Studies of the Nonlinear Response of Stainless Steel Structures

A thesis submitted to the University of London
for the degree of Doctor of Philosophy

By

Marios Theofanous

Department of Civil and Environmental Engineering
Imperial College London
London SW7 2AZ

January 2010

ABSTRACT

Current design guidance on stainless steel structures is largely based on assumed analogies with carbon steel, thereby neglecting stainless steels' actual material behaviour in favour of simplicity. However, its high initial cost warrants the development of improved design guidance which is rational, safe, efficient and in accordance with the actual nonlinear material behaviour.

Within the current research project, all reported test data on stainless steel cross-sections (beams and stub columns) have been gathered and utilized to update current European design guidance and to propose alternative novel design methods which account for actual material behaviour and allow for more efficient material use. Existing design methods which allow for the effect of element interaction on cross-section capacity of carbon steel plated sections have been adapted to stainless steel and a modification to the continuous strength method has been proposed, which leads to a significant decrease in the scatter of the predictions.

Moreover, the possibility of expanding the scope of the current codified provisions of Eurocode 3: Part 1-4 to new material grades and cross-sections has been investigated through experimental and numerical studies. A series of tests and finite element (FE) analyses on stainless steel Oval Hollow Section (OHS) members was carried out to investigate the structural behaviour of these sections. Similarly, experimental and numerical studies on a new grade of stainless steel with a low nickel content, termed lean duplex stainless steel (EN 1.4162) were also conducted and its applicability for structural applications was verified.

Finally, a series of tests on continuous stainless steel beams has been undertaken to investigate the effect of moment redistribution on the capacity of indeterminate stainless steel structures and assess the applicability of nonlinear structural analysis procedures, equivalent to the plastic design of carbon steel structures, to indeterminate stainless steel structures. It was found that plastic design can be safely applied to stainless steel structures and an extension to the continuous strength method has been proposed.

ACKNOWLEDGEMENTS

The work presented in this thesis was carried out under the supervision of Dr Leroy Gardner, to whom I would like to express my sincere gratitude for his continuous encouragement and support and his valuable advice and sharp insights throughout the course of my postgraduate studies.

I would also like to acknowledge the financial support received from the Outokumpu Stainless Research Foundation, and would especially like to thank Dr David Dulieu for his valuable comments and for giving me the opportunity to present my work to an audience of engineers and metallurgists at the seminars organised by Outokumpu.

The experimental part of this project has been carried out in the Structures Laboratory of the Department of Civil and Environmental Engineering, Imperial College London. Hence, I would like to thank the technicians Gordon Herbert and Les Clark for their hard work. Thanks are also due to fellow PhD students Facheng Wang and Nadiah Saari for their assistance in the lab.

The quiet and inspiring working environment provided by the academic and administrative staff of the Department has significantly contributed in the timely completion of this thesis. In particular, I would like to thank Dr Miguel Castro, Dr Tak-Ming Chan, Dr Katherine Cashell, Christina Völlmecke and Ada Law who made Room 429 an ideal working environment. Special thanks are also due to Dr Ahmer Wadee and Stylianos Yiatros, who gave me the opportunity to work on a very interesting research topic beyond the scope of the herein presented research.

The patience exhibited by Nick Loizos, Alkis Papadopoulos, Dimitrios Karypidis and Thomas Tsantikos, while I was trying to play basketball, and their support during the last four years is also gratefully acknowledged. Special thanks are due to Marianthi Leon for tolerating me during the course of my postgraduate studies.

Finally, I would like to thank my mother for the unconditional love and support, without which the completion of this thesis would not have been possible.

CONTENTS

CHAPTER 3 – CROSS-SECTION BEHAVIOUR

CHAPTER 4 – STAINLESS STEEL OVAL HOLLOW SECTIONS

CHAPTER 5 – LEAN DUPLEX STAINLESS STEEL COMPONENTS

CHAPTER 6 – PLASTIC DESIGN OF STAINLESS STEEL STRUCTURES

CHAPTER 7 – CONCLUSIONS AND SUGGESTIONS FOR FUTURE RESAERCH

NOTATION

A	cross-sectional area
A_{cor}	corner area of cross-section
a_m	mean major half-axis measured along centrelines of elliptical hollow section
B	outer width of the section
b_m	mean minor half-axis measured along centrelines of elliptical hollow section
CHS	circular hollow section
CSM	continuous strength method
COV	coefficient of variation
c	flat width of plate element
D	outer depth of the section
D_e	equivalent diameter for OHS and EHS
DSM	direct strength method
d	outer diameter of CHS
E	Young's modulus
E_0	Young's modulus
$E_{0.2}$	tangent modulus at 0.2% offset strain
e_0	global imperfection amplitude

EHS elliptical hollow section

FE finite element

F_{coll} plastic collapse load

F_{hl} load corresponding to the formation of the first plastic hinge

F_u ultimate load

$F_{u,FE}$ predicted ultimate load based on finite element analysis

$F_{u,pred}$ predicted ultimate load

F_y theoretical squash load

f_y yield stress

I second moment of area

L length between centerlines of supports

LVDT linearly varying displacement transducer

L_0 initial length

N_{cl} axial resistance accounting for local buckling according to the DSM

OHS oval hollow section

PFC parallel flange channel

RHS rectangular hollow section

SHS square hollow section

t thickness of plate element average thickness of cross-section

r local radius of curvature

r_i average internal corner radius

w_0 maximum measured local imperfection

$w_{0.5}$ maximum measured local imperfection based on the middle half-length of the specimen

M bending moment

MA major axis

MI minor axis

M_{crl} elastic critical moment causing local buckling of the cross-section

M_{el} elastic moment resistance

$M_{hinge,1}$ moment resistance at the location of the first plastic hinge

$M_{hinge,i}$ moment resistance at the location of the i^{th} plastic hinge

M_{pl} plastic moment resistance

M_u ultimate moment

N axial force

N_u ultimate column buckling load

n strain hardening exponent used in Ramberg-Osgood model

$n'_{0.2,1.0}$ strain hardening exponent used in compound Ramberg-Osgood model

P_m circumference of elliptical hollow section based on centreline dimensions

R rotation capacity of plastic hinge

R-O Ramberg-Osgood

α imperfection factor for column buckling

δ vertical displacement

δ_u end-shortening at ultimate load

ε strain, or material factor defined in EN 1993-1-4 $\left(\sqrt{\frac{235}{\sigma_{0.2}}\frac{E}{210000}}\right)$

ε_f plastic strain at fracture based on elongation over the proportional gauge length $5.65\sqrt{A}$

ε_{LB} strain at which local buckling occurs

ε_{ln}^{pl} logarithmic plastic strain

ε_{nom} engineering strain

$\varepsilon_{t0.2}$ total strain at $\sigma_{0.2}$

$\varepsilon_{t1.0}$ total strain at $\sigma_{1.0}$

θ rotation of a cross-section

θ_m total rotation corresponding to ultimate moment M_u at plastic hinge

θ_{pl} elastic part of the total rotation at midspan when M_{pl} is reached on the ascending branch

θ_u total rotation at plastic hinge when the moment-rotation curve falls back below M_{pl}

k_σ plate element elastic buckling factor

κ_{pl} elastic part of the total curvature at midspan when M_{pl} is reached on the ascending branch

κ_u total curvature at plastic hinge when the moment-rotation curve falls back below M_{pl}

$\bar{\lambda}$ non-dimensional slenderness

$\bar{\lambda}_0$ limiting slenderness for column buckling

$\bar{\lambda}_c$ non-dimensional cross-section slenderness of CHS

$\bar{\lambda}_l$ non-dimensional cross-section slenderness utilised in the direct strength method

$\bar{\lambda}_p$ non-dimensional local plate slenderness

$\bar{\lambda}_{p.f}$ non-dimensional local plate slenderness of flange

$\bar{\lambda}_{p.w}$ non-dimensional local plate slenderness of web

λ plate element slenderness specified in SEI/ASCE-8 (ASCE 2002)

ν Poisson's ratio

ρ reduction factor due to local buckling

σ_{cr} elastic critical buckling stress of plate element

σ stress

σ_{nom} engineering stress

σ_{LB} stress corresponding to local buckling strain ε_{LB}

σ_{true} true stress

σ_u ultimate tensile stress

$\sigma_{u,mill}$ ultimate tensile stress as given in the mill certificate

$\sigma_{0.2}$ proof stress at 0.2% offset strain

$\sigma_{0.2,mill}$ proof stress at 0.2% offset strain as given in the mill certificate

$\sigma_{1.0}$ proof stress at 1.0% offset strain

$\sigma_{1.0,mill}$ proof stress at 1.0% offset strain as given in the mill certificate

χ buckling reduction factor

ψ ratio of end stresses in a compression element

2a larger outer diameter of OHS or EHS

2b smaller outer diameter of OHS or EHS

LIST OF FIGURES

LIST OF TABLES

CHAPTER 1

INTRODUCTION

1.1 BACKGROUND

The term stainless steel refers to a broad family of iron-chromium (Fe-Cr) alloys that contain at least 11% chromium by mass. When exposed to oxygen, the chromium forms a passivation layer of chromium oxide (Cr_2O_3), which protects the underlying metal from corrosion. Other alloying elements typically found in stainless steels are nickel (Ni), which is added to ensure a balanced microstructure, and molybdenum (Mo). According to their crystalline structure, stainless steels are classified as austenitic, ferritic, duplex (austenitic-ferritic), precipitation hardening and martensitic (EN 10088-1, 2005). Austenitic stainless steels were pioneered by Strauss and Maurer in 1912, Dansitzen and Becket industrialized ferritic stainless steels, whereas the commercial birth of martensitic stainless steels is attributed to Brearley, in 1913.

Depending on the alloying elements and heat treatment, a vast range of stainless steel grades with different properties can be produced to suit the needs of many applications (including structural, industrial, automotive and aerospace) and products. Moreover, numerous surface finishes are available for each stainless steel grade, according to the required aesthetic. Typical structural stainless steel products forms include sheet, plate, tube, bar, fasteners and structural sections (either hot-rolled or

cold-formed). Stainless steel grades are classified according to various designation systems; in this thesis the European system (EN 10088-1, 2005) is adopted.

This study is concerned with structural applications of stainless steel. Among the five broad families of stainless steels mentioned before, the austenitic and duplex grades are the most commonly used in the construction industry and hence these stainless steel grades are considered herein.

1.2 STAINLESS STEEL IN THE CONSTRUCTION INDUSTRY

The physical characteristics of stainless steel make it well suited to use in construction; it possesses high strength and stiffness (comparable with carbon steel), very high ductility (approximately two times that of carbon steel), and excellent corrosion resistance, which means, suitably specified that it requires no protective coatings (Gardner, 2005). Stainless steel also offers better retention of strength and stiffness than carbon steel at elevated temperatures (Gardner and Baddoo, 2006; Gardner, 2007).

Owing to its aesthetic appeal stainless steel is often employed for monumental structures (for example the Atomium in Brussels and the US Air Force Memorial in Arlington) and exposed structural elements, a number of examples of which are given by Baddoo et al. (1997). Some of the earliest applications of stainless steel in construction include the cladding of the Chrysler Building in New York, shown in Figure 1.1 and the St. Louis Gateway Arch, erected in 1965. More recently, stainless steel has been used as the principal structural material in numerous road bridges and footbridges (Gedge, 2008). Figure 1.2 depicts a stainless steel footbridge erected in 2008 in Sienna, Italy.

The principal disincentive for the more widespread application of stainless steel in construction is the initial material cost, though considered on a whole life basis, cost comparisons with carbon steel become more favourable (Gardner et al., 2007). Structural design guidance is available for stainless steel, as discussed in Chapter 2.

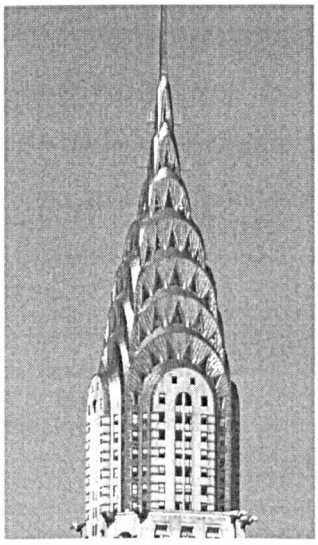

Figure 1.1: *Chrysler Building*

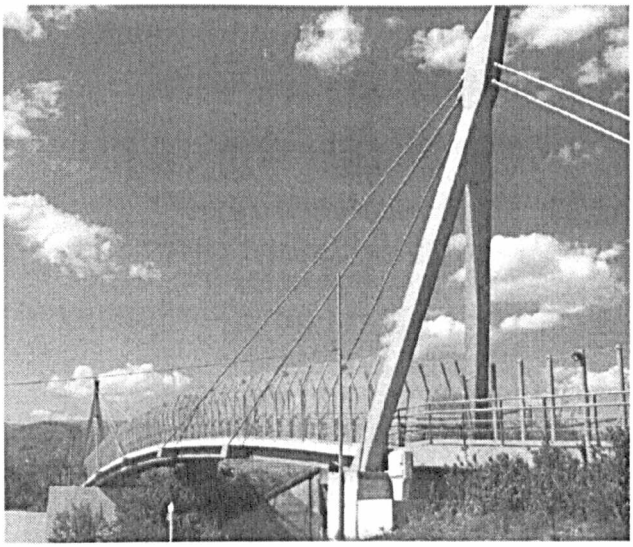

Figure 1.2: *Footbridge in Sienna, Italy*

In most design standards, the design rules are harmonised, where possible, with those developed for structural carbon steel; this enables a relatively straightforward transition between the two materials, but at the expense of design efficiency. It is the intention of this study to enhance design efficiency by proposing more efficient design rules to reflect stainless steels' particular material response.

1.3 OUTLINE OF THESIS

In this chapter, stainless steel and its applications within the construction industry have been briefly introduced. An overview of the thesis follows. It should be noted that throughout the thesis the European structural stainless steel design specifications EN 1993-1-4 (2006) are utilized and assessed, whilst American (SEI/ASCE 8-02, 2002) and Australian/New Zealand (AS/NZS 4673, 2001) design provisions on stainless steel tubular members are assessed only in Chapter 5.

In Chapter 2, a broad literature review of structural stainless steel design guidance, relevant test data and finite element (FE) modelling of stainless steel components is provided, whilst a more focused review on specialized topics is given in the relevant chapters.

Chapter 3 describes the codified design provisions for local buckling set out in EN 1993-1-4 (2006), presents a thorough assessment of the codified slenderness limits and proposes the adoption of revised slenderness limits and effective width equations, thereby enhancing design efficiency. Moreover, advanced design methods for the treatment of local buckling are outlines and assessed on the basis of extensive FE analysis and relevant test data, and modifications to the continuous strength method (CSM), introduced by Gardner (2002), are proposed.

Chapter 4 focuses on the structural response of cold-formed stainless steel oval hollow section (OHS) compression and flexural members and comparisons are made with the results from previous studies on carbon steel elliptical hollow sections (EHS). Based on test and FE results, design provisions for stainless steel OHS in line with EN 1993-1-4 (2006) are proposed. It should be noted that the reported tests are the first tests on stainless steel OHS to be published in the literature.

Chapter 5 focuses on the structural behaviour of lean duplex stainless steel (EN 1.4162) components and assesses the applicability of current design guidance for this new grade of stainless steel.

A discussion on plastic analysis and design, which is currently not allowed for stainless steel structures in any design standard, is presented in Chapter 6. A series of tests on stainless steel continuous beams is reported and some preliminary proposals to expand plastic design to stainless steel structures are described.

Finally, Chapter 7 contains a summary of the findings of this study and gives an overview of the contribution of this research project to structural stainless steel design. Suggestions for further research, some of which already underway, are also provided.

CHAPTER 2

LITERATURE REVIEW

2.1 INTRODUCTION

In this chapter a broad review of previous research into the behaviour and design of stainless steel structures is provided. The development of structural stainless steel design guidance is summarised, with the focus lying on European, American and Australian/New Zealand design Standards, followed by a summary of published test data on stainless steel stub columns, beams and long columns. These test results are extensively utilised throughout the thesis to verify the suitability of current and proposed design approaches. Finally, important findings on numerical modelling of stainless steel components, including the modelling of material behaviour, the effect residual stresses and initial geometric imperfections, are presented. More focused reviews of specialised topics are given in the relevant chapters

2.2 INTERNATIONAL DESIGN STANDARDS

Central to the current codified provisions for stainless steel structures is the adoption of a material-specific limiting stress value, termed the yield strength, which is

assumed to be the maximum attainable stress value for any structural member other than those subjected to pure tension. The adoption of such a limiting stress value seems justified for materials with a sharply defined yield point, whereupon a significant reduction in stiffness occurs, such as carbon steel. For stainless steel, such an assumption is merely a simplistic convention which does not reflect actual structural response. Nonetheless, all current codes for stainless steel adopt the stress corresponding to 0.2% permanent strain $\sigma_{0.2}$, as an equivalent yield stress and assume bilinear (elastic, perfectly-plastic) behaviour for stainless steel as for carbon steel, since departing from the familiar bilinear material model and the associated design philosophy would increase complexity in design and discourage practicing engineers from using stainless steel.

The earliest structural stainless steel design code was the "Specification for the design of cold-formed stainless steel structural members", published by the American Iron and Steel Institute (AISI) in 1968. It was based on the research on austenitic stainless steels reported by Johnson and Winter (1966). Subsequent research, conducted by Wang and Winter (1969), led to revisions published in 1974 by AISI and 1991 by ASCE. The latest American design guidance on structural stainless steel design is the SEI/ASCE 8-02 "Specification for the design of cold-formed stainless steel structural members" published by ASCE (2002). A full account of the improvements of this revised design specification is given by Lin et al. (2005). Based on the American design specifications, the Australian/New Zealand design code for cold-formed stainless steel structures AS/NZS 4673 (2001) was published in 2001. A brief description of its design provisions regarding stainless steel tubular structures is given in Chapter 5, where its suitability for the treatment of lean duplex stainless steel beams is assesses. A detailed account of its development is provided by Rasmussen (2000).

The latest international design standard on stainless steel structures is the European standard EN 1993-1-4 (2006), published in 2006 by CEN. It stems from the respective prestandard, published in 1996, which was based on the second Edition of Euro Inox Design Manual for Stainless Steel (Euro Inox, 1994). A third Edition of the Design Manual for Stainless Steel was also published in 2006 (Euro Inox, 2006), with its commentary published in 2007 (Euro Inox, 2007). Extensive reference to EN

1993-1-4 (2006) is made throughout this thesis and the design provisions codified therein are assessed and compared with design approaches proposed herein.

2.3 LABORATORY TEST RESULTS

As mentioned in the previous section, all structural stainless steel design codes are based on assumed analogies with carbon steel, in an attempt to find a balance between efficiency and simplicity. Given the high material cost of stainless steel, improving existing design guidance is warranted. Improvements can be made either by devising more accurate design approaches in line with actual material response or by optimizing the existing ones. In any case, the existence of a large pool of relevant test data, against which existing and novel design methods can be calibrated and optimized, is vital. Hence the first step towards improving structural stainless steel design guidance involves the gathering of all available test data on structural stainless steel components.

All major structural stainless steel design codes (SEI/ASCE 8-02, 2002; AS/NZS 4673, 2001 and EN 1993-1-4, 2006)) are largely based on test data, the majority of which were reported in the 1950s and the 1960s, as documented in the Commentary to the third edition of Design Manual for Structural Stainless Steel (Euro Inox, 2007). Since their development, considerable further research has been conducted on structural stainless steel. Hence many additional experimental results on cross-section behaviour and member resistance, that were not available during the development of the design specifications, now exist and are utilised throughout this project.

A total of 183 stub column tests results have been gathered from published sources and a further 14 are reported in Chapters 4 and 5. All stub column test data are summarised in Table 2.1, where the section types considered, number of tests conducted, material grade and relevant references are also shown. These are utilized in Chapter 3 to establish appropriate Class 3 slenderness limits for stainless steel internal and outstand elements and CHS, and to assess the suitability of novel design approaches for the treatment of local buckling.

Table 2.1: *Stub column tests*

Reference	Section type	No. of tests	Material grade
Kuwamura (2003)	Angle	12	1.4301 1.4318
	Channel	11	
	Lipped channel	12	
	I (welded)	16	
	SHS	12	
	CHS	10	
ECSC (2000)	I (welded)	4	1.4301 1.4462
Gardner and Nethercot (2004a)	SHS	17	1.4301
	RHS	16	
	CHS	4	
Talja and Salmi (1995)	SHS	1	1.4301
	RHS	2	
Rasmussen and Hancock (1993a)	SHS	2	1.4306
	CHS	3	
Liu and Young (2003)	SHS	4	1.4301
Young and Liu (2003)	RHS	8	1.4301
Young and Lui (2006)	SHS	6	Duplex
	RHS	3	
Young and Ellobody (2006)	SHS	2	1.4462
	RHS	3	
Gardner et al. (2006)	SHS	4	1.4318
	RHS	4	
Young and Hartono (2002)	CHS	4	1.4301
Burgan et al. (2000)	CHS	3	1.4435 1.4541
Bardi and Kyriakides (2006)	CHS	18	1.4410
Lam and Gardner (2008)	CHS	2	1.4401
Theofanous et al. (2009b)	OHS	6	1.4401
Theofanous and Gardner (submitted)	SHS	6	1.4162
	RHS	2	

Furthermore, a total of 76 bending tests have been collected in order to derive class 3 and class 2 limits for stainless steel cross-sections in Chapter 3. Moment-rotation or moment-curvature relationships were not reported for all tests, but, where available, these have been used for the determination of class 1 limits. All published bending test results are summarised in Table 2.2 and include 6 three point bending tests on OHS and eight three point bending tests on lean duplex stainless steel RHS and SHS, reported in Chapters 4 and 5 respectively.

Table 2.2: *Three and four point bending tests*

Reference	Section type	No. of tests	Material grade
Rasmussen and Hancock (1993b)	SHS	1	1.4306
	CHS	1	
Talja and Salmi (1995)	SHS	3	1.4301
	RHS	6	
ECSC (2000)	I (welded)	4	1.4301 1.4462
	CHS	11	
Real and Mirambell (2005)	SHS	2	1.4301 1.4306
	RHS	2	
	I (welded)	2	
Gardner and Nethercot (2004b)	SHS	5	1.4301
	RHS	4	
Zhou and Young (2005)	SHS	8	1.4301 Duplex
	RHS	7	
Gardner et al. (2006)	SHS	2	1.4318
	RHS	4	
Theofanous et al. (2009b)	OHS	6	1.4401
Theofanous and Gardner (submitted)	SHS	6	1.4162
	RHS	2	

Flexural buckling tests are utilised in Chapter 4 to assess the applicability of the European buckling curve codified in EN 1993-1-4 (2006) for stainless steel hollow section columns. For completeness, test data on columns employing open cross-sections have also been gathered and summarised in Table 2.3. Test data on six OHS

columns reported in Chapter 4 and twelve lean duplex stainless steel RHS and SHS columns reported in Chapter 5 are also included.

Table 2.3: *Flexural buckling tests*

Reference	Section type	No. of tests	Material grade
Rasmussen and Hancock (1993a)	SHS	3	1.4306
	CHS	4	
Talja and Salmi (1995)	SHS	3	1.4301
	RHS	6	
Bredenkamp and van den Berg (1995)	I (welded)	13	1.4003
Ala-Outinen and Oksanen (1997)	SHS	2	1.4301
Burgan et al. (2000)	CHS	6	1.4435 1.4541
	I (welded)	15	1.4301 1.4462
Rhodes et al. (2000)	Lipped channel	22	1.4301
Young and Hartono (2002)	CHS	12	1.4301
Young and Liu (2003)	RHS	16	1.4301
Liu and Young (2003)	SHS	8	1.4301
Gardner and Nethercot (2004b)	SHS	8	1.4301
	RHS	14	
Young and Lui (2006)	SHS	16	duplex
	RHS	8	
Gardner et al. (2006)	SHS	12	1.4318
Theofanous et al (2009a)	OHS	6	1.4401
Theofanous and Gardner (in press)	SHS	6	1.4162
	RHS	6	

2.4 NUMERICAL MODELLING

Owing to the increasing computational efficiency of modern computers and the development of sophisticated finite element (FE) codes, FE analysis is nowadays

widely utilised, complementary to laboratory testing, by both practising engineers and researchers for the investigation of the structural response of cold-formed components. To this end FE models are generated and validated against a set of test data. Once the FE models are deemed capable of replicating test results with sufficient accuracy, parametric studies are conducted to further investigate the effect of key parameters on the structural response in a quick and inexpensive way compared to physical testing.

All FE analyses, reported in Chapters 3, 4 and 5 have been conducted by means of the general purpose FE software ABAQUS (ABAQUS, 2006). In depth research on the FE modelling of stainless steel structural components has been carried out by Gardner and Nethercot (2004c) and Ashraf et al. (2006b), the conclusions of which are utilised in this project. Some remarks regarding modelling assumptions pertinent to this thesis are discussed hereafter. These include the employed element type, the adopted analysis techniques, material modelling, residual stresses and geometric imperfections.

2.4.1 Element type and analysis techniques

Shell elements are customarily adopted to simulate thin-walled structural components. The ABAQUS element library (ABAQUS, 2006) contains a range of shell elements. The element employed in the present study is S4R, a 4-noded doubly curved general-purpose shell element, with reduced integration and finite membrane strains, which has performed well in numerous similar applications (Ellobody and Young, 2005; Lecce and Rasmussen, 2006).

The behaviour of thin-walled structures is affected by material nonlinearity, geometric nonlinearity and the interaction thereof. Modelling of material nonlinearity in stainless steel structures is discussed hereafter. In all FE analyses conducted in the present study, the Riks method (ABAQUS, 2006) has been employed, which accounts for geometric nonlinearities and enables tracing of the structural response beyond the ultimate load.

2.4.2 Material modelling

Stainless steel exhibits a rounded stress-strain relationship with no sharply defined yield point. Traditionally its stress-strain relationship has been described by the Ramberg-Osgood model (Ramberg and Osgood, 1943)), as modified by Hill (1944). However the Ramberg-Osgood model has been found to overestimate the stress at high strains. An improved material model, based on a two stage Ramberg-Osgood equation was introduced by Mirambell and Real (2000) and further developed by Rasmussen (2003) and Gardner and Nethercot (2004a). This compound Ramberg-Osgood model is defined by Equations (2.1) and (2.2) and is utilised herein, as it is deemed accurate for the strain range considered. A three-stage full-range stress-strain model for stainless steel has recently been proposed by Quach et al. (2008). It is intended for applications involving modelling of forming processes, where very high strains can occur, and hence need not be adopted in the present study.

$$\varepsilon = \frac{\sigma}{E_0} + 0.002\left(\frac{\sigma}{\sigma_{0.2}}\right)^n \quad \text{for } \sigma \leq \sigma_{0.2} \tag{2.1}$$

$$\varepsilon = \frac{(\sigma - \sigma_{0.2})}{E_{0.2}} + \left(\varepsilon_{t1.0} - \varepsilon_{t0.2} - \frac{\sigma_{1.0} - \sigma_{0.2}}{E_{0.2}}\right)\left(\frac{\sigma - \sigma_{0.2}}{\sigma_{1.0} - \sigma_{0.2}}\right)^{n'_{0.2,1.0}} + \varepsilon_{t0.2} \quad \text{for} \quad \sigma_{0.2} < \sigma < \sigma_u \tag{2.2}$$

where E_0 and $E_{0.2}$ are the Young's modulus and the tangent modulus at 0.2% offset strain, respectively, $\sigma_{0.2}$ and $\sigma_{1.0}$ are the proof stresses at 0.2% and 1% offset strains, respectively, $\varepsilon_{t0.2}$ and $\varepsilon_{t1.0}$ are the total strains at $\sigma_{0.2}$ and $\sigma_{1.0}$, respectively and n and $n'_{0.2,1.0}$ are strain hardening exponents. These material parameters for the compound Ramberg-Osgood model are determined experimentally.

In this study, the resulting stress-strain curve has to be thereafter transformed in the true stress σ_{true} - log plastic strain ε_{ln}^{pl} format, as required by ABAQUS (2006) and defined by Equations (2.3) and (2.4):

$$\sigma_{true} = \sigma_{nom}(1 + \varepsilon_{nom}) \tag{2.3}$$

$$\varepsilon_{ln}^{pl} = \ln(1+\varepsilon_{nom}) - \frac{\sigma_{true}}{E} \tag{2.4}$$

where σ_{nom} and ε_{nom} are the engineering stress and strain respectively and E is the Young's modulus.

Regarding the incorporation of the material model into the FE simulations, another issue arises since a piecewise linear approximation of the actual continuous engineering stress-strain curve has to be derived, which can be thereafter converted into the desired format using Equations (2.3) and (2.4). An optimized distribution of the approximation points, which maximises the accuracy of the fit for a given number of discretisations, is pursued. In a similar investigation (Koltsakis and Preftitsi, 2008), it was concluded that the density of the points defining the multilinear curve should be proportional to the curvature of the Ramberg-Osgood model. This approach has been followed in the present study, with a slight modification since a compound Ramberg-Osgood curve rather than the original single expression is used. The engineering stress-strain curve is initially divided into two regions; the first one being limited by the 0.2% proof stress $\sigma_{0.2}$, whilst the second one is limited by the ultimate tensile stress σ_u. From the number of points to be used for the discretisation of the stress-strain curve, three are reserved for the representation of the origin and the end of the curve and the point corresponding to $\sigma_{0.2}$, whilst the remaining points are then divided between the first and the second region in proportion to the $\sigma_{0.2}/(\sigma_u - \sigma_{0.2})$ ratio. Finally, the points to be used in each region are distributed so that their density is proportional to the curvature of each sub-curve comprising the whole material response.

Equations (2.1) and (2.2) express strains as a function of stress. However, in some applications (e.g. when applying the continuous strength method (CSM) outlined in Chapter 3), the evaluation of stress values corresponding to strain (i.e. deformation capacity) values is required. Since Equation (2.1) and (2.2) cannot be exactly inverted to express stress as a function of strain, approximate inversion formulae proposed by Abdella (2006, 2007, 2009) are utilised.

2.4.3 The effect of residual stresses

Residual stresses in cold-formed tubular sections may be categorised as (1) bending residual stresses that vary through the thickness of the sections and arise as a result of plastic deformation during forming and (2) membrane residual stresses that are induced during the seam-welding operation to complete the tube. Careful measurements, reported by Cruise and Gardner (2008a), have shown the latter to be relatively insignificant in stainless steel hollow sections and largely swamped by the dominant bending residual stresses.

Furthermore, the effect of the bending residual stresses is inherently present in the material stress-strain properties (Rasmussen and Hancock, 1993a; Cruise and Gardner, 2008a) since the residual stresses that are released during the cutting of the coupons (causing longitudinal curvature) are essentially reintroduced by straightening of the coupons during testing, provided the coupons were not straightened (by plastic deformation) prior to testing. Residual stresses were therefore not explicitly introduced into the FE models, but the influence of bending residual stresses was inherently present in the material modelling.

2.4.4 Geometric imperfections

Initial geometric imperfections are introduced into structural sections during production, fabrication and handling and can significantly influence structural behaviour of any structural component prone to instability. It is common practice to assume that geometric imperfections have the form of the lowest relevant (i.e. local or global) elastic buckling mode shape, as it is the shape according to which a perfect structure would buckle and eventually fail. To this end an elastic eigenvalue buckling analysis is initially performed to extract the buckling mode shapes which are utilised in subsequent analyses to perturb the idealised geometry. This approach has been followed in the present study.

The buckling mode shapes provide only a perturbation pattern and the incorporation of an imperfection amplitude into the FE models is required. This can be derived from laboratory measurements, be assumed to be a fraction of a characteristic dimension of the modelled structure, or be determined from predictive models (Dawson and Walker, 1972; Schafer and Peköz, 1998a; Cruise and Gardner, 2006).

2.5 DISCUSSION

In this chapter an overview of the recent developments in laboratory testing, design guidance and numerical modelling has been given, whilst additional more focused literature is introduced and discussed within the relevant chapters.

Current design guidance is largely based on assumed analogies with carbon steel and does not allow for the actual material response. In light of additional experimental results, the suitability of codified provisions is reassessed and improvements to EN 1993-1-4 (2006) are proposed. Novel design methods for stainless steel structures are introduced and existing ones are further developed throughout this thesis; their incorporation into future design guidance is supported.

CHAPTER 3

CROSS-SECTION BEHAVIOUR

3.1 INTRODUCTION

Most structural stainless steel components are either cold-formed or welded, comprising plated elements of varying slenderness and are hence susceptible to local buckling when subjected to high compressive stresses. The occurrence of local buckling limits the exploitation of the material's full potential and is particularly detrimental to cross-sections employing high strength stainless steel grades.

The treatment of local buckling within the framework of EN 1993-1-4 (2006), the European structural design rules for stainless steel, draws heavily from the respective design guidance for carbon steel EN 1993-1-1 (2005) and follows the familiar cross-section classification approach. The constituent plate elements of a cross-section are placed into discrete behavioural classes by comparing their width to thickness ratio with codified slenderness limits, which depend on the element's boundary conditions, the applied stress gradient and the manufacturing process (whether cold-formed or welded). The cross-section itself is classified according to its most slender constituent element. Since the constituent plate elements are treated in isolation, the effect of element interaction on both the elastic buckling and ultimate response is neglected. Boundary conditions at element junctions are assumed to be simply-supported (i.e.

zero rotational stiffness), as reflected in the plate buckling coefficients k_σ specified in EN 1993-1-5 (2006). However, the embedded conservatism is not uniform for all cross-sections, but varies, depending on how close the actual boundary conditions are to the assumed ones. In a uniformly compressed square hollow section, for example, the four elements offer equal restraint to one another, effectively resulting in simply-supported boundary conditions for each element. In a uniformly compressed rectangular hollow section, on the other hand, the two shorted faces of the section offer greater restraint to the two longer faces; as the aspect ratio increases, the restraint afforded to the two longer faces increases, and the boundary conditions approach fixed supports.

Ignoring element interaction is a simplifying assumption common to both carbon steel and stainless steel. A further simplifying assumption which has greater significance for stainless steel is that of a bilinear (elastic, perfectly-plastic) material response, which ensures consistency between carbon steel and stainless steel design specifications. This assumption is of little significance for very slender elements, the failure of which is governed by stiffness, but severely compromises accuracy and design efficiency in the case of stocky stainless steel plated elements, failure of which is mainly governed by material response.

With the increasing usage of high strength stainless steel grades, which effectively leads to more slender cross-sections, together with the high initial material cost associated with the material, reassessment of the validity of the aforementioned assumptions and elimination of any associated conservatism is warranted. The codified slenderness limits for stainless steel elements are assessed on the basis of all relevant published test data. New slenderness limits are proposed in an attempt to enhance design efficiency within the framework of EN 1993-1-4 (2006). Advanced design methods that allow for element interaction, actual material response or both, which have been previously employed or proposed for carbon steel and/or stainless steel components, are discussed in the following section. The suitability and performance of these methods is assessed thereafter on the basis of a series of FE parametric studies on stainless steel RHS, I sections and PFC stub columns covering a wide range of element slendernesses and aspect ratios. The findings of this research

have been reported by Gardner and Theofanous (2008) and Gardner and Theofanous (2008, submitted).

3.2 CLASSIFICATION AND SLENDERNESS LIMITS

The concept of cross-section classification as a means of codified treatment for local buckling of cross-sections that are partly or fully in compression was originally developed for materials that closely follow an idealised bilinear stress-strain response such as carbon steel. The existence of a sharply defined yield point, beyond which a sudden drop in stiffness occurs and hence instability is triggered, defines distinct behavioural groups, based on whether the attainment of this yield stress in any part of the cross-section is limited by the occurrence of local buckling. For the fundamental case of pure compression, cross-section failure may occur either by material yielding and inelastic local buckling in the case of stocky cross-sections (class 1-3) or by local buckling at an average stress below the yield stress for slender cross-sections (class 4). For cross-sections in bending, failure may occur by local buckling prior to reaching the yield stress in the case of slender sections (class 4), by inelastic local buckling above the elastic moment capacity but below the plastic moment capacity following extreme fibre yielding for intermediate sections (class 3), or by inelastic local buckling above the plastic moment capacity following extensive yielding for stocky sections (classes 1-2). Distinction is made between class 1 and 2 cross-sections depending on whether they can sustain their plastic moment with increasing deformation and allow sufficient moment redistribution to take place in the structure for a collapse mechanism to form, in which case plastic analysis may be applied (class 1), or local buckling limits their deformation capacity (class 2) and elastic analysis need be applied.

Given the relatively recent emergence of stainless steel as a structural material, efforts have been made to maintain consistency with carbon steel design guidance. However, unlike carbon steel, stainless steel exhibits a rounded non-linear stress-strain relationship with no strictly defined yield point, as shown in Figure 3.1, and hence no sharp behavioural transition occurs at any specific stress, thereby complicating any

design process traditionally based on a characteristic stress level. This complexity is overcome by defining the yield point as the stress level corresponding to 0.2% permanent strain $\sigma_{0.2}$, and assuming bilinear stress-strain behaviour for stainless steel as for carbon steel. The substantial differences in the structural response between the two materials are neglected in favour of simplicity, generally resulting in conservative slenderness limits for stainless steel cross-sections.

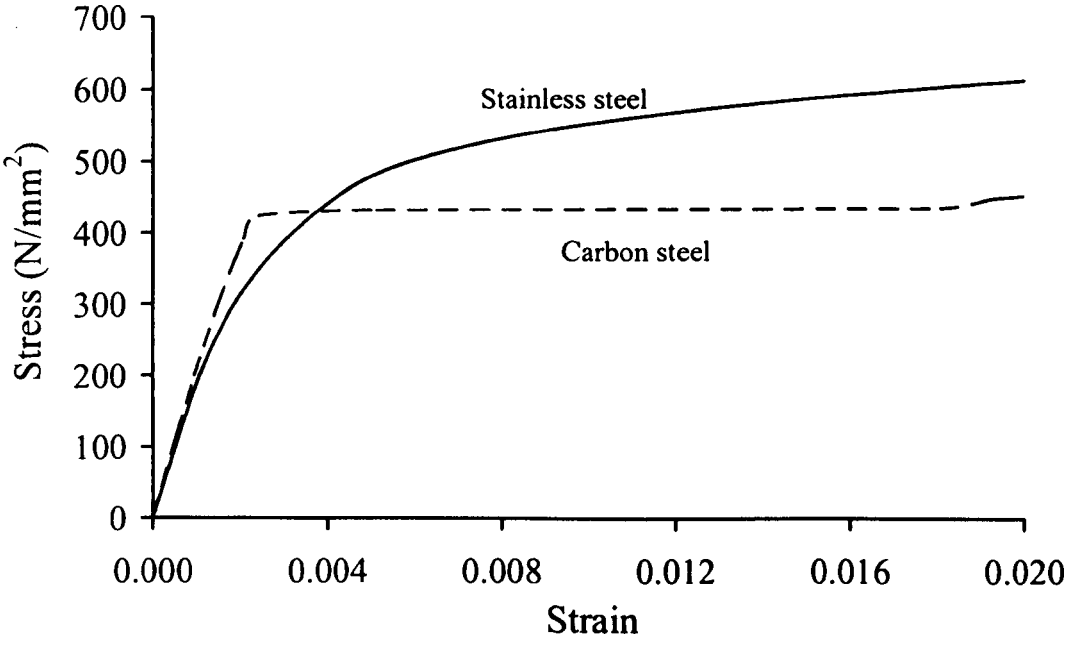

Figure 3.1: *Indicative carbon steel and stainless steel stress-strain curves*

3.2.1 Current slenderness limits for stainless steel sections

The classification process employed in the current codified treatment of local buckling for stainless steel cross-sections mirrors that applied to carbon steel. Squash load F_y, elastic moment capacity M_{el} and plastic moment capacity M_{pl} of stainless steel cross-sections are defined with respect to the conventional yield (0.2% proof) stress $\sigma_{0.2}$, and relevant classes are based on susceptibility to local buckling and cross-sectional deformation capacity as for carbon steel. Cross-sectional response is assumed to relate to the behaviour of its most slender plate element, thereby neglecting the interaction of constituent plate elements, which are individually classified according to their width-to-thickness ratios, as compared to codified

slenderness limits. These limits depend on each element's boundary conditions (internal or outstand), manufacturing process (welded or cold-formed) and stress gradient.

Determination of slenderness limits is ideally based on relevant experimental results; stub column and/or bending tests for the derivation of the class 3 limit and bending tests only for the class 2 and class 1 limits. However, unlike carbon steel, only a limited number of test results existed at the time of the development of most stainless steel design codes. These included 46 stub column and 11 bending tests on cross-sections comprising internal and outstand (either welded or cold-formed) plate elements, reported by Johnson and Winter (1966), Wang and Winter (1969) and Yamada et al. (1988), which were primarily intended to investigate the effective width of class 4 plate elements in compression. These tests are appropriate only for the derivation of the class 3 limit for plate elements in compression. The remaining slenderness limits for compressed elements were derived based on engineering judgment and assumed analogies with carbon steel, whereas the relevant classification limits for plate elements in bending and combined compression and bending were based on adjustment to the respective compression limits by appropriate buckling factors derived from elastic solutions of perfect plates subjected to stress gradients. Hence the existing class 1 and class 2 limits are largely unverified, while the class 3 limit has been experimentally justified but only by a relatively limited number of test results.

3.2.2 Assessment of existing slenderness limits

Since the development of EN 1993-1-4 (2006), considerable further research has been conducted on structural stainless steel. Many additional experimental results on cross-sectional resistance, that were not available during the development of the code, now exist. These include both stub column and bending tests, summarised in Tables 2.1 and 2.2 respectively, which are utilized herein to assess the applicability of current slenderness limits.

In this section, existing slenderness limits are compared with all published stainless steel experimental results to assess their applicability. Determination of the

slenderness parameters follows the provisions of EN 1993-1-4 (2006). Experimental results are shown in Figures 3.2-3.10 and 3.12-14. The corresponding class limits for carbon steel and stainless steel, as specified by EN 1993-1-1 (2005) and EN 1993-1-4 (2006) respectively, are also depicted for comparison. For all cross-sections the relevant response characteristic ($F_u/A\sigma_{0.2}$, M_u/M_{el}, M_u/M_{pl}, or rotation capacity R) is plotted against the slenderness of the most slender constituent element in the cross-section, where F_u and M_u are the ultimate loads and moments as determined from the experiments and M_{el} and M_{pl} are the conventional elastic and plastic moment capacities. In determining element slenderness, due account of the stress distribution and element support conditions has been made through the buckling factor k_σ, as defined in EN 1993-1-5 (2006). The following symbols are employed: c = compressed flat width; d = outer diameter; t = element thickness; $\varepsilon = [(235/f_y)(E/210000)]^{0.5}$. Note that this definition of ε for stainless steel, as given in EN 1993-1-4 (2006) differs from that given in EN 1993-1-1 (2005), to allow for variation in Young's modulus. However, given that the difference in Young's modulus between stainless steel and carbon steel is small (approximately 5%), in comparison to the scatter of experimental data, it is believed that in the interest of simplicity and harmonisation the familiar carbon steel definition of $\varepsilon = (235/f_y)^{0.5}$ could be utilized for both materials.

3.2.2.1 Class 3 slenderness limit

Cross-sections capable of reaching their yield stress ($\sigma_{0.2}$ in the case of stainless steel) prior to the onset of local buckling are classified as class 3 or better. Both stub column and bending tests are utilized to assess appropriate class 3 limits, as shown in Figures 3.2-3.7.

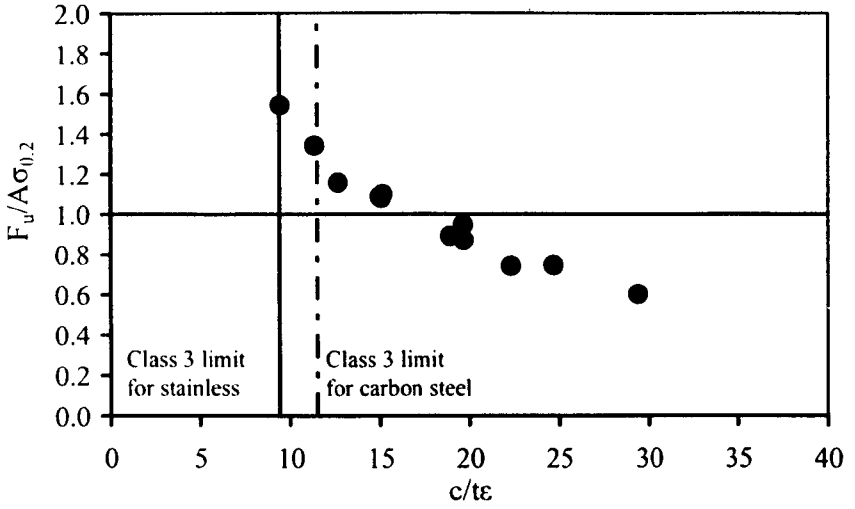

Figure 3.2: *Class 3 limit for angles in compression*

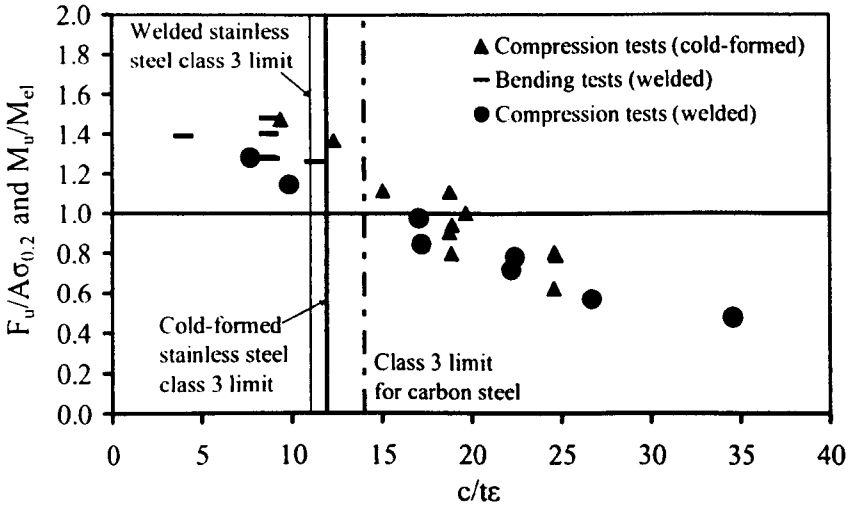

Figure 3.3: Class 3 limit for outstand elements in compression

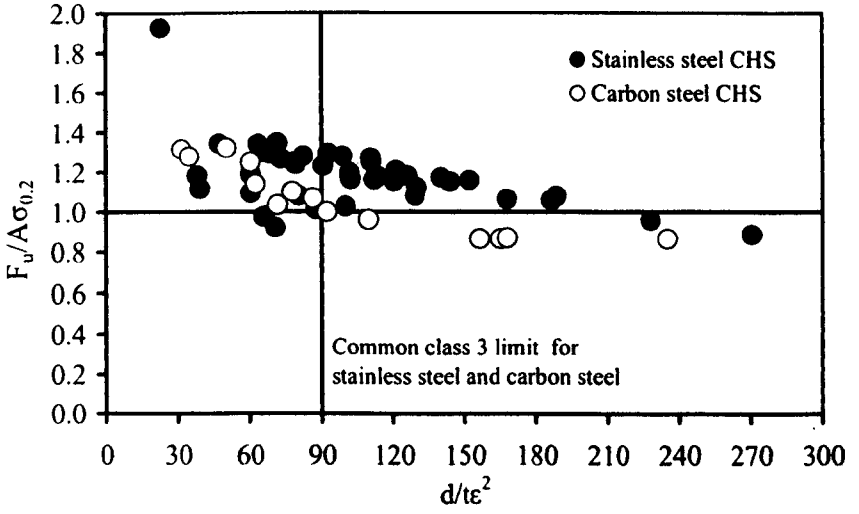

Figure 3.4: *Class 3 limit for CHS in compression*

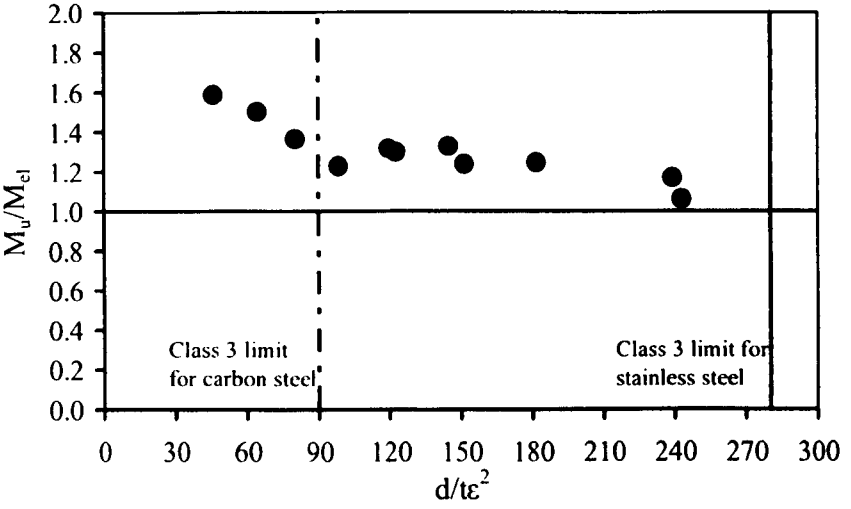

Figure 3.5: *Class 3 limit for CHS in bending*

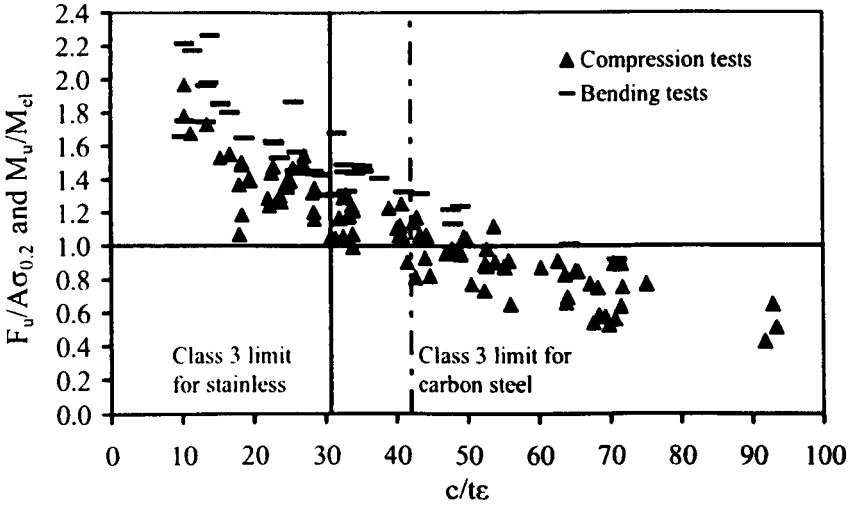

Figure 3.6: *Class 3 limit for internal elements in compression*

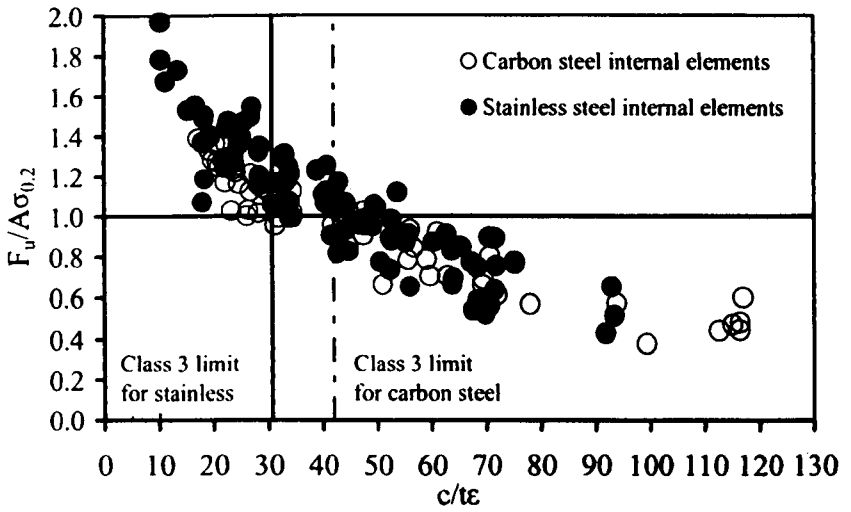

Figure 3.7: Class 3 limit for carbon steel and stainless steel internal elements in compression (stub column tests only)

In Figures 3.4 and 3.7, carbon steel data have been included for comparison purposes as will be discussed in Section 3.2.3. The carbon steel data were obtained from stub column tests on CHS conducted by O'Shea and Bridge (1997) and Elchalakani et al. (2002) and on cross-sections comprising flat internal elements conducted by Akiyama et al. (1992) and Uy (1998).

3.2.2.2 Class 2 slenderness limit

Cross-sections capable of reaching their full plastic moment capacity are classified as class 2 or better. A series of bending tests have been utilized to assess the current class 2 limits as illustrated in Figures 3.8-3.10. For CHS (Figure 3.8) and cross-sections comprising internal parts in compression (Figure 3.10), a reasonable number of test results exist, but for outstand elements, test data are scarcer. Figure 3.9 shows results from six I-section beam tests. No bending tests have been reported on cross-sections comprising cold-formed outstand elements to date.

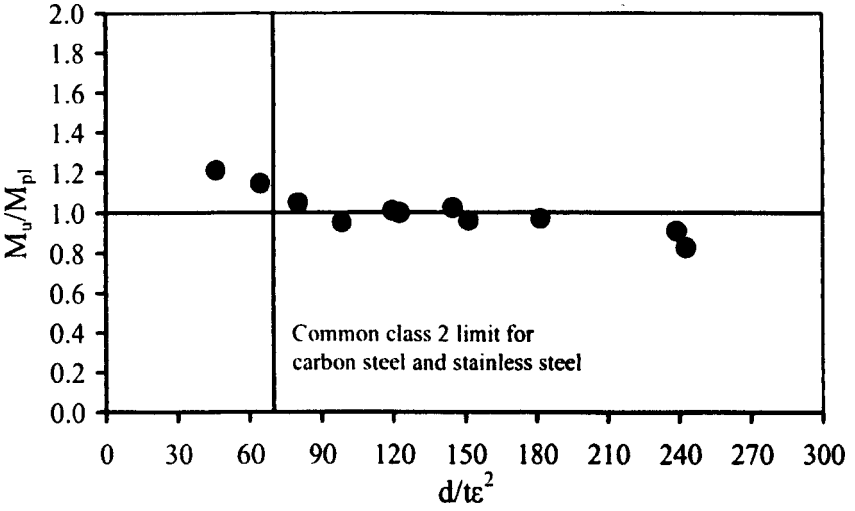

Figure 3.8: *Class 2 limit for CHS in bending*

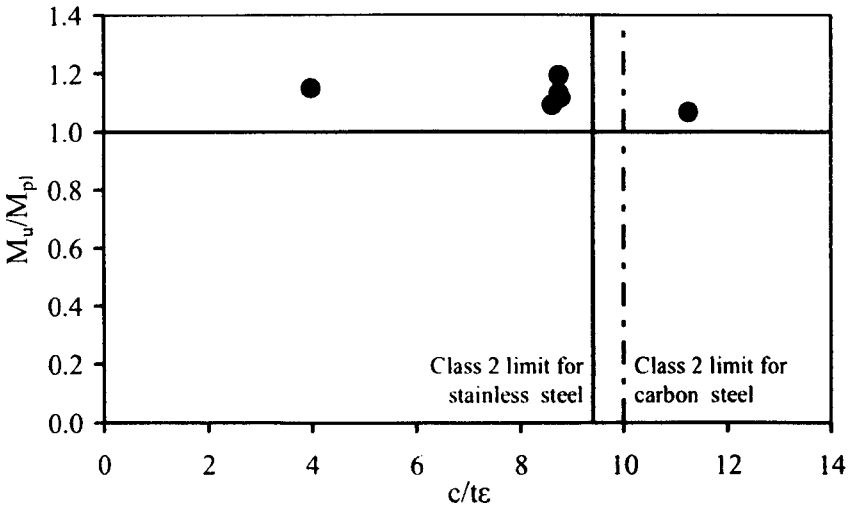

Figure 3.9: Class 2 limit for welded outstand elements in compression (I-section tests)

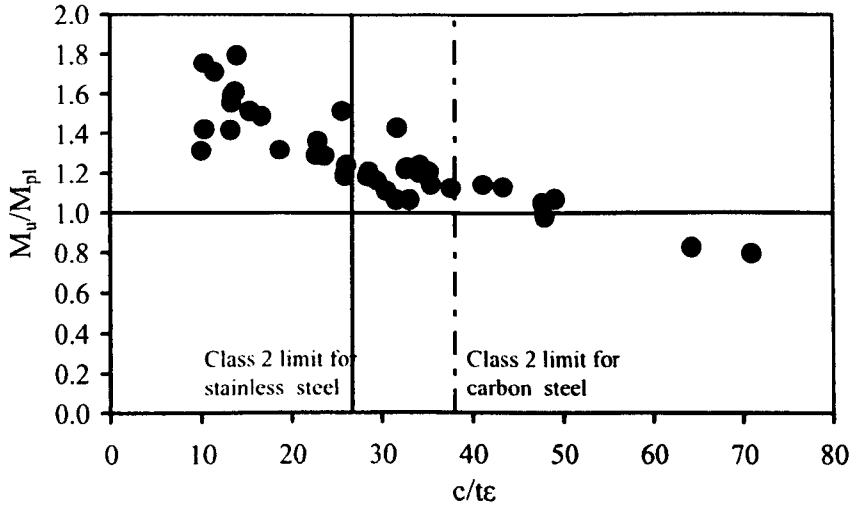

Figure 3.10: Class 2 limit for internal elements in compression (SHS and RHS bending tests)

3.2.2.3 Class 1 slenderness limit

Cross-sections capable of reaching and maintaining their plastic moment capacity with sufficient deformation capacity to be used in plastic design, are classified as class 1. The term deformation refers either to the rotation at the theoretical plastic hinge location (i.e. most heavily stressed cross-section in the case of specimens under a moment gradient e.g. 3-point bending tests), or to the constant curvature developed in the uniform moment region of specimens under pure bending (typically achieved in

the central region of symmetrical 4-point bending tests). In either case the deformation capacity is quantified through Equation (3.1), where k_u (θ_u) is the curvature k (rotation θ) at the point at which the falling branch of the moment-curvature (moment-rotation) curve falls below M_{pl}, and k_{pl} (θ_{pl}) is the elastic curvature (rotation) corresponding to M_{pl} as illustrated in Figure 3.11.

$$R = \frac{k_u}{k_{pl}} - 1 \text{ (based on M-k relationship)}$$
$$R = \frac{\theta_u}{\theta_{pl}} - 1 \text{ (based on M-}\theta\text{ relationship)} \quad (3.1)$$

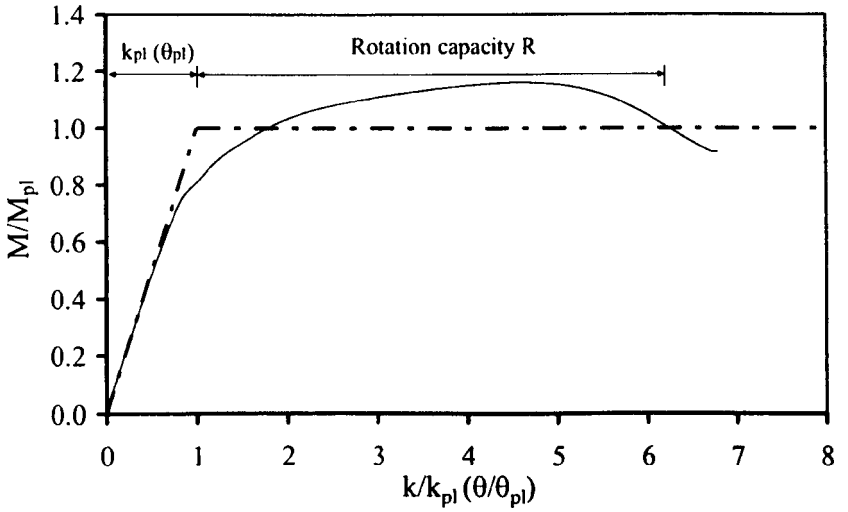

Figure 3.11: *Definition of deformation capacity*

In the absence of a codified deformation capacity requirement for class 1 stainless steel cross-sections (no rules for plastic global analysis are given in EN 1993-1-4 (2006), as discussed in chapter 6), the equivalent carbon steel requirement of R = 3 reported by Bild et al. (1989) and Sedlacek and Feldmann (1995) has been adopted. In some cases, experiments were stopped upon attainment of the maximum moment capacity and the full deformation capacity was not reached. Since there is no accurate way of extrapolating the reported experimental curves, the deformation capacity in those cases was conservatively defined by using the maximum reported curvature k_{max} (for 4-point bending tests) or rotation θ_{max} (for 3-point bending tests) in place of k_u (θ_u) in Equation (1). The tests results are shown in Figures 3.12-3.14; the specimens that reached their full deformation capacity are depicted with shaded symbols, while those that did not are depicted with blank symbols.

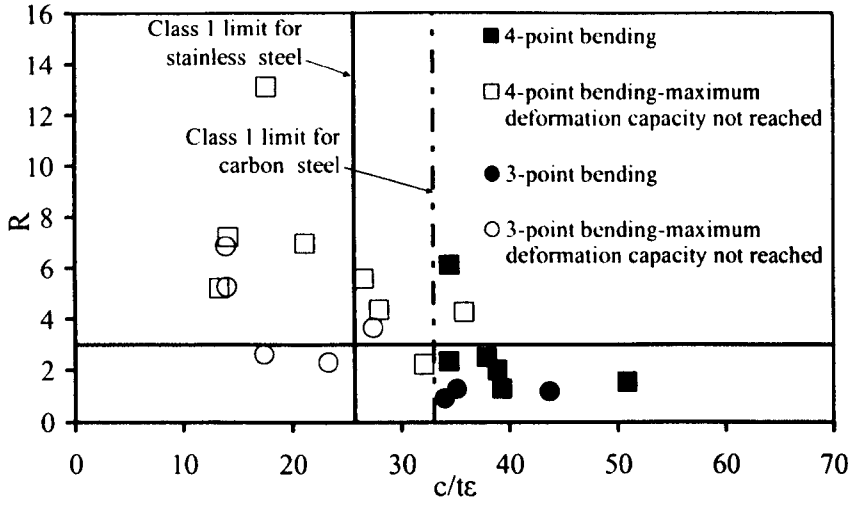

Figure 3.12: Class 1 limit for internal elements in compression

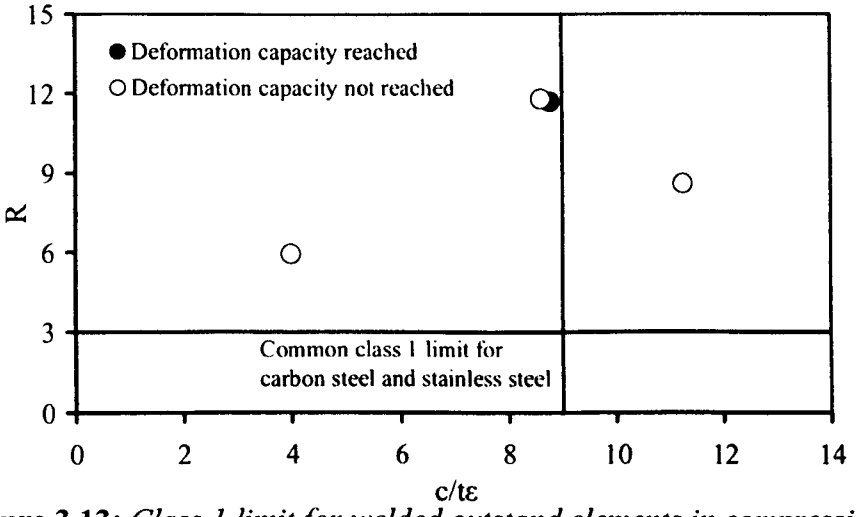

Figure 3.13: *Class 1 limit for welded outstand elements in compression*

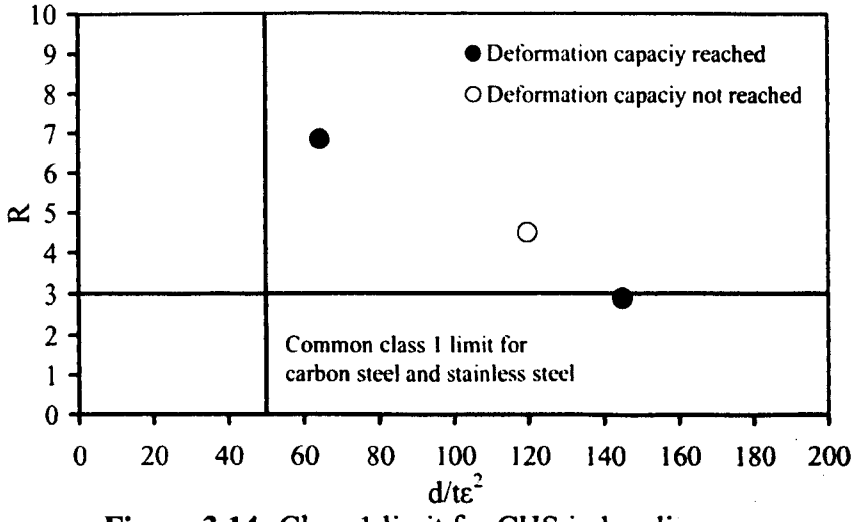

Figure 3.14: Class 1 limit for CHS in bending

3.2.3 Proposal for new slenderness limits

Analysis of the presented test data reveals that current slenderness limits for stainless steel are overly conservative and that harmonisation with the equivalent carbon steel limits may be justified. For class 1 and class 2 limits, Figures 3.8-3.14 indicate that the equivalent carbon steel limits may be safely adopted for stainless steel, although the number of tests reported for outstand elements in compression is rather limited and further test results are required.

The current class 3 limits for stainless steel angles and outstand elements is unduly strict and all reported test results support the adoption of the equivalent carbon steel limits. Furthermore, the distinction made in EN 1993-1-4 between cold-formed and welded outstand parts is not clearly justified by the relevant test results. Although the cold-formed outstand elements generally exhibit superior capacity to their welded counterparts in the stocky range, attributed to the enhanced corner properties brought about by the forming process and the less severe residual stresses, the disparity in response becomes insignificant at higher slendernesses. Hence, it is recommended that the current carbon steel class 3 limit for outstand elements (including both welded and cold-formed elements) be adopted for both cold-formed and welded stainless steel outstand elements. Regarding the class 3 limit for CHS in bending, Figure 3.5 suggests that the current stainless steel slenderness limit of $280\varepsilon^2$ is reasonable. However no test data exist in the vicinity of this limit and any extrapolation should be conducted with caution. The current corresponding slenderness limit for carbon steel CHS of $90\varepsilon^2$ is clearly inappropriate for stainless steel, and its suitability for carbon steel has also been questioned by Gardner and Chan (2007). Finally, the comparison between carbon steel and stainless steel test data for CHS and internal elements in compression, shown in Figures 3.4 and 3.7, demonstrate that stainless steel CHS and flat internal elements in compression perform similarly to their carbon steel counterparts.

The class 3 slenderness limit for CHS in compression currently lies at $90\varepsilon^2$ for both carbon steel and stainless steel, and this value is supported by the presented test data. For flat internal elements in compression, the current class 3 slenderness limit for

stainless steel is conservative, but harmonisation with the carbon steel limit is not supported by the test data, and an intermediate limit is therefore proposed.

The above recommendations are summarised in Table 3.1, where specific slenderness limits are given for each behavioural class and for all loading conditions. The recommended class 2 and class 3 slenderness limits for internal and outstand (both cold-formed and welded) elements in compression, CHS in compression and bending and the class 3 limit for angles in compression have been validated by means of statistical analysis according to Annex D of EN 1990 (2002) against all available test data summarised in Tables 2.1 and 2.2 and were deemed safe for design in conjunction with a partial safety factor of γ_{M1}=1.1, as specified in EN 1993-1-4 (2006). For consistency, it is proposed that the effective width formulae specified in EN 1993-1-4 (2006) be modified to Equations (3.2) and (3.3), which have also been statistically validated according to EN 1990 (2002). It should be noted that statistical data on the mechanical strength (i.e. average actual 0.2% proof stress values and corresponding standard deviations) of various stainless steel grades, reported by Groth and Johansson (1990) have been utilized in the statistical validation of the slenderness limits and effective width equations proposed herein.

$$\rho = \frac{1}{\bar{\lambda}_p} - \frac{0.188}{\bar{\lambda}_p^{\,2}} \leq 1 \qquad \text{for outstand elements (cold-formed or welded)} \qquad (3.2)$$

$$\rho = \frac{0.772}{\bar{\lambda}_p} - \frac{0.079}{\bar{\lambda}_p^{\,2}} \leq 1 \qquad \text{for internal elements (cold-formed or welded)} \qquad (3.3)$$

where ρ is the reduction factor for local buckling and $\bar{\lambda}_p$ is the element slenderness, as defined in EN 1993-1-4 (2006).

For elements under stress gradients, the slenderness limits recommended in Table 3.1 have been derived on the basis of modification of the proposed limits for compression by appropriate buckling factors k_σ EN 1993-1-5 (2006), though due to lack of experimental data, no statistical validation has been performed. Moreover, no statistical analysis has been performed for the proposed class 1 limits due to the highly

Table 3.1: *Carbon steel (CS), stainless steel (SS) and proposed slenderness limits for compression elements*

Element	Class 1			Class 2			Class 3		
	CS limit	SS limit	Proposed limit	CS limit	SS limit	Propose d limit	CS limit	SS limit	Proposed limit
Internal element in compression	33ε	25.7ε	33ε	38ε	26.7ε	35ε	42ε	30.7ε	37ε
Internal element in bending	72ε	56ε	72ε	83ε	58.2ε	76ε	124ε	74.8ε	90ε
Internal element subject to bending and compression: $a > 0.5$ or $\psi > -1$	$\frac{396\varepsilon}{13a-1}$	$\frac{308\varepsilon}{13a-1}$	$\frac{396\varepsilon}{13a-1}$	$\frac{456\varepsilon}{13a-1}$	$\frac{320\varepsilon}{13a-1}$	$\frac{420\varepsilon}{13a-1}$	$\frac{42\varepsilon}{0.67+0.33\psi}$	$15.3\varepsilon\sqrt{k_\sigma}$	$18.5\varepsilon\sqrt{k_\sigma}$
Internal element subject to bending and compression: $a \le 0.5$ or $\psi \le -1$	$36\varepsilon/a$	$28\varepsilon/a$	$36\varepsilon/a$	$41.5\varepsilon/a$	$29.1\varepsilon/a$	$38\varepsilon/a$	$62\varepsilon(1-\psi)\sqrt{-\psi}$	$15.3\varepsilon\sqrt{k_\sigma}$	$18.5\varepsilon\sqrt{k_\sigma}$
Cold-formed outstand element in compression	9ε	10ε	9ε	10ε	10.4ε	10ε	14ε	11.9ε	14ε
Cold-formed outstand subject to bending and compression (tip in compression)	$9\varepsilon/a$	$10\varepsilon/a$	$9\varepsilon/a$	$10\varepsilon/a$	$10.4\varepsilon/a$	$10\varepsilon/a$	$21\varepsilon\sqrt{k_\sigma}$	$18.1\varepsilon\sqrt{k_\sigma}$	$21\varepsilon\sqrt{k_\sigma}$
Cold-formed outstand subject to bending and compression (tip in tension)	$\frac{9\varepsilon}{a\sqrt{a}}$	$\frac{10\varepsilon}{a\sqrt{a}}$	$\frac{9\varepsilon}{a\sqrt{a}}$	$\frac{10\varepsilon}{a\sqrt{a}}$	$\frac{10.4\varepsilon}{a\sqrt{a}}$	$\frac{10\varepsilon}{a\sqrt{a}}$	$21\varepsilon\sqrt{k_\sigma}$	$18.1\varepsilon\sqrt{k_\sigma}$	$21\varepsilon\sqrt{k_\sigma}$
Welded outstand element in compression	9ε	9ε	9ε	10ε	9.4ε	10ε	14ε	11ε	14ε
Welded outstand subject to bending and compression (tip in compression)	$9\varepsilon/a$	$9\varepsilon/a$	$9\varepsilon/a$	$10\varepsilon/a$	$9.4\varepsilon/a$	$10\varepsilon/a$	$21\varepsilon\sqrt{k_\sigma}$	$16.7\varepsilon\sqrt{k_\sigma}$	$21\varepsilon\sqrt{k_\sigma}$
Welded outstand subject to bending and compression (tip in tension)	$\frac{9\varepsilon}{a\sqrt{a}}$	$\frac{9\varepsilon}{a\sqrt{a}}$	$\frac{9\varepsilon}{a\sqrt{a}}$	$\frac{10\varepsilon}{a\sqrt{a}}$	$\frac{9.4\varepsilon}{a\sqrt{a}}$	$\frac{10\varepsilon}{a\sqrt{a}}$	$21\varepsilon\sqrt{k_\sigma}$	$16.7\varepsilon\sqrt{k_\sigma}$	$21\varepsilon\sqrt{k_\sigma}$
Angles in compression	-	-	-	-	-	-	11.5ε	9.1ε	11.5ε
CHS in compression	$50\varepsilon^2$	$50\varepsilon^2$	$50\varepsilon^2$	$70\varepsilon^2$	$70\varepsilon^2$	$70\varepsilon^2$	$90\varepsilon^2$	$90\varepsilon^2$	$90\varepsilon^2$
CHS in bending	$50\varepsilon^2$	$50\varepsilon^2$	$50\varepsilon^2$	$70\varepsilon^2$	$70\varepsilon^2$	$70\varepsilon^2$	$90\varepsilon^2$	$280\varepsilon^2$	$280\varepsilon^2$

(a=depth of plastic compression zone over total element width, ψ=elastic compressive over elastic tensile stress ratio, k_σ defined in EN 1993-1-5)

scattered nature of the rotation capacities of the sections. Poor correlation between rotation capacity and codified slenderness parameters was also reported for carbon steel specimens by Bild et al. (1989) and Sedlacek and Feldmann (1995) where the scatter was attributed to the effect of other parameters, such as moment gradient, material properties and the interaction of constituent plate elements. Hence, as for carbon steel, a degree of engineering judgement has been required for the assessment of the class 1 limits given in Table 3.1. It is recommended that the proposed slenderness limits (Table 3.1) and effective width formulae (Equations (3.2) and (3.3)) be incorporated into future revisions of EN 1993-1-4 (2006).

3.3 ADVANCED METHODS FOR THE TREATMENT OF LOCAL BUCKLING

Although conceptually simple, application of the effective width method is often cumbersome, since having established the effective width of the individual elements, calculation of the properties of the effective cross-section is then required. Moreover, it may have to be applied iteratively, when a shift of a cross-section's neutral axis and a corresponding modification of the applied stress distribution is caused by the loss of effectiveness of some parts of the cross-section. As previously discussed, element interaction and material nonlinearity are not accounted for within the classification framework. Failure to account for element interaction leads to overly conservative design for both carbon steel and stainless steel components in cases where the slenderness of the constituent plate elements varies significantly (e.g. RHS with large aspect ratios), whilst less conservative results are obtained when all plate elements have similar slenderness (e.g. SHS). On the other hand, the effect of the actual material response on ultimate cross-section capacity is more important for stainless steel due to its pronounced strain-hardening and becomes increasingly significant with decreasing cross-section slenderness.

The shortcomings of the codified provisions have been highlighted by many researchers and more advanced design methods, allowing for element interaction and

material strain-hardening, have been proposed. Some of these methods, including a statistical method proposed by Kato (1989; 1990), the Direct Strength Method (DSM) and the Continuous Strength Method (CSM), are briefly summarised herein and assessed on the basis of an extensive FE parametric study. An overview of the methods considered, their origin and whether or not they account for material nonlinearity and element interaction is given in Table 3.2.

Table 3.2: *Various design methods for the treatment of local buckling*

Design methods	Originally devised for	Element interaction	Material response
Classification/ Effective width	Hot-rolled steel	Not considered	Bilinear
Linear regression analysis	Hot-rolled I sections	Yes	Bilinear
Direct Strength Method	Cold-formed steel	Yes	Bilinear
Continuous Strength Method	Stainless steel	Not considered	Actual

3.3.1 Ultimate capacity predictions based on regression analysis

During his studies on the rotation capacity of carbon steel structures, Kato (1989; 1990) acknowledged both the mutual restraint between the flanges and the web of I-sections and the strain-hardening exhibited by carbon steel at high strains. He devised a semi-analytical method for predicting the rotation capacity of an I-section as an explicit function of the stress at which local buckling occurs, normalised by the yield stress. The general form of the normalised buckling strength, referred to as σ_{cr}/σ_y by Kato (1989; 1990), is given by Equation (3.4)

$$\frac{\sigma_y}{\sigma_{cr}} = A + \frac{B}{a_f} + \frac{C}{a_w} \tag{3.4}$$

where a_f and a_w are slenderness parameters for the flange and the web respectively and A, B and C are parameters determined by multivariable linear regression analysis of stub column test data. The stress at which local buckling occurs is denoted σ_{LB} herein, whilst the equivalent yield stress of stainless steel is taken as the 0.2% proof stress $\sigma_{0.2}$.

This method was shown to be quite accurate (Kato 1989; 1990) for carbon steel I section stub columns and was able to correctly predict the ultimate capacity of stocky cross-sections above the yield load, whilst the flange-web interaction was explicitly accounted for. Once calibrated on the basis of stub column tests, the method can be extended to predict the ultimate moment capacity of beams. Daali and Korol (1995) adapted the method to predict the ultimate capacity of carbon steel I section beams, whilst a similar approach was followed by Beg and Hladnik (1996) for high strength steel I section beams.

To date this method has been applied to the prediction of the ultimate capacity of carbon steel and high strength steel I section stub columns and beams failing by local buckling, but is, in principle, applicable to other plated cross-section types and materials, provided that a sufficiently large set of stub column test data exists for its calibration. Its accuracy, simplicity, explicit nature and its ability to account for both element interaction and strain-hardening, render this method an attractive alternative to cross-section classification. However its mere statistical nature and the need for calibration and derivation of a separate design equation for each cross-section type are its main drawbacks.

3.3.2 The Direct Strength Method (DSM)

Increasingly sophisticated manufacturing facilities and the desire to minimise material use in cold-formed carbon steel structures have lead to the emergence of very slender cross-sections, frequently employing edge stiffeners and intermediate stiffeners of various geometries to delay the onset of local buckling. The complexity of many recently developed cross-sections and their deviation from the traditional

assembly of flat plated elements renders application of the effective width method questionable and awkward. Moreover, optimization of the properties of cold-formed steel cross-sections may result in the triggering of numerous buckling modes (e.g. local, distortional and global) at similar load levels, leading to interaction phenomena.

The cumbersome nature of the effective width method when applied to slender cold-formed steel cross-sections of complex geometries and concerns about its ability to account for all possible failure modes including interaction buckling, led to the development of the Direct Strength Method (DSM) by Schafer and Peköz (1998b), a review of which is given by Schafer (2008). The DSM is based on determining the strength of a structural component as an explicit function of its gross cross-sectional properties, elastic critical buckling stresses for all relevant instability modes (i.e. global buckling, local buckling and distortional buckling) and yield strength. To this end, a linear eigenvalue buckling analysis of the full cross-section by means of the constrained finite strip method is utilised (Schafer and Ádány, 2006; Ádány and Schafer, 2008) and the relevant critical stresses are obtained. The software CUFSM (Schafer and Ádány, 2006) has been utilised herein.

The DSM has been calibrated on the basis of numerous test data on cold-formed carbon steel components and has been adopted in the North American (AISI, 2004) and Australian (AS/NZS 4600, 2005) specifications for cold-formed steel design as an alternative design method to the effective width approach. Following its successful application to cold-formed steel, the DSM was subsequently extended to structural stainless steel members in compression by (Becque et al., 2008) and aluminium alloy flexural members (Zhu and Young, 2009).

Its versatility, capability of treating complex cross-sections, loading cases and failure modes and ease of application, provided that a suitable software for the calculation of the critical stresses and buckling modes is available, are the main merits of the DSM. It should be noted that the DSM assumes a bilinear elastic-perfectly plastic material response and is therefore best suited to the treatment of slender cross-sections and components, the failure of which is mainly governed by elastic buckling and post-buckling and remains largely unaffected by strain-hardening. The capacity of stocky stainless steel (Becque et al., 2008) and aluminium (Zhu and Young, 2009) cross-

sections and members is underpredicted by the DSM, since it does not allow for stresses greater than the yield stress $\sigma_{0.2}$ to be achieved. Furthermore, DSM does not apply to CHS.

3.3.3 The Continuous Strength Method (CSM)

The Continuous Strength Method (CSM) was initially proposed for the treatment of local buckling of stainless steel cross-sections by Gardner and Nethercot (2004a) and Ashraf et al. (2006a) subjected to compression or/and bending. The basic concept underpinning the CSM is that the occurrence of local buckling is the only physical limit to the exploitation of material's strain-hardening capacity. Indeed, the continuous nature of stainless steel's stress-strain law and the absence of a sharply defined yield point, beyond which a dramatic loss of stiffness occurs and instability is triggered, implies a continuous variation in the maximum attainable stress by a cross-section, which is not limited by $\sigma_{0.2}$. Hence the maximum attainable stress at failure is not a material-specific stress (i.e. the $\sigma_{0.2}$ proof stress), but is rather a continuous function of material properties, geometry of the cross-section and imposed stress gradient, all of which are incorporated into a cross-section slenderness parameter.

For plated cross-sections, the relevant cross-section slenderness parameter is related to the plate slenderness $\bar{\lambda}_p$ of the most slender constituent element (which is also the case for the traditional classification approach) as given by Equation (3.5), whilst the corresponding cross-section slenderness for CHS $\bar{\lambda}_c$ is given by Equation (3.6) (Allen and Bulson, 1980):

$$\bar{\lambda}_p = \sqrt{\frac{\sigma_{0.2}}{\sigma_{cr}}} = \frac{\sqrt{12(1-\nu^2)}\sqrt{235}}{\pi\sqrt{210000}\sqrt{k_\sigma}}\frac{b}{t\varepsilon} \tag{3.5}$$

$$\bar{\lambda}_c = \frac{\sigma_{0.2}}{\sigma_{cr}} = \frac{\sqrt{3(1-\nu^2)}235}{2\times 210000}\frac{(d-t)}{t\varepsilon^2} \tag{3.6}$$

where σ_{cr} is the elastic critical buckling stress of the plate element or CHS, b is the flat element width measured between centrelines of adjacent faces, d is the CHS outer diameter, t is the plate or CHS thickness, v is Poisson's ratio, E is Young's modulus, $\varepsilon = [(235/f_y)(E/210000)]^{0.5}$ and k_σ is a buckling factor allowing for differing boundary and loading conditions (i.e. stress gradients) specified in EN 1993-1-5 (2006). For CHS no buckling factor is applied and Equation (3.6), which is derived for CHS in compression, is conservatively adopted for bending.

The basis of the method lies in an experimentally derived 'base' curve, calibrated against all available stub column test data, which relates a cross-section's slenderness, denoted $\bar{\lambda}_p$ ($\bar{\lambda}_c$ for CHS), to its deformation capacity, denoted ε_{LB}. The deformation capacity ε_{LB} is the maximum attainable strain for a given cross-section in compression or the outer fibre strain of an assumed linear strain distribution of a cross-section in bending. It is defined by Equation (3.7) as the compressive strain corresponding to ultimate load ε_{LB}, obtained by dividing the axial shortening δ_u at ultimate load (as shown in Figure 3.15) by the stub column's initial length L_0. This deformation capacity is normalised to the elastic strain corresponding to the 0.2% proof stress $\sigma_{0.2}$, henceforth denoted ε_0, as defined by Equation (3.8).

$$\varepsilon_{LB} = \frac{\delta_u}{L_0} \tag{3.7}$$

$$\varepsilon_0 = \frac{\sigma_{0.2}}{E} \tag{3.8}$$

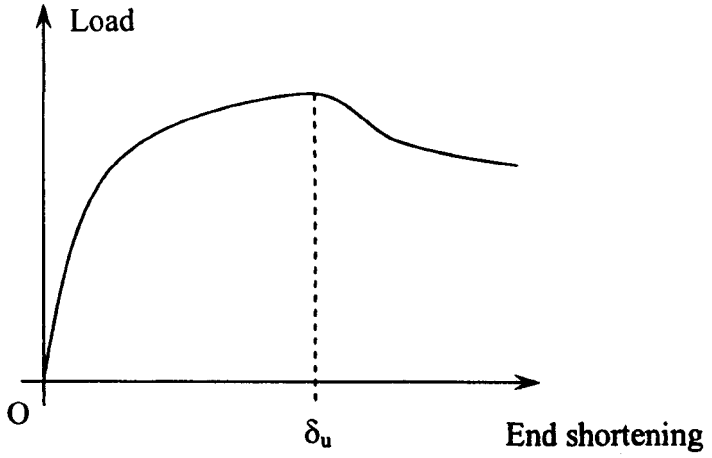

Figure 3.15: *Typical stub column load-end shortening curve*

The resulting normalised deformation capacity is approximated as a function of cross-section slenderness ($\bar{\lambda}_p$ or $\bar{\lambda}_c$) by Equation (3.9) for plated sections and Equation (3.10) for CHS, as reported by Ashraf et al. (2008a) and Ashraf et al. (2008b) respectively. A comparison between the normalised deformation capacity $\varepsilon_{LB}/\varepsilon_0$ predicted from Equations (3.9) and (3.10) and the actual deformation capacity obtained from test results is shown in Figure 3.16 for plated cross-sections and Figure 3.17 for CHS.

$$\frac{\varepsilon_{LB}}{\varepsilon_0} = \frac{1.43}{\bar{\lambda}_p^{\,2.71-0.69\bar{\lambda}_p}} \tag{3.9}$$

$$\frac{\varepsilon_{LB}}{\varepsilon_0} = \frac{0.18}{\bar{\lambda}_c^{\,1.24+1.70\bar{\lambda}_c}} \tag{3.10}$$

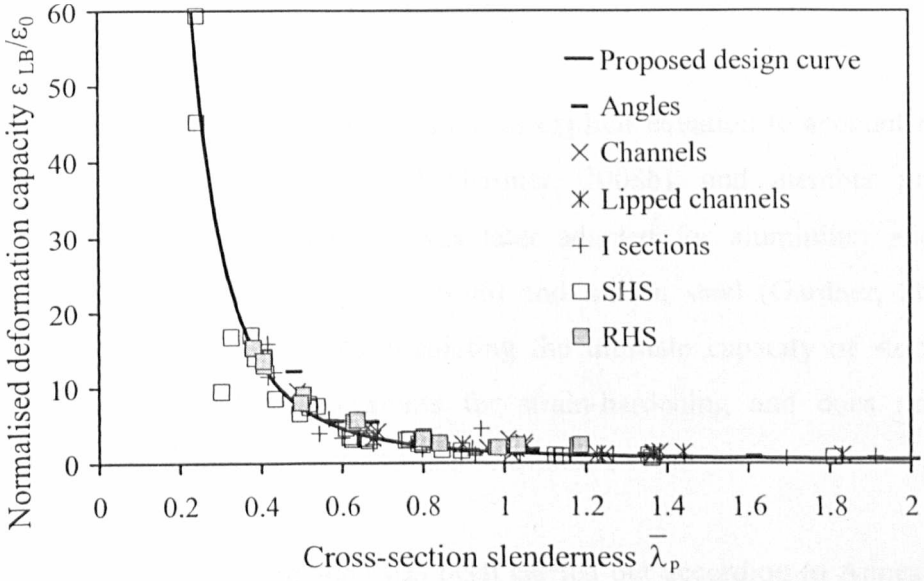

Figure 3.16: *Normalised deformation capacity against cross-section slenderness for plated cross-sections*

The deformation capacity is utilized in conjunction with an accurate material law, which in the case of stainless steel is a compound Ramberg-Osgood model (Mirambell and Real, 2000; Rasmussen, 2003), to obtain the corresponding stress σ_{LB}. For cross-sections in compression, the local buckling stress σ_{LB} is multiplied by the gross cross-section area to yield the cross-section compression resistance $N_{c,Rd}$,

whereas for cross-sections in bending, the obtained stress distribution is integrated over the cross-section to yield the ultimate moment capacity $M_{c,Rd}$.

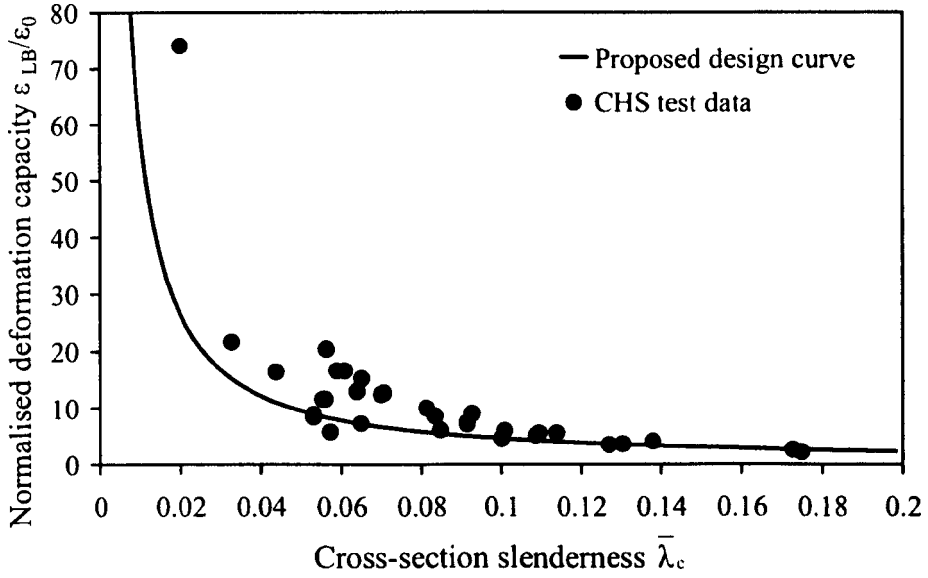

Figure 3.17: *Normalised deformation capacity against cross-section slenderness for CHS*

Additional features of the method include an explicit equation to account for corner strength enhancements (Cruise and Gardner, 2008b), and member instabilities (Ashraf et al., 2008a). The CSM was later adapted for aluminium alloys, high strength steel (Gardner and Ashraf, 2006) and carbon steel (Gardner, 2008). The method is capable of accurately predicting the ultimate capacity of stocky cross-sections, since it explicitly accounts for strain-hardening and does not impose unnecessary limitations on the maximum attainable stress.

Statistical analysis of the method has been carried out according to Annex D of EN 1990 (2002) and it has been concluded that the CSM may be safely adopted for the design of CHS and plated sections with a slenderness value $\bar{\lambda}_p$ less than 1.8 in both compression and bending in conjunction with a safety factor γ_{M0}=1.1 (Gardner and Theofanous, 2008). However, the method does not account for the effect of element interaction on the local buckling capacity of plated cross-sections and utilizes only the slenderness of the most slender constituent plate element. This leads to conservative predictions of the capacity of cross-sections consisting of plated elements of varying slenderness and optimistic predictions of the capacity of cross-sections employing

elements of similar slenderness (e.g. the capacity of RHS is marginally underpredicted whilst that of SHS is marginally overpredicted by Ashraf et al. (2006a)).

3.4 NUMERICAL MODELLING

The accuracy of the described design methods is assessed in Section 3.5 of this chapter on the basis of an extensive numerical study conducted on stainless steel stub columns by means of the general purpose finite element (FE) programme ABAQUS (2006). The FE models were developed following the guidelines given by Gardner and Nethercot (2004c) and Ashraf et al. (2006b), which were shown to give accurate capacity predictions. FE models of stainless steel SHS, RHS, PFC, lipped channel section, I section and angle stub columns were developed and validated against 136 test data by Ashraf et al. (2006b). The FE models were shown to marginally overpredict the capacity by 1% with a coefficient of variation of 0.08 and were deemed acceptable for the purpose of the current study.

The cross-sections considered herein include RHS (with SHS as a special case), PFC and I sections with the focus being on local buckling alone. All cross-sections had an outer flange width of 100 mm, whilst the web height and cross-section thickness were varied to obtain a wide range of local slendernesses and aspect ratios. For all RHS and PFC sections the internal root radii were assumed to be equal to the cross-section thickness. A uniform section thickness was assumed for RHS and PFC, whereas two flange to web thickness ratios were considered for the I sections. Each stub column length was fixed to three times the largest cross-section dimension. A total of 65 geometric configurations were considered, a summary of which is given in Table 3.3.

The models were discretized with the reduced integration 4-noded doubly curved general-purpose shell element S4R with finite membrane strains (ABAQUS, 2006). Symmetry was exploited to reduce computational time and hence half the cross-sections of the I sections and PFC and a quarter of the RHS were modelled, with suitable boundary conditions applied along the axes of symmetry. All degrees of

freedom were fixed at the stub columns' ends except for the vertical displacement at the loaded edge. Kinematic coupling was employed to impose uniform end-shortening at the loaded edge.

Table 3.3: *Geometric configurations modelled in the parametric studies*

Cross section	Outer flange width (mm)	Ratio of web to flange outer dimensions (aspect ratio)	Flange thickness (mm)	Web to flange thickness ratio	No. of geometric configurations considered
RHS	100	1, 2, 3	8, 6, 5, 4, 3	1	15
I sections	100	1, 1.5, 2	8, 6, 5, 4, 3	1, 0.6	30
PFC	100	1, 2, 3, 4	8, 6, 5, 4, 3	1	20

A linear eigenvalue buckling analysis was initially conducted to extract the lowest buckling mode shape for each cross-section; this was thereafter introduced as the geometric imperfection pattern in the subsequently performed geometrically and materially non-linear analyses. Typical lowest elastic buckling mode shapes for the different cross-section types are depicted in Figure 3.18. The amplitude of the geometric imperfection was given by a modification to the Dawson and Walker (1972) model, proposed by Gardner and Nethercot (2004c) and Ashraf et al. (2006b). The non-linear analyses employed the modified Riks method (ABAQUS, 2006), which enabled tracing the post-ultimate response of the modelled stub columns. All stub columns failed by local buckling as shown in Figure 3.19.

The compound Ramberg-Osgood model (Mirambell and Real, 2000; Rasmussen, 2003) as modified by Gardner and Nethercot (2004a, 2004c) was incorporated in the FE models in the true stress–logarithmic plastic strain format, as discussed in Chapter 2. Two sets of material properties were considered in the parametric studies for each modelled cross-section, resembling a typical austenitic stainless steel and a typical duplex stainless steel. For both materials, the Young's modulus E was taken as 200000 N/mm^2 and typical values for the ratio of 1% proof stress to 0.2% proof stress

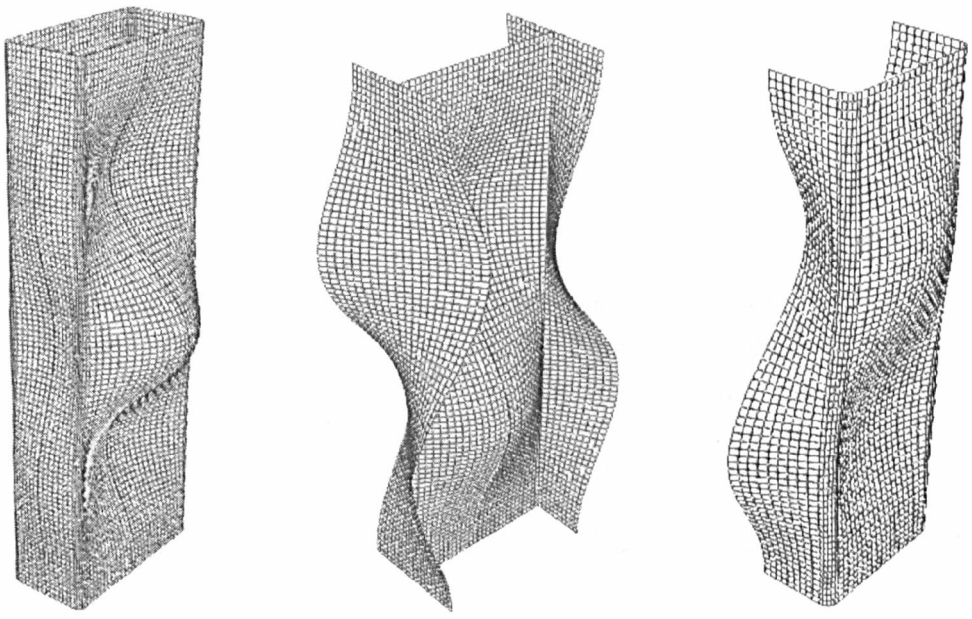

(a) RHS (b) I section (c) PFC

Figure 3.18: *Typical lowest elastic buckling mode shapes for stub columns*

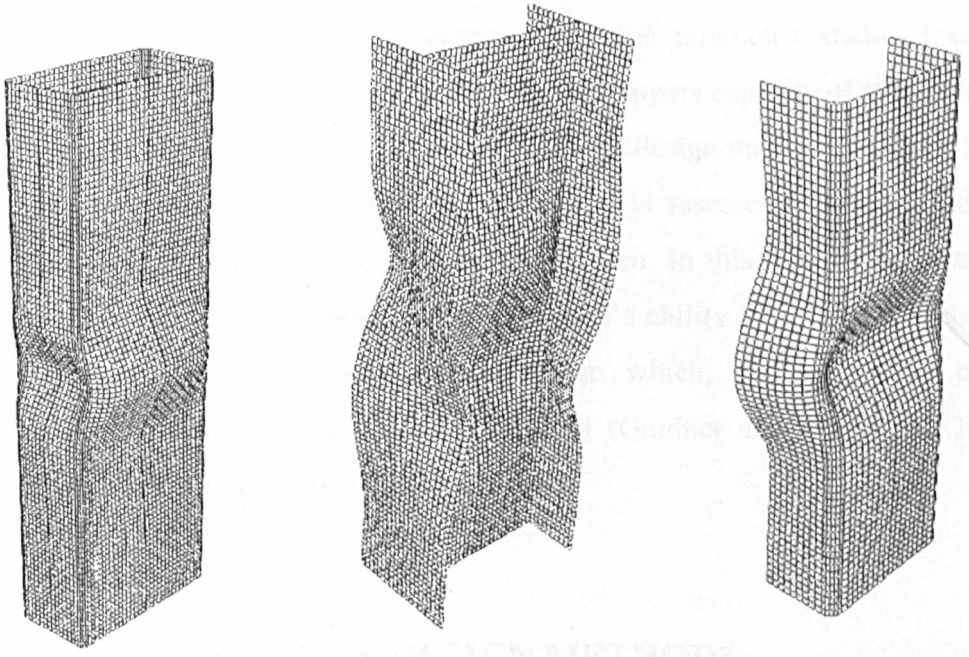

(a) RHS (b) I section (c) PFC

Figure 3.19: *Typical stub column failure modes*

$\sigma_{1.0}/\ \sigma_{0.2}$, and strain-hardening exponents n and $n_{0.2,1.0}$ obtained by averaging numerous coupon test results, were adopted. The considered 0.2% proof stresses $\sigma_{0.2}$ were 306.1 N/mm^2 and 592 N/mm^2 for the austenitic and duplex material respectively, in accordance with the statistical analysis on mill certificate data carried out by Groth and Johansson (1990). All adopted material properties are given in Table 3.4.

Table 3.4: *Material properties employed in the parametric studies*

Material	E (N/mm^2)	$\sigma_{0.2}$ (N/mm^2)	$\sigma_{1.0}/\sigma_{0.2}$	n	$n_{0.2,1.0}$
Austenitic	200000	306.1	1.20	5.6	2.7
Duplex	200000	592.0	1.15	5.0	3.4

Given the inherent high scatter and uncertainty in the distribution and magnitude of the residual stresses and the small effect they have been found to have on the ultimate capacity of stainless steel stub columns, it was decided not to incorporate residual stresses in the models. Moreover, it was decided not to explicitly incorporate the enhanced corner properties typically present in press-braked (PFC) and roll-formed (RHS) (Cruise and Gardner, 2008b) sections, since the parametric studies focus on determining the effect of element interaction on the ultimate capacity of stub columns rather than on replicating test data. For simplicity, the design methods outlined in the preceding section are calibrated, and their accuracy is assessed, assuming uniform material properties throughout the whole cross-section. In this way the accuracy of each design approach solely depends on the method's ability to account for element interaction and actual material response, after which, the effect of corner enhancements on ultimate capacity can be added (Gardner and Nethercot, 2004a; Ashraf et al., 2006b; Cruise and Gardner, 2008b).

3.5 ASSESSMENT OF THE DESIGN METHODS

The ultimate capacities of the 130 modelled stub columns are utilised in this section to assess the suitability of the various design methods for the treatment of local

buckling of stainless steel plated cross-sections and highlight their relative merits and drawbacks. The cross-section classification procedure with the slenderness limits codified in EN 1993-1-4 (2006) is utilized in conjunction with effective width equations for Class 4 internal and outstand elements, also specified in EN 1993-1-4 (2006), to predict the ultimate capacity of the modelled stub columns. Additionally, the revised slenderness limits (Table 3.1) and effective width equations (Equations (3.2) and (3.3)), proposed in Section 3.2.3, are also assessed.

The ultimate capacity predictions of the codified (EN 1993-1-4, 2006) and revised (Gardner and Theofanous, 2008) effective width equations are normalized by the squash load ($A\sigma_{0.2}$) and plotted against the normalized FE compressive resistances in Figure 3.20. Similar trends were observed for all types of cross-sections considered and hence no distinction is made between them in Figure 3.20.

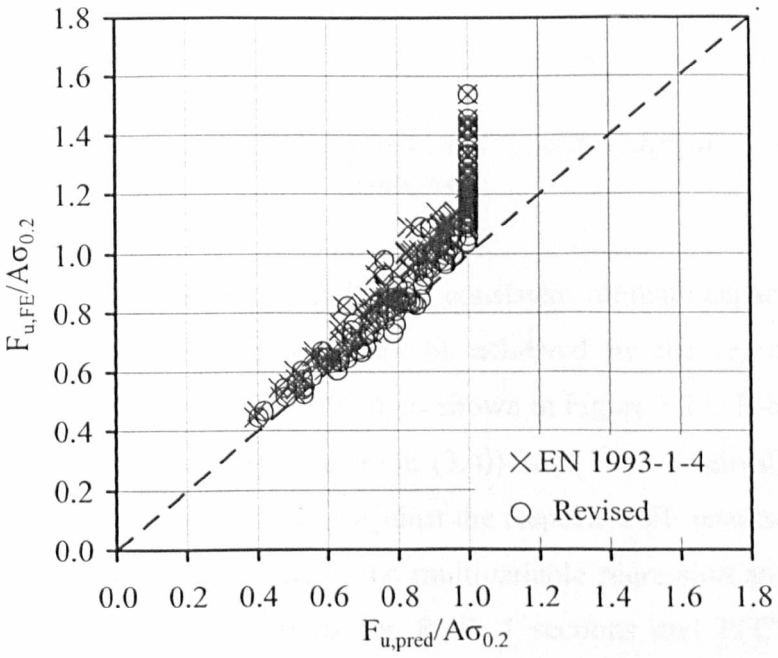

Figure 3.20: *Comparison between FE and predicted compression resistances for EN 1993-1-4 and the modification proposed herein*

Both the original and revised effective width equations result in predictions of similar scatter, with the revised ones being marginally less conservative. However the predicted compressive resistances are limited to $A\sigma_{0.2}$ while the observed capacities $F_{u,FE}$ can considerably exceed this value, as evidenced by the vertical distribution of the data points in Figure 3.20. This results in excessive conservatism for stocky cross-

sections. The inconsistent degree of conservatism achieved by the effective width approach is clearly illustrated in Figure 3.21, which depicts the variation of the predicted compression capacities, normalized by the respective FE ultimate loads, with the plate slenderness of the most slender constituent plate element.

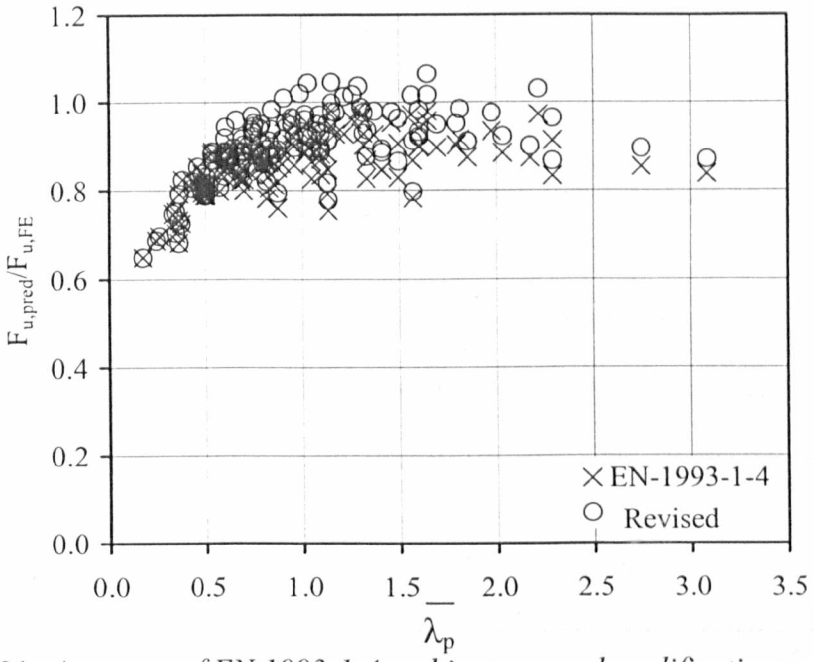

Figure 3.21: *Accuracy of EN 1993-1-4 and its proposed modification as a function of slenderness*

A significant reduction in scatter and more consistent ultimate capacity predictions over the full range of slenderness may be achieved by the regression analysis approach proposed by Kato (1989, 1990), as shown in Figure 3.22. The parameters A, B and C of the design equation (Equation (3.4)) have been obtained separately for each cross-section type by calibration against the respective FE results. Both material grades considered have been used in the multivariable regression analysis for each cross-section. The design equations for RHS, I sections and PFC are given by Equations (3.11), (3.12) and (3.13) respectively.

$$\frac{\sigma_{0.2}}{\sigma_{LB}} = 0.53 + \frac{0.10}{\bar{\lambda}_{p,f}} + \frac{0.60}{\bar{\lambda}_{p,w}} \tag{3.11}$$

$$\frac{\sigma_{0.2}}{\sigma_{LB}} = 0.50 + \frac{0.40}{\bar{\lambda}_{p,f}} + \frac{0.30}{\bar{\lambda}_{p,w}} \tag{3.12}$$

$$\frac{\sigma_{0.2}}{\sigma_{LB}} = 0.47 + \frac{0.32}{\bar{\lambda}_{p.f}} + \frac{0.59}{\bar{\lambda}_{p.w}} \tag{3.13}$$

It should be noted that in the investigations carried out by Kato (1989, 1990), Daali and Korol (1995) and Beg and Hladnik (1996), the squares of the flange slenderness and the web slenderness were incorporated into the design equations. The reasoning for this stems from definition of the slenderness as the square root of the yield stress $\sigma_{0.2}$ divided by the elastic critical plate buckling stress σ_{cr}. This is not necessarily appropriate however for ultimate capacity, since, when post-buckling effects are considered, normalized capacity tends towards $1/\bar{\lambda}_p$ rather than $1/\bar{\lambda}_p^{\,2}$. In this study, regression analysis has been based on the flange slenderness $\bar{\lambda}_{p.f}$ and the web slenderness $\bar{\lambda}_{p.w}$, rather than their squares, as this was shown to result in more consistent predictions.

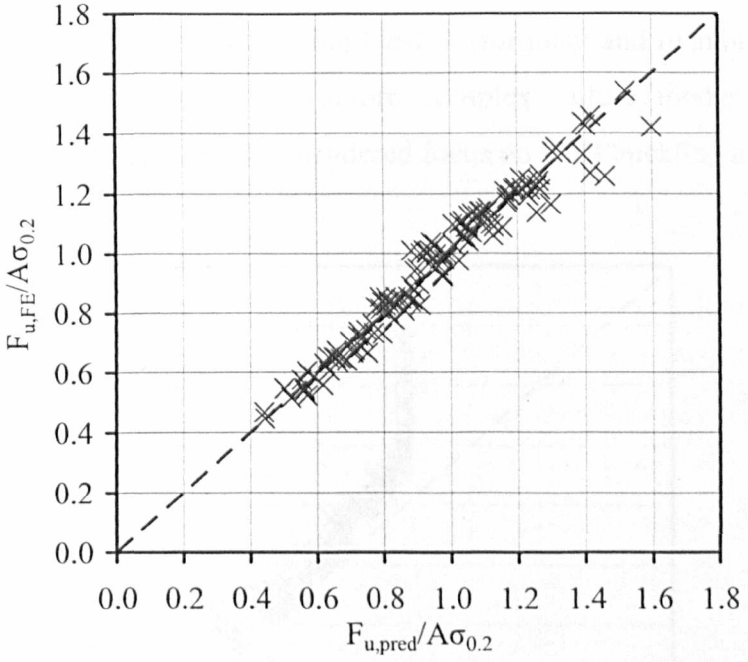

Figure 3.22: *Comparison between FE and predicted compression resistances for the regression analysis approach*

The direct strength equation utilized in the present study (Equation 3.14) is the one proposed by Becque et al (2008) for stainless steel members, which, in the absent of member buckling, reads:

$$N_{cl}=\begin{cases} A\sigma_{0.2} & \text{for} \quad \lambda_l \leq 0.55 \\ \left(\frac{0.95}{\lambda_l}-\frac{0.22}{\lambda_l^2}\right)A\sigma_{0.2} & \text{for} \quad \lambda_l>0.55 \end{cases} \tag{3.14}$$

where N_{cl} is the axial resistance accounting for local buckling according to the DSM and $\lambda_l = \sqrt{\frac{\sigma_{0.2}}{\sigma_{crl}}}$, in which σ_{crl} is the elastic critical local buckling stress of the cross-section.

A comparison between the normalised FE resistance and that predicted by the DSM is shown in Figure 3.23. As expected the DSM suffers from the same shortcoming as the effective width approach due to the limitation of the maximum attainable stress; stresses beyond the $\sigma_{0.2}$ are not allowed, and hence strain-hardening of stocky cross-sections is not accounted for, whilst similar scatter to the effective width approach is displayed. It should be noted that Equation (3.14) has been calibrated by Becque et al. (2008) against numerous test data involving local, distortional and member buckling and is hence capable of dealing with more complex failure modes and their interactions, whereas all other method considered focus on local buckling alone.

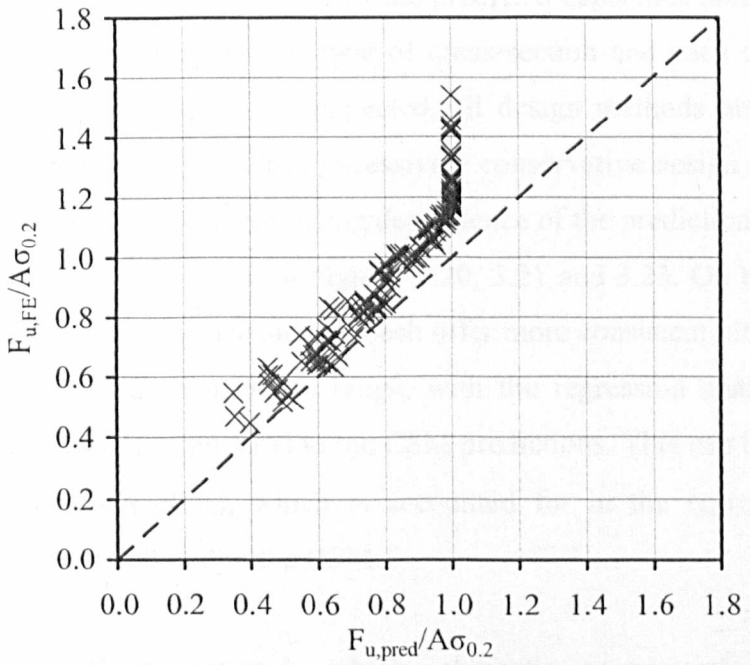

Figure 3.23: *Comparison between FE and predicted compression resistances for the DSM*

The CSM predictions are compared with the FE compressive resistances in Figure 3.24. As expected, similar level of scatter can be observed for all cross-sections, since strain-hardening is allowed for.

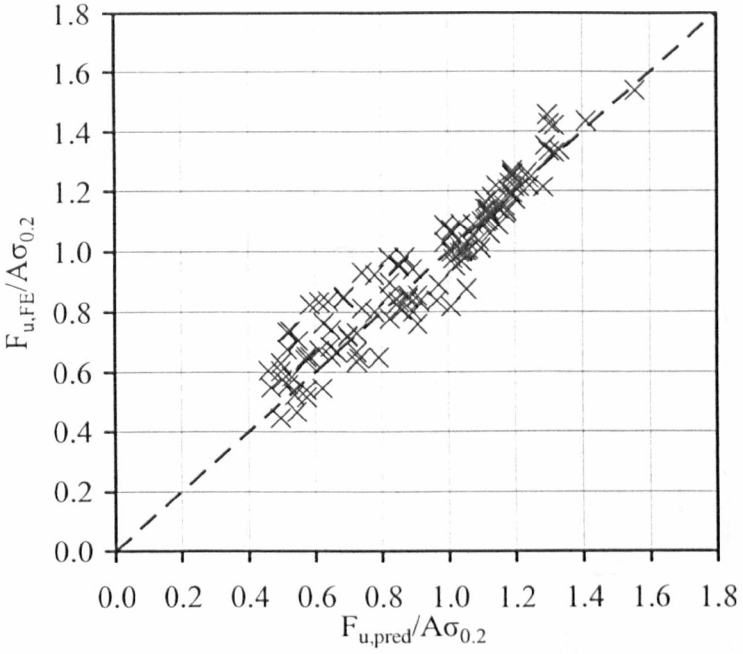

Figure 3.24: *Comparison between FE and predicted compression resistances for the CSM*

An overview of the accuracy attained by each method is given in Table 3.5, where the mean value and coefficient of variation of the predicted capacities normalized by the FE ultimate load are given for each type of cross-section and each design method considered in the present study. As expected, all design methods not allowing for stresses greater than the $\sigma_{0.2}$ result in excessively conservative design resistances for stocky cross-sections and a corresponding dependence of the predictions on the cross-sectional slenderness, as depicted in Figures 3.20, 3.21 and 3.23. On the other hand, the CSM and the regression analysis approach offer more consistent ultimate capacity predictions over the full slenderness range, with the regression analysis approach displaying a lower scatter compared to the CSM predictions. This can be attributed to the element interaction effect, which is accounted for in the regression analysis approach, but disregarded within the CSM.

The regression analysis approach, which inherently accounts for both strain-hardening and element interaction, may be seen to provide accurate predictions of

Table 3.5: *Comparison between design method predictions of compression resistance and FE results*

Cross-section	EN 1993-1-4		Modification proposed by Gardner and Theofanous (2008)		Regression analysis		DSM		CSM	
	Mean Pred/FE	COV	Mean Pred/FE	COV	Mean Pred/FE	COV	Mean Pred/FE	COV	Mean Pred/FE	COV
RHS	0.86	0.09	0.89	0.11	1.00	0.04	0.84	0.09	1.00	0.08
I sections	0.86	0.07	0.90	0.08	1.00	0.05	0.84	0.07	0.94	0.11
PFC	0.86	0.08	0.90	0.10	1.00	0.07	0.88	0.08	1.02	0.11
All	0.86	0.08	0.90	0.09	1.00	0.05	0.85	0.08	0.98	0.11

resistance and is thus a promising design approach for stainless steel cross-sections. However, the validity of the regression analysis parameters is limited to the slenderness range, aspect ratios, cross-section types and material grades of the data pool utilized for the calibration of the method. Hence the derivation of separate design equations is needed for each type of cross-section and possibly for different material grades considered, thereby limiting its scope. It is therefore attempted to improve the existing design methods, so that both element interaction and material nonlinearity are explicitly accounted for within a generic design framework applicable to all cross-sections and material grades.

3.6 THE CONTINUOUS STRENGTH METHOD ALLOWING FOR ELEMENT INTERACTION

As previously discussed, the DSM accounts for element interaction and the CSM accounts for material nonlinearity. Hence the DSM seems the appropriate design approach for slender cross-sections, which are least affected by material nonlinearity, whereas the CSM should be used for stocky cross-sections, where strain-hardening is significant. However the majority of stainless steel cross-sections used in structural applications are affected by both element interaction and material nonlinearity, and hence a combination of the merits of both design methods is desirable.

Expanding the DSM to account for material nonlinearity by specifying direct strength equations that are not bounded by the $\sigma_{0.2}$ would alleviate the embedded conservatism. However the format of the direct strength equations incorporates only the conventional yield stress $\sigma_{0.2}$ and Young's modulus E, since it was originally derived for carbon steel. Hence different design equations should be specified for different material grades. On the other hand the CSM relies on relating the cross-sectional geometry to its deformation capacity and thereafter obtaining the ultimate resistance via accurate material modeling; hence the geometrical effects are decoupled from the effect of material nonlinearity. It is therefore attempted to improve the CSM so that element interaction is explicitly accounted for.

To this end, the definition of the cross-sectional slenderness utilized in the DSM is adopted herein as a modification to the CSM; hence the critical buckling stress of the whole cross-section, derived by means of CUFSM (Schafer and Ádány, 2006), is incorporated into the definition of cross-section slenderness. The cross-section slenderness is thereafter utilized to obtain the normalized deformation capacity $\varepsilon_{LB}/\varepsilon_0$, and finally the stress at failure σ_{LB} via the compound Ramberg-Osgood constitutive law. The CSM design equation for plated cross-sections (Equation (3.9)) has to be modified in light of the revised slenderness definition. The modified CSM equation Equation (3.15), as derived on the basis of the FE results, reads:

$$\frac{\varepsilon_{LB}}{\varepsilon_0} = \frac{1.22}{\lambda_l^{2.71-0.69\lambda_l}} \leq 15 \quad \text{for } \lambda_l \leq 1.8 \tag{3.15}$$

where λ_l is the local buckling slenderness of the whole cross-section, which it is proposed to be employed in place of the slenderness of the most slender plate element $\bar{\lambda}_p$, as utilised in the original CSM. The predictions of the modified CSM are plotted together with those of the original CSM in Figure 3.25, where a significant reduction in scatter may be observed.

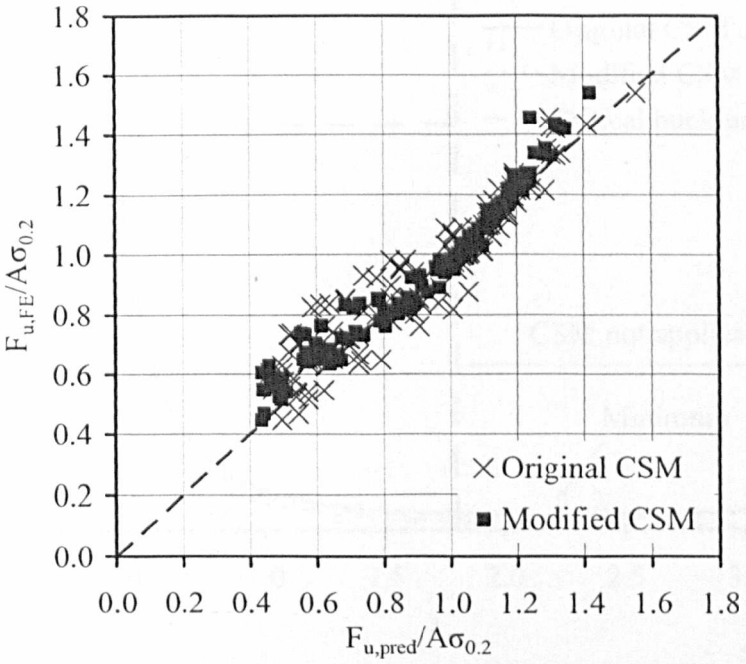

Figure 3.25: *Comparison between FE and predicted compression resistances for the original and modified CSM*

The 'base' curves for plated cross-section defined by Equations (3.9) and (3.15) have a minimum at $\bar{\lambda}_p \approx 2.2$ and therefore overpredict the deformation capacity ε_{LB} and hence the failure stress σ_{LB} of cross-sections beyond this slenderness value. Moreover, it has been observed in previous studies (Gardner and Nethercot, 2004a; Ashraf et al., 2006a; Ashraf et al., 2008) that the CSM overestimates the ultimate capacity of very slender cross-sections. For these reasons and given that the importance of strain-hardening vanishes at high slenderness, it is proposed that the applicability of the CSM is limited to a maximum slenderness value. An upper slenderness limit $\bar{\lambda}_l=1.8$ (or $\bar{\lambda}_p=1.8$ when using the most slender element) is therefore proposed herein. Cross-sections of higher slenderness should be designed according to the effective width approach or the DSM. Additionally, adoption of an upper limit of $\varepsilon_{LB}/\varepsilon_0=15$ on the exploitation of strain-hardening, in accordance with the minimum ductility requirements specified in EN 1993-1-4 (2006) and EN 1993-1-1 (2005), is also proposed. The new CSM curve relating the cross-section slenderness to its deformation capacity is plotted together with the original CSM curve and the elastic critical buckling curve in Figure 3.26. The proposed limitations on slenderness and deformation capacity are also depicted as cut-offs on the CSM curve.

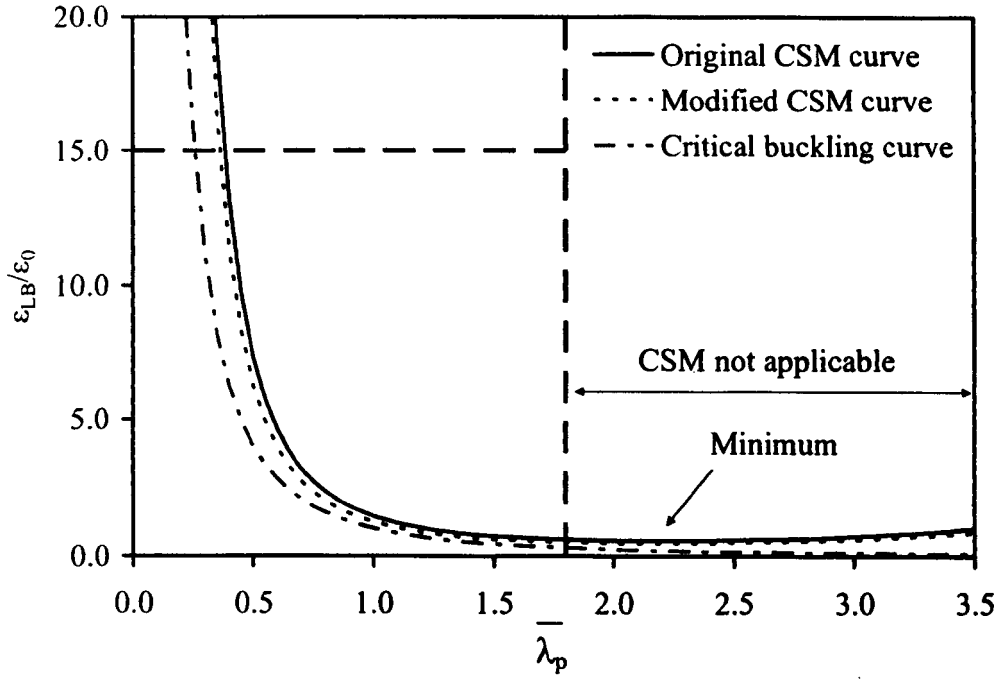

Figure 3.26: *Elastic critical buckling curve, original CSM design curve and modified CSM design curve*

The accuracy of the modified CSM is assessed in Table 3.6. The mean values and coefficients of variation of the predicted ultimate capacities normalized by the corresponding FE capacities are shown for each cross-section type and for the original CSM, the modified CSM without slenderness and deformation capacity limitations and the modified CSM with limitations. It can be seen that, while the mean predictions are similar, significant reductions in scatter are achieved by the modified CSM compared to the original proposal. The bounds imposed on the slenderness and deformation capacity do not significantly affect the results, since the vast majority (118/130) of the FE data considered lie within the specified limits.

Table 3.6: *Comparison of original and modified CSM predictions of compression resistance with FE results*

Cross-section	Original CSM		CSM with element interaction		CSM with element interaction and cut-offs	
	Mean Pred/FE	COV	Mean Pred/FE	COV	Mean Pred/FE	COV
RHS	1.00	0.08	0.96	0.08	0.96	0.08
I sections	0.94	0.11	0.96	0.09	0.97	0.08
PFC	1.02	0.11	1.00	0.04	0.99	0.04
All	0.98	0.11	0.97	0.08	0.97	0.07

3.7 COMPARISON WITH TEST DATA

In this section, the accuracy of the modified CSM, including the proposed limitations on deformation capacity and slenderness, is assessed on the basis of available test data. To this end, all published test data on stainless steel I section, RHS and PFC stub columns, summarised in Table 2.1, are utilised. The predictions of the other four methods considered herein are also assessed. The effect of the corner strength enhancements is accounted for via a corner enhancement factor derived according to the proposals of Ashraf et al. (2006a), Cruise and Gardner (2008b) and Ashraf et al.

(2008a), which is multiplied by the regression analysis, original CSM and modified CSM predictions. No account for the corner enhancements was taken for the remaining design methods.

The mean values and coefficients of variation of the predicted ultimate capacities normalized by the corresponding test results are shown in Table 3.7. Similarly to the comparison based on FE results (Table 3.5), all methods not accounting for material strain-hardening significantly underpredict the compressive resistance and display a relatively large scatter in the predictions, mainly due to their poor predictions of the capacity of stocky cross-sections. As before, the regression analysis approach and the CSM (both original and modified) offer more accurate predictions and a significant reduction in scatter, with the modified CSM displaying the lowest coefficient of variation of 0.08.

The accuracy of the various design methods in predicting the cross-section capacity of beams tested in 3- and 4-point bending is also assessed. To this end, the relevant published test data on stainless steel beams, summarised in Table 2.2, have been utilised. However the tests reported by Zhou and Young (2005) could not be utilized to assess the CSM, as insufficient data on material strain-hardening were reported. For consistency, the tests reported by Zhou and Young (2005) were also disregarded for the remaining design methods.

The effect of the stress gradient on the web slenderness was accounted for by means of the appropriate buckling factor k_σ specified in EN 1993-1-5 (2006). For the effective width approach, the original version of the CSM and the regression analysis method, the design equations specified for compression were then used. For the modified CSM and the DSM the slenderness of the cross-sections subjected to bending was obtained by performing constrained finite strip analyses with the CUFSM software (Schafer and Ádány, 2006). Within the framework of the CSM (both original and modified), the ultimate moment resistance was determined by means of numerical integration of the stress distribution, which was derived from an assumed linearly-varying strain distribution with an extreme value equal to ε_{LB}.

Table 3.7: *Comparison between design method predictions and stub column test results*

Cross-section	EN 1993-1-4		Proposed modification		Regression analysis		DSM		Original CSM		Modified CSM	
	Mean	COV	Mean	COV	Mean	COV	Mean	COV	Mean	COV	Mean	COV
RHS	0.81	0.14	0.83	0.15	1.00	0.11	0.79	0.14	1.01	0.13	1.00	0.09
I sections	0.90	0.10	0.94	0.11	1.09	0.09	0.93	0.10	1.00	0.09	1.02	0.06
PFC	0.85	0.11	0.90	0.12	1.03	0.04	0.88	0.11	1.02	0.10	1.05	0.05
All	0.83	0.14	0.86	0.15	1.02	0.10	0.82	0.15	1.01	0.12	1.01	0.08

To date, no specific direct strength equations for stainless steel in bending have been proposed. Therefore the direct strength equation codified for cold-formed carbon steel in Appendix 1 of the North American Specification (AISI, 2004) and the one proposed for aluminium alloy beams by Zhu and Young (2009) have been utilized in the present study and are given by Equations (3.16) and (3.17) respectively. Both yield similar results as the difference between them, is relatively small.

$$M_{cl}=\begin{cases} W_{el}\sigma_{0.2} & \text{for } \lambda_l \le 0.776 \\ \left[1-0.15\left(\frac{M_{crl}}{W_{el}\sigma_{0.2}}\right)^{0.4}\right]\left(\frac{M_{crl}}{W_{el}\sigma_{0.2}}\right)^{0.4} W_{el}\sigma_{0.2} & \text{for } \lambda_l > 0.776 \end{cases} \quad (3.16)$$

$$M_{cl}=\begin{cases} W_{el}\sigma_{0.2} & \text{for } \lambda_l \le 0.713 \\ \left[1-0.15\left(\frac{M_{crl}}{W_{el}\sigma_{0.2}}\right)^{0.3}\right]\left(\frac{M_{crl}}{W_{el}\sigma_{0.2}}\right)^{0.3} W_{el}\sigma_{0.2} & \text{for } \lambda_l > 0.713 \end{cases} \quad (3.17)$$

where M_{crl} is the elastic critical moment causing local buckling of the cross-section

The predictions of all design methods, normalised by the respective numerical results, are summarized in Table 3.8, from which similar conclusions to the ones mentioned for the case of compression can be drawn. The low coefficient of variation exhibited by the modified CSM for both compression (0.08) and bending (0.06) is due to the incorporation of both element interaction and material nonlinearity in the design approach and demonstrates the applicability of the method for the treatment of local buckling of stainless steel cross-sections.

The regression analysis approach and the DSM apply only to plated cross-sections. The local buckling of CHS, for which no element interaction exists, can be treated either with the effective width approach or with the CSM. The mean values and coefficients of variation of the predicted ultimate capacities of CHS stub columns and beams, summarized in Tables 2.1 and 2.2, have been normalized by the corresponding test results and are depicted in Table 3.9. The CSM can be seen to offer

Table 3.8: *Comparison between design method predictions and bending test results*

Cross-section	EN 1993-1-4		Proposed modification		Regression analysis		DSM		Original CSM		Modified CSM	
	Mean	COV	Mean	COV	Mean	COV	Mean	COV	Mean	COV	Mean	COV
RHS	0.65	0.15	0.72	0.14	0.89	0.10	0.66	0.13	1.01	0.07	0.99	0.06
I sections	0.87	0.05	0.87	0.05	1.00	0.07	0.74	0.06	0.99	0.04	1.00	0.04
All	0.68	0.17	0.74	0.14	0.89	0.12	0.67	0.13	1.00	0.06	0.99	0.06

improved capacity predictions compared to the respective design provisions codified in EN 1993-1-4 (2006) for both compression and bending, resulting in more efficient material use. It should be noted that, despite CHS bending capacity being over-predicted by the CSM, the approach is found to be statistically reliable according to Annex D of EN 1990 (2002), owing to material over-strength and a low coefficient of variation.

Table 3.9: *Comparison of CHS test results with EN 1993-1-4 and CSM*

Loading type	EN 1993-1-4 (2006)		CSM		CSM/EN predictions
	Mean EN/Test	COV	Mean CSM/Test	COV	
Compression	0.85	0.15	1.00	0.09	1.18
Bending	0.81	0.07	1.06	0.05	1.30

3.8 CONCLUDING REMARKS

A comprehensive assessment of the current treatment of local buckling in stainless steel elements according to EN 1993-1-4 (2006) has been carried out. All relevant experimental results have been gathered, analysis of which has highlighted conservatism within the current design process. Based on the experimental results, new statistically validated slenderness limits for each behavioural class and for all loading conditions, have been proposed. The new slenderness limits allow more efficient exploitation of the material and greater harmonisation with the corresponding slenderness limits for carbon steel. Furthermore, the existing effective width formulae have been updated to maintain consistency with the proposed slenderness limits. It is recommended that the proposed slenderness limits and effective width formulae be adopted in future revisions of EN 1993-1-4.

Reassessment of the slenderness limits for stainless steel has also highlighted the differences in structural response between carbon steel and stainless steel, and in

particular, the shortcomings associated with limiting the maximum compressive stress to the material 0.2% proof stress and ignoring element interaction in the treatment of plated cross-sections. Various design methods for the treatment of local buckling in stainless steel cross-sections have been outlined herein and their relative merits and drawbacks have been highlighted. Among the methods considered, the cross-section classification coupled with effective width approach is the simplest from a conceptual point of view, as it treats plate elements individually and assumes a bilinear elastic perfectly-plastic material constitutive law. More advanced methods include the direct strength method (DSM), which accounts for element interaction but not for material strain-hardening, the continuous strength method (CSM), which accounts for the material strain-hardening but ignores element interaction, and a method based on regression analysis, which accounts implicitly for both element interaction and material nonlinearity.

Based on an extensive parametric study on stainless steel stub columns, all methods have been assessed and the value of incorporating both element interaction and material nonlinearity within one design method was highlighted. A modification to the CSM for plated cross-sections, by redefining the considered slenderness to include element interaction, has been described. The modified CSM combines the merits of both the original CSM and the DSM and has been shown to offer accurate capacity predictions for cross-sections in compression, based on both FE and published test results from the literature. Furthermore the applicability of the method to cross-sections subjected to bending has been demonstrated and the incorporation of the method into future design guidance is proposed.

CHAPTER 4

STAINLESS STEEL OVAL HOLLOW SECTIONS

4.1 INTRODUCTION

Tubular construction is becoming increasingly popular for stainless steel structural applications. The traditional family of structural hollow sections comprises square, rectangular and circular hollow sections. The general choice of section for carrying predominantly axial loading is either square or circular, while when bending is introduced, a rectangular section will generally be more efficient.

The natural counterpart to a rectangular hollow section, but with a smooth external profile is an oval or elliptical hollow section. Hot-rolled carbon steel elliptical hollow sections (EHS) and cold-formed stainless steel oval hollow sections (OHS) have been recently introduced as tubular construction products. These sections offer the architectural attributes of circular hollow sections, together with the structural advantages associated with sections of differing properties about the two principal axes. However no structural guidance on stainless steel OHS exists to date, thereby inhibiting their more widespread usage in construction.

Previous research into the structural response of carbon steel EHS has included analytical and numerical investigations of elastic buckling and post-buckling (Kempner and Chen, 1968; Ruiz-Teran and Gardner, 2008; Silvestre, 2008), experimentation and derivation of slenderness limits (Gardner and Chan, 2007; Chan and Gardner, 2008a; Chan and Gardner, 2008b) and examination of shear (Gardner et al., 2008a) and flexural buckling (Chan and Gardner, 2009) behaviour. The resistances of EHS under combined loading (Nowzartash and Mohareb, 2009) and with concrete infill (Yang et al., 2008; Roufegarinejad and Bradford, 2007; Zhao et al., 2007) have also been studied, as have a range of EHS connection types (Martinez-Saucedo et al., 2008; Choo et al., 2003; Willibald et al., 2006).

This chapter reports a series of experimental and numerical investigations on the structural response of cold-formed stainless steel oval hollow section components subjected to the fundamental loading cases of compression and bending. Comparisons are made with the results from previous studies on carbon steel EHS (Chan, 2008) and stainless steel CHS reported by various researchers and design rules for stainless steel OHS, principally in line with EN 1993-1-4 (2006) are proposed. The findings of this research have been reported by Gardner et al. (2008b) and Theofanous et al. (2009a, 2009b).

4.2 EXPERIMENTAL STUDY

A laboratory testing programme comprising material tests, compressive stub column tests, 3-point bending tests and flexural buckling tests was conducted to investigate the structural behaviour of stainless steel oval hollow section compression and flexural members. All tests were performed in the Structures laboratory of the Department of Civil and Environmental Engineering at Imperial College London. Three section sizes were employed for the stub column tests and the beam tests - OHS 121×76×2, OHS 121×76×3 and OHS 86×58×3, whilst all flexural buckling tests were conducted on OHS 86×58×3. All tested material was austenitic stainless steel, grade 1.4401 (316), which contains approximately 18% chromium and 10% nickel (EN 10088-2, 2005). All specimens were cold-rolled and seam welded. The

minimum specified yield strength (0.2% proof strength) for grade 1.4401 stainless steel is 240 N/mm^2 for cold-rolled sheet material (up to 8 mm in thickness) and 220 N/mm^2 for hot-rolled sheet material (up to 13.5 mm in thickness) according to EN 10088-4 (2009). However, the material strength of stainless steel is considerably enhanced during the sheet and section forming processes due to cold-working, as indicated by previous test results (Talja and Salmi, 1995; Young and Lui, 2003; Gardner et al., 2006) and verified in the present study. This section summarises the testing apparatus, the experimental procedures and the test results obtained.

4.2.1 Tensile coupon tests

Tensile coupon tests were performed to establish the basic material stress-strain response; this was subsequently utilised during the analysis of the member test results and in the development of numerical models. The tests were carried out in accordance with EN 10002-1 (2001).

Parallel coupons were machined longitudinally from the two flattest portions of the cross-sections (i.e. along the centrelines of the minor axis) using a tipped slot-drill. Longitudinal curving of the coupons was observed as machining progressed, indicating the presence of through-thickness residual stresses. However, no attempt was made to straighten the coupons (by plastic bending) prior to tensile testing. The nominal dimensions of the tensile coupons were 350×20 mm. Holes were drilled and reamed 20 mm from each end of the coupons for pins to be inserted to prevent slippage of the coupons in the jaws of the testing machine. Proportional gauge lengths were marked along the coupons to calculate the strain at fracture. A summary of the mean measured dimensions for the tensile coupons are given in Table 4.1. Two coupon tests, designated TC1 and TC2, were performed for each section size.

Linear electrical strain gauges were affixed at the midpoint of each side of the tensile coupons. Load, strain, displacement and input voltage were all recorded using the data acquisition equipment DATASCAN and logged using the DALITE computer package. All data were recorded at one second intervals. The tensile tests were

performed using an Amsler 100 kN hydraulic testing machine. Strain rates were within the limits prescribed by EN 10002-1 (2001).

Table 4.1: *Mean measured dimensions of tensile coupons*

Coupon designation	Width b (mm)	Thickness t (mm)	Cross-sectional area A (mm^2)	Original gauge length (mm)
OHS 121×76×2 - TC1	19.21	1.82	34.97	32.0
OHS 121×76×2 - TC2	19.19	1.83	35.14	32.0
OHS 121×76×3 - TC1	19.97	3.00	59.93	42.0
OHS 121×76×3 - TC2	20.02	2.98	59.58	42.0
OHS 86×58×3 - TC1	20.02	3.15	63.00	44.0
OHS 86×58×3 - TC2	19.98	3.13	62.59	44.0

The key results from the six coupon tests are summarised in Table 4.2, where E_0 is the initial tangent modulus, $\sigma_{0.2}$ and $\sigma_{1.0}$ are the 0.2% and 1% proof strengths respectively, σ_u is the ultimate tensile strength, ε_f is the plastic strain at fracture and n and $n_{0.2,1.0}$ are strain hardening exponents for the compound Ramberg-Osgood model described in Chapter 2.

Table 4.2: *Measured material properties from tensile coupons*

Coupon designation	E_0 (N/mm^2)	$\sigma_{0.2}$ (N/mm^2)	$\sigma_{1.0}$ (N/mm^2)	σ_u (N/mm^2)	ε_f	Modified R-O coefficients	
						n	$n'_{0.2,1.0}$
121×76×2 - TC1	193900	380	426	676	0.61	7.8	2.9
121×76×2 - TC2	193300	377	419	672	0.60	8.9	2.9
121×76×3 - TC1	194100	420	460	578	0.58	9.7	4.0
121×76×3 - TC2	190400	428	467	583	0.58	8.2	4.0
86×58×3 - TC1	194500	339	368	586	0.62	14.0	1.8
86×58×3 - TC2	194500	331	349	597	0.62	13.5	1.3

4.2.2 Stub column tests

A total of six stainless steel oval hollow section (OHS) stub columns were tested in pure axial compression to assess load carrying capacity and deformation capacity and enable the determination of a suitable Class 3 limit for stainless steel OHS in compression. Full load-end shortening curves were recorded, including into the post-ultimate range.

The specimens were cut roughly to length using a rotary hacksaw. Their ends were milled flat and square to a tolerance of ±0.02 mm to achieve accurate seating in the testing machine. Prior to testing, strain visualisation grids were marked onto the surface of the specimens, and measurements of geometry, including initial imperfections were taken. The nominal lengths of the stub columns were chosen such that they were sufficiently short not to fail by overall buckling, yet still long enough to contain representative distributions of residual stresses and geometric imperfections. The stub column lengths were taken as two times the larger cross-sectional dimension.

The stub column tests were carried out in a self-contained 300 T Amsler hydraulic testing machine as shown in Figure 4.1. The tests were load-controlled through an Amsler control cabinet. The end platens of the testing apparatus were fixed flat and parallel. Alignment of the specimens was necessary to ensure that the compressive load was introduced concentrically. This was carried out by applying a small alignment load to the specimens, approximately 10% of the predicted failure load $F_{u,pred}$ and observing the variation in strain around the cross-section. In all cases the variation between strains at any point from the average strain was less than 5%. Linearity of the stress-strain plot was used to confirm that the alignment load was below the proportional limit.

Four linear variable displacement transducers (LVDTs) were used to determine the end shortening of the stub columns between the end platens of the testing machine. Figure 4.2 shows a schematic view of their layout. Four linear electrical resistance strain gauges were affixed to each specimen at mid-height, and at a distance of four

times the material thickness from the major axis. The strain gauges were initially used for alignment purposes, and later to modify the end shortening data from the LVDTs to eliminate the elastic deformation of the end platens (Gardner and Nethercot, 2004a). Load, strain, displacement, and input voltage were all recorded at 2 second intervals.

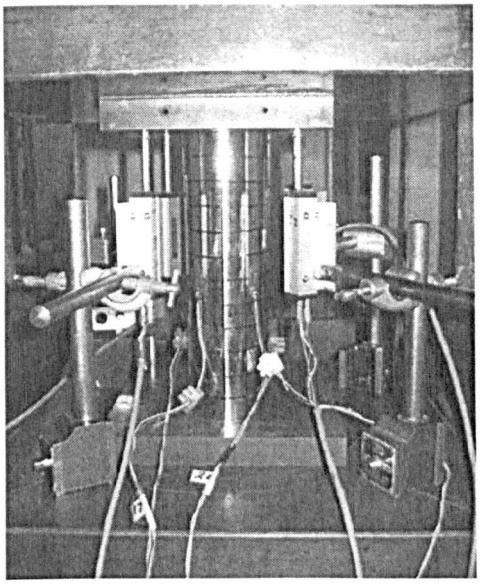

Figure 4.1: *Stub column testing apparatus*

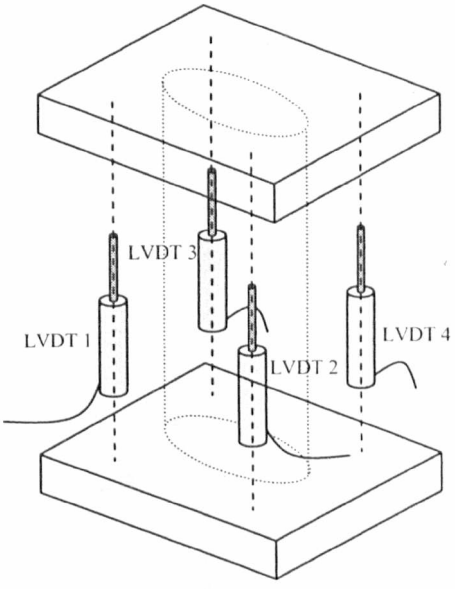

Figure 4.2: *Location of LVDTs*

Measurements of major and minor axis diameters, material thickness and stub column length were taken at four different points for each specimen. The mean measured dimensions for the six stub column specimens are presented in Table 4.3; cross-section geometry and notation is defined in Figure 4.3. Two stub column tests, designated SC1 and SC2, were performed for each section size.

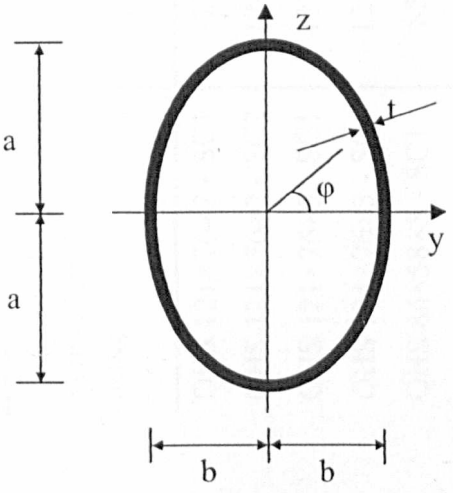

Figure 4.3: *Geometry and notation for oval hollow sections*

Table 4.3: *Mean measured dimensions of stub columns*

Stub column designation	Larger outer diameter 2a (mm)	Smaller outer diameter 2b (mm)	Thickness t (mm)	Cross-sectional area A (mm^2)	Length L (mm)	Imperfection amplitude w_0 (mm)	Imperfection amplitude $w_{0.5}$ (mm)
OHS 121×76×2 - SC1	123.70	76.94	1.84	577.3	242.0	1.06	0.31
OHS 121×76×2 - SC2	124.14	76.60	1.84	577.1	242.0	0.96	0.27
OHS 121×76×3 - SC1	121.53	77.14	2.94	902.1	241.7	0.96	0.21
OHS 121×76×3 - SC2	121.56	77.09	2.95	904.0	241.2	1.19	0.33
OHS 86×58×3 - SC1	85.63	57.22	3.11	674.4	171.9	0.78	0.20
OHS 86×58×3 - SC2	84.67	58.98	3.12	678.4	171.6	1.01	0.29

The circumferences of the oval specimens were traced to determine their exact cross-sectional profiles. These were subsequently fitted with the equation of an ellipse, which was found to provide a suitably accurate representation of the geometry, an example of which is shown in Figure 4.4. The cross-sectional area A of the test specimens was calculated as the circumference P_m (determined along the centreline of the thickness and calculated from Equation (4.1) multiplied by the material thickness t, as recommended by Chan and Gardner (2008a).

$$P_m = \pi(a_m + b_m) \times (1 + 0.25h_m) \tag{4.1}$$

in which $a_m = (2a - t)/2$, $b_m = (2b - t)/2$ and $h_m = (a_m - b_m)^2/(a_m + b_m)^2$.

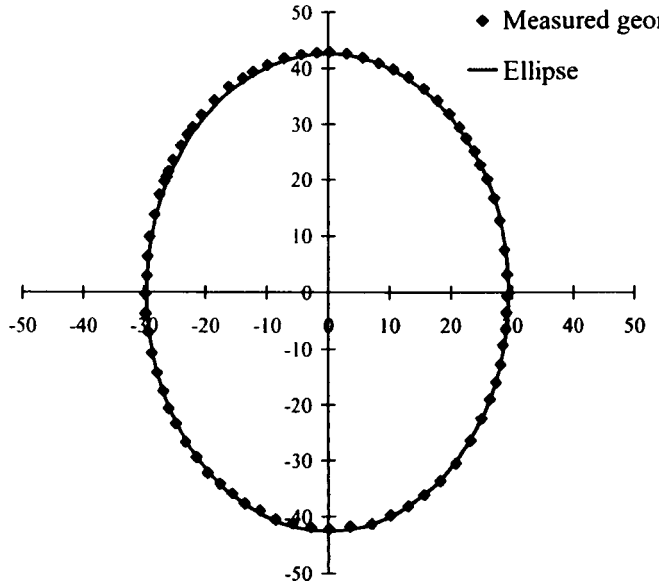

Figure 4.4: *Measured mid-surface geometry of OHS and elliptical representation*

Measurements of local initial geometric imperfections are important in aiding the explanation of structural response and in the development of numerical models. Schafer and Peköz (1998a) conducted a detailed assessment of initial geometric imperfections in cold-formed channel sections. In their experimental set-up, the specimens were mounted on the table of a milling machine, and a displacement transducer, fitted in the head of the milling machine, was employed to trace the local geometric imperfections. A similar arrangement was adopted by Gardner and Nethercot (2004a) and in the present study. Readings were taken at 20 mm intervals

along the centrelines of the minor and major axes of the specimens. The datum line for the imperfection measurements was initially taken as a straight line connecting the ends of each stub column face. However, it was observed that the release of residual stresses following cutting to length induced flaring at the ends of the stub columns. The resulting imperfection amplitudes w_0 were therefore not representative of the general geometric imperfection distribution in specimens. The effect of the end flaring was therefore removed by considering only the middle 50% of the specimens' length in the definition of the datum line, as proposed by Cruise and Gardner (2006). The imperfection amplitudes based on this modified datum line, henceforth referred to as $w_{0.5}$, are included in Table 4.3 together with w_0.

Measured end shortening readings from the LVDTs were modified on the basis of the strain gauge readings to account for the elastic deformation of the end platens that are present in the LVDT measurements according to the recommendations of the Centre for Advanced Structural Engineering (1990). Thus true end shortening values were derived, and are utilised in the remainder of this study. Load-end shortening curves from the six stub column tests are shown in Figure 4.5, whilst a summary of the key test results including ultimate load F_u and end shortening at ultimate load δ_u is given in Table 4.4. In general, the test results indicate good correlation between the repeated stub column tests (SC1 and SC2).

Table 4.4: *Summary of results from stub column tests*

Stub column designation	Ultimate load F_u (kN)	End shortening at ultimate load δ_u (mm)
OHS 121×76×2 - SC1	234	1.55
OHS 121×76×2 - SC2	235	1.63
OHS 121×76×3 - SC1	444	2.77
OHS 121×76×3 - SC2	442	2.71
OHS 86×58×3 - SC1	259	4.69
OHS 86×58×3 - SC2	260	4.25

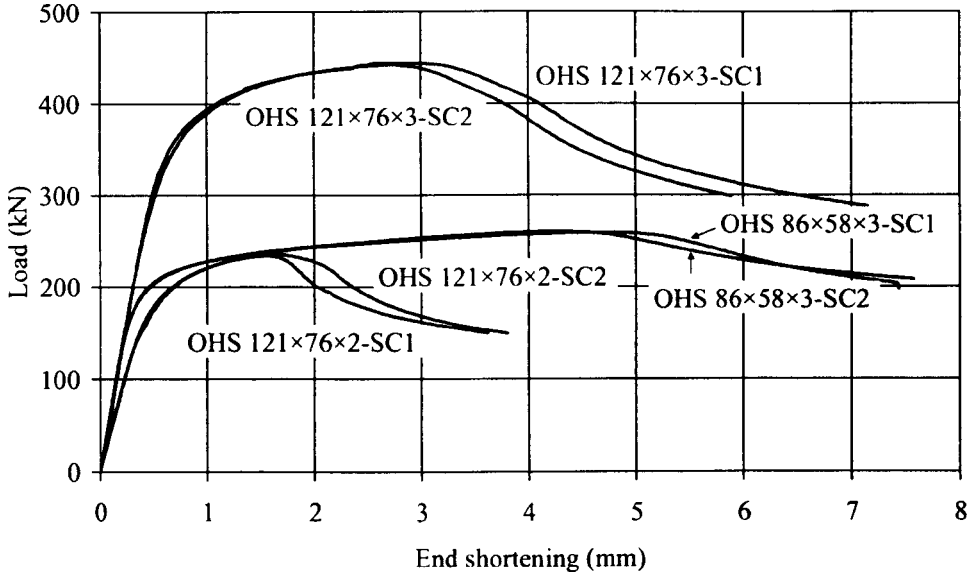

Figure 4.5: *Load-end shortening curves for OHS stub columns*

Compression tests on stub columns reveal the average compressive response of the cross-sections and include implicitly the effects of strain-hardening and residual stresses induced during the cold-forming process. The compound Ramberg-Osgood model described in Chapter 2 has been used to capture the average compressive stress-strain response, as determined from the stub column tests, the resulting parameters for which are presented in Table 4.5.

Table 4.5: *Measured material properties from stub column tests*

Coupon designation	E_0 (N/mm^2)	$\sigma_{0.2}$ (N/mm^2)	$\sigma_{1.0}$ (N/mm^2)	Modified R-O coefficients	
				n	$n'_{0.2,1.0}$
OHS 121×76×2 - SC1	185000	380	426	7.9	4.1
OHS 121×76×2 - SC2	189000	380	426	8.3	4.1
OHS 121×76×3 - SC1	176800	444	492	10.1	4.2
OHS 121×76×3 - SC2	176650	438	489	8.3	4.1
OHS 86×58×3 - SC1	178000	317	361	10.9	4.1
OHS 86×58×3 - SC2	182000	318	360	9.1	4.1

Ultimate failure was due to local buckling of the cross-sections. All the stub columns exhibited a similar failure mode whereby the two flatter portions of the specimens (i.e. the regions of maximum radius of curvature) buckled locally. Photographs of the deformed specimens 121×76×2 are shown in Figure 4.6.

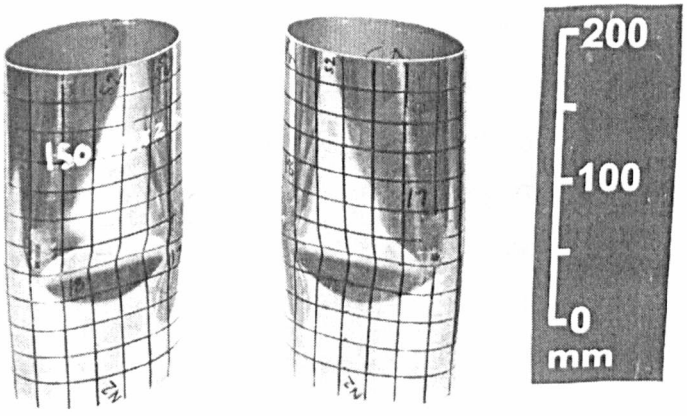

Figure 4.6: *Deformed OHS 121×76×2 stub columns*

4.2.3 Beam tests

Three section sizes - OHS 121×76×2, OHS 121×76×3 and OHS 86×58×3 - were employed in the three-point bending tests to encompass a variety of section slenderness values and cover a range of structural responses. One major and one minor axis bending test was conducted for each section size. The specimens were cut to the required length using a rotary hacksaw and measurements of their geometry were taken prior to testing. Strain visualisation grids were marked onto the specimens at a spacing of 20 mm.

Initial geometric imperfections were measured to aid in the assessment of the structural behaviour of the beams and in the development of the numerical models. Due to the high tosrional stiffness brought about by the closed shape of the OHS, lateral-tosrional buckling was not an issue for the span lengths considered in this study and hence global imperfections were not examined. Measurements of local imperfections were conducted following the procedure described for stub columns in the preceding section. The imperfection pattern at the ends of the simple beam

specimens tested herein has little influence on their flexural response, since the maximum moment arises at mid-span and hence this is where local imperfections are of greatest importance. Hence the middle 50% of the specimens' length was considered in the definition of the datum line.

All measured geometric data (defined in Figure 4.3), the section moduli for the relevant axis of bending and the maximum measured initial imperfection amplitudes are summarised in Table 4.6. The section moduli (i.e. $W_{el,y}$, $W_{el,z}$, $W_{pl,y}$ and $W_{pl,z}$) were calculated by assuming the OHS to have a constant thickness (which was verified by the measurements taken) and numerically integrating along the mid-surface of the ellipse, as proposed by Chan and Gardner (2008b). The designation of the specimens adopted in the present study includes the section type (OHS), the nominal major and minor axis outer dimensions, the nominal thickness and the axis of bending (MA for major and MI for minor axis bending).

The beams were simply supported between rollers, which were placed 50 mm inward from each end of the beam as depicted in Figure 4.7. Steel collars (25 mm in width) machined to the profiles of the oval sections, were employed at the points of load introduction and support. Profiled wooden blocks with a width of 25 mm were inserted in the tubes at the loading point and at the support points to prevent local bearing failure. A linearly varying displacement transducer (LVDT) was placed at mid-span to measure the mid-span vertical deflection, whilst two additional LVDTs were positioned at each end of the specimens in order to determine the rotation of the beams at the support points, as shown in Figure 4.7. Strain gauges were also attached to each beam at a distance of 50 mm from the mid-span to measure the strain at the extreme tensile and compressive fibres of the cross-sections. Load, strain, displacement, and input voltage were all recorded at 2 second intervals using the data acquisition system DATASCAN.

Table 4.6: *Mean measured dimensions of bending specimens*

Beam specimen designation	Axis of bending	Larger outer diameter 2a (mm)	Smaller outer diameter 2b (mm)	Thickness t (mm)	Length between supports L (mm)	Elastic section modulus W_{el} (mm^3)	Plastic section modulus W_{pl} (mm^3)	Measured maximum local imperfection $w_{0.5}$ (mm)
OHS 121×76×2 - MI	Minor	123.82	77.27	1.92	1006	12361	15596	0.42
OHS 121×76×2 - MA	Major	121.79	78.44	1.91	1003	15689	21134	0.38
OHS 121×76×3 - MI	Minor	121.79	77.08	3.01	1016	18312	23458	0.39
OHS 121×76×3 - MA	Major	121.35	78.74	3.03	1008	24049	32697	0.19
OHS 86×58×3 - MI	Minor	85.68	57.21	3.18	701	9697	12676	0.12
OHS 86×58×3 - MA	Major	85.47	57.17	3.17	702	12203	16760	0.12

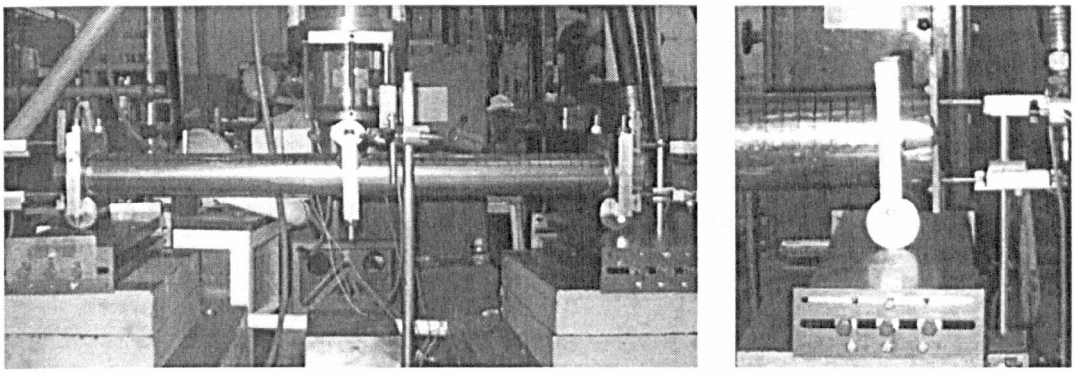

Figure 4.7: *Three-point bending tests*

Load was applied at mid-span using a 50 T Instron hydraulic actuator, which was connected to a load cell and controlled through an Instron control cabinet. Displacement control was utilized in order to capture the full moment-rotation response, including into the post-ultimate region. The obtained moment-rotation curves are depicted in Figures 4.8 and 4.9 for the major and minor axis bending specimens respectively. It should be noted that the reported rotation refers to the total rotation at mid-span (location of the idealised plastic hinge), which is calculated as the sum of the measured end rotations, whilst the applied bending moment was calculated directly from the applied force.

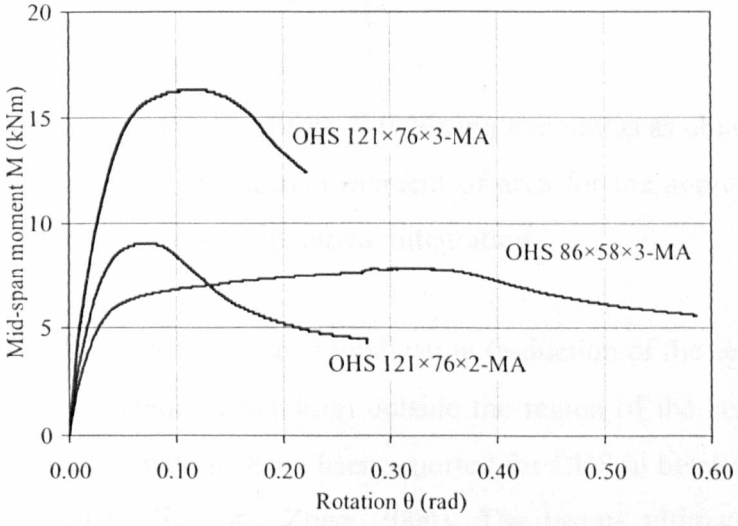

Figure 4.8: *Moment-rotation responses of specimens subjected to major axis bending*

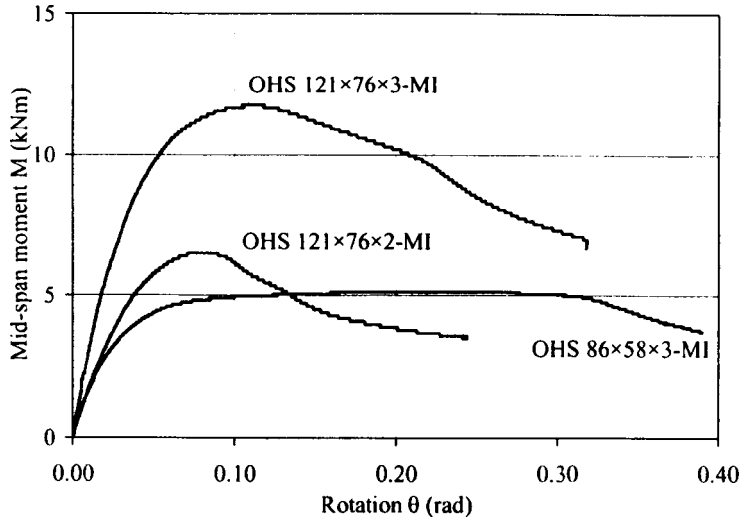

Figure 4.9: *Moment-rotation responses of specimens subjected to minor axis bending*

For comparison purposes, all curves have also been plotted in non-dimensional form in Figure 4.10, where for each section the applied moment has been normalised by the respective plastic moment capacity M_{pl} (calculated as the plastic modulus W_{pl} multiplied by the tensile 0.2% proof strength $\sigma_{0.2}$ given in Table 4.2), whilst the corresponding total rotation at mid-span has been normalised by the elastic component of the total rotation corresponding to M_{pl}, defined as θ_{pl} and given by Equation (4.2):

$$\theta_{pl} = \frac{M_{pl}L}{2EI} \tag{4.2}$$

where L is the span between the supports, E is Young's modulus as obtained from the tensile coupon tests and I is the second moment of area for the appropriate axis of bending as calculated by means of numerical integration.

All six specimens displayed evidence of ovalization (reduction of the section's height due to flattening in the plane of bending) outside the region of the central collar at high strains. Similar observations have been reported for CHS in bending in previous studies (Sherman, 1976; Jiao and Zhao, 2004). The beams ultimately failed by inelastic local buckling of the compression (upper) portion of the sections in the region of maximum moment near the point of loading (See Figure 4.11). For specimens tested about their minor axis, local buckling initiated at the point of

greatest radius of curvature (i.e. the flattest part of the section), which coincided with the point of maximum compressive stress. For specimens tested in major axis bending local buckling initiated near the extreme compressive fibre though deformations spread further down the section towards the neutral axis. This pattern of local buckling may be expected since, in major axis bending, although the compressive stress is reducing towards the neutral axis, the local stiffness of the section (which is strongly influenced by the local curvature) is also reducing.

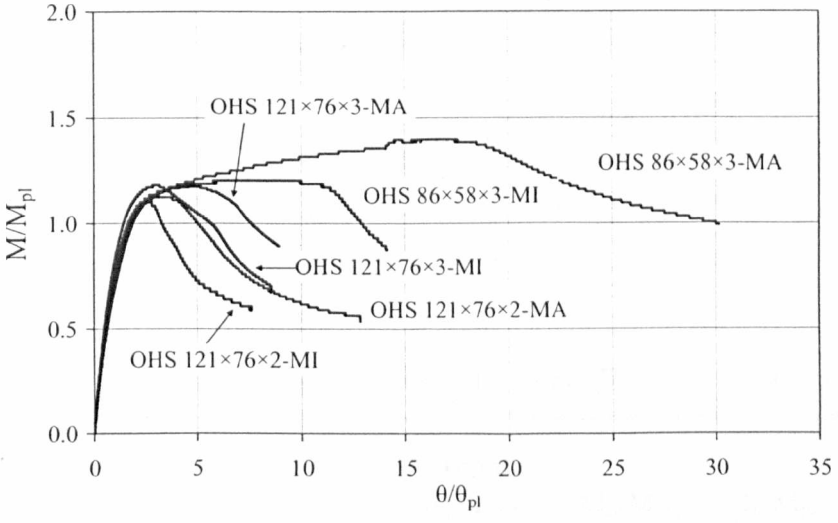

Figure 4.10: *Normalised moment-rotation curves for all specimens*

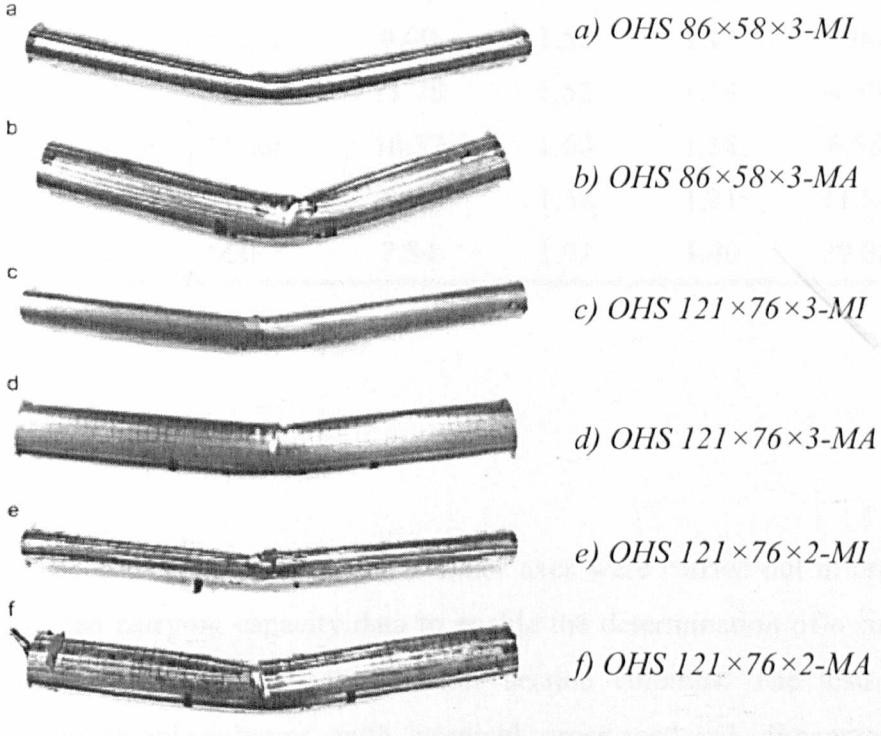

Figure 4.11: *OHS specimen failure modes*

All key experimental results are summarised in Table 4.7. The elastic and plastic moment capacities, M_{el} and M_{pl} were evaluated by multiplying the relevant section modulus (W_{el} or W_{pl} given in Table 4.6) by the measured tensile 0.2% proof strength $\sigma_{0.2}$, whilst the rotation capacities R were evaluated using Equation (4.3):

$$R = \frac{\theta_u}{\theta_{pl}} - 1 \tag{4.3}$$

where θ_{pl} is the elastic component of the rotation when M_{pl} is reached as defined by Equation (4.2) and θ_u refers to the total rotation at mid-span when the moment-rotation curve falls back below M_{pl} and is obtained from the test results. All test results together with the numerical results generated from subsequent parametric studies are discussed in detail in Section 4 of this Chapter.

Table 4.7: *Summary of test results from 3-point bending tests*

Beam specimen designation	Axis of bending	Ultimate moment M_u (kNm)	M_u/M_{el}	M_u/M_{pl}	Rotation capacity R
OHS 121×76×2 - MI	Minor	6.51	1.39	1.10	2.28
OHS 121×76×2 - MA	Major	9.00	1.52	1.13	4.06
OHS 121×76×3 - MI	Minor	11.78	1.52	1.18	4.59
OHS 121×76×3 - MA	Major	16.32	1.60	1.18	6.58
OHS 86×58×3 - MI	Minor	5.13	1.58	1.21	11.84
OHS 86×58×3 - MA	Major	7.84	1.92	1.40	29.02

4.2.4 Flexural buckling tests

Flexural buckling tests about the major and minor axes were carried out in order to obtain ultimate load carrying capacity data to enable the determination of a suitable buckling curve for stainless steel oval hollow section columns. The tests were conducted on pin-ended columns with nominal cross-sectional dimensions of 86×58×3 mm. The buckling lengths considered ranged from 700 mm to 3100 mm;

these lengths were chosen to cover a spectrum of member slendernesses, as defined by Equation (4.4), ranging between 0.34 and 2.07.

$$\bar{\lambda} = \sqrt{A\sigma_{0.2}/N_{cr}} \tag{4.4}$$

where A is the cross-sectional area, $\sigma_{0.2}$ is the material 0.2% proof strength as determined from tensile coupon tests and N_{cr} is the elastic buckling load of the column.

The specimens were cut to the required lengths by a rotary hacksaw and the ends were milled flat to ensure full contact with the end plates. Subsequently, measurements of specimen geometry and initial global imperfections e_0 were taken and are presented in Table 4.8. The designations 'CMI' and 'CMA' refer to minor and major axis buckling respectively.

Table 4.8: *Measured geometric properties of columns*

Specimen	Larger outer diameter 2a (mm)	Smaller outer diameter 2b (mm)	Thick-ness t (mm)	Cross-sectional area A (mm^2)	Buckling length (mm)	Global imper-fection amplitude e_0 (mm)
86×58×3-CMI1	85.41	57.16	3.11	672.7	699.5	0.08
86×58×3-CMA1	85.48	56.84	3.09	668.5	700.6	0.11
86×58×3-CMI2	86.05	56.21	3.11	672.9	1499.6	1.43
86×58×3-CMA2	85.91	56.70	3.15	681.4	1500.5	2.17
86×58×3-CM13	86.18	56.22	3.11	674.2	2299.3	2.78
86×58×3-CMI4	86.02	56.33	3.12	675.0	3100.3	1.73

The tests were carried out in a 400 T capacity rig (Figure 4.12). The load was applied through end plates that were attached to hardened steel knife-edges (Figure 4.13) designed to replicate pinned end conditions. The buckling lengths reported in Table 4.8 were measured between the pinned ends of each column, i.e. between the knife edges. The columns were aligned such that the centrelines of the cross-sections

coincided with the middle of the knife edges, though, as discussed later, an unintentional eccentricity of approximately L/1250 (additional to the initial global geometric imperfections) was also present in all tests.

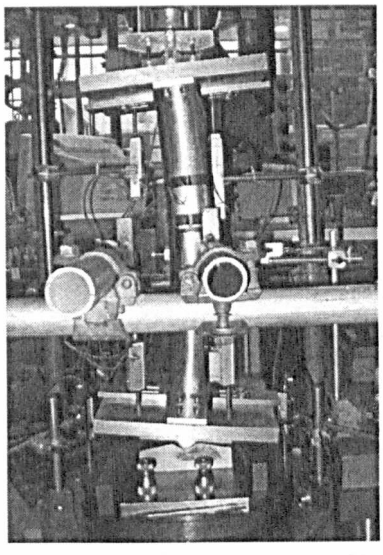

Figure 4.12: *Test setup for flexural buckling tests*

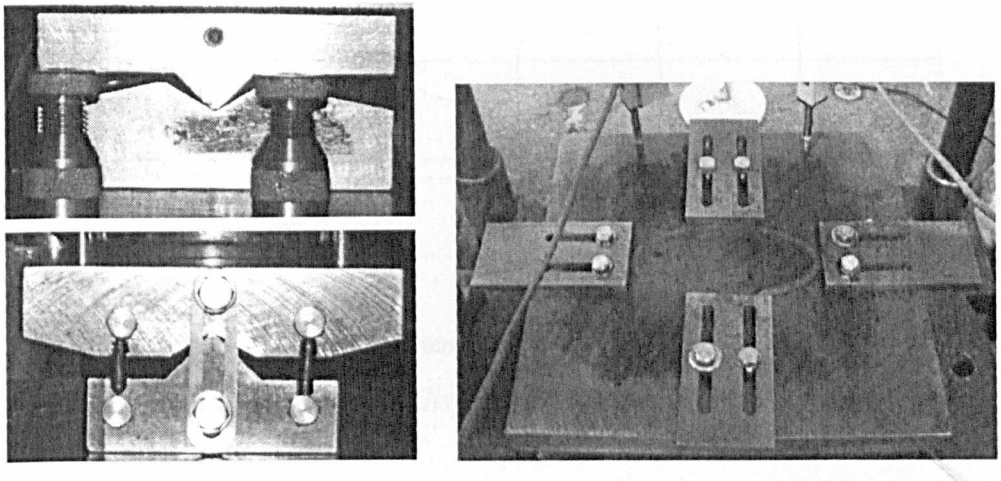

Figure 4.13: *Knife-edges and sliding clamps employed for the flexural buckling tests*

Two displacements transducers were placed at the mid-height of the columns to measure the lateral deflection. Two further displacement transducers were placed on each of the end-plates to measure end rotations, while an additional two were employed to measure the end shortening. Four stain gauges were attached at a 50 mm distance from mid-height at each section's major and minor axis. Test data from the transducers, strain gauges, compressive load and the horizontal and vertical

displacements were recorded at two second intervals. Key results from the column tests are summarised in Table 4.9 and load-lateral displacement at mid height curves are shown in Figure 4.14 both for major and minor axis buckling columns.

Table 4.9: *Key results from flexural buckling tests*

Specimen	Non - dimensional slenderness $\bar{\lambda}$	Ultimate load N_u (kN)	Lateral deflection at N_u (mm)
86×58×3 - CMI1	0.46	181.8	9.5
86×58×3 - CMA1	0.34	196.9	3.8
86×58×3 - CMI2	1.00	116.1	17.8
86×58×3 - CMA2	0.72	150.8	5.8
86×58×3 - CMI3	1.54	72.3	17.5
86×58×3 - CMI4	2.07	40.6	29.9

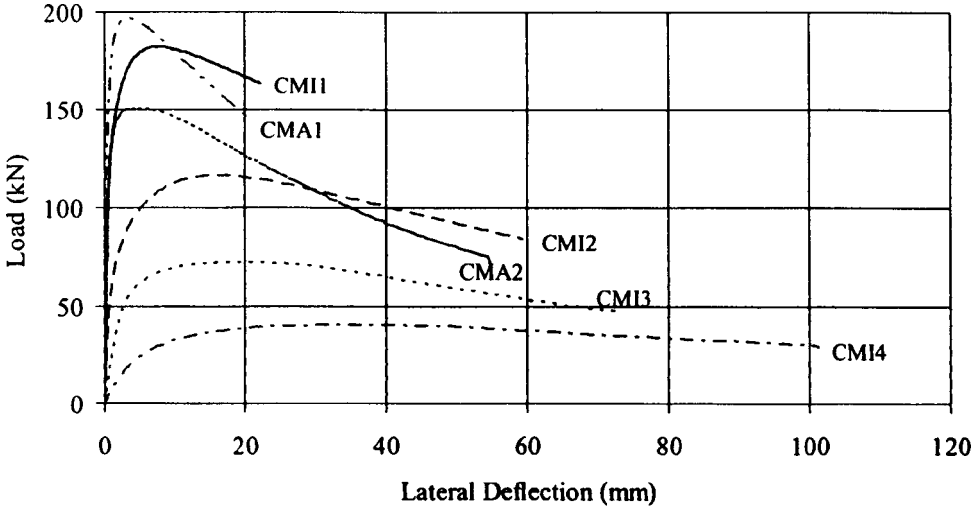

Figure 4.14: *Load-lateral displacement curves for OHS columns*

As expected, all the columns failed principally by global buckling, with the maximum lateral displacement occurring at mid-height. Upon detailed examination of the response of the tested specimens, it was observed that a small loading eccentricity with respect to the axis of buckling was introduced during testing - the value of this eccentricity was approximately L/1250, as estimated from the strain gauge data. This eccentricity has been included in subsequent numerical models. Typical column failure modes are shown in Figure 4.15. The results of all tests are discussed in Section 4 of this chapter.

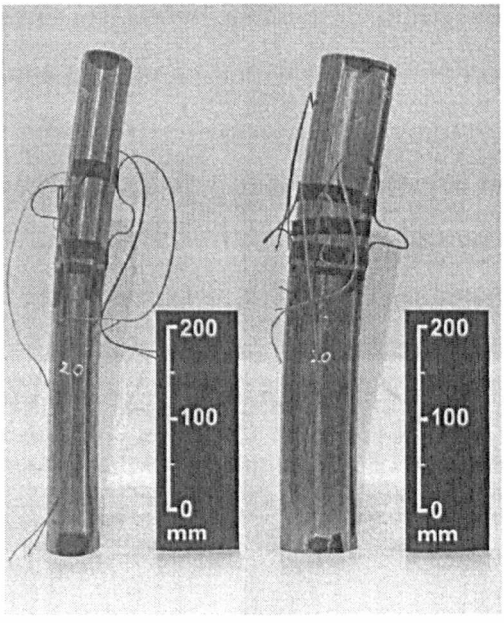

Figure 4.15: *Typical failure modes of OHS columns*

4.3 NUMERCAL MODELLING

A numerical modelling programme was performed in parallel with the testing programme, using the non-linear finite element analysis package ABAQUS version 6.6 (ABAQUS, 2006). Two types of numerical analyses were performed for each model; linear elastic buckling analyses were initially carried out to determine buckling mode shapes, which were subsequently incorporated in geometrically and materially non-linear analyses as a representation of geometric imperfections. The modified Riks method (ABAQUS, 2006) was employed for the non-linear analyses, which enabled the post-ultimate load response (i.e. the unloading branch of the load-displacement curves) of the models to be captured.

The 4-noded doubly curved general-purpose shell element S4R was adopted to simulate the stainless steel oval hollow section components, as discussed in Chapter 2. A mesh convergence study based on elastic eigenvalue buckling analyses was performed to choose a mesh size that would produce accurate results whilst remaining computationally efficient. A uniform mesh along the circumferential and longitudinal directions of size 2a/10(a/b)×2a/10(a/b) (where a and b are defined in Figure 4.3) was

deemed suitable and was employed for all models. Assumptions regarding material modelling, residual stresses and initial geometric imperfections were discussed in Chapter 2 and apply to the remainder of this section.

The initial aim of the numerical study was to replicate the experimental results and assess the sensitivity of the models to mesh density, material properties and initial geometric imperfections. Once validated, a series of parametric studies were carried out to investigate the influence of key variables (in particular cross-section slenderness and aspect ratio for the stub columns and beams and global slenderness, aspect ratio and axis of buckling for the long columns) and generate further results.

4.3.1 Numerical modelling of stub columns

Geometry, end restraints, loading and experimentally observed failure modes were symmetric about both the major and minor axes for all stub column tests. This symmetry was exploited in the FE simulations by modelling only one quarter of the cross-section and applying appropriate symmetry boundary conditions along the major and minor axes of the sections. Kinematic coupling was employed to constrain the vertical displacement of all nodes at the loaded end. The ends of the stub column models were fixed against all degrees of freedom except for the vertical displacement at the loaded edge in accordance with other numerical studies on stub columns (Ashraf et al., 2006b; Ellobody and Young, 2005). However, it was later observed that the circumferential expansion of the cross-sections due to the Poisson effect during the non-linear analyses effectively induced an additional geometric imperfection near the loaded ends of the models, which were not allowed to expand. This additional induced imperfection was found generally to be more significant than the critical geometric imperfection itself (incorporated by means of the lowest buckling mode shape) even for high imperfection amplitudes. The result of this was to induce an elephant's foot failure mode and a smooth post-ultimate response, which deviated from the experimental observations. Although the pre-buckling response prior reaching the ultimate load was relatively insensitive to the in-plane boundary conditions imposed on the ends of the model, the unloading response and failure mode was affected. Therefore, despite accurate predictions of the ultimate load still

being possible with restrained ends, it was decided not to restrain the in-plane translations at the ends of the models in the non-linear analyses, to enable the entire load-displacement response and failure mode to be consistently and accurately be captured.

Measured geometric and material properties were used in each model to replicate the corresponding test behaviour. Both tensile coupon and stub column material properties were obtained during the experimental phase of this study (Tables 4.2 and 4.5) and were incorporated into the models. Hence, two series of numerical analyses were carried out; one utilizing tensile material properties and one utilizing stub column material properties. The material stress-strain parameters were averaged for each nominal cross-section size and applied uniformly around the cross-sections of the models in a multi-linear form.

The amplitude of the initial geometric imperfections, a typical pattern of which is shown in Figure 4.16, was varied to assess the sensitivity of the models. Five imperfection amplitudes were considered: the maximum measured amplitudes from the testing programme w_0 and $w_{0.5}$ and three different fractions of the cross-sectional thickness t (t/10, t/100 and t/500). Results and comparison with test behaviour for the five imperfection amplitudes are shown in Tables 4.10 and 4.11 for tensile and stub column material properties respectively.

The response of the FE models was found to be sensitive to the amplitude of the geometric imperfection, as shown in Tables 4.10 and 4.11. It may also be seen that incorporation of the measured imperfection amplitude w_0 (including flaring deformations at the ends of the stub columns) in the numerical models leads to a considerable underprediction of their load-carrying capacity. On the other hand, incorporation of the $w_{0.5}$ imperfection amplitude (based on the central 50% of the stub columns' length) resulted in improved predictions of load-carrying capacity. Regarding the choice of material properties, it can be concluded that adoption of stub column material properties in the FE models yields more accurate results than incorporation of the tensile coupon properties. The improved accuracy resulting from the use of the stub column properties is believed to relate to basic differences in

stress-strain curves in tension and compression and the inherent presence of the varying level of cold-work around the section in the stub column properties.

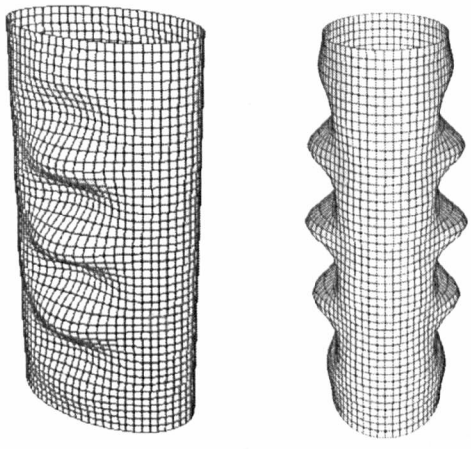

Figure 4.16: *Typical stub column lowest elastic buckling mode shape*

Overall, the FE models have been found to be capable of replicating the experimentally observed fundamental structural response characteristics of the stainless steel OHS stub columns. The initial stiffnesses, peak loads, post-ultimate responses and failure modes of all modelled stub columns are generally well-predicted for both tensile and stub column properties. Excellent agreement with experimental results was obtained for an imperfection amplitude of t/100 and using stub column material properties. The numerical load-displacement curves for OHS 121×76×3-SC1 and OHS 86×58×3-SC1 using stub column material properties and an imperfection amplitude of t/100 are compared with the respective experimental curves in Figures 4.17 and 4.18 respectively. Comparison of the numerical failure mode of OHS 86×58×3-SC1 with the experimental one is depicted in Figure 4.19.

Table 4.10: *Comparison of stub column test results with FE results for varying imperfection amplitudes and tensile material properties*

Stub column designation	w_0		$w_{0.5}$		t/10		t/100		t/500	
	FE F_u/ Test F_u	FE δ_u/ Test δ_u	FE F_u/ Test F_u	FE δ_u/ Test δ_u	FE F_u/ Test F_u	FE δ_u/ Test δ_u	FE F_u/ Test F_u	FE δ_u/ Test δ_u	FE F_u/ Test F_u	FE δ_u/ Test δ_u
OHS 121×76×2 - SC1	0.78	0.63	0.91	0.60	0.92	0.72	1.01	1.08	1.04	1.39
OHS 121×76×2 - SC2	0.78	0.58	0.92	0.58	0.91	0.68	1.00	1.00	1.03	1.26
OHS 121×76×3 - SC1	0.82	0.40	0.91	0.65	0.89	0.44	0.95	0.96	0.96	1.12
OHS 121×76×3 - SC2	0.80	0.39	0.89	0.44	0.89	0.44	0.96	0.93	0.97	1.17
OHS 86×58×3 - SC1	0.87	0.23	0.96	0.54	0.94	0.52	1.06	1.15	1.13	1.57
OHS 86×58×3 - SC2	0.85	0.25	0.95	0.62	0.95	0.61	1.08	1.36	1.14	1.85
Mean	0.82	0.41	0.92	0.57	0.92	0.57	1.01	1.08	1.04	1.39
COV	0.04	0.40	0.03	0.13	0.03	0.21	0.05	0.15	0.07	0.20

Table 4.11: *Comparison of stub column test results with FE results for varying imperfection amplitudes and stub column material properties*

Stub column designation	w_0		$w_{0.5}$		t/10		t/100		t/500	
	FE F_u/ Test F_u	FE δ_u/ Test δ_u	FE F_u/ Test F_u	FE δ_u/ Test δ_u	FE F_u/ Test F_u	FE δ_u/ Test δ_u	FE F_u/ Test F_u	FE δ_u/ Test δ_u	FE F_u/ Test F_u	FE δ_u/ Test δ_u
OHS 121×76×2 - SC1	0.78	0.65	0.92	0.62	0.96	0.73	1.02	0.99	1.03	1.19
OHS 121×76×2 - SC2	0.79	0.60	0.92	0.60	0.95	0.69	1.01	0.93	1.03	1.03
OHS 121×76×3 - SC1	0.85	0.43	0.94	0.70	0.95	0.66	1.00	1.00	1.01	1.11
OHS 121×76×3 - SC2	0.83	0.42	0.95	0.64	0.96	0.68	1.01	1.02	1.02	1.19
OHS 86×58×3 - SC1	0.87	0.33	0.96	0.57	0.94	0.46	1.01	1.02	1.06	1.33
OHS 86×58×3 - SC2	0.85	0.27	0.94	0.43	0.94	0.42	1.02	0.94	1.05	1.36
Mean	0.83	0.45	0.94	0.59	0.95	0.61	1.01	0.98	1.03	1.20
COV	0.04	0.33	0.02	0.16	0.01	0.22	0.01	0.04	0.02	0.10

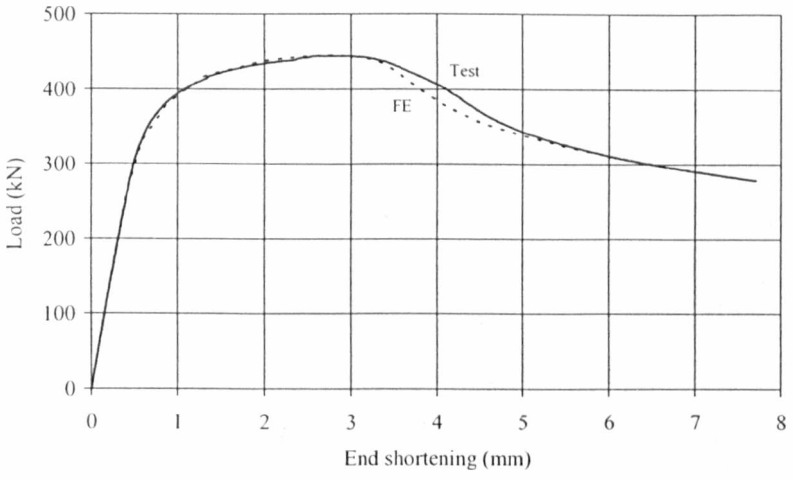

Figure 4.17*: Experimental and numerical load-end shortening curves for OHS 121×76×3-SC1*

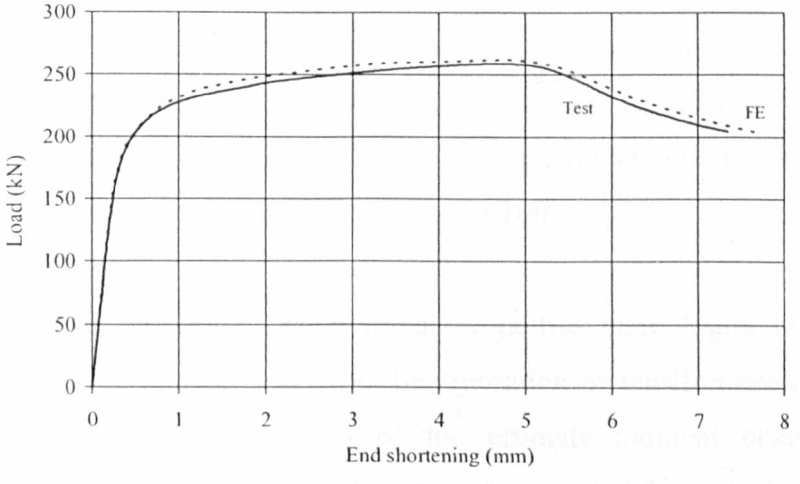

Figure 4.18: *Experimental and numerical load-end shortening curves for OHS 86×58×3-SC1*

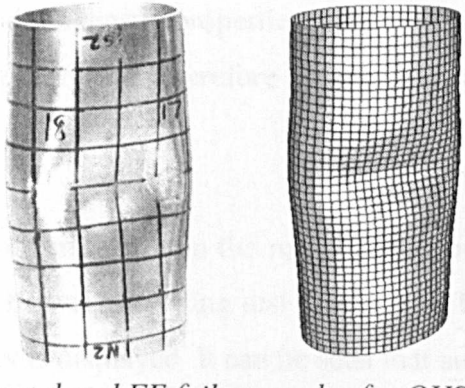

Figure 4.19: *Experimental and FE failure modes for OHS 86×58×3-SC1*

4.3.2 Numerical modelling of simply supported beams

All failure modes observed during testing were symmetric with respect to the plane of bending. In order to further reduce computational time, only one half of each section was modelled and suitable symmetry boundary conditions were applied along the plane of bending. The effect of the steel collars and wooden blocks located at the supports and at mid-span was taken into account in the FE simulations by ensuring that the respective cross-sections remained undeformed at these locations, using kinematic coupling. Results were found to be insensitive to whether a single cross-section (i.e. one line of nodes) or a 25 mm length of beam (corresponding to the width of the collar and wooden block) were restrained; thus the former approach was employed at the loading point and supports. Simple support conditions were simulated by restraining suitable degrees of freedom at the ends of the beams. The beam was restrained longitudinally at one end only. The imperfection amplitude was varied to assess the sensitivity of the models and four cases were considered: the maximum measured imperfection $w_{0.5}$ as given in Table 4.6, zero imperfection and two fractions of the cross-sectional thickness, namely t/10 and t/100.

Initial imperfection amplitude and material properties were found to be the key features affecting the models' response. Incorporation of tensile material properties resulted in marginal overpredictions of the ultimate moment observed in the corresponding tests, whilst the use of compressive material properties (as derived from stub column tests) improved the predictions in terms of strength but did not improve the accuracy in terms of rotations. The closest agreement between test and FE results was obtained when the stub column properties were assigned to the part of the model in compression and the tensile properties were assigned to the part that was stressed in tension. This approach was therefore followed throughout the numerical study.

The effect of the imperfection amplitude on the response can be assessed from Table 4.12 where the comparison between bending test results and FE results for varying local imperfection amplitudes is displayed. It can be seen that accurate results in terms of moment capacity are obtained for all considered imperfection amplitudes, whereas

Table 4.12: *Comparison of the in-plane bending test results with FE results for varying imperfection amplitudes*

Beam specimen designation	t/10		t/100		no imperfection		$w_{0.5}$	
	FE M_u/ Test M_u	FE R/ Test R	FE M_u/ Test M_u	FE R/ Test R	FE M_u/ Test M_u	FE R/ Test R	FE M_u/ Test M_u	FE R/ Test R
OHS 121×76×2 - MI	0.99	0.61	1.01	0.83	1.01	1.45	0.96	0.41
OHS 121×76×2 - MA	1.04	0.84	1.05	1.18	1.05	1.20	1.01	0.63
OHS 121×76×3 - MI	1.00	0.91	1.00	0.86	1.00	1.36	1.00	0.88
OHS 121×76×3 - MA	1.05	1.40	1.06	1.43	1.06	1.50	1.05	1.61
OHS 86×58×3 - MI	1.02	0.85	1.04	1.06	1.04	1.65	1.03	0.99
OHS 86×58×3 - MA	1.02	1.01	1.05	1.13	1.05	1.15	1.03	1.03
Mean	1.02	0.94	1.04	1.08	1.04	1.38	1.01	0.92
COV	0.02	0.28	0.02	0.21	0.02	0.14	0.03	0.44

the rotation capacity R was found to be more sensitive to imperfections. As in the tests, ovalization of the specimens was evident in the geometrically and materially non-linear FE analyses. This ovalization resulted in a decrease in flexural rigidity of the beams and promoted the onset of local buckling even in the case where no initial local imperfection was incorporated into the non-linear analysis. Approaching ultimate moment, the magnitude of the additional imperfection caused by ovalization overshadowed the initial geometric imperfection amplitude incorporated in the models. Therefore, the response of the models, particularly in terms of maximum attained moment, was relatively insensitive to the prescribed initial imperfection amplitudes.

In general, the FE models displayed good agreement with the experimental results and were capable of replicating the experimentally observed structural response of the specimens. Best agreement in terms of both peak moments and rotations was obtained for an initial imperfection amplitude of t/10, as shown in Table 4.12. In all cases, experimental and numerical failure modes were similar, as indicated in Figures 4.20 and 4.21. The full moment-rotation response, including initial stiffness, peak moment and post-ultimate response was generally well predicted by the FE simulations, as displayed in Figures 4.22 and 4.23 where the numerical moment-rotation curves for OHS 121×76×3-MI and OHS 86×58×3-MA are compared with the respective experimental curves. The initial elastic stiffness is included in both figures for comparison purposes.

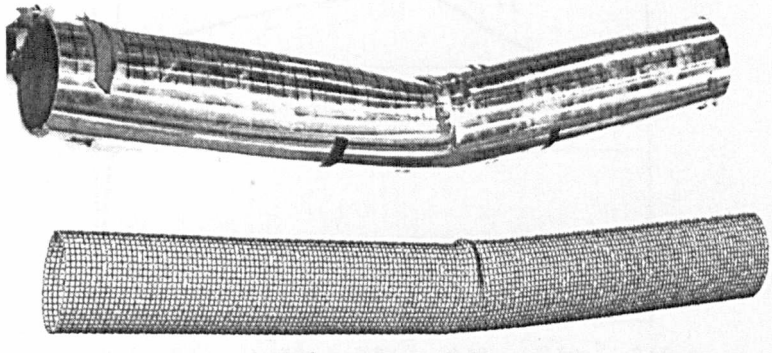

Figure 4.20: *Experimental and numerical failure modes for bending about the major axis (OHS 121×76×2-MA)*

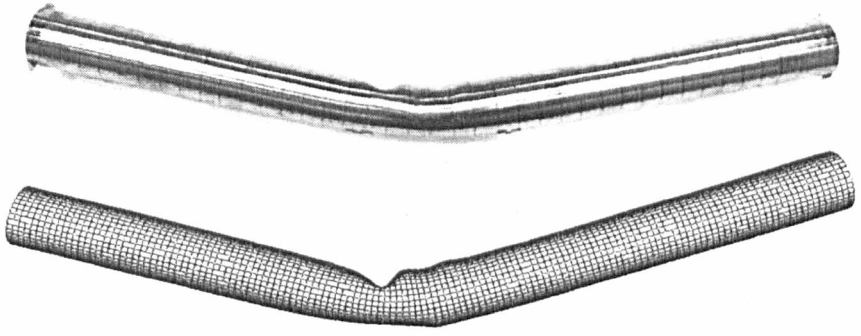

Figure 4.21: *Experimental and numerical failure modes for bending about the minor axis (OHS 86×58×3-MI)*

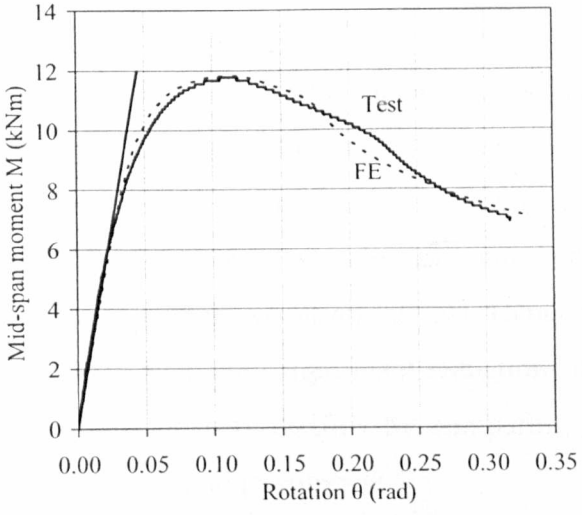

Figure 4.22: *Experimental and numerical moment-rotation curves for OHS 121×76×3-MI specimen*

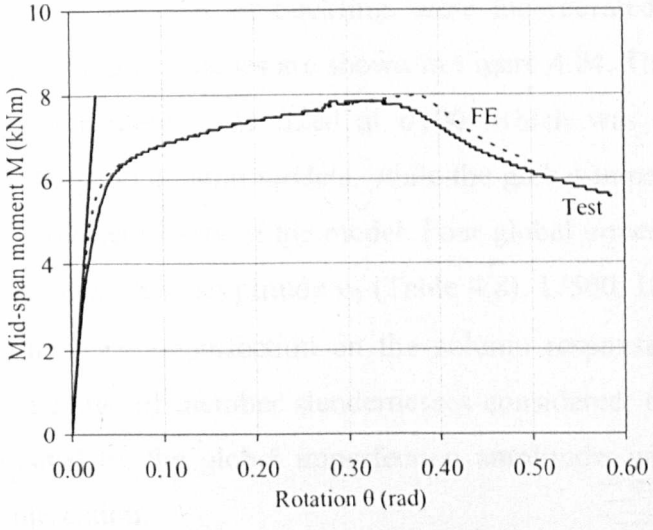

Figure 4.23: *Experimental and numerical moment-rotation curves for OHS 86×58×3-MA specimen*

4.3.3 Numerical modelling of flexural buckling members

Numerical simulations of the OHS flexural buckling tests were conducted similarly to the stub column tests. The boundary conditions imposed at the end cross-sections were similar to those applied to the stub column models allowing in-plane deformation of the cross-sections, but the columns' ends were also free to rotate about the axis of buckling. Kinematic coupling was employed to constrain both the vertical displacement of the loaded cross-section and the rotation of the end cross-sections about the axis of buckling considered.

Cross-section geometry, end restraints, loading and test failure modes were all symmetric with respect to the plane perpendicular to the axis of buckling for all tested specimens. This symmetry was exploited by modelling only half of the cross-section and employing symmetry boundary conditions. Furthermore, with a symmetric imperfection pattern, all FE failure modes were also symmetric with respect to the plane perpendicular to their member axis at mid-height. Hence only half the member length was modelled, thereby achieving significant reductions in computational time. This latter symmetry assumption was verified by comparing full-length with half-length models; the results were found to coincide.

Both global and local initial geometric imperfections in the form of the lowest elastic global and local buckling modes, together with the observed loading eccentricity of L/1250 with respect to the axis of buckling, were incorporated into the models. Typical local and global mode shapes are shown in Figure 4.24. The amplitude of the local imperfections considered was fixed at t/100, which was shown to provide accurate results for the stub column models, while the global imperfection amplitude was varied to assess the sensitivity of the model. Four global imperfection amplitudes were considered; the measured amplitude e_0 (Table 4.8), L/500, L/1000 and L/1500. The influence of the local imperfection on the column response was found to be insignificant for the range of member slendernesses considered; the response of the models was dominated by the global imperfection amplitude, with no evidence of significant mode interaction.

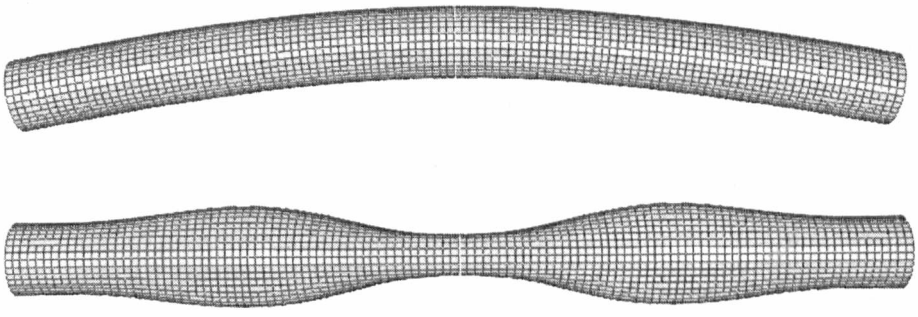

Figure 4.24: *Typical column local and global buckling mode shapes*

Both tensile coupon and stub column properties were incorporated into the FE models for each considered imperfection amplitude. Although accurate replication of tests ultimate loads could be obtained for both cases, provided that a suitable global imperfection amplitude was chosen, the stub column properties were found to give more consistent results and were able to more accurately overall load-lateral deflection response. For this reason, the stub column material properties were used in all subsequent FE models.

Table 4.13: *Comparison of column test results with FE results for varying imperfection amplitudes, a loading eccentricity of L/1250 and stub column properties*

Column designation	FE F_u / Test F_u			
	Measured e_0	L/500	L/1000	L/1500
86×58×3 - CMI1	1.02	0.96	0.99	1.00
86×58×3 - CMA1	1.03	0.99	1.01	1.02
86×58×3 - CMI2	0.97	0.93	1.00	1.03
86×58×3 - CMA2	0.98	0.95	1.00	1.02
86×58×3 - CM13	0.92	0.87	0.93	0.96
86×58×3 - CMI4	1.03	0.95	1.01	1.03
Mean	0.99	0.95	0.99	1.01
COV	0.05	0.04	0.03	0.03

Table 4.13 presents the ratios of numerical to experimental ultimate loads for the case of stub column material properties, a local imperfection amplitude of t/100 and various global imperfection amplitudes. For a global imperfection amplitude of

L/1000, an average value of numerical over experimental ultimate load of 0.99 with a corresponding coefficient of variation of 0.03 was obtained. Figures 4.25 and 26 depict comparisons between numerical and experimental load-lateral deflection curves for column specimens CMA2 and CMI4 respectively.

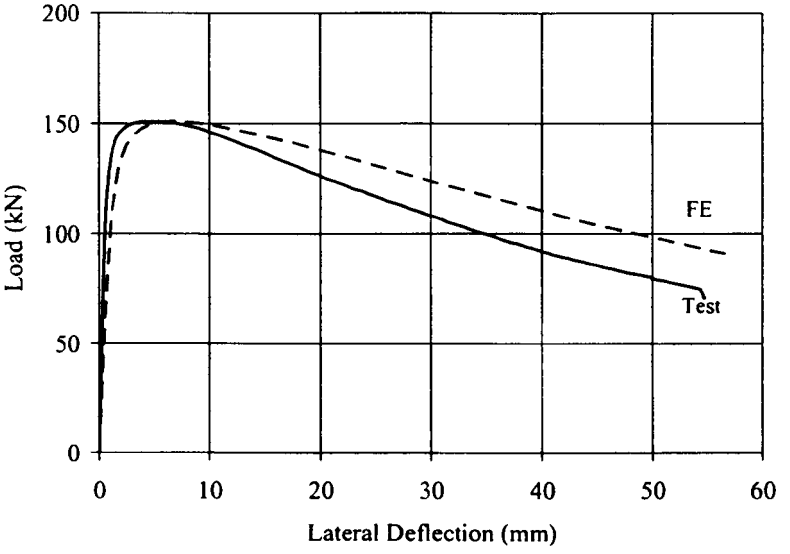

Figure 4.25: *Experimental and numerical load-lateral deflection curves for CMA2*

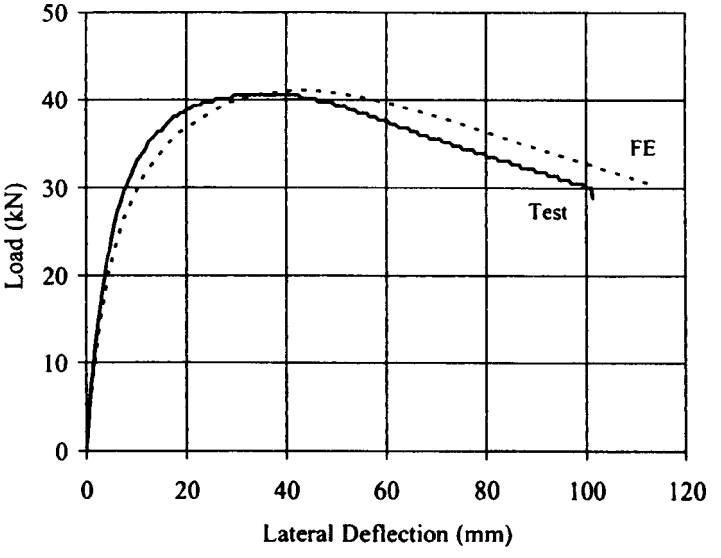

Figure 4.26: *Experimental and numerical load-lateral deflection curves for CMI4*

4.3.4 Parametric studies

Having demonstrated the ability of the numerical models to replicate the observed structural behaviour of stainless steel oval hollow components, parametric studies were performed to investigate the structural response of OHS stub columns, beams and long columns over a wider range of local and global slendernesses and derive suitable design rules.

For OHS stub columns the imperfection pattern was taken as the lowest buckling mode shape with an amplitude of t/100, while the material properties derived from the stub column tests on the two OHS 121×76×2 specimens were averaged and incorporated into the FE models. The effect of aspect ratio on cross-sectional response was also investigated, by considering two aspect ratios - 1.5 and 2. The aspect ratio of 1.5 coincides with the aspect ratio of the test specimens presented in Section 4.2, while the aspect ratio of 2 corresponds with carbon steel EHS examined by Chan and Gardner (2008a). In the developed models, the larger outer diameter and length of the stub columns were fixed at 120 mm and 240 mm respectively, whereas the smaller outer diameter and thickness dimensions were varied to achieve the desired aspect ratio and slenderness values. The results of the stub column parametric studies are presented and discussed in Section 4.4.2.

Parametric studies were also carried out to investigate the behaviour of stainless steel OHS in bending over a wider range of cross-section slenderness in order to derive suitable slenderness limits. Both major and minor axis bending were studied. Local imperfections assumed the pattern of the elastic lowest buckling mode shape with an amplitude of t/10, whilst the material properties of OHS 121×76×3 were incorporated in the models (tensile material properties for the lower (tension) part of the beam and stub column properties for the upper (compression) part). Two aspect ratios, 1.5 and 2 were considered, similarly to the stub column models. All modelled cross-sections had a larger outer diameter of 120 mm and a length of 1000 mm, whilst the smaller diameter was set to either 80 mm or 60 mm to achieve an aspect ratio of 1.5 or 2 respectively. The thickness of the models was varied between 0.4 mm and 8.9 mm for the OHS 120×80 sections and between 0.6 mm and 11.8 mm for the 120×60 sections,

thereby covering a slenderness range $D_e/t\varepsilon^2$ (described in Section 4.4.1) between 40 and 320 for both major and minor axis bending. The obtained results are discussed in Section 4.4.3, where comparisons with carbon steel EHS and stainless steel CHS are also displayed.

Regarding OHS columns, both major and minor axis buckling was studied. In the parametric studies, the non-dimensional slenderness $\bar{\lambda}$ of the columns was varied between 0.2 and 2.4 in increments of 0.2 for both axes. Two cross-section aspect ratios, 1.5 and 2, were considered for each axis of buckling. The modelled columns had cross-sections of OHS 86×57.33×3 and OHS 86×43×4 (providing aspect ratios of 1.5 and 2 respectively), with lengths varying between 224 mm and 5022 mm to achieve the desired non-dimensional slenderness values. The cross-sections considered were relatively stocky and assumed to be fully effective. The models incorporated stub column material properties (from the 86×58×3 stub columns) and included both local and global imperfections of amplitudes t/100 and L/1000 respectively. Loading eccentricities were not included in the parametric studies, since these were primarily related to the experimental setup and are not an inherent characteristic of the sections considered herein. The results are presented and discussed in 4.4.4.

4.4 DISCUSSION AND DESIGN RECOMMENDATIONS

In this section, all test data and numerically generated results on stainless steel OHS stub columns, beams and long columns are analysed and discussed. Comparisons are made with existing compression test data and bending test data on carbon steel elliptical hollow sections (EHS). The applicability of current design guidance for classification and column buckling to OHS members is assessed and new design recommendations are proposed. It should be noted that in all code comparisons presented in this section, the measured material properties (derived from tensile coupon tests) and measured geometry have been employed.

4.4.1 Slenderness parameters

Due to the recent introduction of OHS in the construction industry, no specific slenderness parameter is currently defined in any code of practice for either carbon steel or stainless steel. Adoption of suitable slenderness parameters is central to the classification process of any cross-section. For cross-sections comprising flat plated elements, each constituent plate element is individually classified based on its width-to-thickness (b/t) ratio independently of the other constituent elements and the whole cross-section is classified by its most slender (least favourably classified) constituent element, as discussed in Chapter 3 . For CHS, the diameter-to-thickness (D/t) ratio is employed as a suitable slenderness parameter. In both cases, the local radius of curvature and hence the local stiffness associated with the element (for plated cross-sections), or cross-section (for CHS) considered, are constant (i.e. ∞ for a plate and D/2 for CHS). For OHS and EHS the local radius of curvature changes around the cross-section as described by Equation (4.5) where φ is defined in Figure 4.3. The local radius of curvature assumes its maximum value $r_{max}=a^2/b$ at $\varphi=0$, which is therefore the least stiff region of the cross-section, and its minimum value $r_{min}=b^2/a$ at $\varphi=\pi/2$, which is therefore the stiffest region of the cross-section.

$$r = \frac{b^2}{a}\left(\sin^2\varphi + \frac{a^2}{b^2}\cos^2\varphi\right)^{3/2} \tag{4.5}$$

Based on the elastic critical stress of an elliptical hollow section in pure compression, Gardner and Chan (2007) and Chan and Gardner (2008a) proposed the following slenderness parameter (Equation (4.6))for carbon steel elliptical hollow sections (EHS):

$$\frac{D_e}{t\varepsilon^2} = 2\frac{(a^2/b)}{t\varepsilon_{cs}^{\ 2}} \tag{4.6}$$

where D_e is an equivalent diameter defined as two times the maximum radius of curvature in an elliptical section which is equal to $2(a^2/b)$, E is Young's modulus, v

is Poisson's ratio and $\varepsilon_{cs} = \sqrt{235/\sigma_{0.2}}$. For application to stainless steel OHS, this slenderness parameter can be slightly modified by defining ε_{ss} as Equation (4.7), in accordance with EN 1993-1-4:

$$\varepsilon_{ss} = \sqrt{\frac{235}{\sigma_{0.2}} \frac{E}{210000}} \tag{4.7}$$

Based on a more precise evaluation of the elastic buckling stress of an elliptical tube following extensive analytical and numerical studies, Ruiz-Teran and Gardner (2008) proposed a more sophisticated slenderness parameter, valid only for elliptical tubes in pure compression, which is given by Equation (4.8):

$$\frac{D_{Eq.OHS}}{t\varepsilon_{ss}^{\ 2}} = \frac{2a}{t\varepsilon_{ss}^{\ 2}}\left(1 + f\left(\frac{a}{b} - 1\right)\right) \tag{4.8}$$

where $D_{Eq.OHS}$ is the equivalent OHS diameter to be used in place of D_e in Equation (4.6) and f is derived from numerical results and given by Equation (4.9):

$$f = 1 - 2.3\left(\frac{t}{2a}\right)^{0.6} \tag{4.9}$$

The equivalent diameter referred to in Equation (4.8) is also limited by a plate bound in (Ruiz-Teran and Gardner, 2008), but this only governs for stocky sections of high aspect ratio, not considered in the present study.

As discussed in Section 4.2.3, for OHS subjected to minor axis bending local buckling initiates at the point of greatest radius of curvature which coincides with the most heavily compressed part of the cross-section, similarly to the OHS stub columns under uniform compression. Therefore the slenderness parameter defined by Equation (4.6) is adopted for OHS in minor axis bending.

For major axis bending, local buckling initiates at a point of the cross-section between the neutral axis and the major axis, since the maximum compressive stress arises at the stiffest part of the cross-section. This issue has been addressed analytically and the location of initiation of local buckling in shells of varying curvature in bending was determined by Gerard and Becker (1957). Based on these findings and experimental observations, Chan and Gardner (2008b) proposed the slenderness parameter defined by Equations (4.10) and (4.11) for major axis bending of carbon steel EHS, which are adopted for stainless steel OHS in the present study.

$$\frac{D_e}{t\varepsilon^2} = 0.8\frac{(a^2/b)}{t\varepsilon^2} \quad \text{for} \quad a/b > 1.357 \tag{4.10}$$

$$\frac{D_e}{t\varepsilon^2} = 2\frac{(b^2/a)}{t\varepsilon^2} \quad \text{for} \quad a/b \leq 1.357 \tag{4.11}$$

The threshold of 1.357 ensures continuity of the two branches defining the slenderness parameter. Its physical meaning is that for aspect ratios less than 1.357 local buckling initiates at the most heavily stressed part of the cross-section despite it also being the stiffest part, while for higher aspect ratios the point of initiation of local buckling moves from the extreme compression fibre towards the neutral axis.

4.4.2 Cross-sections in compression

The F_u/F_y (ultimate load over squash load) ratio of all experimental and FE data on stainless steel OHS stub columns has been plotted against the cross-section slenderness parameter defined by Equation (4.6) in Figure 4.27. For comparison purposes, existing experimental data on carbon steel EHS stub columns reported by Chan (2008) have been added to Figure 4.27; their slenderness parameter is based on ε_{cs}. The current European codified slenderness limit of 90 for carbon steel (EN 1993-1-1, 2005) and stainless steel (EN 1993-1-4, 2006) CHS in pure compression are also depicted. Cross-sections with a F_u/F_y ratio greater than unity are capable of reaching their squash load and are therefore fully effective (Class 1-3), whilst the remaining

cross-sections are prone to local buckling prior to the attainment of their squash load and are therefore characterized as slender (Class 4).

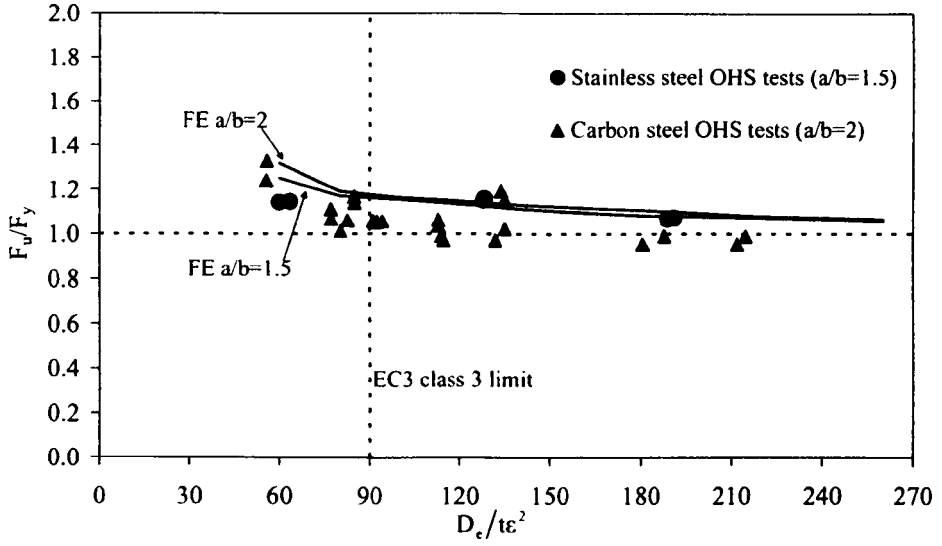

Figure 4.27: *Comparison between carbon steel and stainless steel OHS test results and FE results*

The parametric studies indicate that the OHS with the higher aspect ratio (2.0) exhibit superior load-carrying capacities to those with the lower aspect ratio (1.5) in the stocky range of the graph. This enhanced performance may be attributed to the stiffer corner regions (with low radius of curvature), which provide restraint to the less stiff flatter regions of the OHS (with high radius of curvature) and allow for greater stains and thus strain-hardening to be achieved before the ultimate load-carrying capacity of the cross-section is reached.

Using this more precise expression as the OHS slenderness parameter given by Equation (4.8), the variation in response between high and low aspect ratio OHS is clearly reduced, as can be seen in Figure 4.28. For comparison, stainless steel CHS test results reported by Rasmussen and Hancock (1993a), Burgan et al. (2000), Kuwamura (2003), Young and Hartono (2002), Bardi and Kyriakides (2006) and Lam and Gardner (2008) have also been included in Figure 4.28. All CHS and OHS data follow a similar trend, throughout the full slenderness range considered, regardless of aspect ratio. Thus, the slenderness parameter given by Equation (4.8) is more complex than that defined by Equation (4.6), but provides a better representation of the

behaviour of stainless steel OHS subjected to compression over a range of aspect ratios.

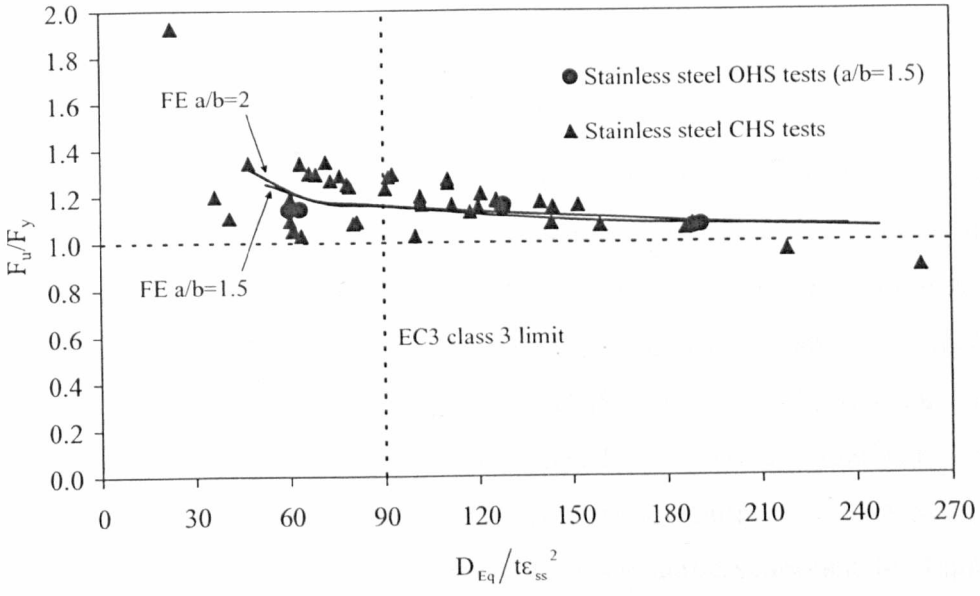

Figure 4.28: *Comparison between stainless steel OHS and CHS test results and FE results*

From both Figures 4.27 and 4.28, it can be seen that load-carrying capacity (normalised by squash load) decreases with increasing slenderness for both experimental CHS and OHS and numerical stainless steel OHS data. The stainless steel OHS may generally be seen to exhibit superior load-carrying in comparison to their carbon steel counterparts, since most of the carbon steel EHS test results (all having an aspect ratio of 2) lie below the corresponding stainless steel curve, as shown in Figure 4.28. Hence the current Class 3 slenderness limit of 90 given in Eurocode 3 for (carbon steel and stainless steel) CHS in pure compression may be safely applied to stainless steel OHS in compression.

4.4.3 Cross-sections in bending

In the following subsections the codified slenderness limits for stainless steel and carbon steel CHS in bending are assessed, based on both experimental and numerical results. In all code comparisons presented in this section, the experimentally obtained

tensile material properties and measured geometry have been used, with all safety factors set to unity.

4.4.3.1 Class 3 limit

Cross-sections able to exceed their elastic moment capacity are classified as Class 3 or better. The M_u/M_{el} (ultimate moment over elastic moment capacity) ratios of all experimental and FE data on stainless steel OHS bending about their minor axis have been plotted against the relevant cross-section slenderness parameter defined by Equation (4.6) in Figure 4.29; stainless steel CHS (ECSC, 2000; Kiymaz, 2005; Rasmussen and Hancock, 1993b) and carbon steel EHS (Chan and Gardner, 2008b) minor axis test data have been included for comparison purposes. The respective major axis data plotted against the cross-section slenderness defined by Equation (4.10) are depicted in Figure 4.30, where the relevant stainless steel CHS and carbon steel EHS have also been included. It should be noted that in the stocky region of the graphs, the curves derived from parametric studies display slightly higher moment capacities than the test results obtained for OHS 86×58×3. This is due to the different strain hardening characteristics inherent in the material properties of OHS 121×76×3 upon which the parametric studies based; a summary of material properties is given in Tables 4.2 and 4.5.

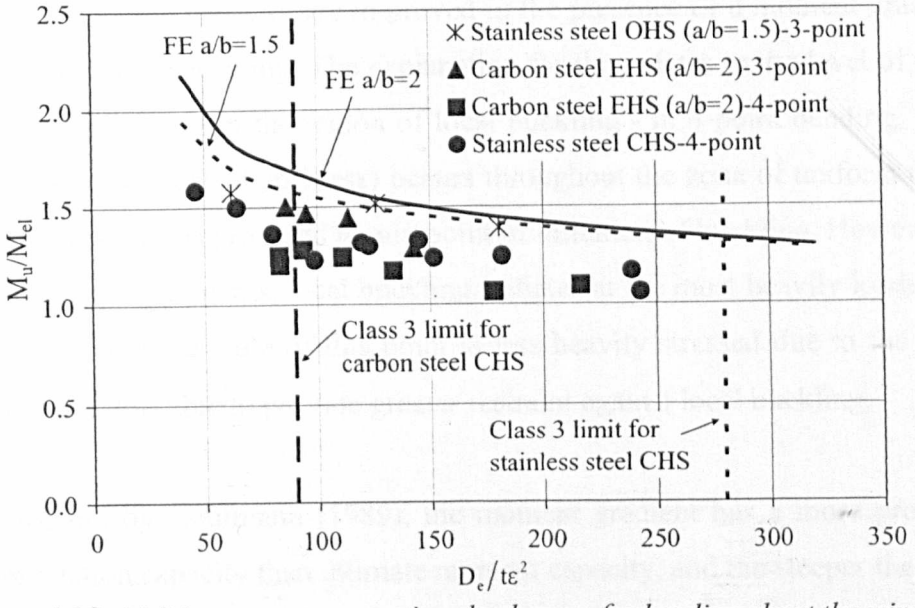

Figure 4.29: *M_u/M_{el} versus cross-section slenderness for bending about the minor axis*

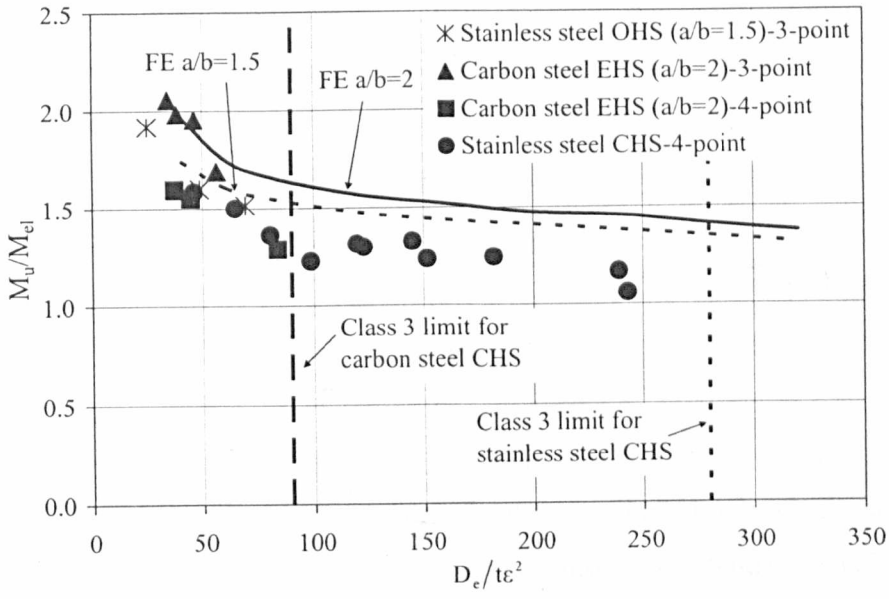

Figure 4.30: *M_u/M_{el} versus cross-section slenderness for bending about the major axis*

It should be noted that all depicted CHS test data have been obtained from 4-point bending tests, whereas all OHS data (both experimental and numerical) have been derived from 3-point bending tests. Carbon steel EHS have been tested in both 3-point and 4-point bending configurations and the respective test points are assigned a different symbol in Figures 4.29 and 4.30. The effect of moment gradient on ultimate moment and rotation capacity of carbon steel I sections has been extensively studied by Kuhlmann (1989). It has generally been concluded that both ultimate moment capacity and rotation capacity are improved in the presence of a moment gradient, as compared to uniform bending. The explanation for this relates to the level of restraint provided to the section in the region of local buckling - in 4-point bending, yielding (and the associated loss of stiffness) occurs throughout the zone of uniform moment, thus limited restraint is provided to any point of initiation of buckling. However, in 3-point bending arrangements, local buckling initiates at the most heavily loaded cross-section; material either side of this point is less heavily stressed due to the moment gradient and is thus able to provide greater restraint against local buckling.

As pointed out by Kuhlmann (1989), the moment gradient has a more pronounced effect on rotation capacity than ultimate moment capacity, and the steeper the moment gradient the higher the rotation capacity. Ultimate moment resistance is generally less

sensitive to moment gradient due to the yield plateau (with increasing deformation only resulting in small increments in load carrying capacity), though for stocky sections that reach the strain-hardening regime or for materials, such as cold-formed carbon steel and stainless steel, that exhibit a more rounded stress-strain response, increases in ultimate moment can be more significant. It can thus be asserted that for a given cross-section slenderness, a stainless steel member subjected to a moment gradient is expected to reach a higher ultimate moment and possess higher rotation capacity than it would under uniform moment.

In both Figures 4.29 and 4.30 the same general trend can be seen: the M_u/M_{el} ratio decreases with increasing cross-section slenderness and, for a given slenderness, performance improves with increasing aspect ratio. The stainless steel OHS test members and the curves derived from the parametric studies display higher moment capacities than their CHS counterparts of similar slenderness. This is believed to relate to both their higher aspect ratio and to the moment gradient that they are subjected to. The stainless steel OHS perform similarly to the carbon steel EHS under 3-point bending, while the influence of varying moment gradient only can be seen by comparing the results of the carbon steel EHS in 3- and 4-point bending.

The codified Class 3 limits for carbon steel (EN 1993-1-1, 2005) and stainless steel (EN 1993-1-4, 2006) CHS are also depicted in Figs 14 and 15. The stainless steel limit of $280\varepsilon^2$ is significantly more relaxed than the carbon steel limit of $90\varepsilon^2$, which appears overly conservative. A more relaxed Class 3 slenderness limit of $140\ \varepsilon^2$ has been previously proposed for both CHS and EHS in bending by Chan and Gardner (2008). It is proposed herein that the current Class 3 limit for stainless steel CHS in bending of $280\varepsilon^2$ may also be applied to stainless steel OHS for both major and minor axis bending. Despite seeming overly conservative for OHS, it should be bourn in mind that the derivation of the stainless steel CHS limit was based on 4-point bending test data, whereas the depicted OHS FE curves are derived for a moment gradient. Hence the superior behaviour of the OHS cannot be attributed solely to the effect of the aspect ratio, but will also reflect the beneficial effect of the moment gradient.

4.4.3.2 Class 2 limit

Cross-sections capable of exceeding their plastic moment capacity are assigned to Class 2. Figures 4.31 and 4.32 depict the M_u/M_{pl} (ultimate moment over plastic moment capacity) ratios as a function of cross-section slenderness for all OHS test and FE data in minor and major axis bending respectively. The relevant carbon steel EHS and stainless steel CHS data are also included as before. Similarly to Figures 4.29 and 4.30, M_u/M_{pl} increases with decreasing slenderness. However the effect of aspect ratio is less pronounced in this case, with the FE curves derived for an aspect ratio of 1.5 and 2 lying very close to each other throughout the considered slenderness range.

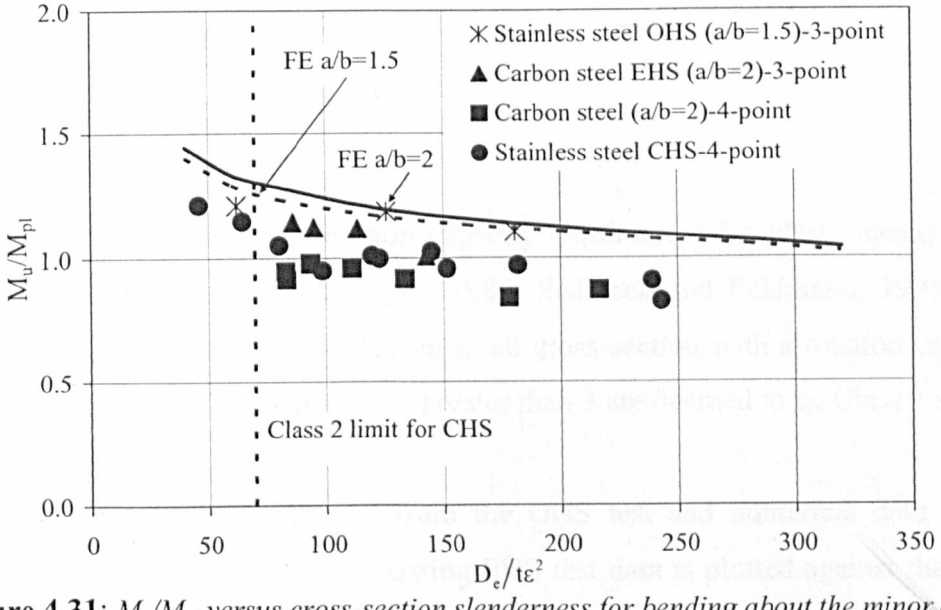

Figure 4.31: *M_u/M_{pl} versus cross-section slenderness for bending about the minor axis*

Previous remarks regarding the effect of moment gradient and the relative performance of stainless steel OHS in comparison to stainless steel CHS and carbon steel EHS are also supported by Figures 4.31 and 4.32. The common stainless steel and carbon steel Class 2 slenderness limit of $70\varepsilon^2$ is suitable for OHS in either major or minor axis bending.

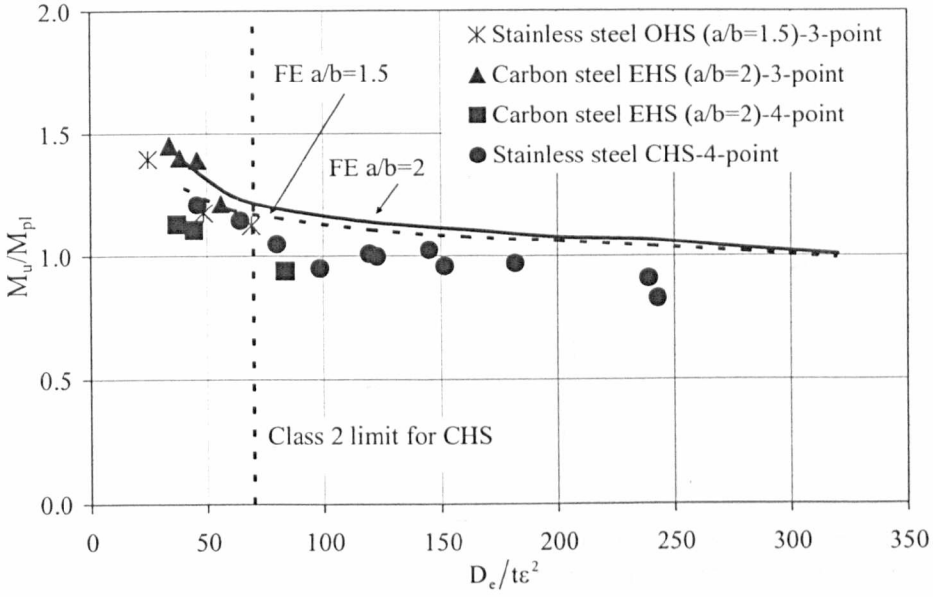

Figure 4.32: *M_u/M_{pl} versus cross-section slenderness for bending about the major axis*

4.4.3.3 Class 1 limit

Similarly to Chapter 3, the rotation capacity requirement for plastic design of R=3 utilised for carbon steel (Bild et al., 1989; Sedlacek and Feldmann, 1995) is also adopted herein for stainless steel. Hence, all cross-section with a rotation capacity as defined in Equation (4.3) equal to or greater than 3 are deemed to be Class 1 sections.

The rotation capacity R derived from the OHS test and numerical data from the present study, together with the existing EHS test data is plotted against the relevant slenderness parameter in Figures 4.33 and 4.34 for minor and major axis bending respectively. Stainless steel CHS data have also been included. Note that the carbon steel EHS subjected to 4-point bending, rotation capacity has been calculated on the basis of Equation (4.12), where $k_{pl,0.95}$ is the elastic rotation at $0.95M_{pl}$ and $k_{rot,0.95}$ is the rotation at which the falling moment branch passes $0.95M_{pl}$. This approach has been applied in previous studies (Chan and Gardner, 2008b; Sherman, 1976) to overcome the problem that the results of 4-point bending tests often exhibit a bending moment plateau just below M_{pl} due to the formation of a plastic zone (in contrast to a more localised plastic hinge associated with a 3-point bending test arrangement) and

possible ovalisation prior to the attainment of strain hardening. Adoption of Equation (4.12) provides a more stable measure of rotation capacity that is comparable with that obtained from 3-point bending tests. For stainless steel, the continuous strain-hardening nature of the material counteracts these effects and the conventional definition of rotation capacity based on the full plastic moment capacity may be calculated through Equation (4.3).

$$R_{0.95} = \frac{k_{rot.0.95}}{k_{pl.0.95}} - 1 \tag{4.12}$$

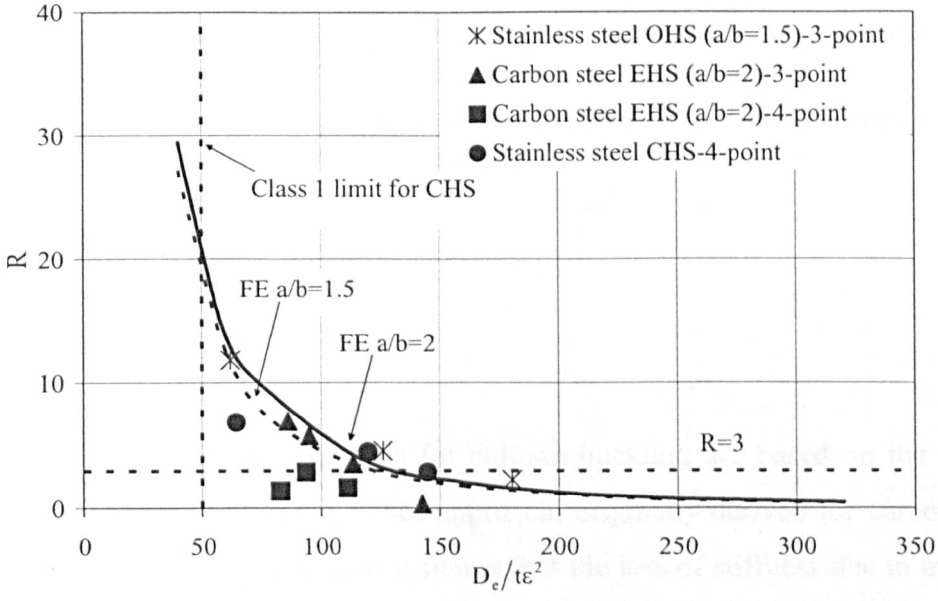

Figure 4.33: *Rotation capacity versus cross-section slenderness for bending about the minor axis*

In Figure 4.33 it can be seen that aspect ratio is not a particularly influential factor in determining rotation capacity as the FE curves derived for aspect ratios of 1.5 and 2 follow a similar path throughout the slenderness range considered, though some deviation may be observed for stocky sections in major axis bending. The results indicate that the current Class 1 slenderness limit of $50\varepsilon^2$ common to both carbon steel and stainless steel may be safely applied to stainless steel OHS in major or minor axis bending.

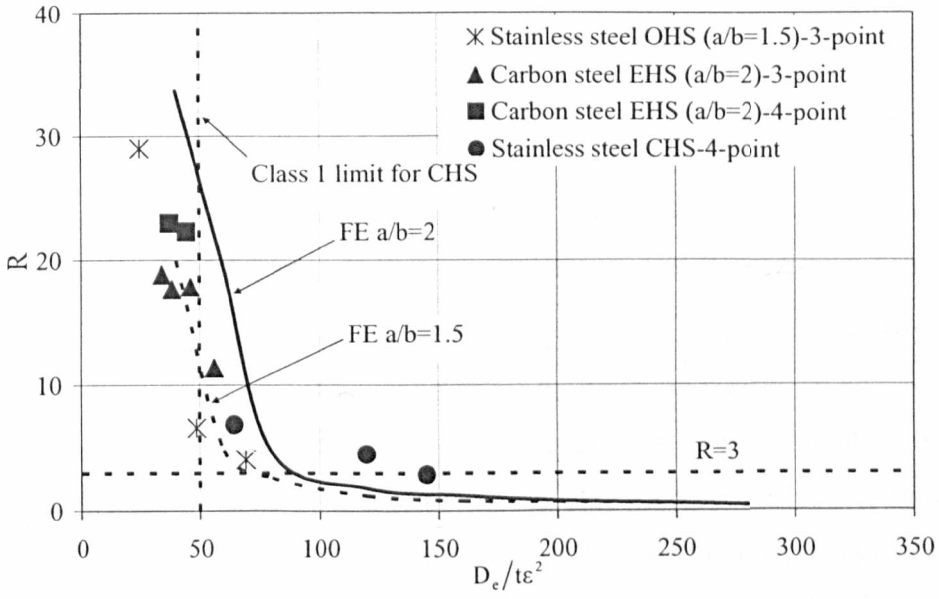

Figure 4.34: *Rotation capacity versus cross-section slenderness for bending about the major axis*

4.4.4 Flexural buckling

Current European codified provisions for column buckling are based on the classic Ayrton-Perry (Ayrton and Perry, 1886) approach, originally derived for carbon steel columns, the underlying principle of which is that the loss of stiffness due to material yielding of the most heavily stressed fibre of the column triggers member instability. Although less clearly applicable to stainless steel columns due to the rounded nature of the material stress-strain curve, the same cross-sectional failure criterion is adopted, which, upon mathematic manipulation, results in the familiar buckling reduction factor formulae codified in EN 1993-1-1 (2005) and EN 1993-1-4 (2006) given by Equation (4.13):

$$\chi = \frac{1}{\Phi^2 + (\Phi^2 - \bar{\lambda}^2)^{0.5}} \leq 1 \tag{4.13}$$

where $\Phi = 0.5(1+\alpha(\bar{\lambda}-\bar{\lambda}_0)+\bar{\lambda}^2)$, in which α is an imperfection factor, $\bar{\lambda}_0$ is the limiting slenderness, below which member buckling effects may be neglected and $\bar{\lambda}$ is the member slenderness defined by Equation (4.4).

Column buckling resistance is determined by multiplying the buckling reduction factor χ by the corresponding cross-section resistance. The imperfection factor α and the limiting slenderness $\bar{\lambda}_0$ allow for the influence of imperfections (principally geometric imperfections and residual stresses) on buckling resistance and depend on cross-section type, axis of buckling and forming process. It is reasonable to assume that all cold-formed hollow sections will display similar residual stresses and geometric imperfections patterns, because of similar production process. Hence the buckling curve specified in EN 1993-1-4 (2006) for stainless steel SHS, RHS and CHS, which is defined by α= 0.49, $\bar{\lambda}_0$ = 0.4, would also be expected to be applicable to stainless steel OHS.

For comparison with codified buckling curves, the ultimate loads attained in stainless steel OHS column tests, normalised by their corresponding squash loads, have been plotted against the member slenderness (as reported in Table 4.9) in Figure 4.35. The codified buckling curve currently applied to stainless steel SHS, RHS and CHS is also depicted. Test data on stainless steel CHS columns and stub columns reported by Rasmussen and Hancock (1993a), Burgan et al. (2000), Kuwamura (2003), Young and Hartono (2002), Bardi and Kyriakides (2006) and Lam and Gardner (2008), as well as OHS stub columns (Section 4.2.2) have also been included in Figure 4.35 for comparison. With the exception of the very stocky members (i.e. stub columns), almost all test points lie below the current buckling curve. Hence, the current codified buckling curve is deemed unsafe for stainless steel CHS and OHS, particularly in the low and intermediate slenderness range and adoption of a revised buckling curve for CHS and OHS columns is necessary to ensure reliable design.

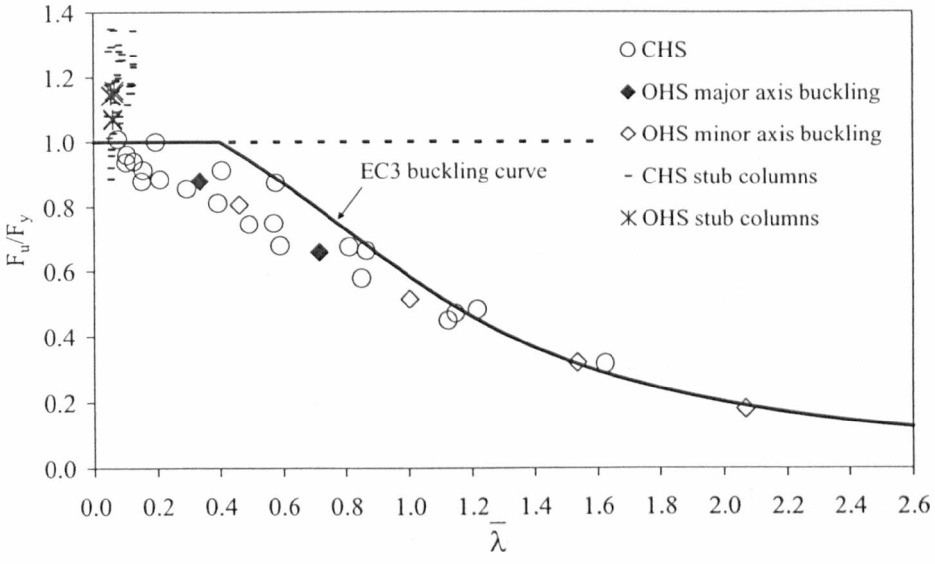

Figure 4.35: *Normalised OHS and CHS test results and column buckling curves*

The shortcomings of the current provisions of EN 1993-1-4 (2006) for CHS column buckling have been previously highlighted by Rasmussen and Rondal (2000) and attributed to the fact that the calibration of the codified strength curve was based primarily on tests of cold-formed SHS and RHS columns for which substantial increases in strength is derived from the highly cold-worked corner regions. Ellobody and Young (2007), following on an extensive finite element investigation, proposed two different buckling curves for stainless steel CHS columns, differentiated by material grade. These proposed curves offer improved fit to available data, but the minimum limiting slenderness $\bar{\lambda}_0$ of 0.2 appears unconservative in the light of the presented test results (see Figure 4.35). Ashraf et al. (2008b) also recognised this deficiency in the current provisions for stainless steel CHS columns and proposed a new buckling curve defined by a limiting slenderness value $\bar{\lambda}_0$ of 0.05 and an imperfection factor α of 0.49, which is found to be in good agreement with both the test data and the numerical results obtained from the OHS column parametric studies, as can be seen in Figure 4.36. The proposed buckling curve has been statistically validated according to Annex D of EN 1990 (2002) against all available CHS and OHS column test results and was deemed safe for design in conjunction with a partial safety factor of γ_{M1}=1.1 as specified in EN 1993-1-4 (2006). Adoption of this curve ($\bar{\lambda}_0$=0.05 and α=0.49) for both CHS and OHS column buckling is therefore proposed herein.

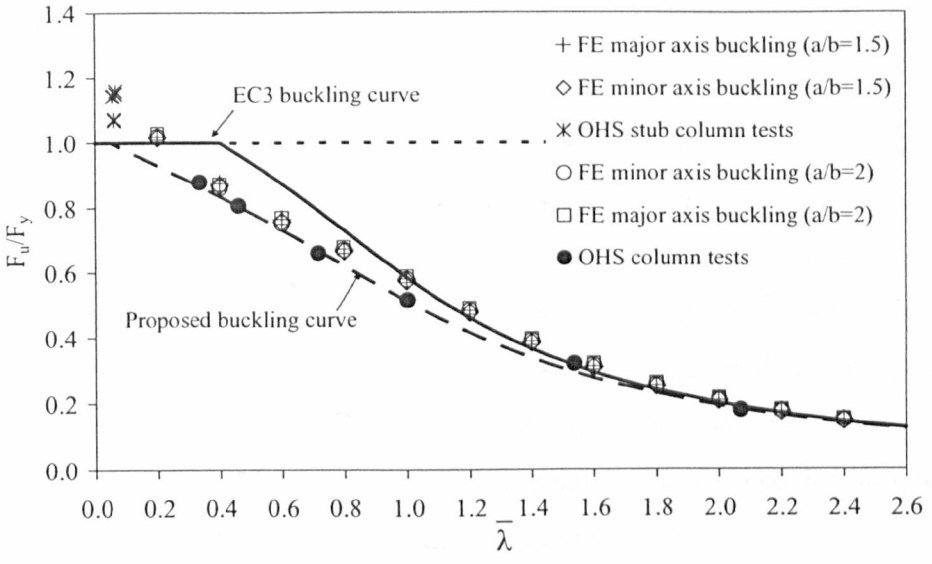

Figure 4.36: *Normalised test and FE OHS results and column buckling curves*

4.5 CONCLUDING REMARKS

Experimental and numerical structural performance data for stainless steel OHS compression members and flexural members have been generated. Six OHS stub columns and six OHS long columns were tested in axial compression, whilst six OHS beams with an aspect ratio of approximately 1.5 and varying cross-section slenderness were tested in major and minor axis bending. These member tests were supplemented by tensile coupon tests on material cut from the cold-formed cross-sections. FE models were developed and validated against the tests. Subsequent parametric studies enabled investigation of the compressive response and flexural response of OHS over a wider range of slendernesses and aspect ratios.

With respect to the cross-sectional response of OHS in compression, two proposed local slenderness parameters, originally derived for carbon steel EHS, were assessed and found to be applicable for design purposes to stainless steel OHS; one being simple and more conservative, the other being more elaborate and accurate. Moreover, it was concluded that the current Class 3 slenderness limit of 90 applied in

Eurocode 3 to both carbon steel and stainless steel CHS in pure compression may be safely used for stainless steel OHS.

Previous studies (Chan and Gardner, 2008b) on carbon steel EHS in major and minor axis bending were utilised and the slenderness parameters originally proposed for carbon steel EHS were adopted in the present study. Both test and FE results were compared with existing test data on stainless steel CHS and carbon steel EHS and the effect of aspect ratio, cross-section slenderness and moment gradient on strength and deformation capacity has been highlighted. It was concluded that current codified slenderness limits for stainless steel CHS may safely be adopted for stainless steel OHS in conjunction with proposed equivalent diameters D_e.

Finally, the current codified buckling curve for stainless steel hollow sections (EN 1993-1-4, 2006) was assessed and was found inappropriate (unsafe) for both OHS and CHS. A new buckling curve for CHS with a limiting slenderness value $\bar{\lambda}_0$ of 0.05 and an imperfection factor α of 0.49 was found to be in excellent agreement with both experimental and numerical test results on OHS columns buckling about either axis, and its adoption for stainless steel OHS and CHS columns is proposed.

CHAPTER 5

LEAN DUPLEX STAINLESS STEEL COMPONENTS

5.1 INTRODUCTION

There is a wide variety of grades of stainless steels, providing a range of material characteristics to suit the demands of numerous, diverse engineering applications. Both overall, and within the construction industry, the austenitic grades feature most prominently (Gardner, 2005). The most commonly employed grades of austenitic stainless steel are EN 1.4301/1.4307 and EN 1.4401/1.4404, which contain around 8-11% nickel according to EN 10088-4 (2009). Nickel stabilises the austenitic microstructure and therefore contributes to the associated favourable characteristics such as formability, weldability, toughness and high temperature properties. However, nickel also represents a significant portion of the cost of austenitic stainless steel and this has led, particularly in recent years to the development and evaluation of alternative grades of stainless steel with low nickel content.

Appropriate material selection, taking due account of in-service performance, economics and environmental conditions, involves matching the material characteristics to the particular demands of the application. Within construction,

although austenitic stainless steels are the most widely specified, their strengths are often not fully utilised; a recently developed 'lean duplex' stainless steel, containing approximately 1.5% nickel, may offer a more appropriate balance of properties for structural applications. The particular grade considered in this study is EN 1.4162, which is generally less expensive and possesses higher strength than the familiar austenitics, while still retaining good corrosion resistance and high temperature properties (Gardner et al., submitted), together with adequate weldability (Nilsson et al., 2008) and fracture toughness (Sieurin et al., 2007). Examples of the use of lean duplex stainless steel in construction have already emerged (Gedge, 2008), including footbridges in Förde, Norway and Siena, Italy; the latter is shown in Figure 5.1.

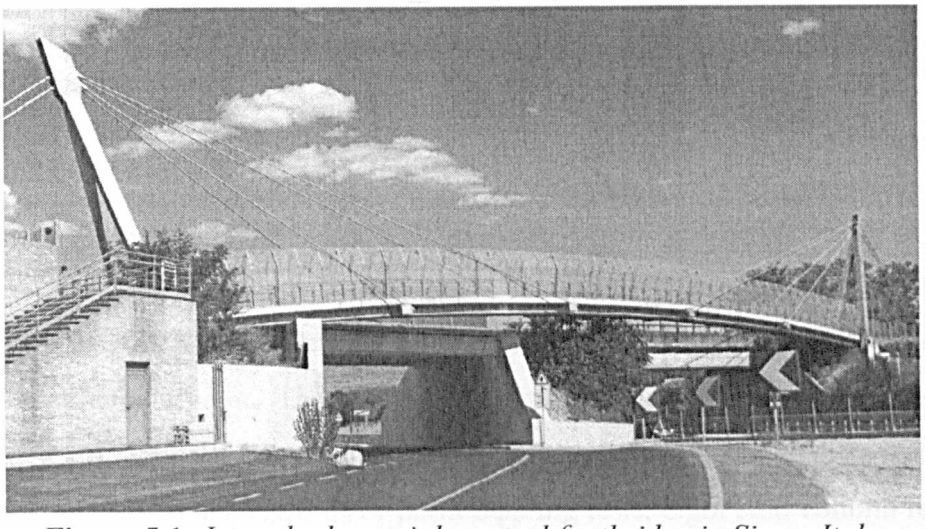

Figure 5.1: *Lean duplex stainless steel footbridge in Siena, Italy*

Despite early applications of lean duplex stainless steel, its structural performance has been relatively unexplored owing to its recent introduction, and to date there has been a lack of experimental data. To assess its structural behavior, a comprehensive laboratory testing programme on grade UNS 32101 (EN 1.4162) stainless steel square and rectangular hollow sections (SHS and RHS) has been conducted at Imperial College London, including tensile, compressive and corner material coupon tests, stub column tests, beam tests and flexural buckling tests.

The test results were used to validate finite element (FE) models, which were thereafter employed in parametric studies, to expand the range of available structural performance data, studying the influence, in particular, of cross-section and member slenderness. Both the experimental and numerical results were used to assess the

applicability of the European structural design provisions for stainless steel EN 1993-1-4 (2006) to lean duplex stainless steel structural components. The American (SEI/ASCE 8, 2002) and Australian/New Zealand (AS/NZS 4673, 2001) codified design provisions for stainless steel components subjected to bending are also assessed on the basis of the beam test and FE results. Comparisons with recent proposals regarding the classification of stainless steel cross-sections, discussed in Chapter 3 and reported by Gardner and Theofanous (2008), as well as comparisons with the structural performance of other commonly used structural stainless steel grades are also included and the significant economic merits of lean duplex stainless steel are discussed. The findings of this research were reported by Theofanous and Gardner (2009a, 2009b, in press).

5.2 EXPERIMENTAL INVESTIGATION

An experimental investigation into the structural performance of lean duplex stainless steel (grade EN 1.4162) SHS and RHS was conducted in the Structures Laboratory at Imperial College London. The laboratory testing program comprised tensile and compressive tests on flat coupons and tensile tests on corner coupons extracted from the cold-formed sections, eight three-point bending tests, eight stub column tests and twelve flexural buckling tests. The chemical composition and the mechanical properties of the tested material, as given in the mill certificates, are displayed in Tables 5.1 and 5.2 respectively.

Table 5.1: *Chemical composition of EN 1.4162 for mill certificates*

Section	C (%)	Si (%)	Mn (%)	P (%)	S (%)	Cr (%)	Ni (%)	N (%)	Mo (%)	Cu (%)
60×60×3	0.025	0.8	4.99	0.02	0.001	21.64	1.5	0.209	0.3	0.31
80×80×4 and 80×40×4	0.028	0.7	4.85	0.021	0.001	21.4	1.6	0.229	0.26	0.29
100×100×4	0.019	0.64	5.05	0.02	0.001	21.41	1.6	0.227	0.28	0.34

Table 5.2: *Mechanical properties stated in mill certificates*

Cross-section	$\sigma_{0.2,mill}$ (N/mm^2)	$\sigma_{1.0,mill}$ (N/mm^2)	$\sigma_{u,mill}$ (N/mm^2)	ε_f (%)
SHS 100×100×4	605	658	777	33
SHS 80×80×4	540	605	752	37
SHS 60×60×3	570	641	770	33
RHS 80×40×4	540	605	752	37

5.2.1 Material testing

A series of tensile and compressive coupon tests were carried out in the Structures laboratory of the Department of Civil and Environmental Engineering at Imperial College London, to obtain the basic material stress-strain response of the lean duplex stainless steel specimens, which was subsequently utilised in numerical modeling and in the analysis of the member test results. All material was extracted from the same length of tubes as the beam, stub column and long column specimens. The tests were conducted in an INSTRON 600 kN machine in accordance with EN 10002-1 (2001). A uniform strain rate of 0.0003 s^{-1} was used throughout all tensile and compressive coupon tests. Strain gauges were affixed at either side of the tested coupons at mid height. Load, cross-head displacement, strain and input voltage were all recorded at one second intervals using the data acquisitions system DATASCAN.

Four section sizes were tested in the present study - SHS 60×60×3, SHS 80×80×4, SHS 100×100×4 and RHS 80×40×4. One tensile flat (labelled TF) and one compressive flat (labelled CF) coupon were machined longitudinally from each of the four faces of each of the four cross-sections (apart from the 80×40×4 for which only two compressive coupons were extracted from the longer faces), resulting in a total of sixteen tensile and fourteen compressive flat coupons. All tensile flat coupons had nominal dimensions of 320×20 mm, while the respective nominal dimensions for the compressive coupons were 72×16 mm. Buckling of the compressive coupons was prevented by means of a bracing jig (Gardner and Nethercot, 2004a), as depicted in Figure 5.2.

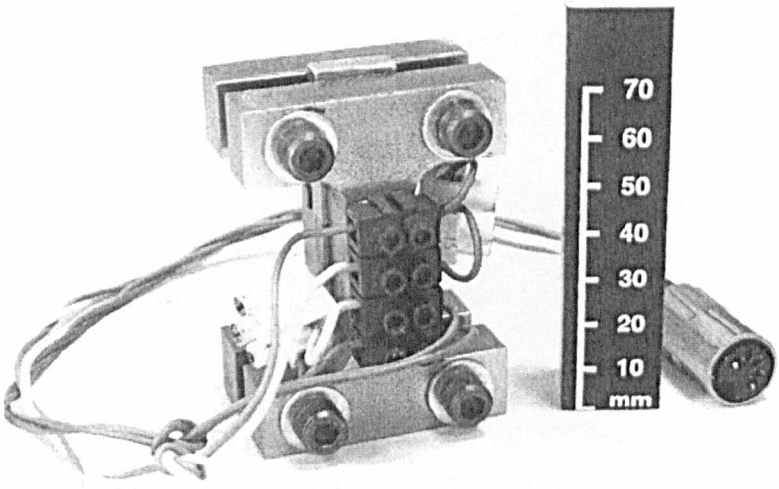

Figure 5.2: *Compressive coupons bracing jig*

It is well-known that work-hardening induced by the cold-forming process leads to significant strength enhancements in the corner regions of both carbon steel (Karren, 1967) and stainless steel (Young and Lui, 2005; Cruise and Gardner, 2008b) cold-formed sections. In order to quantify these strength enhancements and to accurately account for them in subsequent FE modeling, one 320 mm long tensile corner coupon (labelled TC) was extracted from the curved portions of each of the cross-sections considered.

Upon machining from the cross-sections, longitudinal curving of all coupon specimens was observed as shown in Figure 5.3, due to the release of the bending residual stresses locked in the cross-sections. No attempt was made to straighten the coupons by plastic deformation prior to testing and hence the obtained stress-strain characteristics inherently include the effect of bending residual stresses, which were reintroduced during gripping in the testing machine's jaws and upon application of light loads (Rasmussen and Hancock, 1993a; Cruise and Gardner, 2008a). Previous studies on cold-formed carbon steel (Schafer and Peköz, 1998) and cold-formed stainless steel members (Young and Lui, 2005) have indicated that the magnitude of membrane residual stresses in cold-formed members is small compared to bending residual stresses. Hence membrane residual stresses have not been measured and were not explicitly accounted for in the numerical investigation detailed later.

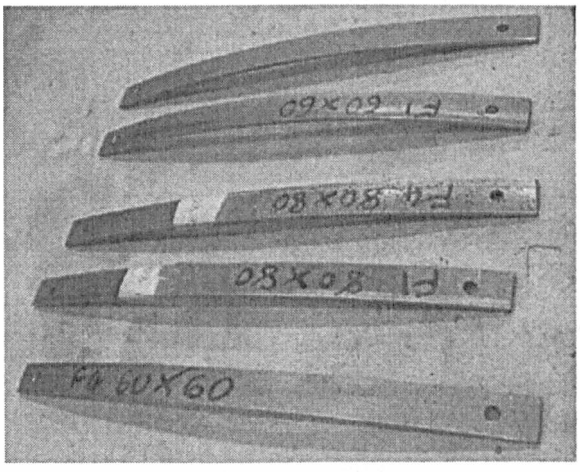

Figure 5.3: *Curved tensile coupons*

The obtained material data for each specimen are given in Table 5.3, whereas the weighted average (based on face width) tensile and compressive material properties of each section are given in Tables 5.4 and 5.5 respectively. The face labelling convention used in Table 5.3 is explained in Figure 5.4. The material parameters reported in Tables 5.3-5.5 are the Young's modulus E, the 0.2% and 1% proof stresses $\sigma_{0.2}$ and $\sigma_{1.0}$, respectively, the ultimate tensile stress σ_u, the plastic strain at fracture ε_f (based on elongation over the standard gauge length $5.65\sqrt{A}$, where A is the cross-sectional area of the coupon), and the strain hardening exponents n and $n'_{0.2,1.0}$ used in the compound Ramberg-Osgood material model (Mirambell and Real, 2000; Rasmussen, 2003; Gardner and Nethercot, 2004a).

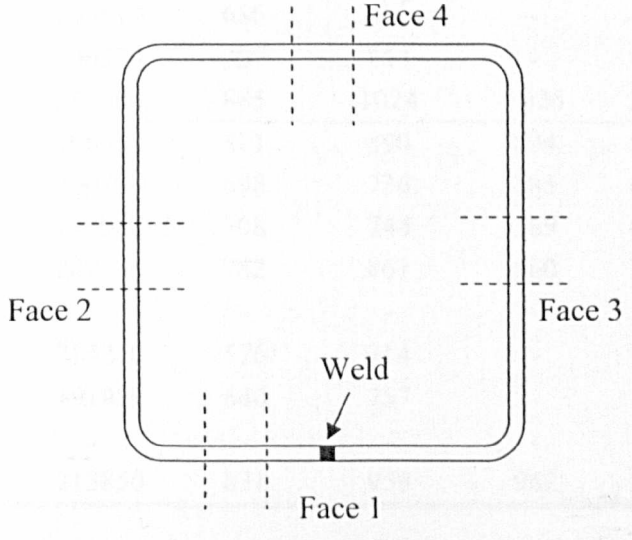

Figure 5.4: *Face labelling convention*

Table 5.3: *Individual coupon test results for each specimen*

Coupon	E (N/mm^2)	$\sigma_{0.2}$ (N/mm^2)	$\sigma_{1.0}$ (N/mm^2)	σ_u (N/mm^2)	ε_f %	Compound R-O coefficients	
						n	$n'_{0.2,1.0}$
100×100×4-TF-1	198820	614	736	767	48	9.0	2.4
100×100×4- TF-2	200160	552	595	748	46	9.2	2.2
100×100×4- TF-3	200180	569	611	760	45	10.7	2.7
100×100×4- TF-4	195920	609	666	767	49	7.1	3.8
100×100×4- CF-1	197330	587	662	-	-	6.9	2.4
100×100×4- CF-2	196040	513	613	-	-	6.1	2.8
100×100×4- CF-3	197180	507	609	-	-	5.9	2.7
100×100×4- CF-4	202410	635	685	-	-	14.3	2.5
100×100×4- TC	206000	811	912	917	32	6.3	4.1
80×80×4- TF-1	191900	686	753	777	40	5.6	5.0
80×80×4- TF-2	199070	665	710	745	42	7.3	3.3
80×80×4- TF-3	201270	642	687	757	43	7.6	3.6
80×80×4- TF-4	207220	723	795	812	44	5.8	4.8
80×80×4- CF-1	195460	692	787	-	-	4.8	2.1
80×80×4- CF-2	197460	622	734	-	-	4.6	2.6
80×80×4- CF-3	201130	630	742	-	-	4.6	2.8
80×80×4- CF-4	194750	684	816	-	-	4.9	2.7
80×80×4- TC	210000	731	942	959	24	5.6	3.7
60×60×3- TF-1	230960	825	906	935	47	5.5	5.1
60×60×3- TF-2	208920	717	770	790	44	5.1	4.1
60×60×3- TF-3	211800	742	793	814	36	6.3	4.0
60×60×3- TF-4	187390	736	809	817	49	7.0	4.0
60×60×3- CF-1	204450	739	869	-	-	6.0	2.7
60×60×3- CF-2	219940	712	860	-	-	4.2	3.1
60×60×3- CF-3	195610	686	811	-	-	4.5	2.3
60×60×3- CF-4	206370	707	844	-	-	5.3	2.7
60×60×3- TC	212400	885	1024	1026	22	6.3	4.0
80×40×4- TF-1	196610	811	890	894	52	7.3	4.3
80×40×4- TF-2	200700	698	736	785	63	10.9	2.9
80×40×4- TF-3	199080	708	744	789	45	11.6	2.7
80×40×4- TF-4	200830	782	861	860	33	8.4	4.7
80×40×4- CF-1	-	-	-	-	-	-	-
80×40×4- CF-2	215270	576	714	-	-	4.4	2.9
80×40×4- CF-3	191980	640	757	-	-	4.8	2.9
80×40×4- CF-4	-	-	-	-	-	-	-
80×40×4- TC	213850	831	959	962	26	4.4	4.0

Table 5.4: *Weighted average tensile flat material properties*

Cross-section	E (N/mm^2)	$\sigma_{0.2}$ (N/mm^2)	$\sigma_{1.0}$ (N/mm^2)	σ_u (N/mm^2)	ε_f %	Compound R-O	
						n	$n'_{0.2,1.0}$
SHS 100×100×4	198800	586	632	761	47	9.0	2.8
SHS 80×80×4	199900	679	736	773	42	6.5	4.2
SHS 60×60×3	209800	755	819	839	44	6.0	4.3
RHS 80×40×4	199500	734	785	817	50	10.1	3.4

Table 5.5: *Weighted average compressive flat material properties*

Cross-section	E	$\sigma_{0.2}$	$\sigma_{1.0}$	Compound R-O coefficients	
	(N/mm^2)	(N/mm^2)	(N/mm^2)	n	$n'_{0.2,1.0}$
SHS 100×100×4	198200	560	642	8.3	2.6
SHS 80×80×4	197200	657	770	4.7	2.6
SHS 60×60×3	206400	711	845	5.0	2.7
RHS 80×40×4	204000	607	734	4.6	2.9

A comparison between the measured the 0.2% and 1% proof stresses with those given in the mill certificates for the coil material is presented in Table 5.6. It should be noted that the properties reported in the mill certificates (see Table 5.2) were derived from tensile tests on transverse coupons (i.e. oriented perpendicularly to the rolling direction) and hence anisotropy inherently influences the comparisons displayed in Table 5.6. Furthermore, possible deviations regarding the strain rate to which the coupon tests were conducted may have also influenced the results. The generally enhanced strengths displayed by the coupons extracted from the complete cross-sections over those given by the mill certificates for the coil material relate largely to strain hardening during the cold-forming production process (Cruise and Gardner, 2008b). The weighted average stress-strain curves for SHS 100×100×4 are depicted in Figure 5.5 as a representative indication of the differences in stress-strain response displayed by tensile flat, compressive flat and tensile corner lean duplex stainless steel material.

Table 5.6: *Comparison of experimental results with mill certificates*

Cross-section	Tensile tests			Compressive tests	
	$\sigma_{0.2}$ / $\sigma_{0.2,mill}$	$\sigma_{1.0}$/ $\sigma_{1.0,mill}$	σ_u / $\sigma_{u,mill}$	$\sigma_{0.2}$ / $\sigma_{0.2,mill}$	$\sigma_{1.0}$ / $\sigma_{1.0,mill}$
SHS 100×100×4	0.97	0.96	0.98	0.93	0.98
SHS 80×80×4	1.26	1.22	1.03	1.22	1.27
SHS 60×60×3	1.32	1.28	1.09	1.25	1.32
RHS 80×40×4	1.36	1.30	1.09	1.12	1.21

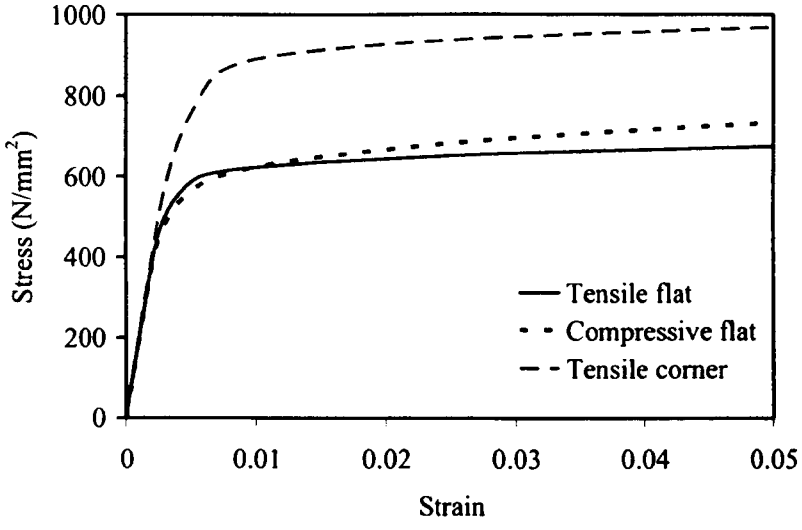

Figure 5.5: *Stress strain curves for flat tensile, flat compressive and corner tensile material extracted from SHS 100×100×4*

5.2.2 Stub column tests

Four section sizes were employed for the stub column tests, namely SHS 100×100×4, SHS 80×80×4, SHS 60×60×3 and RHS 80×40×4. Two repeated concentric compression tests were carried out for each of the cross-section sizes to enable the determination of a suitable Class 3 limit for lean duplex stainless steel internal elements in compression. All specimens were cold-rolled and seam welded. A stub column length equal to four times its mean nominal cross-sectional width was chosen, which is deemed long enough to include a representative pattern of residual stresses and geometric imperfections, yet short enough to avoid overall flexural buckling (Galambos, 1998).

Measurements of the basic geometry and initial geometric imperfections of the specimens were conducted prior to testing. The geometric imperfections measurements followed the procedure reported by Schafer and Peköz (1998a) and described in Chapter 4. As for the OHS, local geometric imperfections were measured only over the middle half of each specimen's length in order to eliminate the effect of end flaring, which results from the release of residual stresses following cutting operations (Cruise and Gardner, 2006). The maximum measured local geometric imperfection w_0 for each nominal stub column dimension is given in Table 5.7. Table 5.7 also includes the measured geometry of each stub column specimen, where L is the stub column length, B is the section width, H is the section depth, t is the thickness and r_i is the internal corner radius.

Table 5.7: *Measured dimensions of stub columns*

Specimen	L (mm)	B (mm)	H (mm)	t (mm)	r_i (mm)	A (mm^2)	w_0 (mm)
100×100×4-SC1	400.0	101.0	102.0	3.93	3.8	1495.2	0.071
100×100×4- SC2	400.0	102.0	103.0	3.97	3.9	1524.7	0.071
80×80×4- SC1	319.7	80.0	80.5	3.88	3.8	1147.4	0.080
80×80×4- SC2	332.2	80.0	80.0	3.81	3.6	1125.0	0.080
60×60×3- SC1	239.8	60.0	60.0	3.09	2.3	683.0	0.062
60×60×3- SC2	240.0	60.0	60.0	3.17	2.1	700.4	0.062
80×40×4- SC1	239.9	39.0	79.5	3.76	3.5	799.8	0.058
80×40×4- SC2	237.8	39.6	79.5	3.81	4.3	808.8	0.058

The employed instrumentation and the testing procedure followed were identical to those described in Chapter 3 for OHS stub column tests, as shown in Figure 5.6. Tests were continued beyond the ultimate load-carrying capacity of the stub columns and the post-ultimate response was recorded. The ultimate load and the corresponding end shortening at ultimate load are given in Table 5.8, while the full load-end shortening curves for the tested specimens are depicted in Figure 5.7. Note that the reported end shortening curves and the end-shortening values given in Table 5.8 refer to the true stub column shortening, obtained on the basis of the recorded LVDT and strain readings, according to the recommendations of the Centre for Advanced Structural Engineering (1990). Failure was due to local buckling though often after considerable plastic deformation; typical failure modes are depicted in Figure 5.8.

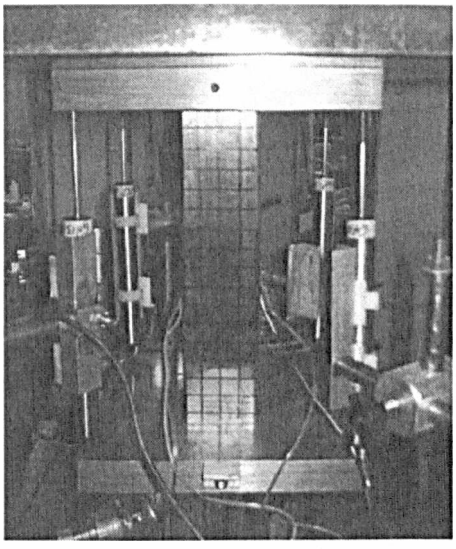

Figure 5.6: *Stub column testing apparatus*

Table 5.8: *Summary of test results for stub columns*

Specimen	Ultimate Load F_u (kN)	End shortening at ultimate load δ_u (mm)
100×100×4-SC1	1022	3.63
100×100×4- SC2	1037	4.01
80×80×4- SC1	923	4.13
80×80×4- SC2	915	3.88
60×60×3- SC1	613	4.09
60×60×3- SC2	616	3.69
80×40×4- SC1	709	4.33
80×40×4- SC2	710	4.12

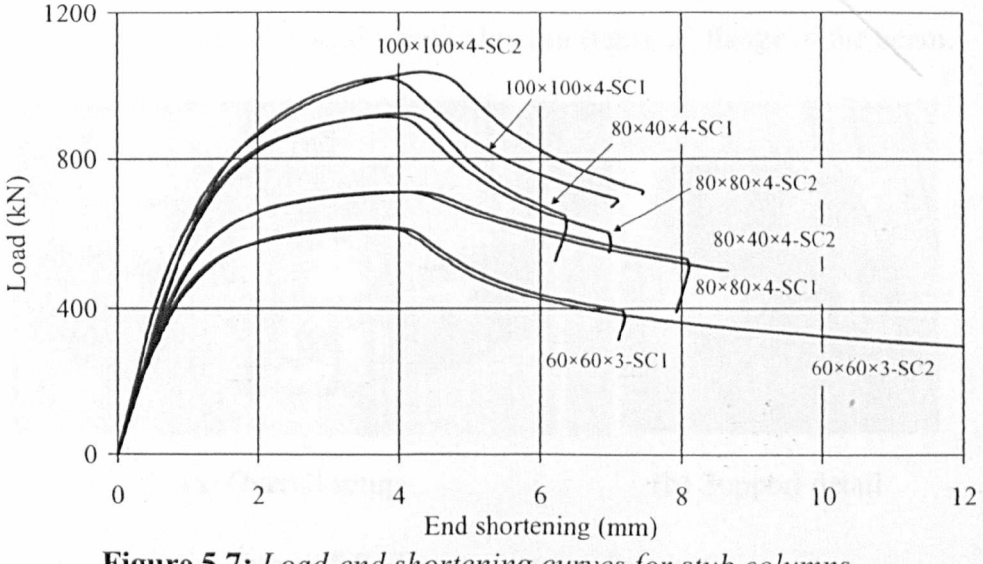

Figure 5.7: *Load-end shortening curves for stub columns*

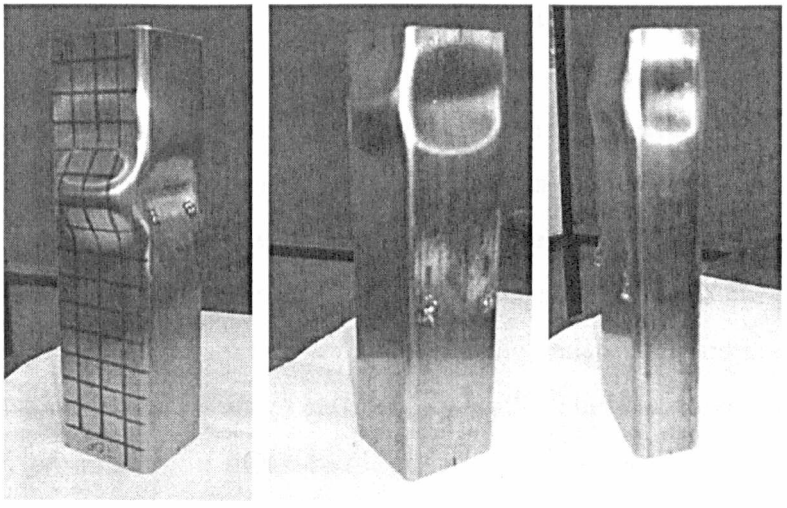

Figure 5.8: *Typical stub column failure modes (from left to right: 60×60×3-SC1, 80×80×4-SC1, 80×40×4-SC1)*

5.2.3 Beam tests

Three-point bending tests were conducted to obtain the basic flexural response characteristics of lean duplex stainless steel cross-sections and assess the applicability of American and European codified slenderness limits and effective width formulae. A total of eight 3-point bending tests (two repeated tests per cross-section labeled B1 and B2) were carried out. The beams had a total length of 1300 mm and were simply supported between rollers, which were placed 100 mm inward from each end of the beam and allow axial displacement of the beams' ends, as depicted in Figure 5.9, resulting in 1100 mm clear span between the centerlines of the supports. The rectangular hollow section – RHS 80×40×4 – was tested about its major axis. In all cases, the face containing the weld was the bottom (tension) flange of the beam.

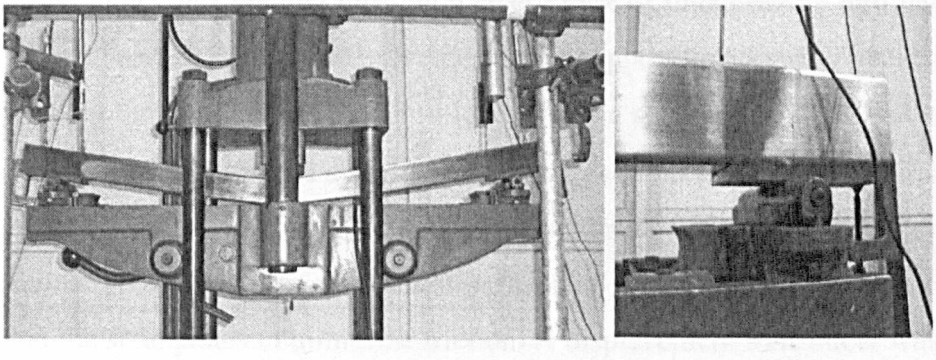

(a) Overall setup (b) Support detail

Figure 5.9: *Three-point bending tests*

Prior to testing, careful measurements of the geometry of the specimens, including initial geometric imperfections were taken. Only local imperfections were considered, since the nature and proportions of the test specimens precluded lateral tosrional buckling. Imperfection measurements were taken along the centerline of the faces of each nominal section size following the procedure described in Chapter 4. Similarly to the OHS beam tests, imperfection measurements were made over the central half of the specimen to eliminate the effect of flaring at the ends of the members due to the release of residual stresses upon cutting to length. The measured cross-sectional geometry and the maximum measured local geometric imperfection are reported in Table 5.9, where L is the length between centerlines of supports, B is the outer width of the section, D is the outer depth of the section, t is the thickness, r_i is the average internal corner radius and w_0 is the maximum measured local imperfection.

Table 5.9: *Measured dimensions of bending specimens*

Specimen	L (mm)	B (mm)	D (mm)	t (mm)	r_i (mm)	w_0 (mm)
100×100×4-B1	1100	103.0	102.3	3.92	3.8	0.071
100×100×4-B2	1100	102.0	102.5	3.83	3.9	0.071
80×80×4-B1	1100	80.0	79.5	3.76	3.5	0.080
80×80×4-B2	1100	80.0	79.6	3.74	4.3	0.080
60×60×3-B1	1100	60.0	60.0	3.15	2.3	0.062
60×60×3-B2	1100	60.0	60.0	3.10	2.8	0.062
80×40×4-B1	1100	39.0	80.0	3.78	3.6	0.058
80×40×4-B2	1100	39.5	80.0	3.84	3.9	0.058

Wooden blocks were placed within the tubes at the loading point to prevent web crippling, and load was applied through a steel block of thickness 15 mm and width 30 mm. Local bearing failure was prevented at the support locations by inserting steel plates between the specimens and the rollers, whilst a steel block of 100×60×25 was inserted between the crosshead and the specimens, thus ensuring a gradual dispersion of the stresses into the section. The loading point detail is depicted, together with a typical failure mode, in Figure 5.10. A thin layer of grease was applied between the rollers and the steel plates to minimize friction. A displacement transducer was placed at mid-span to measure the vertical deflection, while two further displacement transducers were positioned at a distance of 50 mm either side of the support at each

end of the specimens in order to determine the end rotation of the beams, as shown in Figure 5.9. Strain gauges were also affixed to the top and bottom flanges of the beams at a distance of 50 mm from the mid-span to measure the strain at the extreme tensile and compressive fibres of the cross-sections. The applied loading rate, in terms of crosshead movement rate, was 3 mm/min. Load, strain, displacement and input voltage were all recorded at 2 second intervals using the data acquisition system DATASCAN.

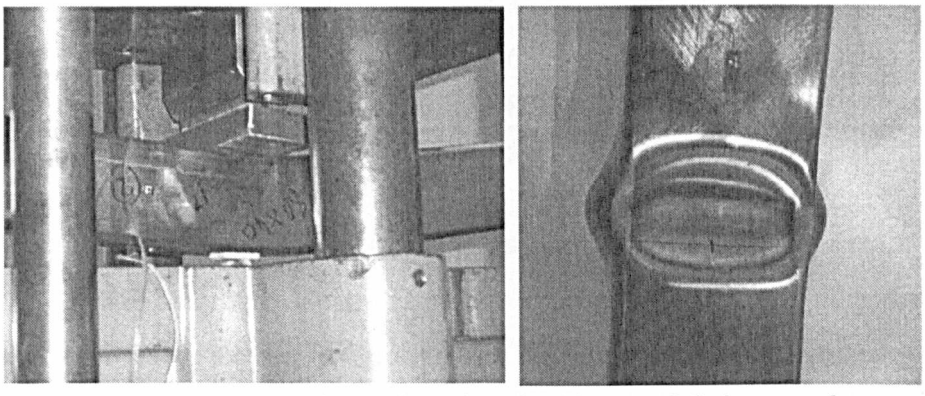

Figure 5.10: *Loading point detail and typical failure mode*

All key experimental results are summarised in Table 5.10, where the elastic and plastic moment capacities M_{el} and M_{pl} were calculated by multiplying the relevant section modulus with the weighted average tensile 0.2% proof stress $\sigma_{0.2}$ of the section, derived from tensile flat coupon tests. The rotation at midspan was assumed to equal the sum of the end rotations, since the observed deformation pattern involved significant localised rotations at mid-span (assumed plastic hinge position) with only negligible deformation occurring in the remainder of the specimen length. The rotation capacities R were evaluated according to Equation 5.1.

$$R = \frac{\theta_u}{\theta_{pl}} - 1 \tag{5.1}$$

in which θ_u is the total rotation at mid-span when the moment-rotation curve falls back below M_{pl} as obtained from the test results and θ_{pl} is the elastic part of the total rotation at midspan when M_{pl} is reached on the ascending branch, defined as $\theta_{pl} = \frac{M_{pl}L}{2EI}$, where I is the second moment of area of the section.

Table 5.10: *Summary of test results from 3-point bending tests*

Specimen	Ultimate moment M_u (kNm)	M_u/M_{el}	M_u/M_{pl}	Rotation capacity R
100×100×4-B1	39.1	1.42	1.21	2.79
100×100×4-B2	36.1	1.35	1.15	1.29
80×80×4-B1	24.9	1.39	1.18	1.35[a]
80×80×4-B2	24.3	1.38	1.16	1.29
60×60×3-B1	12.8	1.38	1.16	1.62
60×60×3-B2	12.9	1.41	1.18	1.94
80×40×4-B1	18.3	1.63	1.26	1.82[a]
80×40×4-B2	20.5	1.80	1.39	2.02[a]

[a] Full rotation capacity not attained; R based on maximum recorded deformation

In some cases (80×80×4-B1, 80×40×4-B1 and 80×40×4-B2) the ultimate rotation capacity was not recorded due to excessive deformations, which necessitated the premature termination of the test before the falling branch of the moment-rotation curve reached the value of M_{pl}. For these cases, the maximum recorded rotation was used instead of θ_u and the corresponding rotation capacities R are noted in Table 5.10. The recorded mid-span moment-rotation responses of the tested beams are depicted in Figure 5.11. All tested specimens failed by local buckling of the upper (compression) flange and the upper part of the web at midspan as shown in Figure 5.10.

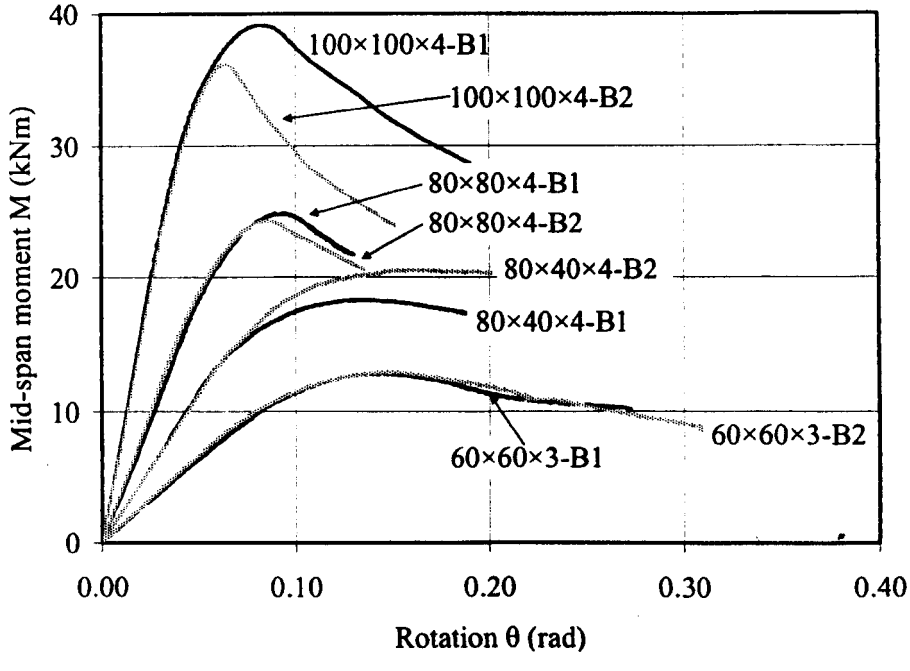

Figure 5.11: *Moment-rotation responses of specimens*

5.2.4 Flexural buckling tests

Having established the basic material and cross-sectional response, twelve flexural buckling tests were carried out in order to obtain ultimate load carrying capacity data. The tests were conducted on pin-ended columns with nominal cross-sectional dimensions of 80×80×4, 60×60×3 and 80×40×4, in a similar fashion to the flexural buckling tests described in Chapter 3. The employed instrumentation may be seen in Figure 5.12 and consisted of a load cell attached to the top knife edge, two pairs of LVDTs at each end of the column measuring end rotations and end shortening and two string pots attached at the mid-height of the columns measuring the lateral deflection of the specimens.

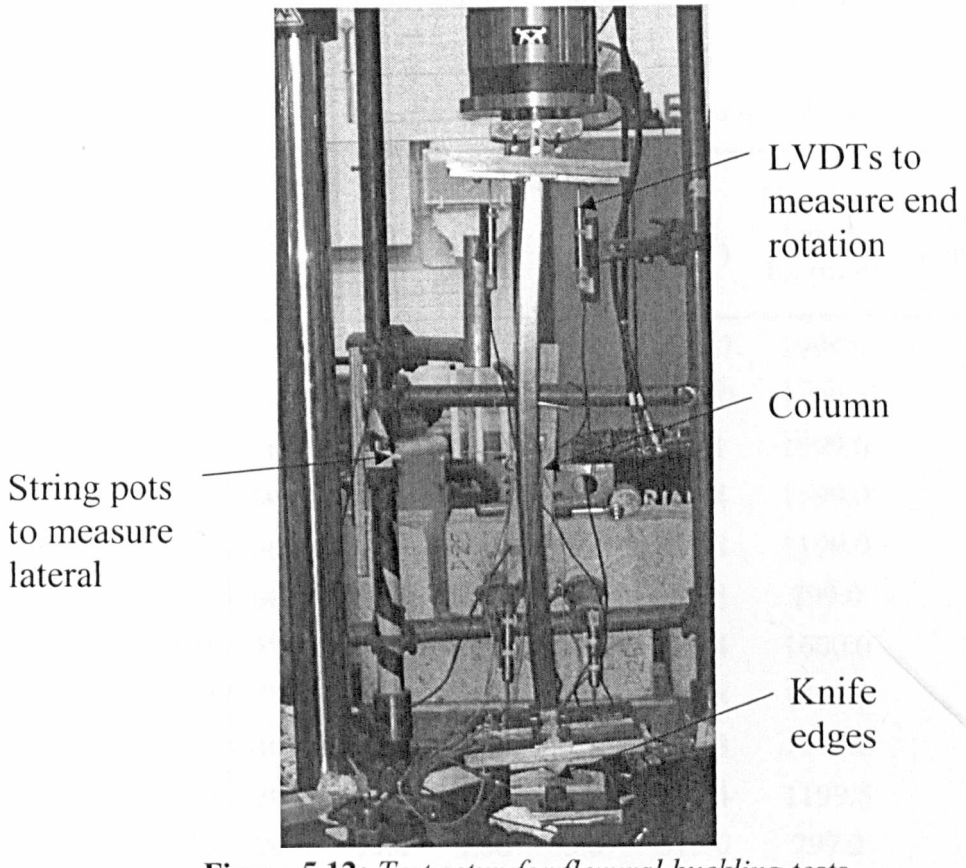

Figure 5.12: *Test setup for flexural buckling tests*

Both minor and major axis buckling were considered for the RHS 80×40×4 specimens. The specimen lengths were chosen such that the buckling lengths (i.e. total distance between knife edges) were equal to 800 mm, 1200 mm, 1600 mm and 2000 mm. This provided a range of non-dimensional member slendernesses, defined by Equation (5.2), in accordance with EN 1993-1-4 (2006), from 0.57 to 2.02.

$$\bar{\lambda} = \sqrt{A\sigma_{0.2}/N_{cr}} \tag{5.2}$$

where A is the cross-sectional area, $\sigma_{0.2}$ is the 0.2% proof stress and N_{cr} is the elastic critical buckling load of the column.

Measurements of the specimen geometry, including initial global geometric imperfections e_0 were conducted prior to testing and are reported in Table 5.11. The measured overall geometric imperfections were generally small and hence the load was applied eccentrically at the ends such that the combined effects of initial bow and loading eccentricity gave a total eccentricity at mid-height of L/1500, where L is the pin-ended column buckling length. This value is the statistical mean of geometric imperfections in steel structural members as reported by Bjorhovde (1972).

Table 5.11: *Measured geometric properties of columns*

Specimen	H (mm)	B (mm)	t (mm)	r_i (mm)	A (mm^2)	Buckling length L_{cr} (mm)	Global imperfection amplitude e_0 (mm)
80×80×4-2000	79.6	79.5	3.80	3.4	1116.7	1999.0	0.41
80×80×4-1200	79.3	79.6	3.72	3.8	1091.0	1199.5	0.10
60×60×3-2000	60.0	60.0	3.13	2.7	689.1	1999.0	0.31
60×60×3-1600	59.6	60.0	3.15	2.4	692.4	1599.0	0.32
60×60×3-1200	60.0	60.0	3.13	2.4	689.8	1199.0	0.26
60×60×3-800	60.0	60.0	3.13	2.4	690.8	799.0	0.23
80×40×4-MI-1600	39.0	79.2	3.80	4.3	800.4	1600.0	0.03
80×40×4-MJ-1600	79.5	39.3	3.95	4.0	835.8	1599.5	0.25
80×40×4-MI-1200	40.0	79.2	3.80	3.8	811.3	1199.0	0.15
80×40×4-MJ-1200	79.6	39.5	3.96	3.6	842.4	1199.5	0.13
80×40×4-MI-800	39.5	79.4	3.80	3.6	810.0	797.2	0.22
80×40×4-MJ-800	79.9	39.5	3.93	4.1	835.6	799.0	0.28

All columns failed by flexural buckling without any visible sign of local buckling. The full load-lateral displacement curves were recorded and are shown in Figures 5.13 and 5.14 for SHS and RHS columns respectively. The key results from the column tests, including the ultimate load and the lateral displacement at ultimate load are reported in Table 5.12. All obtained test results have been used in the validation

of the numerical models, as described hereafter, and are analysed and discussed in detail in Section 4 of the present Chapter.

Table 5.12: *Key results from flexural buckling tests*

Specimen	Non-dimensional slenderness $\bar{\lambda}$	Ultimate load F_u (kN)	Lateral deflection at F_u (mm)
80×80×4-2000	1.21	361.9	20.0
80×80×4-1200	0.73	672.5	4.7
60×60×3-2000	1.66	162.3	19.5
60×60×3-1600	1.34	231.7	15.4
60×60×3-1200	0.99	326.9	10.4
60×60×3-800	0.66	445.9	5.9
80×40×4-MI-1600	2.02	160.4	4.1
80×40×4-MJ-1600	1.14	406.3	3.8
80×40×4-MI-1200	1.47	237.4	9.9
80×40×4-MJ-1200	0.86	497.7	7.7
80×40×4-MI-800	0.99	366.6	9.0
80×40×4-MJ-800	0.57	546.2	6.3

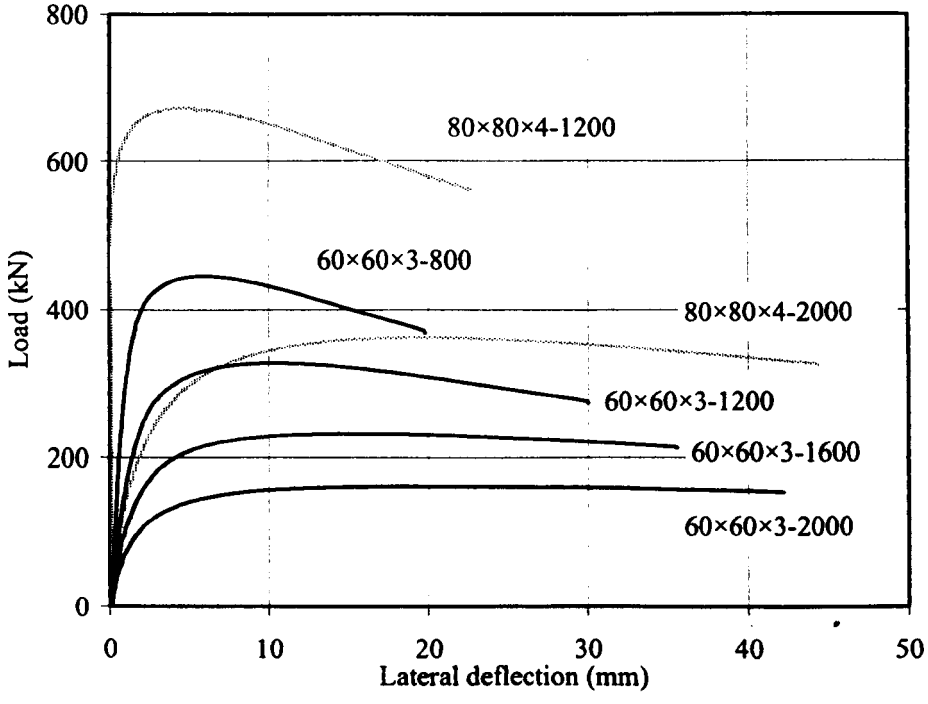

Figure 5.13: *Load-lateral displacement curves for SHS columns*

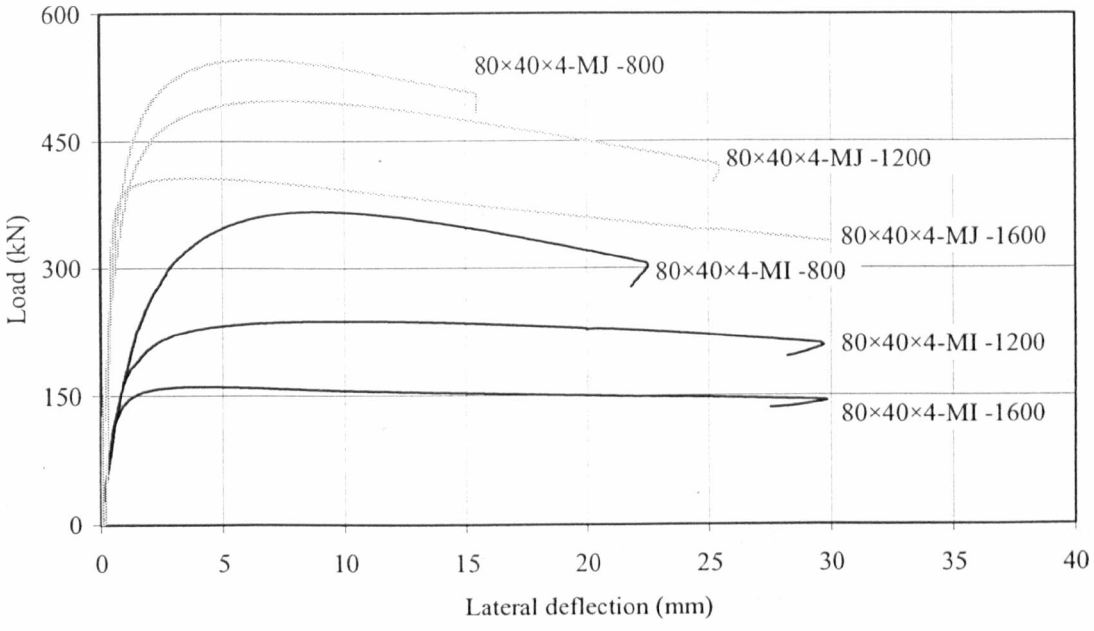

Figure 5.14: *Load-lateral displacement curves for RHS columns*

5.3 NUMERICAL MODELLING

5.3.1 Basic modelling assumptions

The tests reported in the previous section have been utilised to validate FE models and generate additional results by means of parametric studies, thus enabling a thorough assessment of the key parameters affecting the structural response of lean duplex stainless steel structural components. The general purpose finite element analysis package ABAQUS (2006) was used for all numerical studies reported herein. The FE simulations followed the guidelines regarding numerical modelling of stainless steel components reported proposed by Gardner and Nethercot (2004c) and Ashraf et al. (2006b) and were similar to those reported in Chapter 4. The employed modelling procedures regarding exploitation of symmetry, boundary conditions, employed element type, material modelling and residual stresses have been described in Chapter 4 and will not be repeated in this section.

The corner properties, as derived from the corner coupon tests, were assumed to extend up to a distance equal to two times the material thickness into the flat region of

each face of the models on either side of the corners, in accordance with Gardner and Nethercot (2004c) and Ashraf et al. (2006b). Two elements were utilised to discretise each of these flat parts adjacent to the corners and hence, in order to maintain a uniform mesh size within all flat parts of the models, an element size equal to the material thickness was required for all models. A coarser, non-uniform mesh was shown to yield results of similar accuracy but given the low computational cost associated with the finer mesh size, a uniform mesh was employed. Three linear elements were employed to approximate the geometry of the curved corners, which were assumed to be circular arcs.

The tensile corner properties (Table 5.3) were assigned to the corner regions and to the flat parts extending to a distance of two times the thickness beyond the corners for all stub column, beam and long column models, whilst the weighted average compressive flat material properties (Table 5.5) were assigned to all flat parts of the stub column and long column models, except for the flat parts adjacent to the corner regions. For the beam models the weighted average tensile flat material properties (Table 5.4) were assigned to the flat tensile regions of the models (i.e. below the neutral axis) and the compressive flat material properties (Table 5.5) were assigned to the flat compressive regions of the models (i.e. above the neutral axis), as shown in Figure 5.15.

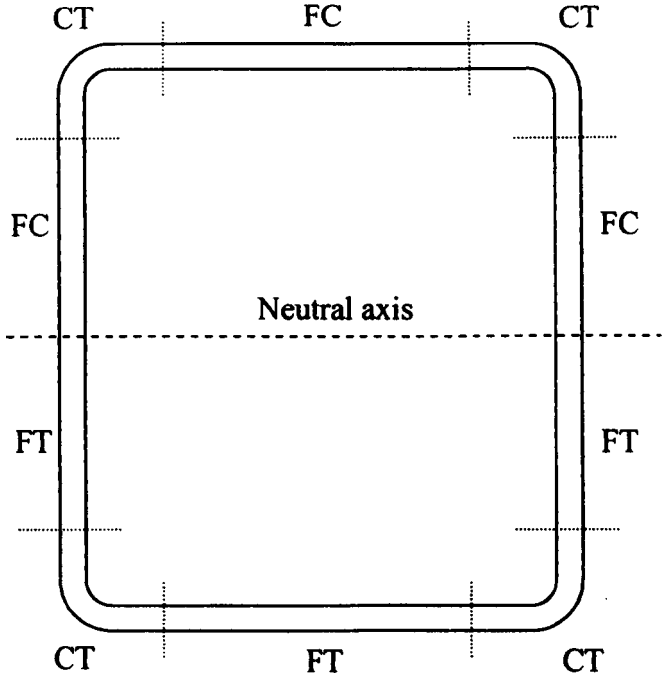

Figure 5.15: *Material properties assigned to the various parts of the beam cross-sections*

Based on the aforementioned modelling assumptions, a series of FE models were generated. Linear eigenvalue buckling analyses using the subspace iteration method were initially performed to extract the buckling mode shapes. These served as initial geometric imperfection patterns used in the subsequent geometrically and materially non-linear analyses. The modified Riks method, which is essentially a variation of the classical arc-length method, was employed for the non-linear analyses to enable the full load-deflection response, including into the post-ultimate range to be simulated.

The lowest local buckling mode shape was utilised to perturb the geometry of the stub column and beam models, while both the first local and first global mode shapes were introduced as geometric imperfections in the flexural buckling models. Four variations of the local imperfection amplitude were considered in the non-linear analyses; the maximum measured imperfection reported in Tables 5.7 and 5.9 for stub columns and beams respectively, 1/10 and 1/100 of the cross-sectional thickness and the imperfection amplitude derived from the predictive model of Dawson and Walker (1972) as adapted for stainless steels by Gardner and Nethercot (2004c), given by Equation (5.3)

$$w_0 = 0.023\left(\frac{\sigma_{0.2}}{\sigma_{cr}}\right)t \tag{5.3}$$

where $\sigma_{0.2}$ is the tensile 0.2% proof stress given in Table 5.4 and σ_{cr} is the elastic critical buckling stress of the most slender of the constituent plate element in the section, determined on the basis of the flat width of the element. Ideally, the constant multiplier in Equation (5.3) is determined by regression analysis on available test data, however, due to the limited measured imperfection data for lean duplex stainless steel, the small plate slenderness range of the specimens considered in this research and the inherent scatter in geometric imperfection measurements, it was decided to adopt the value of 0.023 proposed by Gardner and Nethercot (2004c) for austenitic stainless steels. For the global imperfection amplitudes employed for the long column models, four fractions of the respective buckling length were considered, namely L/500, L/1000, L/1500 and L/2000, noting that L/1500 represents the experimental imperfection.

5.3.2 Validation of models

In this section the results of the numerical simulations and the tests are compared, and the sensitivity of the models to the key modelling parameters, particularly the imperfection amplitudes, are examined. Comparisons with the test results are made to assess the accuracy of the models and verify their suitability for performing parametric studies.

5.3.2.1 Stub columns

Table 5.13 presents the ratios of the numerical to experimental ultimate loads and corresponding displacements at ultimate load for the varying imperfection amplitudes. The ultimate load is generally well-predicted for the measured imperfection amplitude, the amplitude predicted by the Dawson and Walker model (Equation (5.3)) and t/100, whereas the use of the t/10 value results in a clear underestimation of the load carrying capacity of the stub columns. The end shortening at ultimate load appears to be more sensitive to the initial imperfection amplitude and is best predicted when an imperfection amplitude from the Dawson and Walker model or t/100 is used. The Dawson and Walker model predicts imperfection amplitudes on the basis of both geometric and material properties of cross-sections. It has been shown, as in the current study, to provide suitable local imperfections for inclusion in numerical models to accurately simulate tests (Gardner and Nethercot, 2004c; Asraf et al., 2006b; Gardner et al., 2006), and to provide a means of predicting measured imperfection amplitudes directly (Cruise and Gardner, 2006). This model was therefore employed in the parametric studies described herein to derive local imperfection amplitudes for both the stub columns and long columns.

Overall excellent agreement between the experimental stub column results and those obtained from the FE simulations was achieved; the compressive response was accurately predicted throughout the full loading history, including initial stiffness, ultimate load, displacement at ultimate load and post-ultimate response. Figures 5.16 and 5.17 depict the experimental and numerical load-end shortening curves using the imperfection amplitude predicted by the Dawson and Walker model for the 80×40×4-

SC2 and 80×80×4-SC2 stub columns, whereas a comparison of experimental and numerical failure modes is displayed in Figure 5.18.

Table 5.13: *Comparison of the stub column test results with FE results for varying imperfection amplitudes*

Stub column designation	Measured amplitude w_0		t/10		t/100		Dawson and Walker model	
	FE F_u/ Test F_u	FE δ_u / Test δ_u	FE F_u/ Test F_u	FE δ_u / Test δ_u	FE F_u/ Test F_u	FE δ_u / Test δ_u	FE F_u/ Test F_u	FE δ_u/ Test δ_u
100×100×4-SC1	0.95	0.71	0.86	0.61	0.98	0.78	0.97	0.73
100×100×4- SC2	0.96	0.64	0.87	0.50	0.98	0.70	0.98	0.69
80×80×4- SC1	1.00	0.68	0.92	0.45	1.01	0.75	1.02	0.80
80×80×4- SC2	1.02	0.81	0.95	0.57	1.05	0.96	1.06	0.98
60×60×3- SC1	0.97	0.86	0.90	0.54	0.98	0.91	0.98	0.91
60×60×3- SC2	0.99	0.89	0.93	0.57	1.00	0.99	1.00	1.02
80×40×4- SC1	1.00	0.83	0.90	0.55	1.03	0.93	1.03	0.93
80×40×4- SC2	0.97	0.76	0.89	0.61	1.01	1.03	1.01	1.04
Mean	0.98	0.77	0.90	0.55	1.00	0.88	1.01	0.89
COV	0.02	0.12	0.03	0.10	0.03	0.14	0.03	0.15

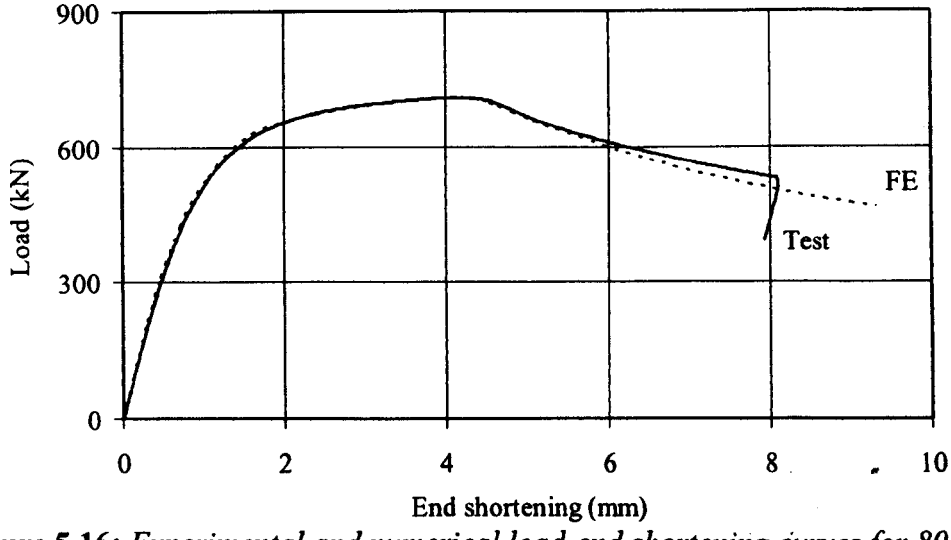

Figure 5.16: *Experimental and numerical load-end shortening curves for 80×40×4-SC2*

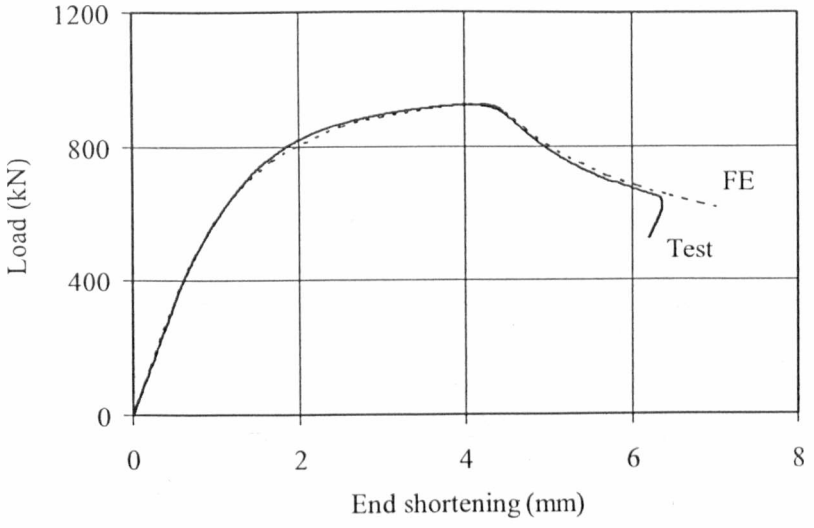

Figure 5.17: *Experimental and numerical load-end shortening curves for 80×80×4-SC2*

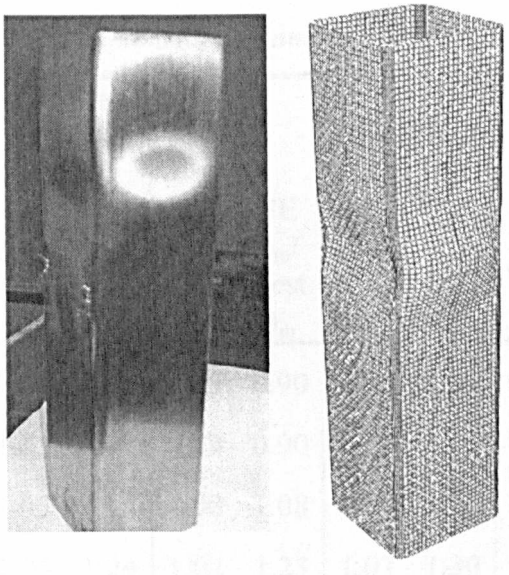

Figure 5.18: *Experimental and FE failure modes for SHS 80×80×4-SC2*

5.3.2.2 Beams

For the beam models, the accuracy of the numerical results was assessed by comparing the maximum moment M_u and the corresponding rotation at maximum moment θ_m at the plastic hinge location (defined as the sum of the end rotations of the beam) with the respective test values. The full moment-rotation curves and the mode of failure were also compared. The results are tabulated in Table 5.14 for the various imperfection amplitudes considered. The incorporated imperfection amplitude can be

seen to have only a modest effect on the ultimate moment capacity, whereas the rotation at ultimate moment seems to be more sensitive. In all cases, the initial stiffness, failure mode and the general shape of the moment-rotation curves of the FE models closely matched those obtained from experiments. Overall, good agreement between experimental and numerical results can be observed, particularly in terms of the predicted ultimate moment capacity; the rotation at the plastic hinge is less accurately, but acceptably, predicted. A typical numerical and experimental failure mode (specimen 60×60×3-B2) is depicted in Figure 5.19; both failure modes display local buckling in the compression flange and the upper part of the web. The corresponding experimental and numerical moment-rotation curves are depicted in Figure 5.20.

Table 5.14: *Comparison of the in-plane bending test results with FE results for varying imperfection amplitudes*

Beam specimen designation	Measured amplitude w_0		t/10		t/100		Dawson and Walker	
	FE M_u/ Test M_u	FE θ_m/ Test θ_m	FE M_u/ Test M_u	FE θ_m/ Test θ_m	FE M_u/ Test M_u	FE θ_m/ Test θ_m	FE M_u/ Test M_u	FE θ_m/ Test θ_m
100×100×4-B1	0.99	0.86	0.95	0.90	0.99	0.86	0.99	0.86
100×100×4-B2	1.02	1.01	0.99	0.90	1.03	1.01	1.01	0.90
80×80×4-B1	1.05	1.24	1.00	1.08	1.05	1.19	1.05	1.19
80×80×4-B2	1.06	1.24	1.02	1.23	1.07	1.30	1.07	1.30
60×60×3-B1	0.99	0.98	0.97	0.89	1.01	1.05	1.01	1.05
60×60×3-B2	1.00	1.01	0.97	0.88	1.00	1.04	1.00	1.01
80×40×4-B1	1.02	1.40	1.00	0.99	1.02	1.34	1.02	1.40
80×40×4-B2	0.92	1.04	0.90	0.86	0.92	1.04	0.93	1.04
Mean	1.01	1.10	0.97	0.97	1.01	1.10	1.01	1.10
COV	0.04	0.16	0.04	0.13	0.04	0.14	0.04	0.17

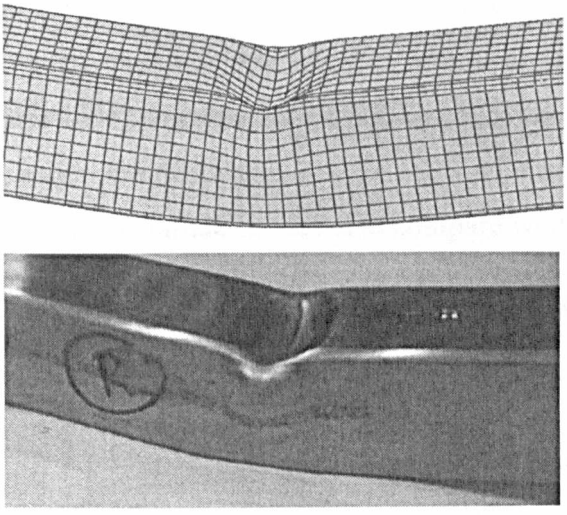

Figure 5.19: *Experimental and numerical failure modes for SHS 60×60×3-B2*

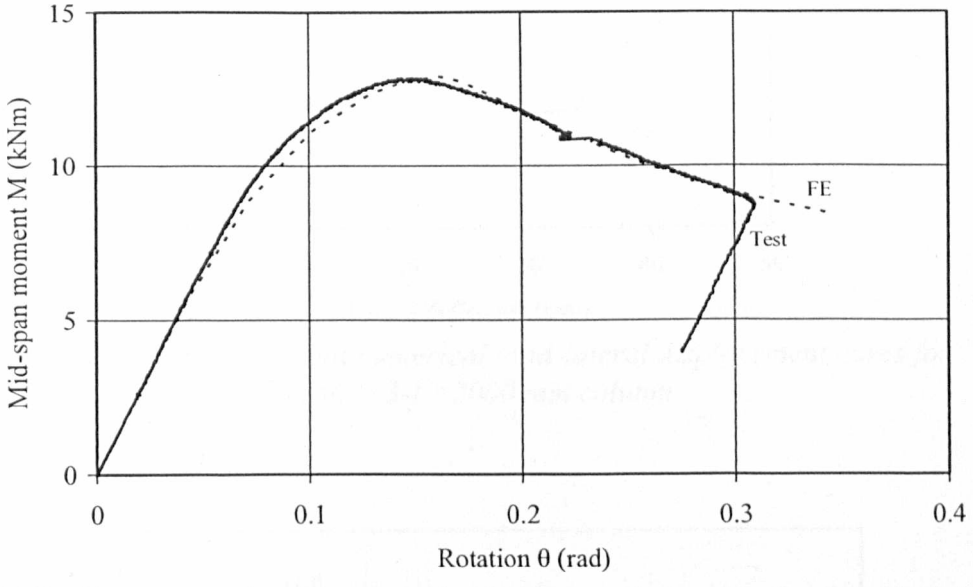

Figure 5.20: *Experimental and numerical moment-rotation curves for 60×60×3-B2*

5.3.2.3 Columns

Good agreement between test and numerical results is also displayed for the flexural buckling specimens. Comparisons are shown in Table 5.15, where it may be seen, as expected, that the ratio of the numerically predicted ultimate buckling load to the experimental buckling load is clearly influenced by the assumed initial global imperfection amplitude. The most accurate and consistent prediction of test response is obtained for an imperfection amplitude of L/1500, which coincides with the total

imperfection amplitude (initial bow imperfection plus eccentricity) present in the tests. Comparisons between experimental and FE results in terms of load versus lateral deflection are depicted in Figures 5.21, 5.22 and 5.23 for an SHS column, an RHS column buckling about the major axis and an RHS column buckling about the minor axis, respectively. The FE failure modes also compare well with the test failure modes, as displayed in Figure 5.24.

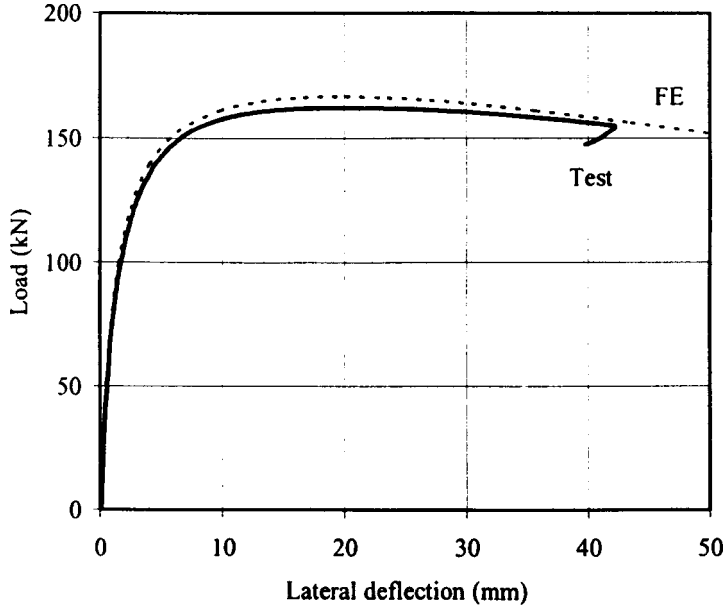

Figure 5.21: *Experimental and numerical load-lateral displacement cures for SHS60×60×3-L=2000 mm column*

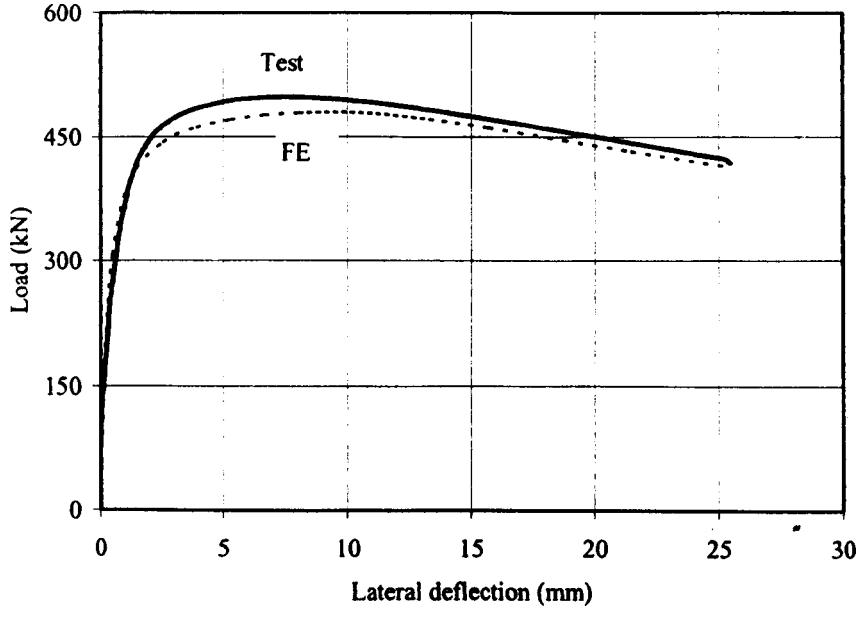

Figure 5.22: *Experimental and numerical load-lateral displacement cures for 80×80×4-MJ-L=1200 mm column*

Table 5.15: *Comparison of the column test results with FE results for varying imperfection amplitudes*

Specimen	FE F_u/ Test F_u			
	L/500	L/1000	L/1500	L/2000
80×80×4-2000	0.96	1.03	1.06	1.08
80×80×4-1200	0.89	0.94	0.95	0.96
60×60×3-2000	0.94	1.00	1.03	1.04
60×60×3-1600	0.93	0.99	1.02	1.04
60×60×3-1200	0.94	1.00	1.03	1.04
60×60×3-800	0.99	1.01	1.02	1.03
80×40×4-MI-1600	0.81	0.87	0.89	0.90
80×40×4-MJ-1600	0.85	0.90	0.93	0.94
80×40×4-MI-1200	0.87	0.93	0.96	0.97
80×40×4-MJ-1200	0.90	0.94	0.96	0.98
80×40×4-MI-800	0.92	0.97	0.99	1.00
80×40×4-MJ-800	1.01	1.05	1.07	1.08
Mean	0.92	0.97	0.99	1.01
COV	0.06	0.06	0.05	0.05

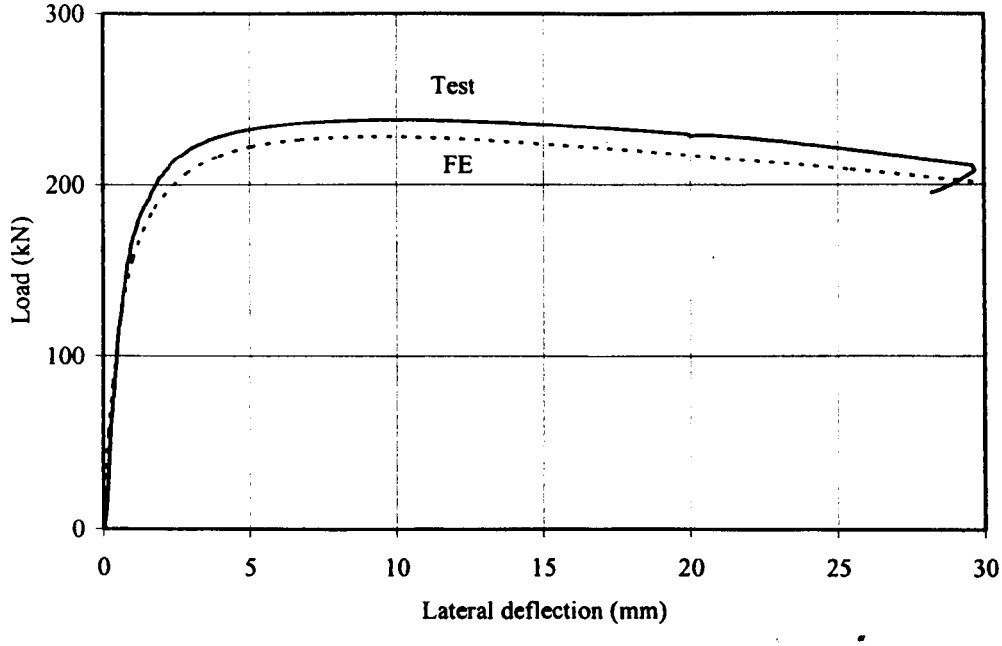

Figure 5.23: *Experimental and numerical load-lateral displacement cures for 80×80×4-MI-L=1200 mm column*

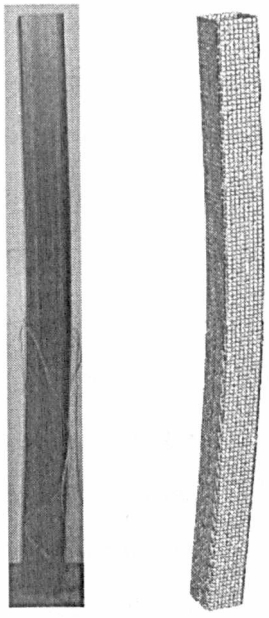

Figure 5.24: *Experimental and FE failure modes for SHS 80×80×4-L=1600 mm column*

5.3.3 Parametric studies

Upon validation of the FE models, parametric studies were conducted to expand the available results over a wider cross-section and member slenderness range and investigate the effect of key factors on the structural response of lean duplex stainless steel compression and flexural members. The generated models adhere to the basic modelling assumptions stated in Section 5.3.1. The material properties adopted in the FE parametric studies were based on the averaged experimental material stress-strain curves. Similarly to validation of the modes, the different material properties (tensile flat, tensile corner and compressive flat) were applied to the appropriate regions of the cross-sections. Local geometric imperfections in the form of the lowest buckling mode shape with an amplitude derived from Equation (5.3) were incorporated for stub column, beam and flexural buckling models, whereas the global imperfection amplitude of the long columns was taken as L/1500.

All stub column and long column cross-sections considered in the parametric studies had an outer width B equal to 100 mm and an outer height H equal to either 100 mm or 200 mm, thereby resulting into aspect ratios of 1.0 and 2.0. The length of the stub column models was set equal to four times their mean outer dimension, hence 400

mm for the SHS and 600 mm for the RHS models, while their thickness varied from 1.6 mm to 13.0 mm to encompass a wide range of cross-sectional slendernesses. The cross-section slenderness was defined as $c/t\varepsilon$ in accordance with EN 1993-1-4 (2006), where c is the flat element width, t is the element thickness and $\varepsilon = \sqrt{(235/f_y)(E/210000)}$.

The modelled beam cross-sections had an overall depth D of 100 mm and an overall width B of either 100 mm or 50 mm thereby generating aspect ratios of 1.0 and 2.0 respectively. The thickness was varied between 0.82 mm and 3.25 mm for the 100×50 cross-sections and between 1.64 mm and 6.51 mm for the 100×100 cross-sections to provide a practical range of slenderness. For each cross-section considered, two beams with lengths of 1000 mm and 2000 mm were analysed in order to assess the effect of moment gradient on the rotation capacity of lean duplex stainless steel beams, which has been found to be quite significant in similar studies on carbon steel flexural members (Kuhlmann, 1989).

Regarding the flexural buckling models, constant thicknesses of 4.75 mm and 9.50 mm were selected for the 100×100 and 100×200 cross-sections respectively, resulting in Class 3 cross-sections according to the slenderness limits given in EN 1993-1-4 (2006) - the actual $c/t\varepsilon$ ratio was 30, compared to the Class 3 slenderness limit of 30.7. The buckling length of the columns was varied to cover a wide spectrum of member slendernesses ranging from 0.4 to 2.4. The generated numerical results are presented and discussed in the following section.

5.4 DISCUSSION AND DESIGN RECOMMENDATIONS

5.4.1 Introduction

In this section, the applicability of the provisions of EN 1993-1-4 (2006), including the Class 3 slenderness limit and effective width formula for internal elements subjected to compression or bending and the buckling curve for hollow section columns to lean duplex stainless steel structural components is assessed on the basis

of both the experimental and numerical results reported herein. The American (SEI/ASCE 8-02, 2002) and Australian/New Zealand (AS/NZS 4673, 2001) design provisions for flexural members are also assessed on the basis of the beam test and FE results. Furthermore, the modified slenderness limits and effective width formulae for stainless steel cross-sections (Gardner and Theofanous, 2008), discussed in Chapter 3, are also assessed. Finally, comparisons of the structural performance of lean duplex stainless steel with that of the more common stainless steel grades in construction are made. In all code comparisons, the measured tensile material properties derived for each cross-section from flat tensile coupon tests were utilised.

5.4.2 Cross-sections in compression

The obtained test and FE data were used to assess the applicability of the codified slenderness limits to lean duplex stainless steel elements. For all experimental and numerical stub column results, the ultimate load divided by the squash load, $F_u/A\sigma_{0.2}$, is plotted against the slenderness of the most slender constituent element in the cross-section in Figure 5.25, where the respective Class 3 limits for carbon steel and stainless steel specified by EN 1993-1-1 (2003) and EN 1993-1-4 (2006), as well as the Class 3 limit proposed by Gardner and Theofanous (2008) (reported in Chapter 3) are also included.

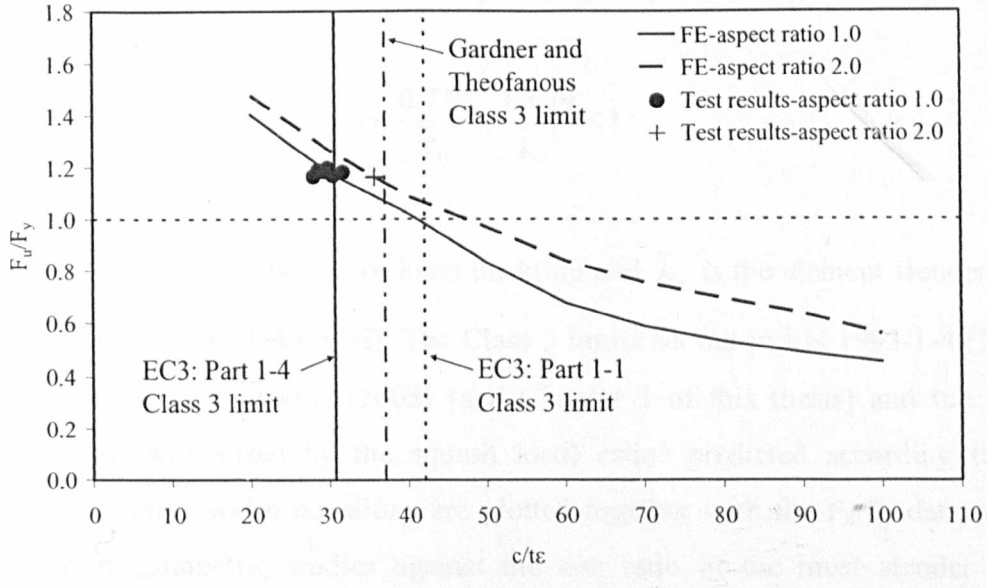

Figure 5.25: *Current and proposed Class 3 slenderness limit for internal elements in compression*

As shown in Figure 5.25, the RHS (H/B=2.0) display superior load carrying capacity to their SHS (H/B=1.0) counterparts of equal cross-sectional slenderness (i.e. c/tε). This is due to the higher level of restraint offered by the narrow faces to the wider (more slender) faces of the RHS and the potential for stress redistribution once local buckling of the wider face plates occurs. For simplicity, the effect of element interaction on the cross-sectional response is not accounted for in EN 1993 -1-4 (2006) and a conservative cross-section classification approach is specified, as discussed in detail in Chapter 3, where more advanced approaches accounting for element interaction are also outlined. Within the current cross-section classification approach codified in EN 1993-1-4, the Class 3 limit (i.e. the limit below which an element can be assumed to be fully effective) of 30.7ε is conservative and could be relaxed to 37ε, as proposed by Gardner and Theofanous (2008) for other grades of stainless steel.

Slender (Class 4) cross-sections are treated in EN 1993-1-4 (2006) following the Von Karman effective width approach, as modified according to experimental data by Winter (1947, 1950) and Johnson and Winter (1966), to account for the occurrence of local buckling prior to reaching the 0.2% proof strength. The effective width equation for internal elements given in EN 1993-1-4 (2006) is compatible with the corresponding codified Class 3 limit of 30.7ε, which has been shown to be rather conservative. For consistency with the revised limit of 37ε, a revised effective width equation, given by Equation (5.4) was proposed in Chapter 3.

$$\rho = \frac{0.772}{\bar{\lambda}_p} - \frac{0.079}{\bar{\lambda}_p^2} \leq 1 \tag{5.4}$$

where ρ is the reduction factor for local buckling and $\bar{\lambda}_p$ is the element slenderness, as defined in EN 1993-1-4 (2006). The Class 3 limits set out in EN 1993-1-4 (2006) and Gardner and Theofanous (2008) (and Chapter 3 of this thesis) and the F_u/F_y (ultimate load normalised by the squash load) ratios predicted according to the respective effective width equations are plotted together with the F_u/F_y data points derived from parametric studies against the c/tε ratio of the most slender plate element in Figure 5.26. The results confirm the adequacy but conservatism of the

current EN 1993-1-4 (2006) provisions and the applicability of the proposed revised formula.

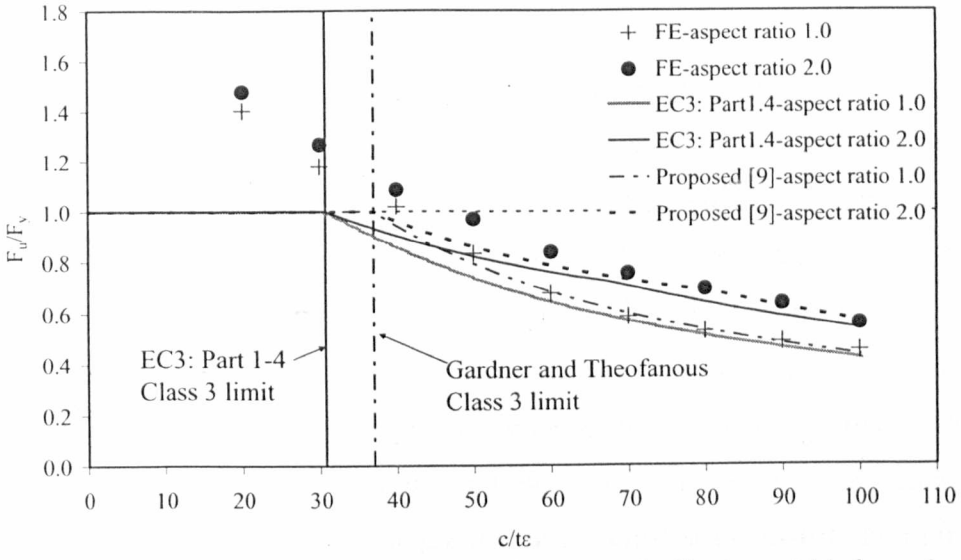

Figure 5.26: *Assessment of EC3: Part 1.4 and proposed effective width formulae for internal elements*

5.4.3 Cross-sections in bending

The obtained test and FE results are compared with the current European, American and Australian/New Zealand design provisions to assess their applicability to lean duplex stainless steel flexural members. The basic features of the cross-section classification process were discussed in detail in Chapter 3 and were briefly outlined in Chapter 4; hence they will not be repeated in this chapter. Since comparisons with the American (SEI/ASCE 8-02, 2002) and Australian /New Zealand (NZS 4673, 2001) code predictions for stainless steel flexural members are made, a brief outline of the respective codified provisions is given herein.

5.4.3.1 American and Australian/New Zealand design provisions for flexural members

The American specification for the design of cold-formed stainless steel structural members, SEI/ASCE 8-02 (2002), provides two alternative procedures for the

determination of flexural capacity. The first procedure, which is similar to the European treatment for Class 3 and Class 4 cross-sections, is based on the initiation of yielding and assumes a linear stress distribution throughout the cross-section with the yield stress as the maximum allowable stress. A slenderness limit is given, beyond which loss of effectiveness occurs and an effective width formula applies. Unlike the European specification, which employs different effective width formulae for internal elements, cold-formed outstand elements and welded outstand elements, a single effective width formula for all plated elements is specified in SEI/ASCE 8-02 (2002). The second procedure utilises the inelastic reserve capacity brought about by the spread of plasticity through the section. This additional capacity may be exploited when certain criteria regarding web slenderness, shear stresses, cross-sectional geometry and the elimination of other possible modes of instability are met. The moment capacity is determined by integrating an assumed stress distribution through the depth of the cross-section, accounting for possible loss of effectiveness by means of effective widths. The plastic moment capacity specified in EN 1993-1-4 (2006) is an upper bound to the design resistance calculated with this method. The second design procedure (based on inelastic reserve capacity) specified by SEI/ASCE 8-02 (2002) has been used where applicable to obtain the flexural resistance.

The Australian/New Zealand design specifications for structural stainless steel AS/NZS 4673 (2001) are in essence the same as to the SEI/ASCE 8-02 (2002) specification, with the only difference lying in additional design provisions specified for tubular members. These provisions allow the attainment of a cross-sections' plastic moment resistance M_{pl}, provided that flange and web slendernesses conform to codified slenderness limits, similarly to EN 1993-1-4 (2006). No provisions for a Class 1 limit are given in either the American or the Australian/New Zealand design standard.

5.4.3.2 Fully effective (Class 3) cross-sections

The suitability of the slenderness limits for fully effective (Class 3) sections is assessed. The moment capacity M_u obtained from the tests and FE analyses is normalised by the elastic moment capacity M_{el} and plotted against the slenderness

parameter c/tε of the most slender constituent plate element of the section (which in all cases was the flange) in Figure 5.27. The slenderness parameter c/tε is specified in Eurocode 3: Part-1-4, where c is the flat width of the plate element considered, t is the plate thickness and $\varepsilon = \sqrt{\frac{235}{\sigma_{0.2}}\frac{E}{210000}}$, $\sigma_{0.2}$ being the 0.2% proof stress and E being the Young's modulus. For internal simply supported elements (buckling factor k_σ=4) the relationship defined by Equations (5.5) between the European measure of slenderness c/tε and the slenderness parameter λ, specified in both the SEI/ASCE 8-02 (2002) and AS/NZS 4673 (2001) holds:

$$\frac{c}{t\varepsilon} = 56.83\lambda \tag{5.5}$$

The Class 3 limit specified in EN 1993-1-4 (2006) is 30.7, whereas the equivalent Class 3 limit of the SEI/ASCE-8 (2002) and AS/NZS 4673 (2001) is 38.3. The Class 3 limit proposed in Chapter 3 for internal elements in compression was 37, which is very close to the slenderness limit of 38.3 codified in both SEI/ASCE-8 (2002) and AS/NZS 4673 (2001).

All three limiting slenderness values are plotted together with the test and FE results in Figure 5.27. The SHS (D/B=1) may be seen to achieve higher normalised moment resistances than their RHS (D/B=2) counterparts with the same flange slenderness, particularly in the slender range of the graph. This is attributed to the lower web slenderness and the greater degree of restraint provided by the webs to the flanges, which delays the onset of local buckling, particularly for flanges of high slenderness, where failure occurs largely within the elastic material range. With decreasing slenderness, higher strains are achieved at ultimate moment and the stiffness is eroded by plasticity, which, in turn, reduces the restraint afforded to the flange. The moment gradient may be seen to have a minimal effect on moment capacity. Similar observations were made for carbon steel beams by Kuhlmann (1989). It can be concluded that the slenderness limit of 30.7 given in EN 1993-1-4 (2006) is overly conservative, whereas the SEI/ASCE-8 (2002) and AS/NZS 4673 (2001) limit and that proposed in Chapter 3 appear more suitable.

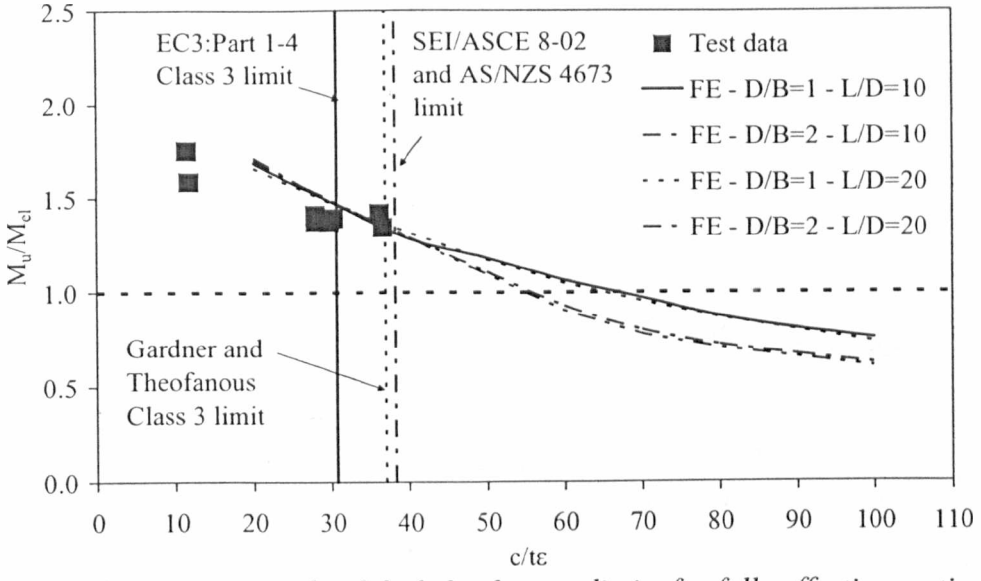

Figure 5.27: *Assessment of codified slenderness limits for fully effective sections (Class 3 sections)*

Figures 5.28 and 5.29 compare the test and FE results with various moment capacity predictions for SHS (D/B=1) and RHS (D/B=2) respectively. In addition to the provisions of EN 1993-1-4 (2006), SEI/ASCE 8-02 (2002) and AS/NZS 4673 (2001), predictions of the flexural capacity based on the revised effective width Equation (5.4) and on the continuous strength method (CSM) are included. The basic features and merits of the CSM have been discussed in Chapter 3. It should be noted that the curves depicted on Figures 5.28 and 5.29 correspond to the original CSM (i.e. without accounting for element interaction).

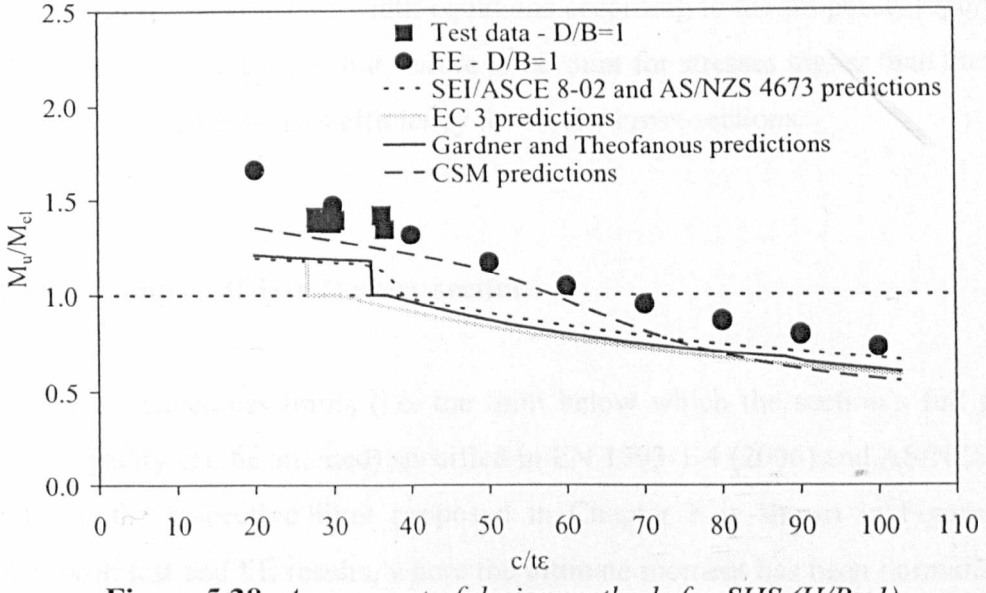

Figure 5.28: *Assessment of design methods for SHS (H/B=1)*

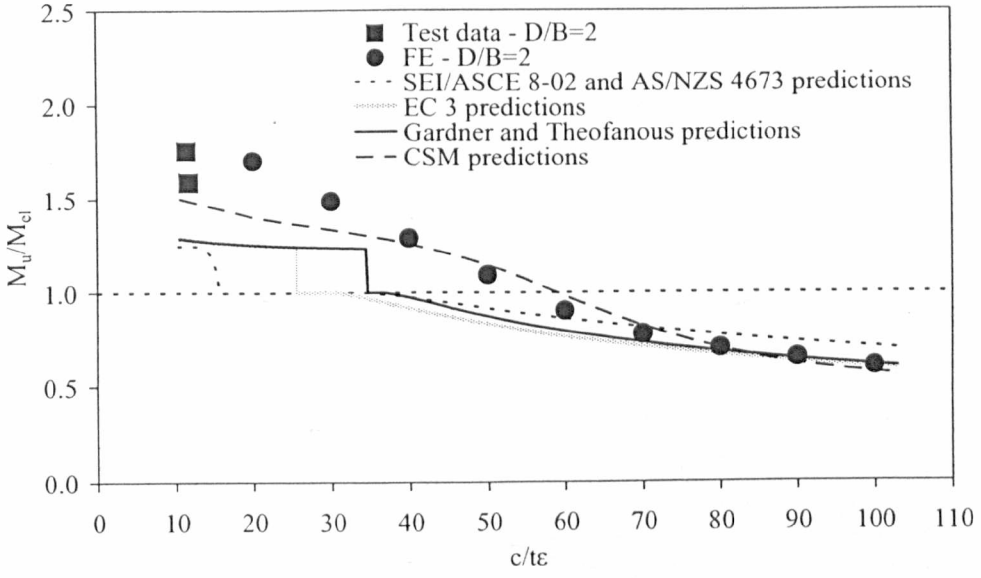

Figure 5.29: *Assessment of design methods for RHS (H/B=2)*

The CSM can be seen to most accurately predict the flexural capacity of the stainless steel beams, particularly in the stocky slenderness range, where stresses far beyond the 0.2% proof stress are reached. The SEI/ASCE 8-02 (2002) and AS/NZS 4673 (2001) predictions compare well with the test and FE results when the design procedure based on inelastic reserve capacity is applicable, whereas the procedure based on the initiation of yielding significantly underestimates the actual structural response of cross-sections with deep webs. The EN 1993-1-4 (2006) method offers good agreement with the test and FE data in the slender range but is unduly conservative for stocky cross-sections due to the strict Class 3 limit adopted. Relaxing the Class 3 limit and effective width equations according to the proposals reported in Chapter 3 improves accuracy, but failure to account for stresses higher than the 0.2% proof stress still compromises efficiency for stocky cross-sections.

5.4.3.3 Compact (Class 2) cross-sections

The Class 2 slenderness limits (i.e. the limit below which the section's full plastic moment capacity can be attained) specified in EN 1993-1-4 (2006) and AS/NZS 4673 (2001) and the respective limit proposed in Chapter 3 is shown in Figure 5.30, together with test and FE results, where the ultimate moment has been normalised by the plastic moment capacity, defined as the plastic section modulus multiplied by the

measured 0.2% proof strength. Similarly to Figure 5.27, the section aspect ratio can be observed to have a marked influence on moment capacity, particularly for slender cross-sections. The Eurocode Class 2 slenderness limit of 26.7 may be seen to be rather conservative, whereas the Australian/New Zealand limit of 33.18 and the more relaxed limit of 35 proposed in Chapter 3 seem more suitable.

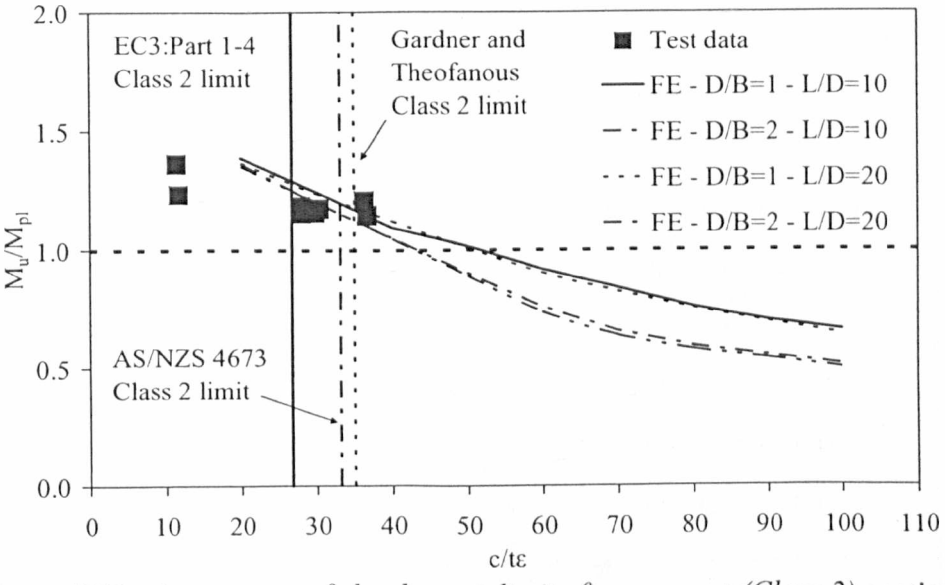

Figure 5.30: *Assessment of slenderness limits for compact (Class 2) sections*

5.4.3.4 Plastic (Class 1) cross-sections

The rotation capacity of both test and FE results, as defined in Equation 5.1, is plotted against the flange slenderness in Figure 5.31, so that the codified limit can be assessed. Both aspect ratio and moment gradient may be seen to influence rotation capacity, with stockier webs and steeper moment gradients significantly enhancing the achievable rotation capacity. No provisions for plastic analysis and design of stainless steel structures are currently specified in any design guidance, as discussed in Chapter 6. Nonetheless a Class 1 slenderness limit of 25.7 is specified in EN 1993-1-4 (2006). In Figure 5.31, the rotation capacity requirement of R=3, adopted for carbon steel (Bild et al., 1989; Sedlacek and Feldmann, 1995) and used as the basis for the Class 1 limit in EN 1993-1-4 (2006), is depicted assuming that this requirement is also applicable to stainless steel. The Class 1 limit of 33 proposed in Chapter 3 (which is the same limit that is applied to carbon steel in EN 1993-1-1 (2005)), judged on the basis of a rotation capacity requirement of R=3, appears unsafe

for lean duplex stainless steel. However the actual material response of stainless steel significantly deviates from the bilinear elastic-perfectly plastic behaviour upon which the plastic design approach, based on concentrated plasticity in discrete plastic hinges, was originally derived. In fact, the gradual yielding of stainless steel and considerable strain hardening, together with the spread of plasticity throughout a plastic zone are believed to significantly reduce the ductility demands imposed on stainless steel structures for plastic design. There is a clear need for research on the inelastic response of indeterminate stainless steel structures.

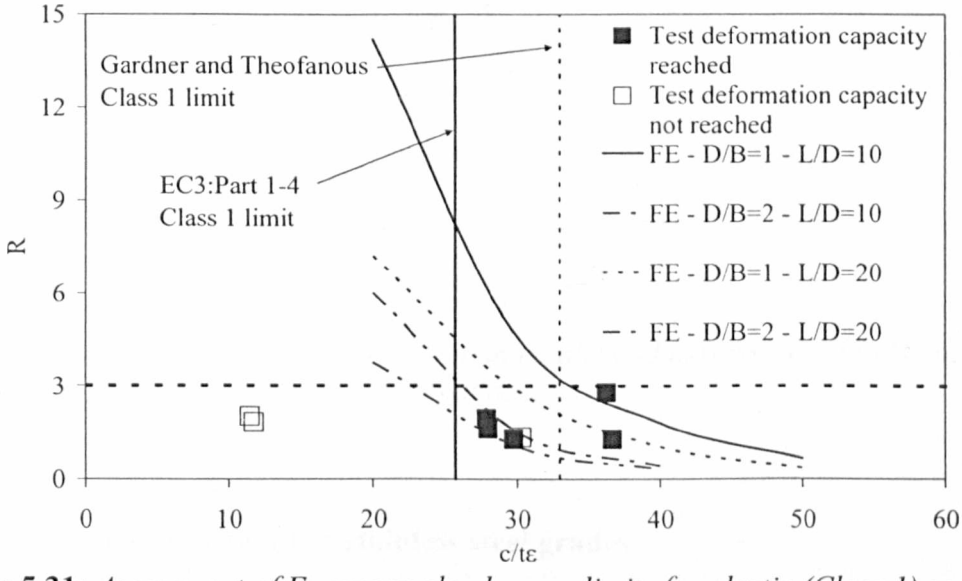

Figure 5.31: *Assessment of European slenderness limits for plastic (Class 1) sections*

5.4.4 Flexural buckling

The applicability of the buckling curve specified in EN 1993-1-4 (2006) for hollow sections to lean duplex stainless steel tubular columns is assessed by comparing the column test and numerical data with the respective codified predictions. For both experimental and FE results, the ultimate load has been normalised by the corresponding squash load (defined as $A\sigma_{0.2}$) and plotted against the non-dimensional slenderness $\bar{\lambda}$ in Figure 5.32, where the stub column test data are also included. The effect of the aspect ratio is insignificant for slender columns, but becomes increasingly important with decreasing member slenderness, because of the increasing influence of cross-sectional behaviour (i.e. local buckling). Good

agreement between the test data and code predictions is observed and hence application of the current buckling curve ($\bar{\lambda}_0 = 0.4$ and $\alpha = 0.49$) to lean duplex stainless steel SHS and RHS columns is proposed herein.

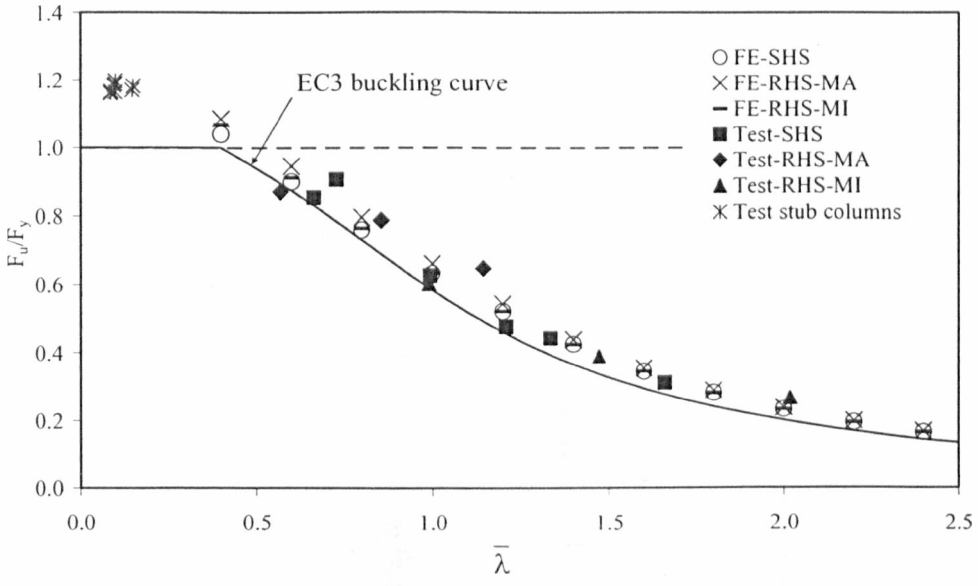

Figure 5.32: *Normalised test and FE column results and assessment of EC3 buckling curve*

5.4.5 Comparison with other stainless steel grades

The initial material cost of stainless steel comprises two components: the basic manufacturing cost and the alloy adjustment factor, which depends on the alloying elements used and hence varies markedly between grades. Lean duplex stainless steel only contains approximately 1.5% nickel, resulting in a relatively low alloy adjustment factor and hence a competitive initial material cost (Outokumpu data sheet, 2009). In Figures 5.33, 5.34 and 5.35 the structural response of stub columns, beams and long columns of the most commonly adopted structural stainless steel grades (i.e. austenitic and duplex grades) is compared with the corresponding lean duplex test data reported herein.

The stub column data included in Figure 5.33 were reported by Gardner and Nethercot (2004a), Kuwamura (2003), Talja and Salmi (1995), Liu and Young (2003), Young and Liu (2003), Young and Lui (2006) and Young and Ellobody

(2006). The beam data of Figure 5.34 were reported by Rasmussen and Hancock (1993b), Talja and Salmi (1995), Gardner and Nethercot (2004b), Real and Mirambell (2005) and Zhou and Young (2005), whereas the flexural buckling data were taken from Talja and Salmi (1995), Liu and Young (2003), Young and Liu (2003), Young and Lui (2006), Gardner and Nethercot (2004b) and Ala-Outinen and Oksanen (1997). In the determination of the slenderness parameter plotted on the horizontal axis of Figures 5.33, 5.34 and 5.35, only geometric properties have been included (c/t for stub columns and beams, and L_{cr}/i, where L_{cr} is the buckling length and i is the radius of gyration, for long columns), so that the effect of material is accounted for only in the vertical axis.

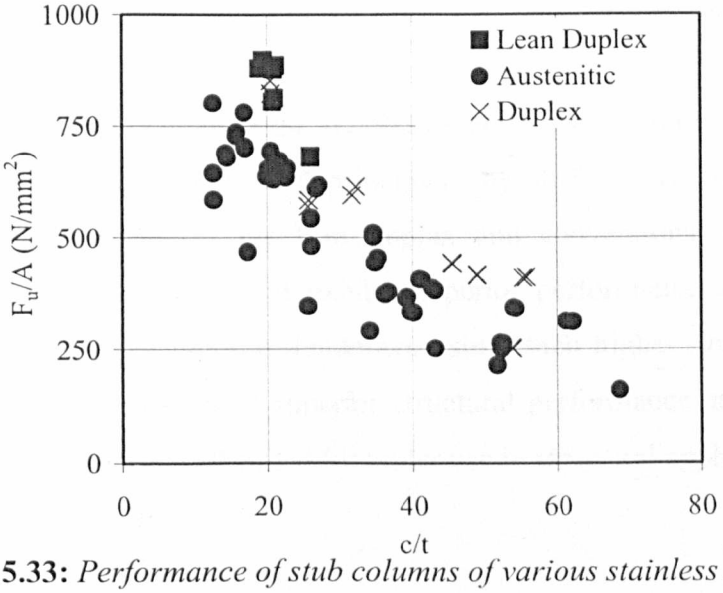

Figure 5.33: *Performance of stub columns of various stainless steel grades*

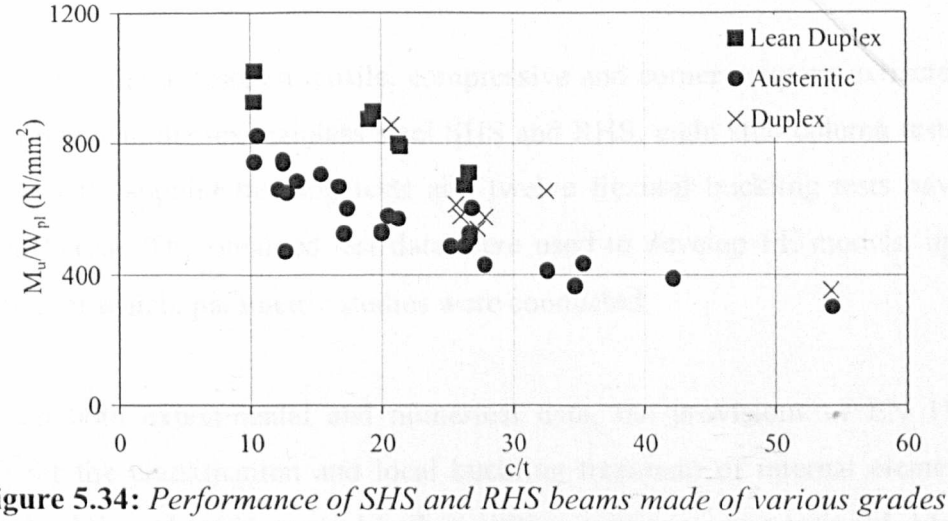

Figure 5.34: *Performance of SHS and RHS beams made of various grades of stainless steel*

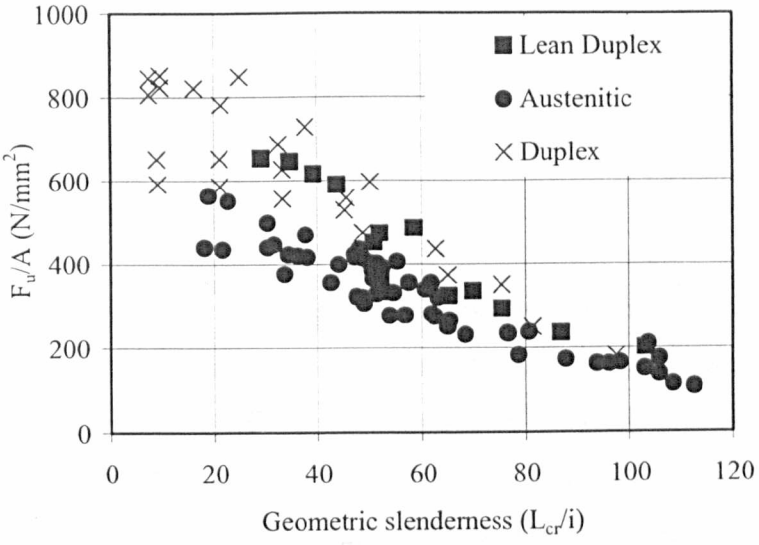

Figure 5.35: *Performance of columns of various stainless steel grades*

In the high slenderness regime all stainless steel grades exhibit similar structural capacities since failure is governed principally by stiffness. However, for stockier cross-sections and members the lean duplex and conventional duplex structural components behave similarly and exhibit superior performance to their austenitic counterparts of similar geometric slenderness, since their higher strength can be fully utilized. With a combination of superior structural performance and lower material cost, lean duplex appears well suited for wider use in structural applications.

5.5 CONCLUDING REMARKS

A series of material tests on tensile, compressive and corner coupons extracted from cold-formed lean duplex stainless steel SHS and RHS, eight stub column tests, eight major axis three-point bending tests and twelve flexural buckling tests have been reported herein. The obtained test data were used to develop FE models, upon the validation of which, parametric studies were conducted.

Based on both experimental and numerical data, the provisions of EN 1993-1-4 (2006) for the classification and local buckling treatment of internal elements and overall buckling of stainless steel hollow section columns, were assessed. Moreover,

the effect of local slenderness, aspect ratio and moment gradient on both the load bearing and deformation capacity of lean duplex stainless steel SHS and RHS was investigated and the suitability of the codified American (SEI/ASCE 8-02, 2002) and Australian (AS/NZS 4673, 2001) provisions for stainless steel tubular cross-sections were assessed.

The European slenderness limits and the corresponding effective width equations for internal elements were shown to be adequate but conservative for stocky cross-sections; the current American and Australian/New Zealand design procedures as well as the more favourable slenderness limits and effective width formulae proposed in Chapter 3 have been shown to more accurately predict the ultimate capacity of lean duplex stainless steel SHS and RHS. Regarding the flexural buckling response of lean duplex stainless steel columns, the current buckling curve for stainless steel hollow sections is deemed suitable.

Overall, lean duplex stainless steel is shown to offer superior structural performance compared to the austenitic grades and at a lower cost (Outokumpu data sheet, 2009), which represents a significant economic advantage and renders lean duplex stainless steel an attractive choice for structural applications.

CHAPTER 6

PLASTIC DESIGN OF STAINLESS STEEL STRUCTURES

6.1 INTRODUCTION

The need for metallic structures to resist high loads that have a small probability of occurrence in an economic way necessitates the exploitation of the inelastic range of the material's stress-strain curve, provided that they possess sufficient ductility. Modern structural design guidance specifies the extent to which the exploitation of the material's inelastic range is allowed, following the cross-section classification procedure, which has been thoroughly discussed in Chapter 3. The European structural design codes for carbon steel (EN 1993-1-1, 2005) and stainless steel (EN 1993-1-4, 2006) specify four behavioural classes of cross-sections according to their susceptibility to local buckling. Indeterminate structures employing carbon steel cross-sections classified as Class 1 may be plastically designed. Despite the high material ductility of structural stainless steels (Gardner, 2005) and the existence of a Class 1 limit in EN 1993-1-4 (2006), plastic design is not permitted for stainless steel structures, which leads to uneconomic design.

In this chapter the applicability of inelastic design procedures to stainless steel indeterminate structures is investigated. The basic features of plastic design, as currently applied to carbon steel structures, are discussed in the following section. Five three-point bending tests and ten two-span continuous beam tests on stainless steel SHS and RHS are reported thereafter. The experimental response of both the simply supported beams and the continuous beams is then compared with the predictions of EN 1993-1-4 (2006). Analysis of the results reveals that current design provisions are overly conservative, since they do not account for material strain-hardening and the significant moment redistribution (in the case of the continuous beams) taking place before collapse occurs. Hence material savings can be achieved if inelastic design procedures are followed at both cross-section level and system level. To this end, the continuous strength method (CSM), outlined in Chapter 3, which allows for the actual material response at cross-sectional level, is adapted to stainless steel indeterminate structures, resulting in more favourable strength predictions. It is envisaged that such procedures will be included in future revisions of structural design guidance, following full experimental and numerical verification.

6.2 Background to plastic design

6.2.1 Basic assumptions

Most of the published analytical and experimental research on plastic design focuses on carbon steel structures employing I sections and RHS (both hot-rolled and cold-formed) whilst publications on stainless steel components primarily deal with ultimate moment capacity rather than rotation capacity. However the key features controlling the rotation capacity of carbon steel sections are expected to remain unchanged for all metallic materials and are therefore presented herein.

In plastic design, unlike conventional elastic design, failure is defined by the formation of a mechanism of plastic hinges at ultimate load, thereby allowing redistribution of bending moments and the exploitation of the structure's reserve strength due to static indeterminacy. The development of a failure mechanism

imposes severe ductility demands on the parts of the structure that are designed to behave as plastic hinges, especially on the first plastic hinge to form. The structure is generally assumed to behave elastically up to the formation of the first plastic hinge upon which, the hinge is assumed to rotate freely maintaining its plastic moment capacity and allowing moment redistribution to other parts of the structure until a sufficient number of hinges forms and the structure collapses.

Since it was originally derived for carbon steel structures, plastic analysis is based on the adoption of an elastic, perfectly-plastic material response. The analysis procedure is significantly simplified by assuming rigid-plastic material response and utilising the classical theorems of plasticity (i.e. upper bound theorem, lower bound theorem, uniqueness theorem). In any case, sufficient rotation capacity is required at the location of the plastic hinges, since the plastic hinges are assumed to maintain their strength while undergoing large rotations, until the collapse mechanism forms. Hence ductility, i.e. the ability of a material, member or structure to undergo large inelastic deformation without significant loss of strength, emerges as a key property for plastic design, and becomes equally important as strength and stiffness.

6.2.2 Available rotation capacity

The rotation capacity of a cross-section is limited by the occurrence of local buckling, which is mainly addressed within the scope of design guidance by limiting the slenderness of the constituent plate elements. The lower the slenderness of the constituent plate elements, the higher the rotation capacity of the overall cross-section and hence maximum slenderness limits are specified for different required structural behaviour, as discussed in Chapter 3. Other factors affecting the rotation capacity, which are, to date, not accounted for in design standards, include local plate slenderness of all constituent plate elements (discussed in Chapter 3), interactive local and lateral torsional buckling (Lay and Galambos 1965, 1967; Kemp 1985, 1992), moment gradient (Kuhlmann, 1989) and material response, such as strain-hardening modulus, length of yielding plateau and ultimate stress to yield stress ratio f_u/f_y (Ricles et al., 1998).

Throughout this thesis, the rotation capacity of a cross-section is defined by Equation (6.1), where θ_u is the rotation θ at the point at which the falling branch of the moment-rotation curve falls below M_{pl}, and θ_{pl} is the elastic rotation corresponding to M_{pl}, as illustrated in Figure 6.1. The rotation capacity of a cross-section is usually derived experimentally from three-point bending tests, the loading of which resembles that to which continuous beams are subjected at their internal supports, or four-point bending tests, in which case, rotation is substituted by curvature.

$$R = \frac{\theta_u}{\theta_{pl}} - 1 \tag{6.1}$$

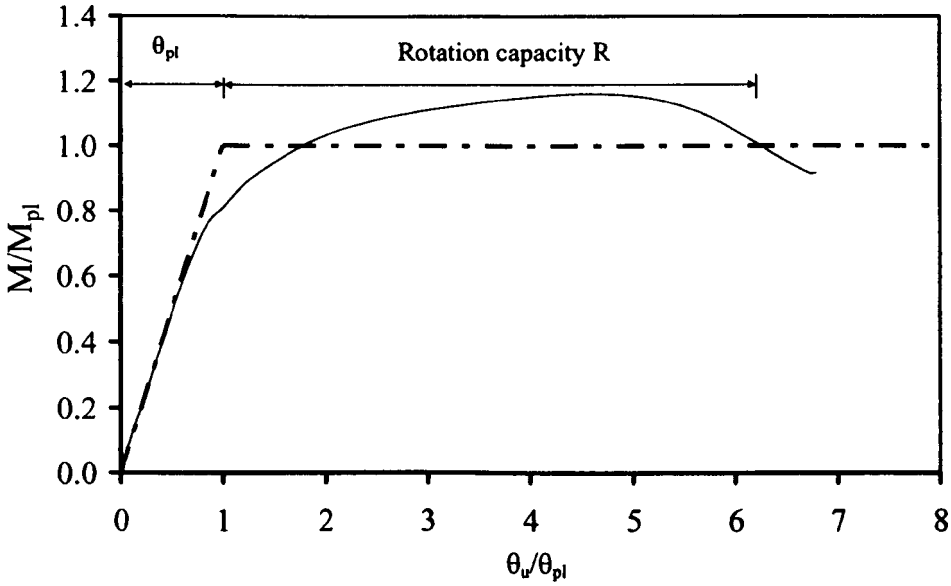

Figure 6.1: *Definition of rotation capacity*

Equation (6.1) has been widely adopted in the literature for the definition of the rotation capacity of carbon steel I-sections (Lukey and Adams, 1969; Kuhlmann, 1989), carbon steel RHS (Korol and Huboda, 1972), high strength steel sections (Ricles et al, 1998) and stainless steel tubular sections (Rasmussen and Hancock, 1993b). It is also adopted in EN 1993-1-1 (2005) according to Bild et al. (1989) and Sedlacek and Feldmann (1995). However, alternative rotation capacity definitions have been proposed by Kemp (1985, 1986), who raised the issue of dependence of the falling branch of the M-θ curve on the stiffness of the testing machine and the subsequent difficulty of duplicating tests to failure with different testing machines.

Kemp (1985, 1986) proposed that rotation capacity be determined at the maximum moment instead of the plastic moment M_{pl}.

6.2.3 Required rotation capacity

McDermott (1969) speculated that a cross-section would have adequate rotation capacity, if local buckling did not occur before the onset of strain-hardening. He proposed a minimum strain of 2% which directly relates to a minimum required curvature capacity for a given cross-section regardless of the structural layout and the loading pattern. However, this proposal does not apply to stainless steel, since it displays no yield plateau but continuous strain-hardening. Moreover, it is evident that the amount of hinge rotation necessary for a mechanism to form depends on the structural arrangement and the loading pattern imposed on the structure. The available rotation capacity at each hinge must be at least equal to the required hinge rotation so that a reliable plastic mechanism can form.

Driscoll (1957, 1958) was among the first researchers to investigate the required rotation capacity for plastic analysis of carbon steel indeterminate structures. He analysed both continuous steel beams and single span steel frames, assuming a bilinear stress-strain (and moment–rotation) response and initially proposed a required rotation capacity R=12 for plastic analysis.

Kemp (1986, 1992) found that the flexibility of bolted connections can significantly increase rotations at critical sections, thereby enhancing moment redistribution and that strain-hardening, which was not accounted for in Driscoll's analysis, spreads rotation requirements to larger portions of the structures and leads to considerably enhanced overall resistance. In his studies on the requirements for plastic design of carbon steel structures, Kemp (1986, 1992) incorporated the effects of strain-hardening and concluded that a rotation capacity of R=5 (or R=3 when rotation capacity is calculated at ultimate moment) is adequate for most practical cases, whilst Yura et al. (1978) proposed a required rotation capacity of R=3.

As pointed out by Korol and Huboda (1972) a highly redundant structure would impose severe rotation demands on the first plastic hinges to form, when the full theoretical collapse load is reached. However, for practical applications, achieving a high proportion of the theoretical collapse load of the structure would suffice and hence only a fraction of the rotation capacity corresponding to the theoretical collapse load of the structure would be required. It was concluded that a rotation capacity of 4 would be adequate for plastic design with the additional requirements of the maximum exceeding the plastic moment capacity and that the area below the actual M-θ curve is not less than the idealized bilinear curve used in plastic design (Korol and Huboda, 1972).

EN 1993-1-1 (2005) is based on a minimum rotation capacity of R=3 (Bild et al., 1989; Sedlacek and Feldmann, 1995) for plastic design of carbon steel structures. This rotation capacity is assumed to be possessed by Class 1 cross-sections. The same rotation capacity value has been adopted in Chapters 3, 4, 5 when Class 1 limits for stainless steel cross-sections were assessed. Clearly more research on this topic is still required. To this end an experimental investigation on stainless steel continuous beams has been conducted, and is reported hereafter.

6.3 EXPERIMENTAL INVESTIGATION

An experimental investigation into the structural response of stainless steel simple and continuous beams has been carried out in the Structures Laboratory at Imperial College London. The employed cross-sections were SHS and RHS in grade EN 1.4301/1.4307 stainless steel with nominal sizes of 50×50×3, 60×60×3, 100×100×3 and 60×40×3. The specimens were extracted from the same lengths as the ones utilised by Nip et al. (in press) in their experimental study on the cyclic behaviour of carbon steel and stainless steel tubular members. Five three-point bending tests were initially performed, to extract fundamental flexural performance data, which were utilised to assess the suitability of current design provisions codified in EN 1993-1-4 (2006). Subsequently ten two-span continuous beam tests (five-point bending) were conducted, which enabled the study of stainless steel indeterminate structures and an

assessment of the current codified provisions. Performing both simply supported and continuous beam tests on the same cross-sections enables the assessment of the effect of moment redistribution on ultimate capacity.

6.3.1 Material tests

In their study, Nip et al. (in press) reported material test data on tensile flat and tensile corner coupons extracted from the finished cross-sections. These test data are utilised herein, as no further material coupon tests were conducted within the current project. The obtained tensile flat and tensile corner material properties are shown in Tables 6.1 and 6.2 respectively, where all symbols have been defined previously. In all code comparisons, the 0.2% proof stress $\sigma_{0.2}$ obtained from tensile flat coupons is utilized to obtain the elastic and plastic moment resistances (M_{el} and M_{pl} respectively).

Table 6.1: *Tensile flat material properties*

Cross-section	E (N/mm^2)	$\sigma_{0.2}$ (N/mm^2)	$\sigma_{1.0}$ (N/mm^2)	σ_u (N/mm^2)	Compound R-O	
					n	$n'_{0.2,1.0}$
SHS 50×50×3	198000	552	608	798	5.50	2.90
SHS 60×60×3	197730	483	546	745	5.25	2.90
SHS 100×100×3	201300	419	470	725	5.25	2.25
RHS 60×40×3	191690	538	592	753	5.00	3.50

Table 6.2: *Tensile corner material properties*

Cross-section	E (N/mm^2)	$\sigma_{0.2}$ (N/mm^2)	$\sigma_{1.0}$ (N/mm^2)	σ_u (N/mm^2)	Compound R-O	
					n	$n'_{0.2,1.0}$
SHS 50×50×3	195000	723	918	927	4.56	3.76
SHS 60×60×3	193440	614	776	855	4.75	4.25
SHS 100×100×3	189520	694	829	839	5.50	3.50
RHS 60×40×3	198530	741	968	984	4.67	4.00

6.3.2 Simply supported beam tests

Five simply supported beam tests have been conducted in the three-point bending configuration. One test was conducted for each of the three SHS employed, whilst two tests were conducted for the RHS 60×40×3 specimen, one about the major axis and one about the minor axis. Prior to testing, measurements of the geometry of the specimens were taken, which are summarised in Table 6.3; the symbols have been defined in Section 5.2.3. No initial geometric imperfections were measured, since, as seen in Chapter 5, they can be relatively accurately predicted using the Dawson and Walker (1972) model as modified by Gardner and Nethercot (2004c).

Table 6.3: *Measured dimensions of three-point bending specimens*

Specimen	Axis of bending	Clear span between supports L (mm)	B (mm)	D (mm)	t (mm)	r_i (mm)
SHS 50×50×3	Major	1100	50.18	50.24	2.76	1.53
SHS 60×60×3	Major	1100	60.37	60.63	2.79	3.50
SHS 100×100×3	Major	1100	99.85	99.93	2.78	2.13
RHS 60×40×3-MA	Major	1100	40.00	60.11	2.75	1.88
RHS 60×40×3-MI	Minor	1100	60.10	39.95	2.75	1.88

All beams had a total length of 1200 mm and were simply supported between rollers, which allowed axial displacement of the beams' ends. The rollers were placed 50 mm inward from each beam end. For the RHS 60×40×3-MA specimen the face containing the weld was the web, whilst in all other cases the face containing the weld was the bottom (tension) flange. The applied loading rate, in terms of crosshead movement rate, was 3 mm/min.

The employed experimental setup and instrumentation were identical to the ones employed for the lean duplex beam tests reported in Section 5.2.3. All key experimental results obtained are summarised in Table 6.4, where the rotation capacity R is defined in Equation (6.1). The rotation at midspan was assumed to equal the sum of the end rotations. All specimens failed by local buckling of the

compression flange and the upper part of the web. All failed specimens are shown in Figure 6.2.

Table 6.4: *Summary of test results from 3-point bending tests*

Specimen	Ultimate moment M_u (kNm)	M_u/M_{el}	M_u/M_{pl}	Rotation capacity R
SHS 50×50×3	7.00	1.68	1.41	3.11 [a]
SHS 60×60×3	8.74	1.62	1.36	5.30
SHS 100×100×3	18.77	1.35	1.16	1.79
RHS 60×40×3-MA	7.99	1.84	1.49	5.12 [a]
RHS 60×40×3-MI	5.69	1.66	1.41	5.50 [a]

[a] Full rotation capacity not attained; R based on maximum recorded deformation

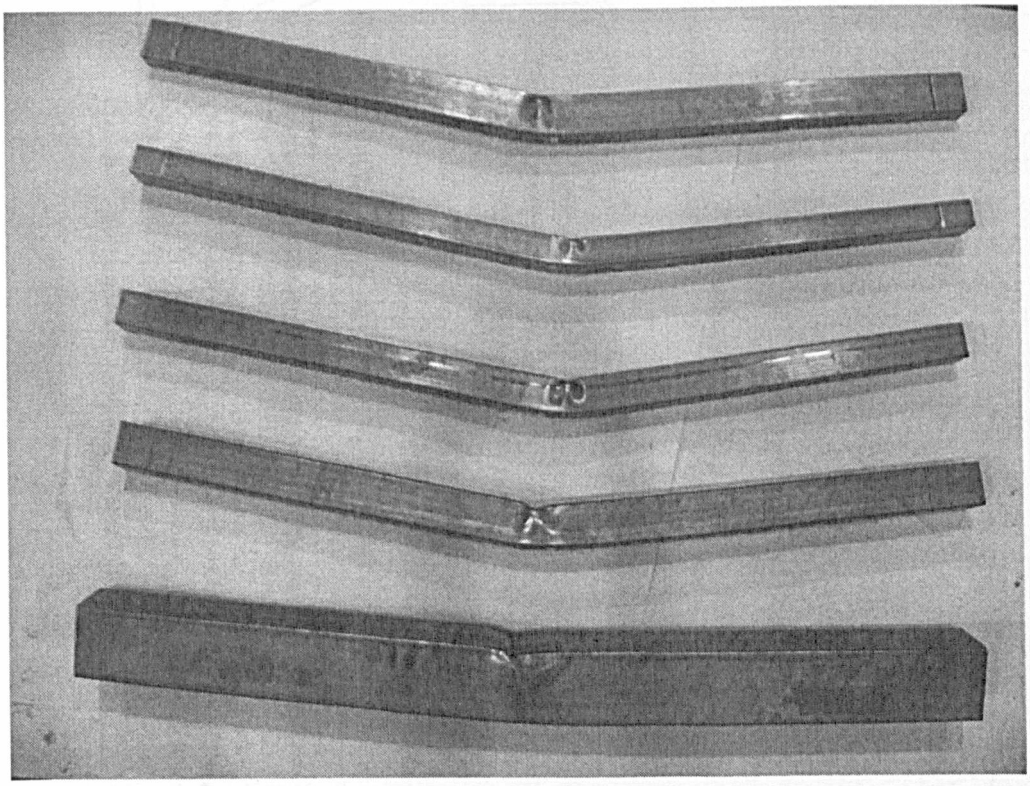

Figure 6.2: *Failure modes for simply supported beams failure modes (from top to bottom: RHS 60×40×3-MA, RHS 60×40×3-MI, SHS 50×50×3, SHS 60×60×3, SHS 100×100×3)*

The recorded mid-span moment-rotation (at plastic hinge) responses of the tested beams are depicted in Figure 6.3. To facilitate comparison between the specimens, the curves are shown in Figure 6.4 in a non-dimensional format; the recorded moment has been normalised by the respective plastic moment resistance, whilst the rotation at plastic hinge has been normalised by the elastic rotation corresponding to M_{pl}, defined as $\theta_{pl} = \frac{M_{pl}L}{2EI}$.

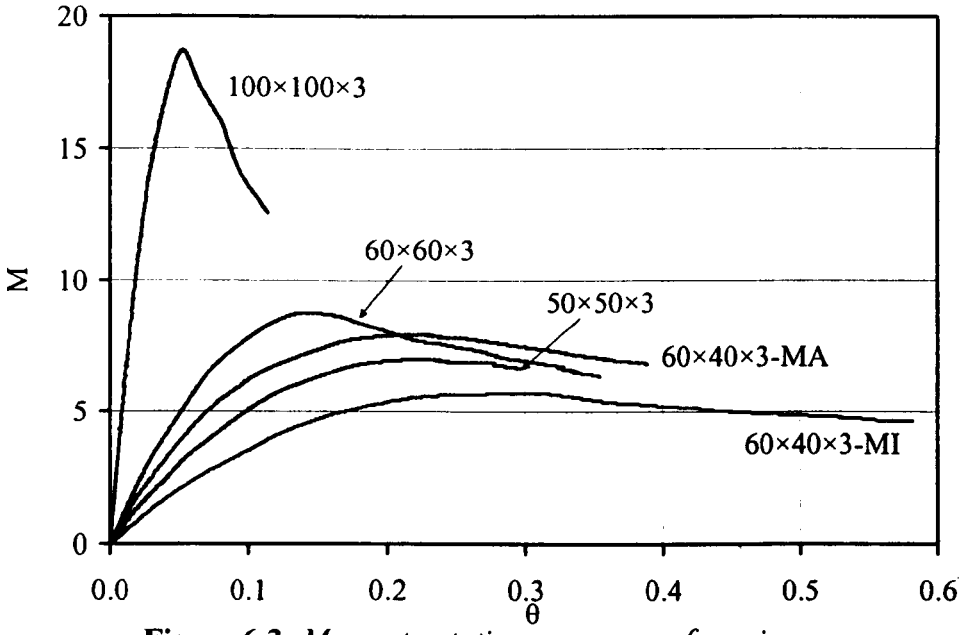

Figure 6.3: *Moment-rotation responses of specimens*

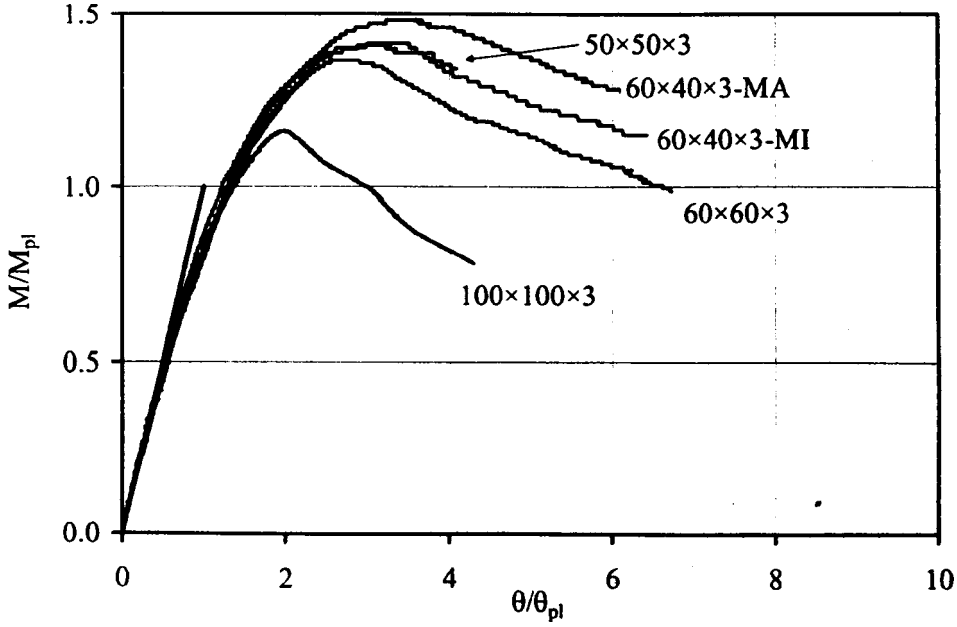

Figure 6.4: *Normalised moment-rotation curves for all specimens*

6.3.3 Continuous beam tests

Ten continuous beam tests were conducted on the same section sizes employed for the simply supported beam tests; two tests were conducted for each cross-section. As before, the RHS 60×40×3 was tested about both its major and minor axes. All beams had a total length of 2400 mm and were resting on three roller supports; the end rollers allowed free axial displacements, while the central roller was fixed against axial displacement. The clear span distance between the roller supports was 1100 mm and a further 100 mm were provided at each specimen end. The measured geometric properties are shown in Table 6.5, where the symbols are as previously defined.

Table 6.5: *Measured dimensions of continuous beam specimens*

Specimen	Axis of bending	Configuration	B (mm)	D (mm)	t (mm)	r_i (mm)
SHS 50×50×3-1	Major	1/2 span	50.22	50.26	2.76	1.38
SHS 50×50×3-2	Major	1/3 span	50.28	50.23	2.76	1.69
SHS 60×60×3-1	Major	1/2 span	60.38	60.68	2.79	3.50
SHS 60×60×3-2	Major	1/2 span	60.36	60.66	2.79	3.50
SHS 100×100×3-1	Major	1/2 span	99.94	99.79	2.78	2.13
SHS 100×100×3-2	Major	1/2 span	99.87	99.85	2.78	2.13
RHS 60×40×3-MA-1	Major	1/2 span	40.05	60.14	2.75	1.88
RHS 60×40×3-MA-2	Major	1/2 span	39.90	60.12	2.75	1.88
RHS 60×40×3-MI-1	Minor	1/2 span	60.10	39.90	2.75	1.88
RHS 60×40×3-MI-2	Minor	1/3 span	60.15	39.90	2.75	1.88

All tests were displacement-controlled with a loading rate of 3mm/min in terms of vertical crosshead movement. Two symmetrical loading configurations were employed to vary the required rotation capacity and moment redistribution before collapse. In the first configuration, denoted '1/2 span' in Table 6.5, the loads were applied at midspan, whilst in the second configuration, 'denoted 1/3 span', the loads were applied at a distance equal to 366.7 mm (1/3 of the clear span length) from the

central support. The two configurations are shown in Figures 6.5 and 6.6, where the employed instrumentation is also depicted. In both figures, all dimensions are in mm. Wooden blocks were inserted at the supports and at the loading points of each specimen and the loads and reactions were applied through a steel block of thickness 15 mm and width 30 mm, to prevent local bearing failure.

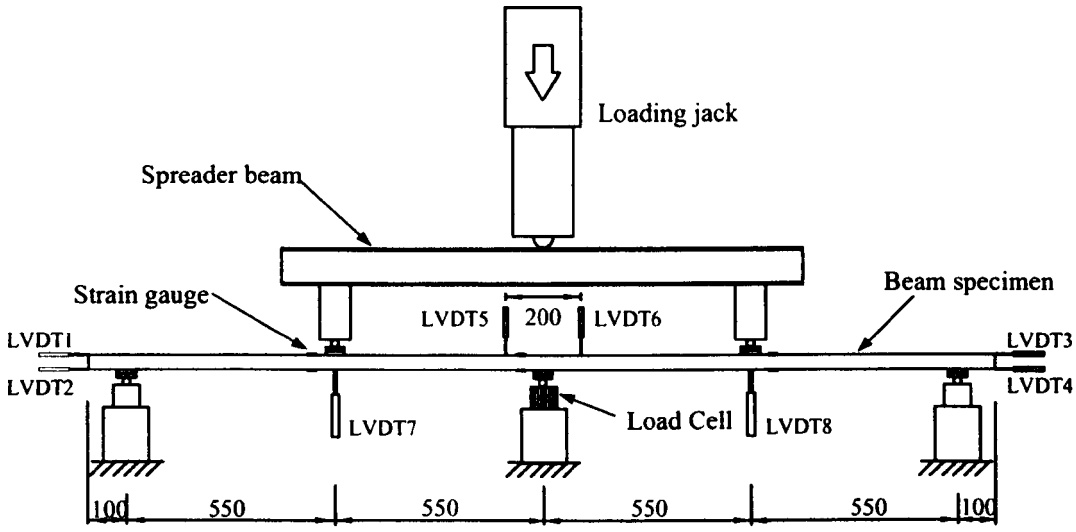

Figure 6.5: *Test configuration '1/2 span' - loads applied at midspan*

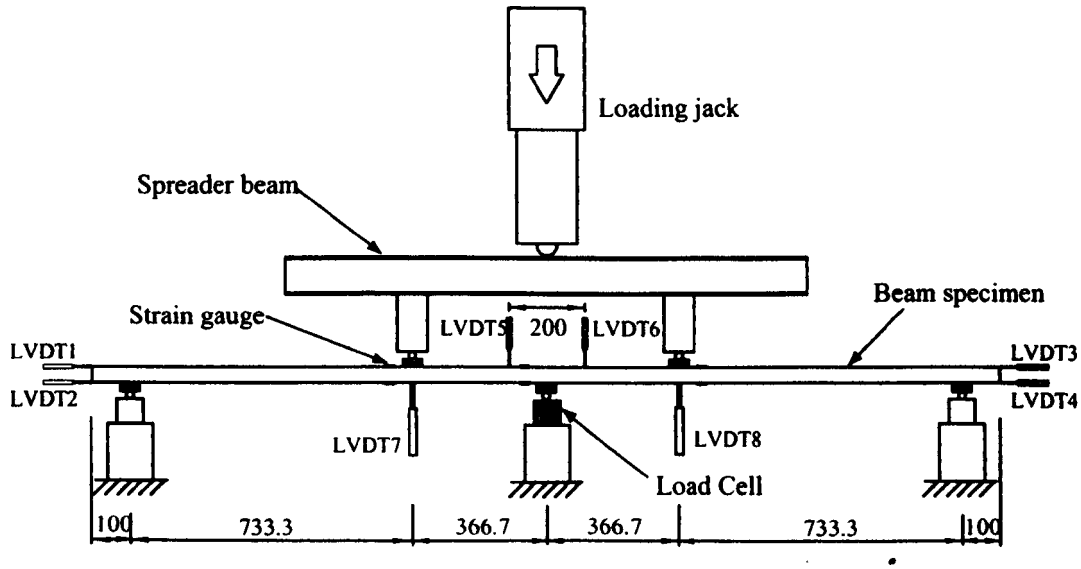

Figure 6.6: *Test configuration '1/3 span' - loads applied at 366.7 mm from central support*

The employed instrumentation consisted of a load cell at the central support, eight LVDTs and six strain gauges, as shown in Figures 6.5 and 6.6. The load cell was utilised to measure the reaction force at the central support, which is necessary to determine the stress condition of each specimen, due to their static indeterminacy. The strain gauges were affixed at the mid-width of the top and bottom flanges at a distance of 60 mm from each loading point and from the central support point. Their readings verified that no axial stress occurred at the specimens and hence the end rollers did not provide any axial restrain. Six LVDTs were employed in pairs of two at the ends of the specimens and the central support, as shown in Figures 6.5 and 6.6, to measure the end rotations and the rotation of the plastic hinge at the central support, whilst two additional LVDTs were employed at the loading points to measure the vertical displacement. The applied load and crosshead movement were also recorded. All readings were taken at 2 sec intervals.

The key experimental results are summarised in Table 6.6, including the ultimate load F_u and the plastic rotation at ultimate load normalised by the corresponding elastic rotation at ultimate load $\theta_{pl,max}/\theta_{el,max}$. The load corresponding to the formation of the first plastic hinge at the central support, denoted F_{hl}, and the theoretical collapse load F_{coll} are also included. The load F_{hl} was determined based on elastic calculations, whereas F_{coll} was determined by classical plastic analysis procedures, assuming rigid-plastic material (and moment-rotation) response. All specimens failed by developing three distinct plastic hinges, one at the central support and one at each loading point. Typical failure modes for both arrangements considered are displayed in Figures 6.7 and 6.8.

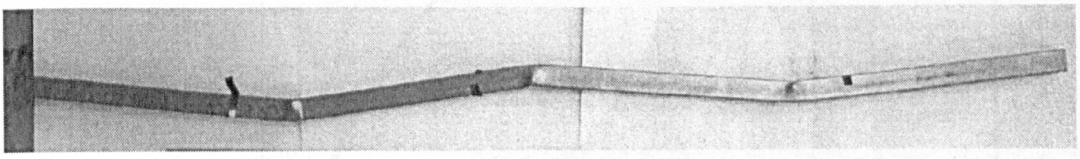

Figure 6.7: *Failure mode of SHS 50×50×3-1 - configuration: 1/2 span*

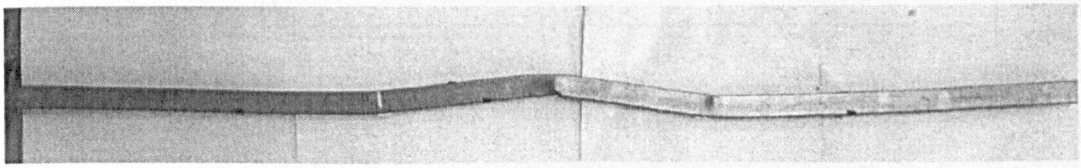

Figure 6.8: *Failure mode of SHS 50×50×3-2 - configuration: 1/3 span*

Table 6.6: *Summary of test results from continuous beam tests*

Specimen	Configuration	F_u (kN)	F_{hl} (kN)	F_{coll} (kN)	$\theta_{pl,max}/\theta_{el,max}$
SHS 50×50×3-1	1/2 span	80.24	48.3	54.35	0.95
SHS 50×50×3-2	1/3 span	98.87	48.8	67.67	1.35
SHS 60×60×3-1	1/2 span	97.08	62.2	70.00	0.70
SHS 60×60×3-2	1/2 span	92.47	62.2	69.94	0.79
SHS 100×100×3-1	1/2 span	173.86	156.3	175.83	0.45
SHS 100×100×3-2	1/2 span	172.21	156.3	175.89	0.20
RHS 60×40×3-MA-1	1/2 span	92.99	52.0	58.54	1.10
RHS 60×40×3-MA-2	1/2 span	91.92	51.9	58.37	1.10
RHS 60×40×3-MI-1	1/2 span	63.94	39.0	43.84	1.00
RHS 60×40×3-MI-2	1/3 span	77.57	39.5	54.84	1.70

The recorded load-deformation response is shown in Figures 6.9-6.13, where the total applied force F is plotted against the jack displacement δ, which equals the average displacement at the loading points. In Figures 6.14-6.18 the total applied load is normalised by the theoretical collapse load F_{coll} and plotted against the average end rotation for each specimen.

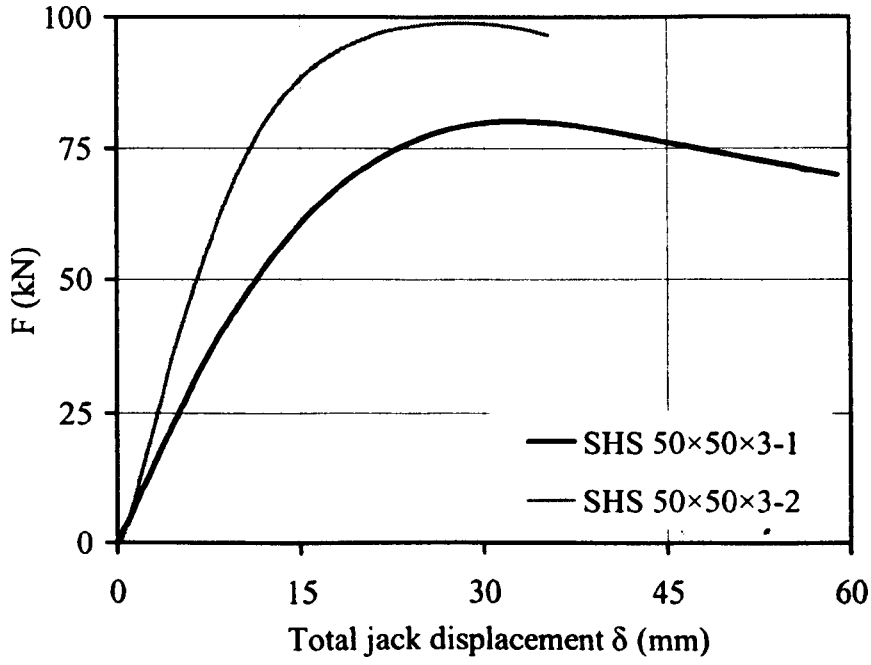

Figure 6.9: *Load-jack displacement curves for SHS 50×50×3 specimens*

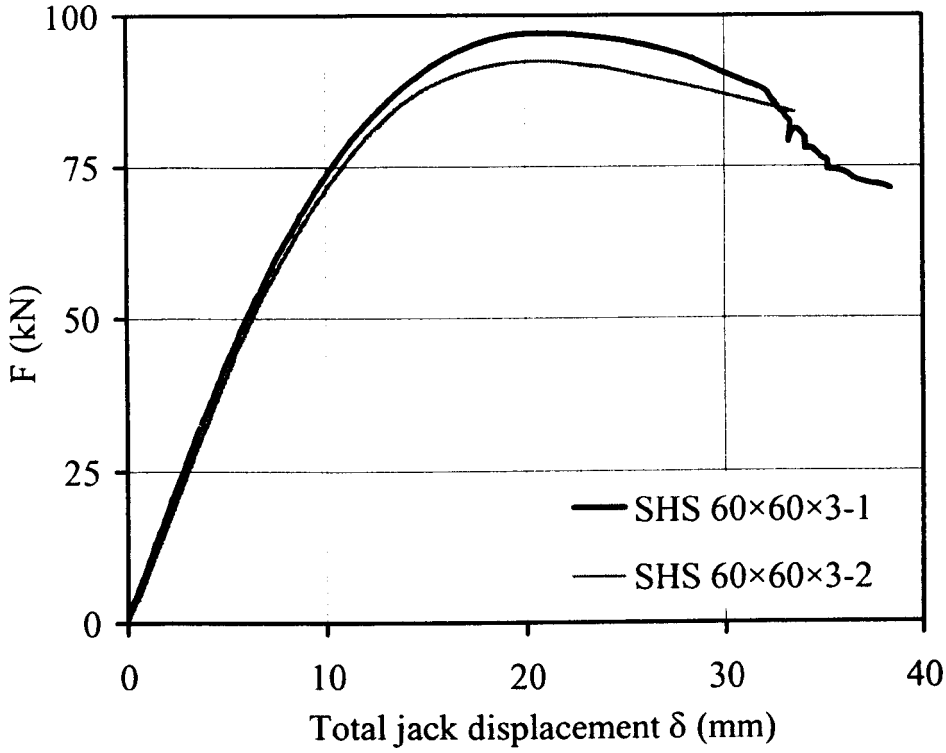

Figure 6.10: *Load-jack displacement curves for SHS 60×60×3 specimens*

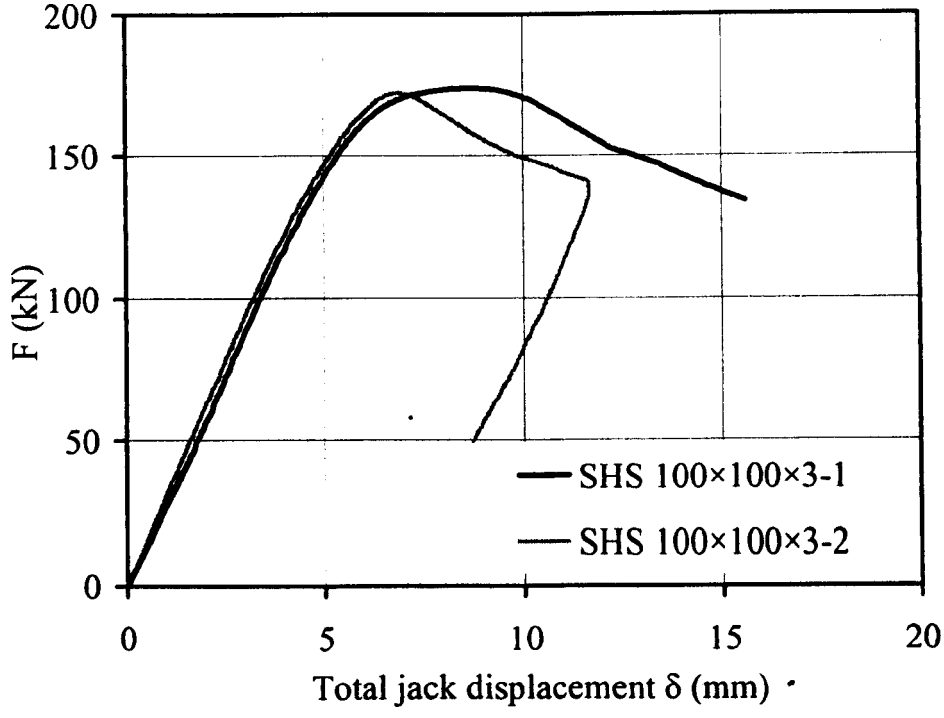

Figure 6.11: *Load-jack displacement curves for SHS 100×100×3 specimens*

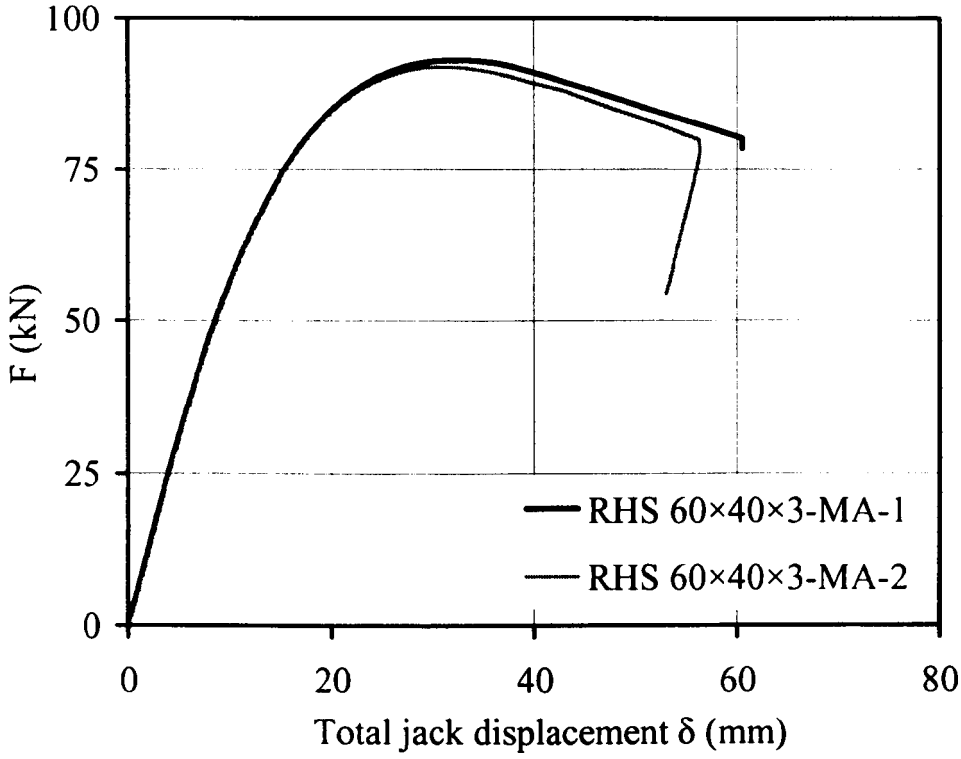

Figure 6.12: *Load-jack displacement curves for RHS 60×40×3-MA specimens*

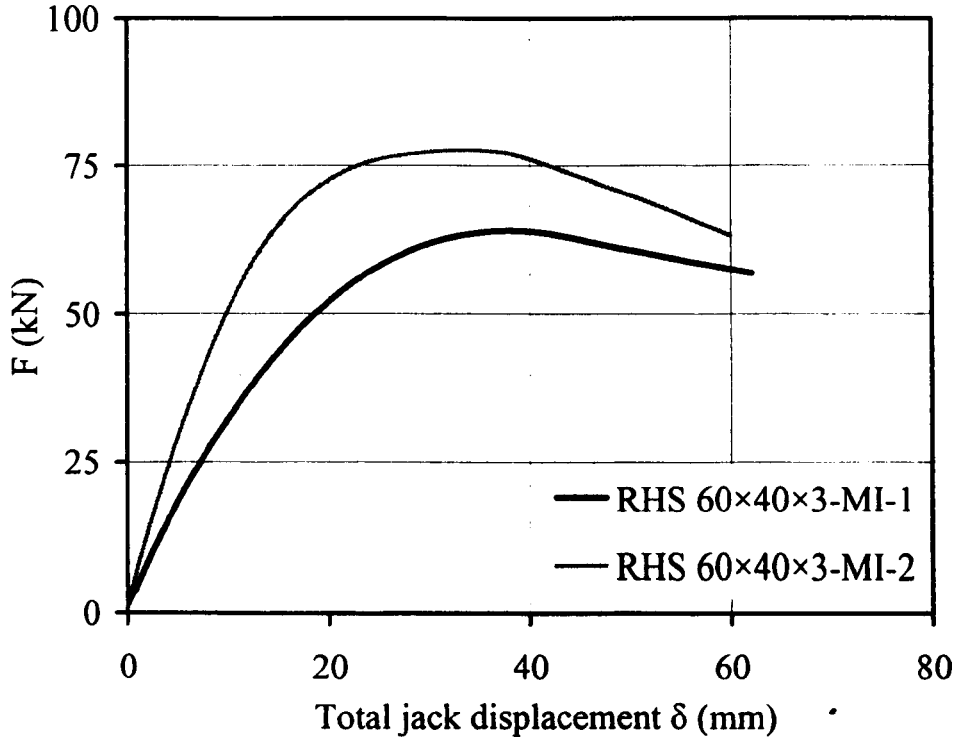

Figure 6.13: *Load-jack displacement curves for RHS 60×40×3-MI specimens*

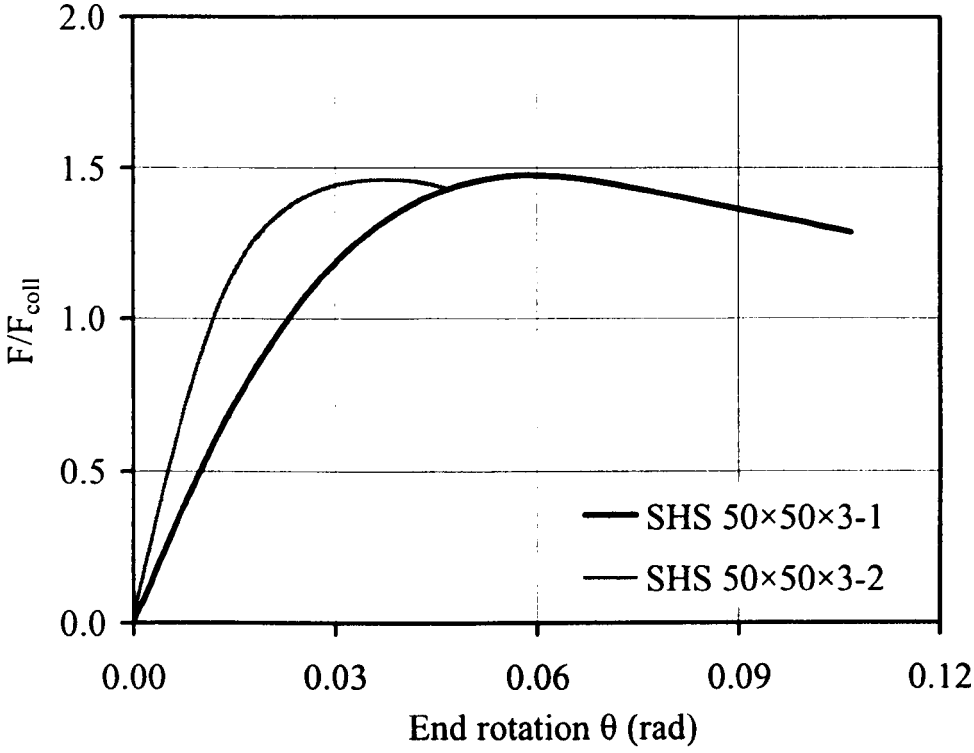

Figure 6.14: *Normalised load-end rotation curves for SHS 50×50×3 specimens*

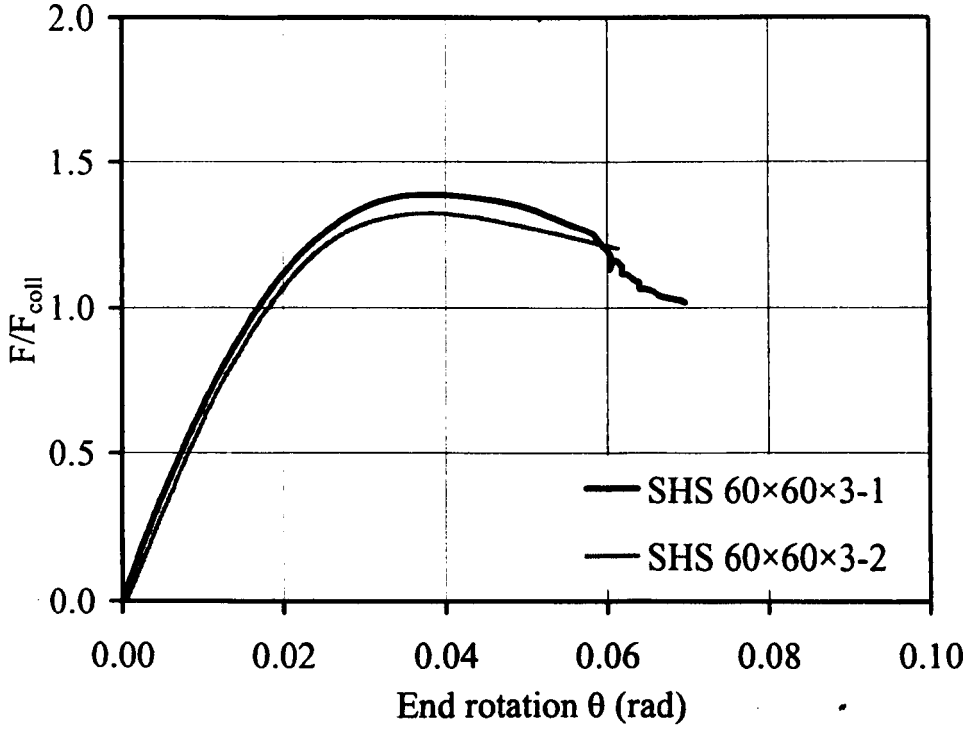

Figure 6.15: *Normalised load-end rotation curves for SHS 60×60×3 specimens*

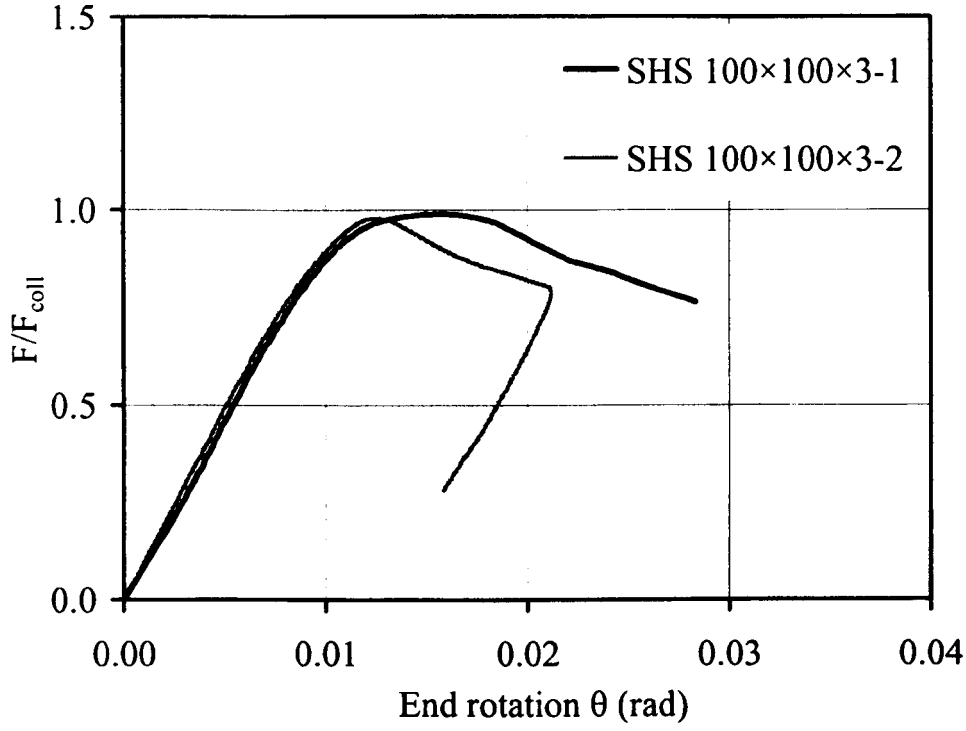

Figure 6.16: *Normalised load-end rotation curves for SHS 100×100×3 specimens*

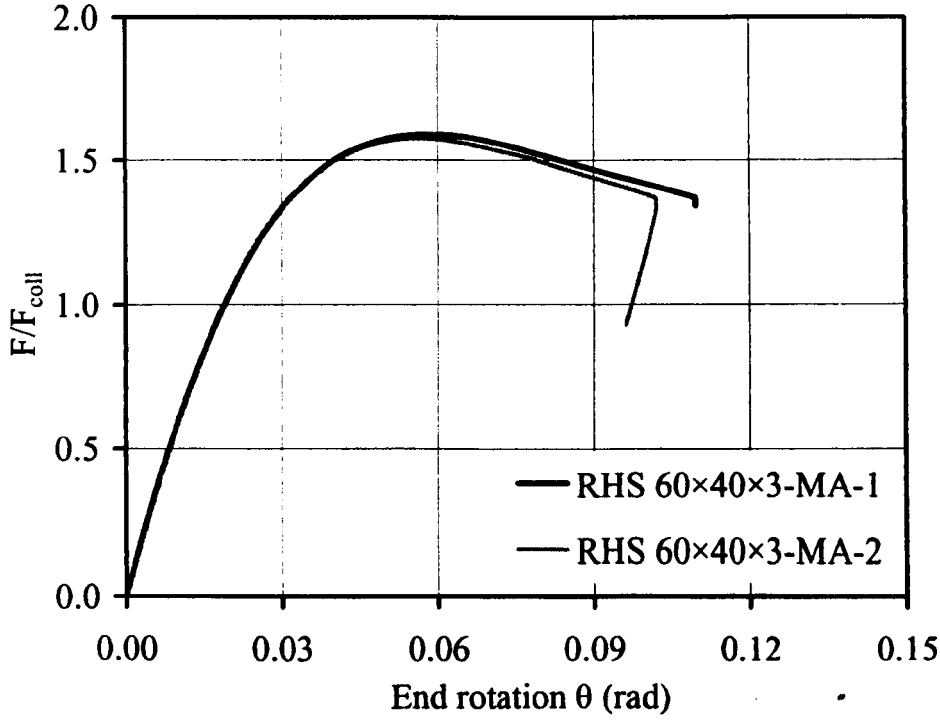

Figure 6.17: *Normalised load-end rotation curves for RHS 60×40×3-MA specimens*

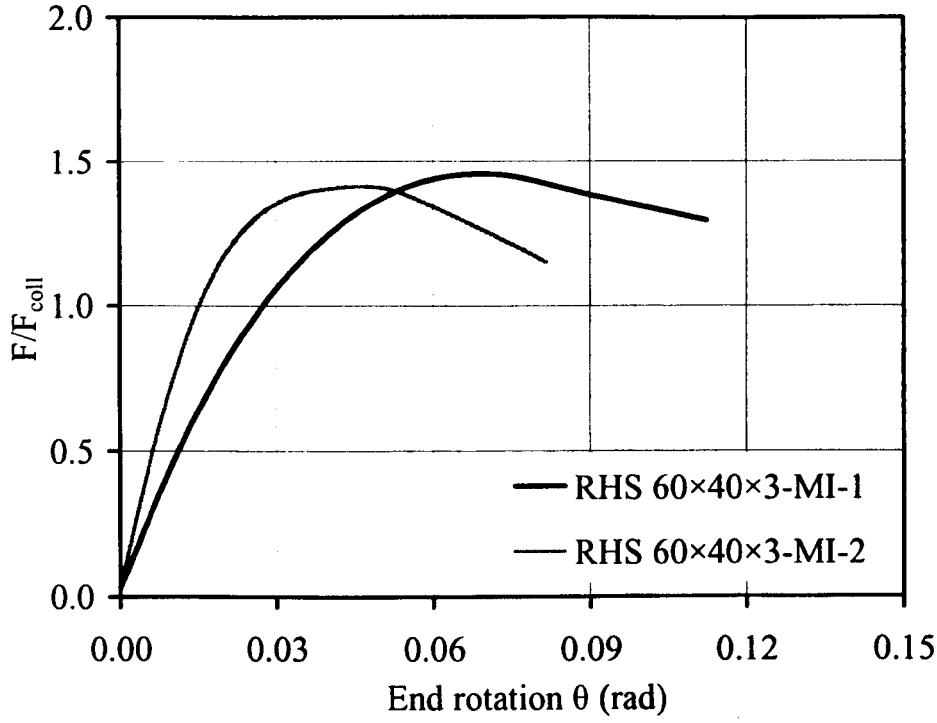

Figure 6.18: *Normalised load-end rotation curves for RHS 60×40×3-MI specimens*

6.4 ANALYSIS OF TEST RESULTS AND DESIGN RECOMMENDATIONS

In this section, the reported test data are analysed and discussed. Various design methods are outlined and their accuracy is assessed on the basis of the test data. These include the design provisions specified in EN 1993-1-4 (2006), the continuous strength method, discussed in Chapter 3, and conventional plastic design, assuming rigid-plastic material behaviour.

For the simply supported beams, discrepancies between the actual resistance and code predictions are due to the effect of material nonlinearity (i.e. strain-hardening) at cross-sectional level, whilst for the continuous beams (indeterminate structures), nonlinearity affects both individual cross-sections, due to material strain-hardening, and the whole structure, due to statical indeterminacy and the corresponding moment redistribution. A method for plastic design of steel structures, which takes into account strain-hardening, was recently proposed by Gardner and Wang (submitted) and its applicability to stainless steel indeterminate structures is assessed herein.

6.4.1 European codified design predictions

As mentioned in the introduction to this chapter, no distinct difference in the treatment of class 1 and class 2 sections exists in EN 1993-1-4 (2006), since plastic design of stainless steel indeterminate structures is not currently allowed, despite the existence of a class 1 slenderness limit. Whether a stainless steel structure is determinate, or indeterminate, elastic analysis need be applied and plasticity may only be accounted for at cross-sectional level, provided that the cross-section is class 2 or better. Moreover, material strain-hardening is ignored, thereby underestimating the actual capacity of both determinate and indeterminate stainless steels structures employing stocky cross-sections.

The codified predictions of EN 1993-1-4 (2006) are overly conservative for the simply supported beams as evidenced in Table 6.4, where even the most slender specimen SHS 100×100×3, classified as Class 4, can be seen to fail beyond its plastic moment resistance. Similar conclusions were drawn in Chapter 3 based on a large pool of beam test data, and revised, more favourable slenderness limits were proposed. The codified and proposed limits are assessed on the basis of the reported test data in Figures 6.19-6.21.

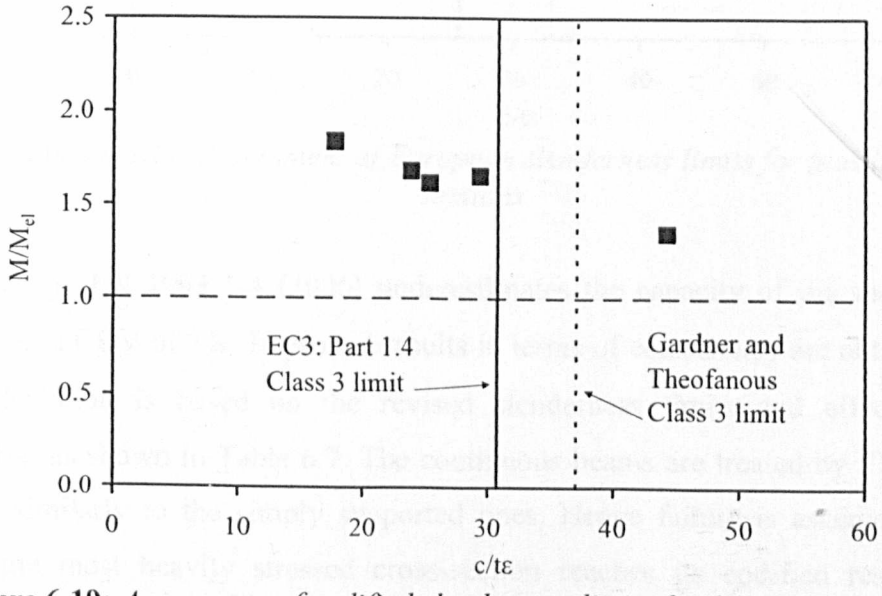

Figure 6.19: *Assessment of codified slenderness limits for fully effective sections (Class 3 sections)*

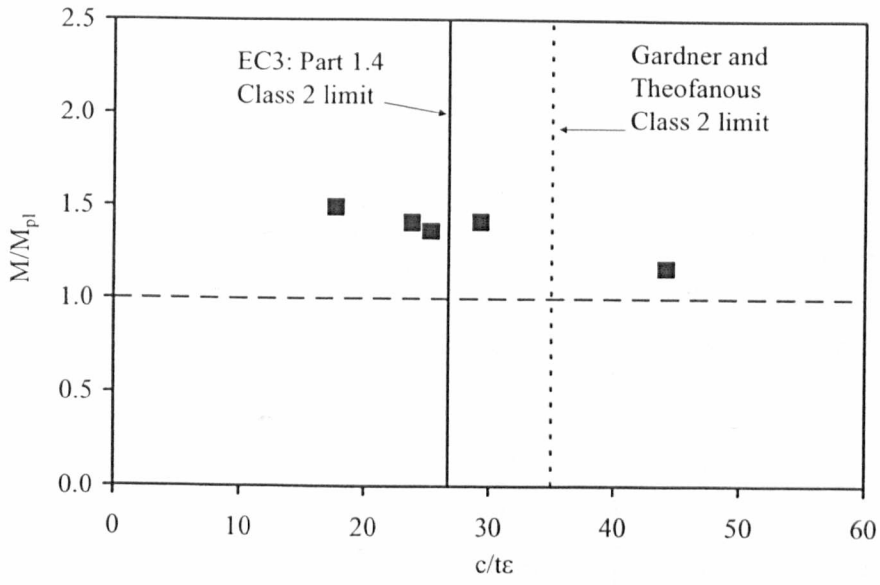

Figure 6.20: *Assessment of slenderness limits for compact (Class 2) sections*

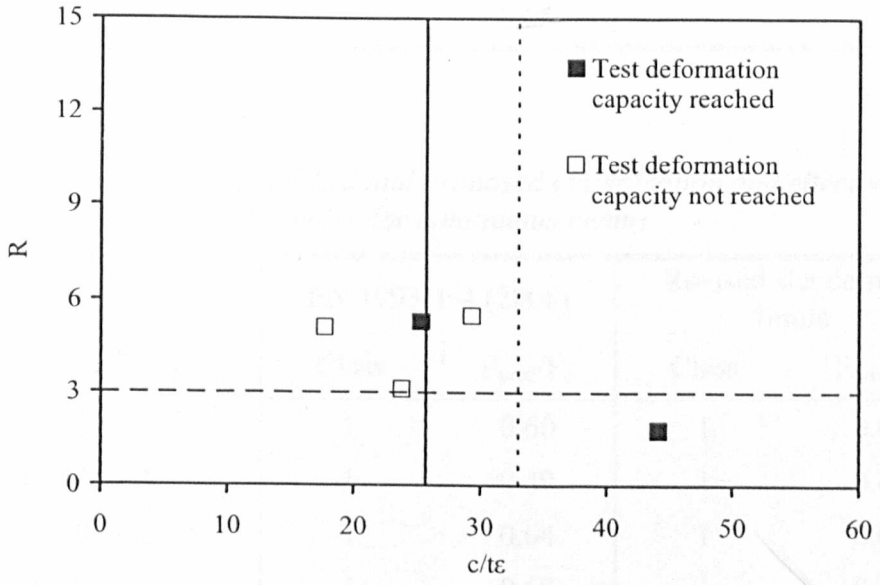

Figure 6.21: *Assessment of European slenderness limits for plastic (Class 1) sections*

On average, EN 1993-1-4 (2006) underestimates the capacity of the specimens by 33% with a COV of 8%. Improved results in terms of consistency are obtained when the calculation is based on the revised slenderness limits and effective width formulae, as shown in Table 6.7. The continuous beams are treated by EN 1993-1-4 (2006) similarly to the simply supported ones. Hence failure is assumed to occur when the most heavily stressed cross-section reaches its codified resistance, as determined through cross-section classification. The codified resistance is compared

to the actual capacity in Table 6.8, where the predictions based on the revised slenderness limits are also included.

Table 6.7: *Assessment of codified and proposed classification and effective width formulae for simply supported beams*

Specimen	EN 1993-1-4 (2006)		Revised slenderness limits	
	Class	M_{pred}/M_u	Class	M_{pred}/M_u
SHS 50×50×3	1	0.71	1	0.71
SHS 60×60×3	1	0.73	1	0.73
SHS 100×100×3	4	0.65	4	0.68
RHS 60×40×3-MA	1	0.67	1	0.67
RHS 60×40×3-MI	3	0.60	1	0.71
MEAN		0.67		0.70
COV		0.08		0.04

Table 6.8: *Assessment of codified and proposed classification and effective width formulae for continuous beams*

Specimen	EN 1993-1-4 (2006)		Revised slenderness limits	
	Class	F_{pred}/F_u	Class	F_{pred}/F_u
SHS 50×50×3-1	1	0.60	1	0.60
SHS 50×50×3-2	1	0.49	1	0.49
SHS 60×60×3-1	1	0.64	1	0.64
SHS 60×60×3-2	1	0.67	1	0.67
SHS 100×100×3-1	4	0.68	4	0.71
SHS 100×100×3-2	4	0.68	4	0.72
RHS 60×40×3-MA-1	1	0.56	1	0.56
RHS 60×40×3-MA-2	1	0.56	1	0.56
RHS 60×40×3-MI-1	3	0.52	1	0.61
RHS 60×40×3-MI-2	3	0.43	1	0.51
MEAN		0.58		0.61
COV		0.15		0.13

6.4.2 Continuous strength method

The continuous strength method (CSM) explicitly accounts for material strain-hardening at cross-sectional level, as discussed in Chapter 3. Hence, more favourable ultimate capacity predictions can be achieved for both simply supported and continuous beams if the cross-section failure is based on the CSM rather than on cross-section classification, as shown in Tables 6.9 and 6.10 for simply supported and continuous beams respectively. In both Tables 6.9 and 6.10, the modified CSM (based on cross-section slenderness), introduced in Chapter 3, has been utilised and the effect of corner strength enhancements has been accounted for according to the proposals of Gardner and Ashraf (2006).

Table 6.9: *Assessment of CSM for simply supported beams*

Specimen	Modified CSM	
	λ_l	M_{pred}/M_u
SHS 50×50×3	0.42	0.90
SHS 60×60×3	0.45	0.95
SHS 100×100×3	0.78	0.91
RHS 60×40×3-MA	0.31	0.87
RHS 60×40×3-MI	0.52	0.87
MEAN		0.90
COV		0.04

As expected, the ultimate capacity of the simply supported beams is very well-predicted and a low COV is observed. For the continuous beams, the CSM gives more favourable strength predictions compared to the classification procedure, but failure to account for moment redistribution results in excessive conservatism. Moreover, a relatively large COV is observed, owing to the dependency of the effect of moment redistribution on the cross-section slenderness. This is clearly seen in the case of the slender continuous beam specimen SHS 100×100×3-1, the capacity of which is well-predicted by the CSM, due to the absence of significant moment redistribution, evidenced in Figures 6.11 and 6.16, where the specimen can be seen to behave almost linearly up to failure.

Table 6.10: *Assessment of CSM for continuous beams*

Specimen	Modified CSM	
	λ_l	F_{pred}/F_u
SHS 50×50×3-1	0.40	0.68
SHS 50×50×3-2	0.40	0.56
SHS 60×60×3-1	0.45	0.73
SHS 60×60×3-2	0.45	0.77
SHS 100×100×3-1	0.71	0.89
SHS 100×100×3-2	0.71	0.90
RHS 60×40×3-MA-1	0.32	0.64
RHS 60×40×3-MA-2	0.32	0.64
RHS 60×40×3-MI-1	0.48	0.67
RHS 60×40×3-MI-2	0.48	0.56
MEAN		0.71
COV		0.17

6.4.3 Conventional plastic analysis

Allowing for the effects of moment redistribution is the key feature of plastic analysis. Despite the deviation of stainless steel's material response from the assumed bilinear elastic, perfectly-plastic model, application of plastic design to stainless steel indeterminate structures is attempted herein. The theoretical collapse load F_{coll} has been calculated for all continuous beam specimens and is given in Table 6.6. The predicted collapse load has been normalised by the ultimate capacity obtained experimentally and is plotted against the flange slenderness in Figure 6.22, where the current Class 1 limit for internal elements in compression codified in EN 1993-1-4 (2006) and that proposed in Chapter 3 are also included. As expected, the capacity of the most slender specimen, which exhibited a linear response up to its failure is overpredicted by plastic design compared to the remaining specimens. Moreover the proposed Class 1 limit seems more appropriate than that codified in EN 1993-1-4 (2006), which is overly conservative. In Table 6.11, the classification procedure

codified in EN 1993-1-4 (2006) and the one proposed in Chapter 3 are once again assessed; in this case the capacity of the specimens with Class 1 cross-sections is calculated by means of plastic design, the resistance of the Class 3 beams is calculated using elastic design and for Class 4 beams, elastic design and effective section properties are used. The revised classification approach seems to offer more consistent ultimate capacity predictions than the one codified in EN 1993-1-4 (2006). However the embedded conservatism remains significant.

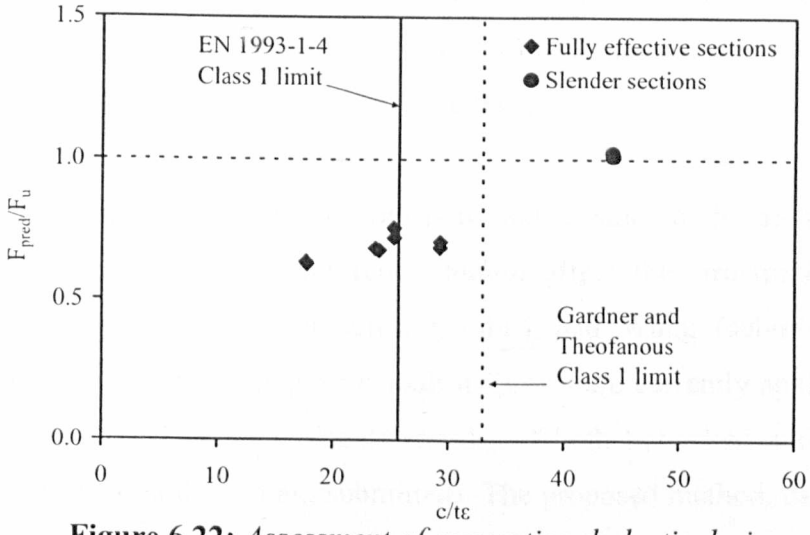

Figure 6.22: *Assessment of conventional plastic design*

Table 6.11: *Assessment of codified and proposed classification and effective width formulae for continuous beams allowing for plastic design*

Specimen	EN 1993-1-4 (2006)		Revised slenderness limits	
	Class	F_{pred}/F_u	Class	F_{pred}/F_u
SHS 50×50×3-1	1	0.68	1	0.68
SHS 50×50×3-2	1	0.68	1	0.68
SHS 60×60×3-1	1	0.72	1	0.72
SHS 60×60×3-2	1	0.76	1	0.76
SHS 100×100×3-1	4	0.68	4	0.71
SHS 100×100×3-2	4	0.68	4	0.72
RHS 60×40×3-MA-1	1	0.63	1	0.63
RHS 60×40×3-MA-2	1	0.63	1	0.63
RHS 60×40×3-MI-1	3	0.52	1	0.69
RHS 60×40×3-MI-2	3	0.43	1	0.71
MEAN		0.64		0.69
COV		0.15		0.06

6.4.4 Continuous strength method for indeterminate structures

Both the CSM and plastic analysis offer significant improvements in terms both design efficiency compared to the current design approach (EN 1993-1-4, 2006). However, plastic analysis seems superior to the CSM in terms of consistency of the predictions. This is due to the fact that, when applying the CSM, the effect of moment redistribution has been ignored, thereby reducing the failure of a structural assembly to the failure of a single cross-section, regardless of the redundancy available and the slenderness of the employed cross-sections, whereas plastic analysis consistently underestimates the capacity at cross-sectional level.

A method combining the merits of both is desirable, since both strain-hardening at cross-sectional level and moment redistribution affect the structural response of stainless steel indeterminate structures. Gardner and Wang (submitted) recently proposed a modification to the plastic analysis procedure currently applied to carbon steel structures, based on experimental results of both hot-rolled and cold-formed continuous beams (Gardner et al., submitted). The proposed method, called the CSM for indeterminate structures, allows for moment redistribution in a similar fashion to traditional plastic analysis. In essence, the method utilises the upper bound theorem of limit analysis and relies on the determination of a suitable collapse mechanism. Initially, all possible collapse mechanisms and the respective locations of plastic hinges are determined, as schematically shown in Figure 6.23 for a two-span continuous beam. The moment capacity $M_{hinge,1}$ at the location of the first plastic hinge to form is calculated by means of the CSM based on its deformation capacity $\varepsilon_{LB,1}$, as discussed in Chapter 3. The ductility demands $\varepsilon_{hinge,i}$ at successive plastic hinge locations i are determined from Equation (6.2) and should be smaller than the available deformation capacity $\varepsilon_{LB,i}$.

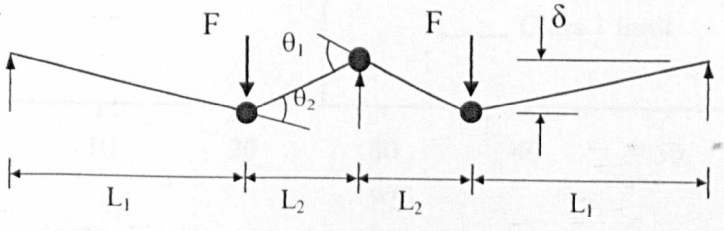

Figure 6.23: Plastic collapse mechanism for a two-span continuous beam

$$\varepsilon_{hinge,i} = \frac{\theta_i}{\theta_1}\frac{D_i}{D_1}\varepsilon_{hinge,1} \leq \varepsilon_{LB,i} \tag{6.2}$$

where D_i, D_1 is the cross-section depth at the location of the first and the i^{th} plastic hinge respectively. The ratio θ_i/θ_1 is determined according to the kinematic relations pertinent to the considered collapse mechanism. Based on the calculated ductility demands (i.e. maximum attainable strain) $\varepsilon_{hinge,i}$, the collapse bending moment diagram is attained. The collapse load F is then calculated by equating the external work done by the loads to the internal work due to the rotation at the plastic hinges, according to the virtual work principle.

This method has been applied to all stainless steel continuous beam specimens tested in this study. The modified CSM, discussed in Chapter 3 has been utilised and due account of the corner strength enhancements has been taken. The predicted collapse load has been normalised by the actual collapse load and is plotted against flange slenderness in Figure 6.23, where the current Class 1 limit for internal elements in compression codified in EN 1993-1-4 (2006) and the one proposed in Chapter 3 are also included.

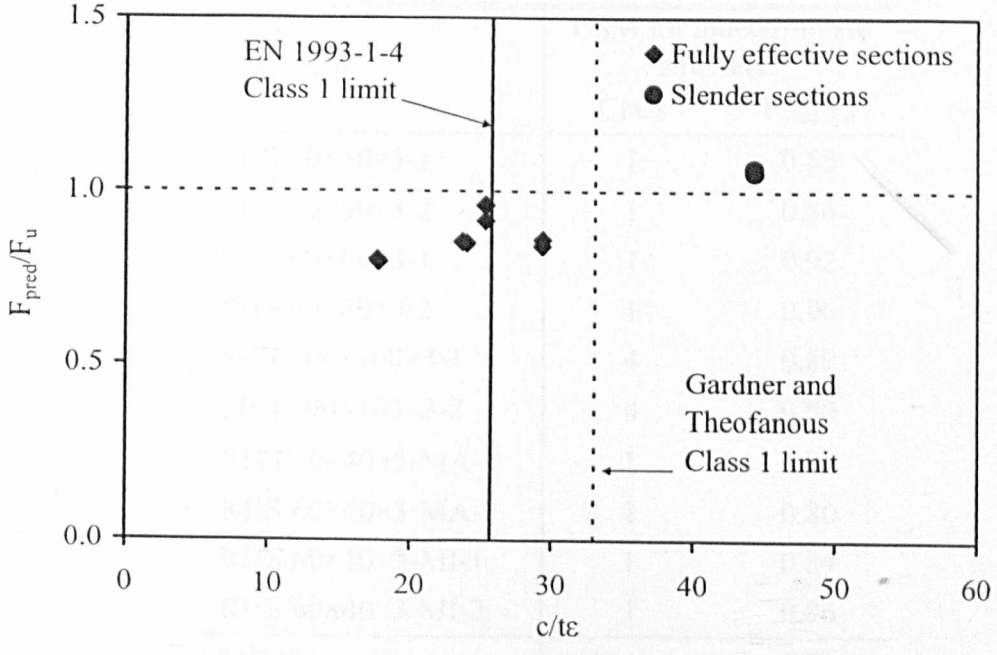

Figure 6.24: *Assessment of the CSM for indeterminate structures*

The method appears suitable for relatively stocky cross-sections, whilst the capacity of the slender SHS 100×100×3, as expected, is overpredicted, due to the assumptions inherent in plastic analysis (i.e. negligible elastic deformations, energy dissipation at plastic hinges etc), which are no longer valid for slender sections failing largely in the elastic range with no significant moment redistribution. Hence the adoption of a suitable slenderness limit, beyond which the proposed method may not be safe, is warranted.

The accuracy of the CSM for indeterminate structures is assessed in Table 6.12, where all cross-sections classified as Class 1 according to the revised slenderness limits proposed in Chapter 3 have been treated with this method. The SHS 100×100×3 specimens, which have a slender (Class 4) cross-section, have been treated with the modified CSM; hence the effect of moment redistribution has not been considered for these sections. Overall, significant enhancement in design efficiency and good agreement with the test results is observed as evidenced by the low COV of 0.06. Hence, the application of the CSM as modified for indeterminate structures is proposed herein for stainless steel indeterminate structures. Further research into the topic is underway.

Table 6.12: *Assessment of the CSM for indeterminate structures*

Specimen	CSM for indeterminate structures	
	Class	F_{pred}/F_u
SHS 50×50×3-1	1	0.85
SHS 50×50×3-2	1	0.86
SHS 60×60×3-1	1	0.92
SHS 60×60×3-2	1	0.96
SHS 100×100×3-1	4	0.89
SHS 100×100×3-2	4	0.90
RHS 60×40×3-MA-1	1	0.80
RHS 60×40×3-MA-2	1	0.80
RHS 60×40×3-MI-1	1	0.84
RHS 60×40×3-MI-2	1	0.86
MEAN		0.87
COV		0.06

6.4.5 Discussion

From the presented analyses, the significance of material nonlinearity for stainless steel indeterminate structures both at cross-section and at system level has been revealed. The current design approach codified in EN 1993-1-4 (2006) accounts for neither and therefore leads to overly conservative strength predictions, particularly for stainless steel indeterminate structures with stocky cross-sections. Best results are obtained when both material strain-hardening and moment redistribution are accounted for and hence the CSM for indeterminate structures with Class 1 cross-sections emerges as a very promising design approach.

Similar conclusions are drawn by analysing the test results on six continuous two-span stainless steel beams reported by Mirambell and Real (2000). Two repeated specimens of each of the nominal section sizes employed were tested. The described design methods are assessed on the basis of these test results in Tables 6.13 and 6.14, for design procedures based on elastic analysis and plastic analysis respectively.

Table 6.13: *Comparison of test data reported by Mirambell and Real (2000) with design predictions based on elastic analysis*

Specimen	EN 1993-1-4 (2006)		Revised slenderness limits		Modified CSM
	Class	F_{pred}/F_u	Class	F_{pred}/F_u	F_{pred}/F_u
SHS 80×80×3	4	0.63	1	0.74	0.83
SHS 80×80×3	4	0.68	1	0.80	0.89
RHS 120×80×4	1	0.72	1	0.72	0.85
RHS 120×80×4	1	0.72	1	0.72	0.85
I 100×100×8	1	0.70	1	0.70	0.80
I 100×100×8	1	0.70	1	0.70	0.80
MEAN		0.69		0.73	0.84
COV		0.05		0.05	0.04

Table 6.14: *Comparison of test data reported by Mirambell and Real (2000) with design predictions based on plastic analysis*

Specimen	Conventional plastic analysis based on EN 1993-1-4 (2006)		Conventional plastic analysis based on revised slenderness limits		CSM for indeterminate structures
	Class	F_{pred}/F_u	Class	F_{pred}/F_u	F_{pred}/F_u
SHS 80×80×3	4	0.63	1	0.83	0.96
SHS 80×80×3	4	0.68	1	0.88	1.02
RHS 120×80×4	1	0.81	1	0.81	0.99
RHS 120×80×4	1	0.81	1	0.81	0.99
I 100×100×8	1	0.79	1	0.79	0.90
I 100×100×8	1	0.79	1	0.79	0.90
MEAN		0.75		0.82	0.96
COV		0.10		0.04	0.05

Further improvements in design efficiency may be achieved if the proposed CSM for indeterminate structures is optimised on the basis of additional experimental and numerical results. Moreover, the assumption of a monotonic moment-rotation response, underpinning the method, may be conservative for stainless steel structures with high redundancy. Accounting for the softening branch of the moment-rotation response may, in some cases, be beneficial since the evolution of plasticity and strain-hardening at successive hinges and the corresponding increase in energy dissipation could increase the ultimate load. However, dealing with softening materials (or moment-rotation characteristics) is a formidable task, although some effective algorithms on the matter have been proposed (Thomopoulos et al., 1996) and applied successfully to continuous cold-formed steel purlins (Laine and Tuomala, 1999) and carbon steel frames (Mistakidis, 1999).

6.5 CONCLUDING REMARKS

An overview of the basic concepts underpinning plastic design has been presented in this chapter. Following an experimental study comprising five three-point bending

tests and ten two-span continuous beam tests (five-point bending), the conservatism embedded in the provisions for stainless steel indeterminate structures codified in EN 1993-1-4 (2006) has been highlighted. The application of conventional plastic analysis to stainless steel indeterminate structures and the accuracy of the CSM, discussed in Chapter 3, have been investigated.

It was concluded that both material strain-hardening at cross-sectional level (at the location of the plastic hinges) and moment redistribution occurring in indeterminate structures, comprising sections with sufficient deformation capacity, are significant and should therefore be accounted for in design. A recently proposed adaptation of the CSM for carbon steel indeterminate structures has been further investigated and applied to stainless steel indeterminate structures, yielding excellent results for stocky cross-sections. However, additional research, both experimental and numerical, is still required in order to further optimise the method. In particular, the determination of suitable slenderness criteria and the possibility of incorporating the falling branch of the moment-rotation response into the method need to be further investigated.

CHAPTER 7

CONCLUSIONS AND SUGGESTIONS FOR FUTURE RESEARCH

7.1 CONCLUSIONS

The key conclusions from this study are summarized in this section and an overview of the contribution of this research project to structural stainless steel design is provided. Suggestions for future research follow thereafter.

Current structural design guidance on stainless steel is largely based on assumed analogies with carbon steel; the substantial differences in the structural behaviour are neglected in favor of simplicity and harmonization with carbon steel design guidance, as discussed in Chapters 2 and 3. However the high initial cost of stainless steel necessitates the development of improved design guidance which is rational, safe, efficient and in accordance with the actual material behaviour. The assessment of current design provisions and derivation of more efficient design rules has been the main objective of this research project, with the focus lying on cross-sectional behaviour and column buckling, for which a significant body of test data exists.

To this end all published test data on stainless steel stub columns and beams failing by local buckling have been summarized in Chapter 2 and are utilized in Chapter 3 to assess the slenderness limits and effective width equations codified in EN 1993-1-4 (2006), which were derived based on a limited number of test data. In light of the additional test results, most slenderness limits were shown to be overly conservative and revised slenderness limits and effective width equations, statistically validated according to Annex D of EN 1990 (2002), were proposed. The revised slenderness limits are, in most cases, harmonized with carbon steel limits and result in more favourable strength predictions. Hence they represent a modest improvement to current European design guidance and result in more efficient design within the framework of EN 1993-1-4 (2006).

More efficient design can be achieved if key parameters affecting cross-section behaviour, such as element interaction and material nonlinearity, are incorporated into the design process. Various advanced design methods allowing for element interaction and material nonlinearity were therefore outlined in Chapter 3, including the direct strength method (DSM), the continuous strength method (CSM) and a design method based on regression analysis. All methods were assessed on the basis of numerical results, and the relative merits and weaknesses of each design approach were highlighted.

A modification to the continuous strength method has been proposed, which allows for the effect of element interaction and leads to more reliable ultimate capacity predictions. Comparisons with available test data were also made to demonstrate the enhanced accuracy of the proposed method and its suitability for the treatment of local buckling in stainless steel cross-sections. The modified CSM has been shown to be very accurate, particularly for relatively stocky cross-sections and its adoption as an alternative design approach in future revisions of EN 1993-1-4 (2006) has been proposed.

Departing from conventional cross-sectional geometries, the response of stainless steel Oval Hollow Sections (OHS) has been investigated in Chapter 4. An experimental study, comprising tensile coupon tests, 6 stub column tests, 6 simply supported beam tests and 6 flexural buckling tests has been reported. These tests were

the first to be reported on stainless steel OHS (Gardner et al., 2008b; Theofanous et al, 2009a; Theofanous et al., 2009b). Numerical studies complemented the experimental investigation. Based on both experimental and numerical data, suitable slenderness parameters and corresponding slenderness limits for stainless steel OHS have been derived and design rules in line with EN 1993-1-4 (2006) have been proposed. Moreover, the buckling curve codified in EN 1993-1-4 (2006) for hollow section columns was assessed and deemed unsafe for both OHS and CHS stainless steel columns; a revised buckling curve was therefore proposed.

As frequently mentioned throughout this thesis, the high initial material cost and price volatility of stainless steel, largely attributed to the high nickel content, hinders its more widespread usage as a primary structural material. A new low nickel stainless steel grade, termed lean duplex stainless steel and designated as EN 1.4162 in EN 10088-4 (2009) has recently emerged. Its structural response has been thoroughly investigated in Chapter 5, where 34 material coupon tests (16 tensile flat coupon tests, 14 compressive flat coupon tests and 4 tensile corner coupon tests), 8 stub column tests, 8 beam test and 12 flexural buckling tests have been reported. The tests on lean duplex stainless steel components were the first to be reported (Theofanous and Gardner 2009a; 2009b; in press). Numerical models were generated and validated against the test data. Parametric studies were subsequently conducted that allowed the assessment of European, American and Australian/New Zealand codified provisions for stainless steel tubular members. It was concluded that current design rules can be safely extended to lean duplex stainless steel components; however the embedded conservatism for stocky cross-sections still remains. Comparisons with test data on austenitic and duplex stainless steel RHS and SHS were made and lean duplex stainless steel was shown to offer superior structural performance and at a lower cost (Outokumpu data sheet, 2009).

Despite the inherent ductility of stainless steel and the provision of a Class 1 limit in EN 1993-1-4 (2006), plastic design is not currently permitted for stainless steel indeterminate structures. This is believed to be primarily due to the absence of test data and the complexities associated with stainless steels' nonlinear material response. However significant savings can be achieved if redistribution of internal forces and moments is allowed for in indeterminate structures.

This issue has been addressed in Chapter 6, where ten two-span continuous beam tests were reported. The experimental ultimate capacity was compared with current codified predictions and the inefficiencies in the current design procedure, associated both with the effect of material strain-hardening and the redistribution of moments, have been highlighted. Alternative design approaches have been presented and the classical plastic design approach has been adapted to stainless steel structures and was shown to offer more accurate ultimate capacity predictions for stocky cross-sections, which possess sufficient rotation capacity. Further research regarding the applicability of the method is ongoing and thorough validation for a variety of structural and loading configurations is required.

Overall, this study has highlighted the deficiencies of current stainless steel design provisions regarding slenderness limits, flexural buckling curves and the treatment of indeterminate structures. Moreover, the structural behaviour of new types of cross-sections (OHS) and new stainless steel grades (lean duplex stainless steel) has been experimentally and numerically studied and design rules in line with EN 1993-1-4 (2006) have been derived. Improvements to EN 1993-1-4 (2006) have also been proposed and alternative design methods for cross-section behaviour and indeterminate stainless steel structures have been presented. The improved design rules were shown to lead to more favourable and more consistent ultimate capacity predictions. Hence, their adoption in future revisions of EN 1993-1-4 (2006) is recommended herein.

7.2 SUGGESTIONS FOR FUTURE RESEARCH

The high initial material cost of stainless steel justifies the efforts for enhancing the efficiency of its usage in construction. The flexural buckling of long columns and the cross-section resistance of stub columns and beams subjected to uniaxial bending have been successfully dealt with, while other aspects of design still need further research.

The required research could, in the author's opinion, follow two distinct paths, since improvement to current design provisions of EN 1993-1-4 (2006) can be achieved either by optimizing the design equations according to experimental and numerical results within the current design format, or by deriving novel design approaches in accordance with the actual material response. As demonstrated in Chapter 3, where both approaches were followed, maintaining current design format ensures consistency with carbon steel design, but at the expense of design efficiency, whilst the derivation of novel design methods leads to more efficient design at the expense of simplicity. Clearly, an acceptable tradeoff between simplicity and design efficiency is sought, and design rules of different levels of complexity could be made available to the designer.

The scope of the modified CSM presented in Chapter 3 should be expanded to more complex load cases, involving cross-sections subjected to combined compression and biaxial moment. Additionally, the derivation of accurate interaction formulae for cross-sections and members subjected to combined compression and biaxial bending within the design format of EN 1993-1-4 (2006) is necessary for the development of an integrated design approach for stainless steel. Similarly the biaxial response of OHS should also be investigated.

Expansion of the modified CSM to components exhibiting member instabilities, such as unrestrained beams and long columns, should also be attempted. This would involve the derivation of base curves relating the maximum attainable strain ε_{LB} to the slenderness corresponding to the considered failure mode and subsequent numerical integration of the corresponding stress field over the cross-section to obtain the respective cross-section resistances. In essence, the approach could be similar to deriving direct strength equations with the difference lying in the equations being defined in terms of strains rather than stresses, the advantage of this being that the effect of material strain-hardening would be explicitly accounted for by means of the stress-strain response.

From a structural engineer's point of view, lean duplex stainless steel behaves similarly to ordinary duplex stainless steel grades. However, in view of the significant financial advantages of lean duplex stainless steel over other stainless steel grades and

the growing global concern regarding environmental issues, further detailed research of lean duplex stainless steel components of various cross-section types is warranted. Comparing lean duplex stainless steel with other structural materials on a whole life basis could potentially promote its usage in the construction industry. Life cycle assessment analyses are hence required.

As discussed in Chapter 6, there is much scope in expanding plastic design for stainless steel indeterminate structures. Further experimental and numerical investigations on stainless steel multi-span beams and frames are required in order to further develop and validate the design method presented in Chapter 6.

All design methods presented herein are, in principle valid for all nonlinear metallic materials exhibiting gradual yielding, such as aluminium alloys and high strength steel. Hence expansion of the scope of the modified CSM and the plastic design proposals to such materials should also be considered.

REFERENCES

ABAQUS. (2006) ABAQUS/Standard user's manual volumes I-III and ABAQUS CAE manual. Version 6.6. (Pawtucket, USA): Hibbitt, Karlsson & Sorensen, Inc.

Abdella, K. (2006). Inversion of a full-range stress-strain relation for stainless steel alloys. International Journal of Non-Linear Mechanics. 41 (3), 456-463.

Abdella, K. (2007). An explicit stress formulation for stainless steel applicable in tension and compression. Journal of Constructional Steel Research. 63 (3), 326-331.

Abdella, K. (2009). Explicit full-range stress–strain relations for stainless steel at high temperatures. Journal of Constructional Steel Research. 65 (4), 794-800.

Ádány, S. and Schafer, B.W. (2008). A full modal decomposition of thin-walled, single-branched open cross-section members via the constrained finite strip method. Journal of Constructional Steel Research. 64 (1), 12-29.

Akiyama, H., Kuwamura, H., Yamada, S. and Chiu, J. (1992). Influences of manufacturing processes on the ultimate behaviour of box-section members. Proceedings of the Third Pacific Structural Steel Conference (PSSC), Tokyo, Japan, 313-320.

Ala-Outinen, T. and Oksanen, T. (1997). Stainless steel compression members exposed to fire, Research Note 1684, VTT Building Technoloy, Finland.

Allen, H.G. and Bulson, P.S. (1980). Background to Buckling. McGraw-Hill. London.

American Society of Civil Engineers (ASCE) (2002). Specification for the design of cold-formed stainless steel structural members (SEI/ASCE 8-02).

Ashraf, M. (2006). Structural stainless steel design : resistance based on deformation capacity. PhD Thesis. Department of Civil and Environmental Engineering, Imperial College London.

Ashraf, M, Gardner, L. and Nethercot, D. A. (2005). Strength enhancement of the corner regions of stainless steel cross-sections. Journal of Constructional Steel Research. 61 (1), 37-52.

Ashraf, M., Gardner, L. and Nethercot, D.A. (2006a). Compression strength of stainless steel cross-sections. Journal of Constructional Steel Research. 62 (1-2), 105-115.

Ashraf, M., Gardner, L. and Nethercot, D.A. (2006b). Finite element modelling of structural stainless steel cross-sections. Thin-walled structures. 44 (10), 1048-1062.

Ashraf, M., Gardner, L. and Nethercot, D. A. (2008a). Structural stainless steel design: Resistance based on deformation capacity. Journal of Structural Engineering, ASCE. 134 (3), 402-411.

Ashraf, M., Gardner, L. and Nethercot, D.A. (2008b). Resistance of stainless steel CHS columns based on cross-section deformation capacity. Journal of Constructional Steel Research. 64 (9), 962-970.

ASTM Standard A240/A240M-09a. (2009). Standard Specification for Chromium and Chromium-Nickel Stainless Steel Plate, Sheet, and Strip for Pressure Vessels and for General Applications. ASTM International, West Conshohocken, PA.

Ayrton, W.E. and Perry, J (1886). On struts. The Engineer, 62, 464-465.

AS/NZS 4673 (2001). Cold-formed stainless steel structures, AS/NZS4673, Standards Australia, Sydney.

AS/NZS 4600 (2005). Cold-formed steel structures, AS/NZS 4600, Standards Australia, Sydney.

Baddoo, N. R., Burgan, R. and Ogden, R. (1997). Architects' Guide to Stainless Steel. SCI-P-179. The Steel Construction Institute, UK.

Bardi, F.C. and Kyriakides, S. (2006). Plastic buckling of circular tubes under axial compression-part I: Experiments. International Journal of Mechanical Sciences. 48 (8), 830-841.

Becque, J., Lecce, M. and Rasmussen, K.J.R. (2008). The direct strength method for stainless steel compression members. Journal of Constructional Steel Research. 64 (11), 1231-1238.

Becque, J. and Rasmussen, K. J. R. (2009). Experimental Investigation of the Interaction of Local and Overall Buckling of Stainless Steel I-Columns. Journal of Structural Engineering, ASCE. 135 (11), 1340-1348.

Beg, D. and Hladnik, L. (1996). Slenderness limit of class 3 I cross-sections made of high strength steel. Journal of Constructional Steel Research. 38 (3), 201-217.

Bild, S., Roik, K., Sedlacek, G., Stutzki, C. and Spangemacher, R. (1989). The b/t-ratios controlling the applicability of analysis models in Eurocode 3, Part 1.1. Background Document 5.02 for chapter 5 of Eurocode 3, Part 1.1, Aachen.

Bjorhovde R. (1972). Deterministic and probabilistic approaches to the strength of steel columns. Bethelehem (PA): Lehigh University.

Burgan, B.A., Baddoo, N.R. and Gilsenan, K.A. (2000). Structural design of stainless steel members – comparison between Eurocode 3, Part 1.4 and test results. Journal of Constructional Steel Research. 54 (1), 51-73.

Centre for Advanced Structural Engineering (1990). Compression tests of stainless steel tubular columns. Investigation Report S770. University of Sydney.

Chan, T.M. (2008). Structural behaviour of elliptical hollow sections. PhD Thesis. Department of Civil and Environmental Engineering, Imperial College London.

Chan, T. M. and Gardner, L. (2008a). Compressive resistance of hot-rolled elliptical hollow sections. Engineering structures. 30 (2), 522-532.

Chan, T.M. and Gardner, L. (2008b). Bending strength of hot-rolled elliptical hollow sections. Journal of Constructional Steel Research. 64 (9), 971-986.

Chan, T.M. and Gardner, L. (2009). Flexural buckling of elliptical hollow section columns. Journal of Structural Engineering, ASCE. 135 (5), 546-557.

Choo, Y. S., Liang, J. X., and Lim, L. V. (2003). Static strength of elliptical hollow section X-joint under brace compression. Proceedings of the 10th International Symposium on Tubular Structures, Madrid, Spain, 253-258.

Cruise, R.B. and Gardner, L. (2006). Measurement and prediction of geometric imperfections in structural stainless steel members. Structural Engineering and Mechanics. 24 (1), 63-89.

Cruise, R.B. and Gardner, L. (2008a). Residual stress analysis of structural stainless steel sections. Journal of Constructional Steel Research. 64 (3), 352-366.

Cruise, R.B. and Gardner, L. (2008b). Strength enhancements induced during cold forming of stainless steel sections. Journal of Constructional Steel Research. 64 (11), 1310-1316.

Daali, M.L. and Korol, R.M. (1995). Prediction of local buckling and rotation capacity at maximum moment. Journal of Constructional Steel Research. 32 (1), 1-13.

Dawson, R.G. and Walker, A.C. (1972). Post-buckling of geometrically imperfect plates. Journal of the Structural Division, ASCE. 98:ST1, 75-94.

Driscoll G.C. (1957). Rotation capacity of a three span continuous beam. Fritz Engineering Laboratory Report No.268.2.

Driscoll G.C. (1958). Rotation capacity requirements for single span frames. Fritz Engineering Laboratory Report No268.5.

ECSC (2000). Final Report. ECSC project – Development of the use of stainless steel in construction. Document RT810, Contract No. 7210 SA/ 842, The Steel Construction Institute, UK.

Elchalakani, M., Zhao, X-L. and Grzebieta, R. (2002). Tests on concrete filled double-skin (CHS outer and SHS inner) composite short columns under axial compression. Thin-Walled Structures. 40 (5), 415-441.

Ellobody, E. and Young B. (2005). Structural performance of cold-formed high strength stainless steel columns. Journal of Constructional Steel Research. 61 (12), 1631-1649.

Ellobody, E. and Young, B. (2007). Investigation of cold-formed stainless steel non-slender circular hollow section columns. Steel and Composite Structures. 7 (4), 321-337.

EN 1990 (2002). Eurocode - Basis of structural design. CEN.

EN 1993-1-1. (2005) Eurocode 3: Design of steel structures - Part 1.1: General rules – General rules and rules for buildings. CEN.

EN 1993-1-4. (2006) Eurocode 3: Design of steel structures - Part 1.4: General rules - Supplementary rules for stainless steel. CEN.

EN 1993-1-5 (2006) Eurocode 3. Design of Steel Structures: Part 1-5: Plated structural elements. CEN.

EN 10002-1 (2001). Metallic materials – Tensile testing – Part 1: Method of test at ambient temperature, CEN.

EN 10088-1. (2005). Stainless steels – Part 1: List of stainless steels. CEN.

EN 10088-4. (2009) Stainless steels – Part 4: Technical delivery conditions for sheet/plate and strip of corrosion resisting steels for general purposes. CEN.

Euro Inox. (1994). Design Manual for Stainless Steel. Second Edition.

Euro Inox (2006). Design Manual for Structural Stainless Steel. Third Edition.

Euro Inox (2007). Design Manual for Structural Stainless Steel. Third Edition. Commentary.

Galambos, T.V. Guide to Stability Design Criteria for Metal Structures. J. Wiley & Sons, New York, 1998 (5th Ed.).

Gardner, L. (2002). A new approach to structural stainless steel design. PhD Thesis. Department of Civil and Environmental Engineering, Imperial College London.

Gardner, L. (2005). The use of stainless steel in structures. Progress in Structural Engineering and Materials. 7 (2), 45-55.

Gardner, L. (2007). Stainless steel structures in fire. Proceedings of the Institution of Civil Engineers - Structures and Buildings. 160 (3), 129-138.

Gardner, L. (2008). The continuous strength method. Proceeding of the Institution of Civil Engineers-Structures and Buildings. 161 (3), 127-133.

Gardner, L. and Ashraf, M. (2006). Structural design for non-linear metallic materials. Engineering Structures. 28 (6), 926-934.

Gardner, L. and Baddoo, N.R. (2006). Fire testing and design of stainless steel structures. Journal of Constructional Steel Research. 62 (6), 532-543.

Gardner, L. and Chan, T. M. (2007). Cross-section classification of elliptical hollow sections. Steel and Composite Structures. 7 (3), 185-200.

Gardner, L., Chan, T. M. and Wadee, M. A. (2008a). Shear response of elliptical hollow sections. Proceedings of the Institution of Civil Engineers - Structures and Buildings. 161 (6), 301-309.

Gardner, L. and Cruise, R.B. (2009). Modeling of Residual Stresses in Structural Stainless Steel Sections. Journal of Structural Engineering. 135 (1), 42-53.

Gardner, L., Cruise, R. B., Sok, C. P., Krishnan, K., Ministro, J. (2007). Life cycle costing of metallic structures. Proceedings of the Institution of Civil Engineers: Engineering Sustainability. 160 (ES4), 167-177.

Gardner, L., Insausti, A., Ng, K. T. and Ashraf, M. (submitted). Elevated temperature material properties of stainless steel alloys. Engineering Structures.

Gardner, L. and Nethercot, D.A. (2004a). Experiments on stainless steel hollow sections - Part 1: Material and cross-sectional behaviour. Journal of Constructional Steel Research. 60 (9), 1291-1318.

Gardner L. and Nethercot D.A. (2004b). Experiments on stainless steel hollow sections - Part 2: Member behaviour of columns and beams. Journal of Constructional Steel Research. 60 (9), 1319-1332.

Gardner, L. and Nethercot D.A. (2004c). Numerical Modeling of Stainless Steel Structural Components - A Consistent Approach. Journal of Structural Engineering, ASCE. 130 (10), 1586-1601.

Gardner, L., Saari, N. and Wang, F. (submitted). Comparative experimental study of hot-rolled and cold-formed structural steel hollow sections. Thin-Walled Structures.

Gardner, L., Talja, A. and Baddoo, N.R. (2006). Structural design of high-strength austenitic stainless steel. Thin-Walled Structures. 44 (5), 517-528.

Gardner, L. and Theofanous, M. (2008). Discrete and continuous treatment of local buckling in stainless steel elements. Journal of Constructional Steel Research. 64 (11): 1207-1216.

Gardner, L., Theofanous, M. and Chan, T.M. (2008b). Buckling of tubular stainless steel columns. In: Proceedings of the 5th International Conference on Coupled Instabilities in Metal Structures 2008.p. 199-207. Sydney, Australia.

Gardner, L. and Wang, F. (submitted). Influence of strain hardening on the behaviour and design of steel structures. International Journal of Structural Stability and Dynamics.

Gedge, G. (2008). Structural uses of stainless steel — buildings and civil engineering. Journal of Constructional Steel Research, 64(11), 1194-1198.

Gerard G and Becker H. (1957). Handbook of structural stability: Part III—Buckling of curved plates and shells. Technical note 3783. NACA.

Groth, H.L. and Johansson, R.E. (1990). Statistics of the mechanical strength of stainless steels. Proceeding of the Nordic Symposium on Mechanical Properties of Stainless Steels SIMR, Sigtuna, Sweden (October 1990), 17-31.

Hill, H.N. (1944). Determination of stress-strain relations from offset yield strength values. Technical Note No 927, National Advisory Committee for Aeronautics. Washington, D.C.

Jiao H. and Zhao X.L. (2004). Section slenderness limits of very high strength circular steel tubes in bending. Thin-Walled Structures. 42 (9), 1257–71.

Johnson, A. L. and Winter, G. (1966). The Structural Performance of Austenitic Stainless Steel Members (Report No. 327). Department of Structural Engineering, School of Civil Engineering, Cornell University.

Karren, K.W. (1967). Corner properties of cold-formed steel shapes. Journal of the Structural Division, ASCE. 93:ST1, 401-432.

Kato B. (1989). Rotation capacity of H-section members as determined by local buckling. Journal of Constructional Steel Research. 13 (2-3), 95-109.

Kato B. (1990). Deformation capacity of steel structures. Journal of Constructional Steel Research. 17 (1-2), 33-94.

Kemp, A.R. (1985). Interaction of plastic local and lateral buckling., Journal of the Structural Division, ASCE. 111 (ST5), 2181-2196.

Kemp, A.R. (1986). Factors affecting the rotational capacity of plastically designed members. The Structural Engineer. 64 (B), 28-35.

Kemp A.R. (1992). Applications of research on ductility of structures. Canadian Journal of Civil Engineering. 19, 86-96.

Kempner J, Chen YN. (1968). Post-buckling of an axially compressed oval cylindrical shell. In: 12th International Congress of Applied Mechanics. Stanford University, 246-256.

Kiymaz, G. (2005). Strength and stability criteria for thin-walled stainless steel circular hollow section members under bending. Thin-Walled Structures. 43 (10), 1534-1549.

Koltsakis, E.K. and Preftitsi, F.G. (2008). Numerical investigation of the plastic behaviour of short welded aluminium double-T beams. Engineering Structures. 30 (7), 2022-2031.

Korol R.M. and Huboda J. (1972). Plastic behaviour of hollow structural sections. Journal of the Structural Division, ASCE. 98 (ST5), 1007-1023.

Kuhlmann, U. (1989). Definition of Flange Slenderness Limits on the Basis of Rotation Capacity Values. Journal of Constructional Steel Research. 14 (1), 21-40.

Kuwamura H. (2003). Local buckling of thin-walled stainless steel members. Steel Structures. 3, 91–201.

Laine, M. and Tuomala, M. (1999). Testing and design of gravity-loaded steel purlins restrained by sheeting. Journal of Constructional Steel Research. 49 (2), 129-138.

Lam, D. and Gardner, L. (2008). Structural design of stainless steel concrete filled columns. Journal of Constructional Steel Research. 64 (11), 1275-1282.

Lay MG, Galambos TV. (1965). Inelastic steel beams under uniform moment. Journal of the Structural Division, ASCE. 91 (6), 67-93.

Lay MG, Galambos TV. (1967). Inelastic beams under moment gradient. Journal of the Structural Division, ASCE. 93 (1), 381-99.

Lecce, M. and Rasmussen, K. J. R. (2006). Distortional buckling of cold-formed stainless steel sections: Finite-element modelling and design. Journal of Structural Engineering, ASCE. 132 (4), 505-514.

Lin, S-H., Yu, W-W., Galambos, T.V. and Wang, E. (2005). Revised ASCE specification for the design of cold-formed stainless steel structural members. Engineering Structures. 27 (9): 1365-1372.

Liu, Y. and Young, B. (2003). Buckling of stainless steel square hollow section compression members. Journal of Constructional Steel Research. 59 (2), 165-177.

Lukey A.F. and Adams P.F. (1969). Rotation capacity of beams under moment gradient. Journal of the Structural Division, ASCE. 95 (ST6), 1173-1188.

Martinez-Saucedo G., Packer J.A., Zhao X.L. (2008). Static design of elliptical hollow section end connections. Proceeding of the Institution of Civil Engineers-Structures and Buildings. 161 (2), 103-113.

Mazzolani, F.M. (1995). Aluminium Alloy Structures. 2nd edition. E & FN Spon, An imprint of Chapman and Hill.

Mc Dermott J.F. (1969). Local plastic buckling of A514 steel members. Journal of the Structural Division, ASCE. 95 (ST9), 1837-1850.

Mirambell, E. and Real, E. (2000). On the calculation of deflections in structural stainless steel beams: an experimental and numerical investigation. Journal of Constructional Steel Research. 54 (1), 109-133.

Mistakidis, E.S. (1999). Evaluation of the total ductility in steel structures through a nonconvex energy optimization approach. Engineering Structures. 21 (9), 810-822.

Nilsson, J. O., Chai, G. and Kivisäkk, U. (2008). Recent development of stainless steels, Proceedings of the Sixth European Stainless steel Conference, Finland, 585-590.

Nip, K.H., Gardner, L. and Elghazouli, A.Y. (2010). Cyclic testing and numerical modelling of carbon steel and stainless steel tubular bracing members. Engineering Structures. 32 (2), 424-441.

North American Specification. Appendix 1: Design of cold-formed steel structural members using the Direct Strength Method. In: 2004 supplement to the North American Specification for the design of cold-formed steel structures. Washington (DC): American Iron and Steel Institute: 2004.

Nowzartash, F. and Mohareb, M. (2009). Plastic Interaction Relations for Elliptical Hollow Sections. Thin-Walled Structures. 47 (6-7), 681-691.

O'Shea, M. D. and Bridge, R. Q. (1997). Local buckling of thin-walled circular steel sections with or without internal restraint. Journal of Constructional Steel Research. 41 (2-3), 137-157.

Outokumpu data sheet (2009). AAF (alloy adjustment factors) for flat products final figures. http://www.outokumpu.com/pages/Page____6001.aspx

Quach, W.M., Teng, J.G. and Chung, K.F. (2008). Three-stage full-range stress-strain model for stainless steel. Journal of Structural Engineering, ASCE. 134 (9), 1518-1527.

Ramberg, W. and Osgood, W. R. (1943). Description of stress-strain curves by three parameters. Technical Note No 902, National Advisory Committee for Aeronautics Washington, D.C.

Rasmussen, K. **J. R.** (2000). The Development of an Australian Standard for Stainless Steel Structures. Proceedings of the Fifteenth International Speciality Conference on Cold-formed Steel Structures. St. Louis, Missouri, USA. 659-671.

Rasmussen, K.J.R. (2003). Full-range stress-strain curves for stainless steel alloys. Journal of Constructional Steel Research. 59 (1), 47-61.

Rasmussen K.J.R. and Hancock G.J. (1993a). Design of cold-formed stainless steel tubular members I: Columns. Journal of Structural Engineering, ASCE. 119 (8), 2349-2367.

Rasmussen, K.J.R. and Hancock, G.J. (1993b). Design of cold-formed stainless steel tubular members II: Beams. Journal of Structural Engineering, ASCE. 119 (8), 2368-2386.

Rasmussen, K.J.R. and Rondal, J. (2000). Column curves for stainless steel alloys. Journal of Constructional Steel Research. 54 (1), 89-107.

Real, E. and Mirambell, E. (2005). Flexural behaviour of stainless steel beams. Engineering Structures. 27 (10), 1465-1475.

Real, E., Mirambell, E. and Estrada, I. (2007). Shear response of stainless steel plate girders. Engineering Structures. 29 (7), 1626-1640.

Ricles J.M., Sause R. and Green P.S. (1998). High strength steel: implications of material and geometric characteristics on inelastic flexural behaviour. Engineering Structures. 20 (4-6), 323-335.

Roufegarinejad, A., and Bradford, M. A. (2007). Local buckling of thin-walled elliptical tubes containing an elastic infill. Proceedings of the 3rd International Conference on Steel and Composite Structures, Manchester, United Kingdom, 943-948.

Ruiz-Teran, A. M. and Gardner, L. (2008). Elastic buckling of elliptical tubes. Thin-Walled Structures. 46 (11), 1304-1318.

Schafer, B.W. (2008). Review: The Direct Strength Method of cold-formed steel member design. Journal of Constructional Steel Research. 64 (7-8), 766-778.

Schafer, B.W., Ádány, S. (2006). "Buckling analysis of cold-formed steel members using CUFSM: conventional and constrained finite strip methods." Eighteenth

International Specialty Conference on Cold-Formed Steel Structures, Orlando, FL. October 2006.

Schafer, B.W. and Peköz, T. (1998a). Computational modelling of cold-formed steel: characterizing geometric imperfections and residual stresses. Journal of Constructional Steel Research. 47 (3), 193-210.

Scahfer, B., Pekoz, T. (1998b). Direct strength prediction of cold-formed steel members using numerical elastic buckling solutions. In: Shanmugam N., Liew, J., Thevendran, V. editors. Thin-walled structures, research and developments. NewYork: Elsevier, p. 127-144.

Sedlacek, G. and Feldmann, M. (1995). The b/t-ratios controlling the applicability of analysis models in Eurocode 3, Part 1.1. Background Document 5.09 for chapter 5 of Eurocode 3, Part 1.1, Aachen.

Sherman DR. (1976). Tests of Circular Steel Tubes in Bending. Journal of the Structural Division, ASCE. 102:ST11, 2181-2195.

Sieurin, H., Sandström, R. and Westin, E.M. (2007). Fracture toughness of the lean duplex stainless steel LDX 2101. Metallurgical and Materials Transactions A. 37 (10), 2975-2981.

Silvestre, N. (2008). Buckling behaviour of elliptical cylindrical shells and tubes under compression. International Journal of Solids and Structures. 45 (16), 4427-4447.

Talja, A. and Salmi, P. (1995). Design of stainless steel RHS beams, columns and beam-columns. Research note 1619. VTT building technology, Finland.

Theofanous, M., Chan, T.M. and Gardner, L. (2009a). Structural response of stainless steel oval hollow section compression members. Engineering Structures. 31 (4), 922-934.

Theofanous, M., Chan, T.M. and Gardner, L. (2009b). Flexural behaviour of stainless steel oval hollow sections. Thin-Walled Structures. 47 (6-7), 776-787.

Theofanous, M. and Gardner, L. (2008). Slenderness limits for stainless steel cross-sections. In: Proceedings of the 5th International Conference on Thin-Walled Structures, Brisbane, Australia. Vol. 2, 899-906.

Theofanous, M. and Gardner, L. (2009a). Structural behaviour of lean duplex stainless steel. In: Proceedings of the 9th International Conference on Steel Concrete Composite and Hybrid Structures (ASCCS 2009), Leeds, UK, 759-766.

Theofanous, M. and Gardner, L. (2009b). Testing and numerical modelling of lean duplex stainless steel hollow section columns. Engineering Structures. 31 (12), 3047-3058.

Theofanous, M. and Gardner, L. (in press). Experimental and numerical studies of lean duplex stainless steel beams. Journal of Constructional Steel Research.

Theofanous, M. and Gardner, L. (submitted). The effect of element interaction and material non-linearity on the ultimate capacity of stainless steel cross-sections. Thin-Walled Structures.

Thomopoulos, K.T., Mistakidis, E.S., Koltsakis, E.K. and Panagiotopoulos, P.D. (1996). Softening behaviour of continuous thin-walled steel beams. Two numerical methods. Journal of Constructional Steel Research. 36 (1). 1-13.

Uy, B. (1998). Local and post-local buckling of concrete filled steel welded box columns. Journal of Constructional Steel Research. 47 (1-2), 47-72.

Wang, S. T. and Winter, G. (1969). Cold rolled Austenitic Stainless Steel: Material Properties and Structural Performance (Report No. 334). Dept. of Structural Engineering, Cornell University.

Willibald, S., Packer, J. A. and Martinez-Saucedo, G. (2006). Behaviour of gusset plate connections to ends of round and elliptical hollow structural section members. Canadian Journal of Civil Engineering. 33 (4), 373-383.

Winter, G. (1947). Strength of thin steel compression flanges. Bulletin No. 35/3, Engrg. Experiment Sta., Cornell University, Ithaca, N.Y.

Winter, G. (1950). Performance of thin steel compression flanges. Bulletin No. 33, Engrg. Experiment Sta., Cornell University, Ithaca, N.Y.

Yamada, S., Kurino, H. and Kato, B. (1988). Ultimate Strength of H-shaped Stub-columns of Stainless Steel. Proceedings of the Institute of Architects, Japan.

Yang, H., Lam, D. and Gardner, L. (2008). Testing and analysis of concrete-filled elliptical hollow sections. Engineering Structures. 30 (12), 3771-3781.

Young, B. and Ellobody, E. (2006). Experimental investigation of concrete-filled cold-formed high strength stainless steel tube columns. Journal of Constructional Steel Research. 62 (5), 484-492.

Young, B. and Hartono, W. (2002). Compression tests of stainless steel tubular members, Journal of structural engineering, ASCE. 128(6), (754-761).

Young, B and Liu, Y. (2003). Experimental investigation of cold-formed stainless steel columns. Journal of Structural Engineering, ASCE. 129 (2), 169-176.

Young, B. and Lui, W.M. (2005). Behavior of cold-formed high strength stainless steel sections. Journal of Structural Engineering, ASCE. 131 (11), 1738-1745.

Young, B. and Lui, W. M. (2006). Tests on cold formed high strength stainless steel compression members. Thin-Walled Structures. 44 (2), 224-234.

Yura J.A., Galambos T.V. and Ravindra M.K. (1978). The bending resistance of steel beams. Journal of the Structural Division, ASCE. 104 (ST9), 1355-1370.

Zhao, X. L., Lu, H. and Galteri, S. (2007). Tests of Elliptical Sections Filled with SCC (Self-Compacting Concrete). Proceedings of the 5th International Conference on Advances in Steel Structures. Singapore, 950-955.

Zhou, F. and Young, B. (2005). Tests of cold-formed stainless steel tubular flexural members. Thin-Walled Structures. 43 (9), 1325-1337.

Zhu, J.-H. and Young, B. (2009). Design of aluminium alloy flexural members using the direct strength method. Journal of Structural Engineering, ASCE. 135 (5), 558-566.